

GAS-PHASE ION/ION REACTION OF BIOMOLECULES

by

Mack Shih

A Dissertation

Submitted to the Faculty of Purdue University

In Partial Fulfillment of the Requirements for the degree of

Doctor of Philosophy



Department of Chemistry

West Lafayette, Indiana

December 2019

THE PURDUE UNIVERSITY GRADUATE SCHOOL
STATEMENT OF COMMITTEE APPROVAL

Dr. Scott A. Mcluckey, Chair

Department of Chemistry

Dr. Mary J. Wirth

Department of Chemistry

Dr. Paul G. Wenthold

Department of Chemistry

Dr. Alexander Laskin

Department of Chemistry

Approved by:

Dr. Christine A. Hrycyna

Head of the Graduate Program

*To my family and friends
Thank you for all your love and support*

ACKNOWLEDGMENTS

First and foremost, I would like to extend my deepest thanks and acknowledgement to my advisor, Dr. Scott McLuckey. It was a privilege to join you and your group for my graduate degree education and I would like to thank you for giving me this opportunity. Thank you for the help and guidance that supported me through my graduate school journey. You have been an excellent research advisor who is already there if I wanted to talk and always providing great insight and ideas not only about research projects but also about life as well. I have learned a lot about how to be a scientist from your example and I will cherish and value what I've learned.

I would also like to express my thanks to the fantastic McLuckey group members. Research is a difficult and at times frustrating journey but I am always encouraged by the close relationships and comradery we share as group as we all venture forth with our research. My time here at Purdue would not be half as enjoyable without you guys. To the senior graduate students who were here when I first joined the group, Alice Pilo, Christine Fisher, Josh Gilbert, Jiexun Bu, Zhou Peng, Stella Betancourt, Eric Dziekonsky, Corinne Demuth, Nicole Redwine, Car Luongo, and Andrew DeBlase, thank you for all the help you've given me, no matter how small. I have learned a lot from you guys and I strive to be as much of help to the younger students now that I'm a senior student. To my peers Feifei Zhao and Nan Wang, it was a privilege to join the group together with you two and I shall always treasure the times we had. To David Foreman, Josh Johnson, Chris Harrilal, Kenny Lee, Caitlin Randolph, Anthony Pitts-McCoy, John Lawler, Elissia Franklin, Sarju Adhikari, His-Chun Chao, Abdirahman Abdillahi, Jay Bhanot, De'Shavon Shenault and Ian Carrick, I've enjoyed our time together and it was always a pleasure to discuss research or any matter with any of you.

To Jim Hager and Larry Campbell, it is always a pleasure when you come to Purdue and thank you for being great collaborators at SCIEX. You have given me tremendous help regarding any question I have with the instruments and I have learned a lot you.

I'd like to thank my parents who have always encouraged me as well as providing valuable advice about life. I am grateful of the efforts you have put into raising me and I will always love you guys. I'd like to thank my best friend Daniel who has been with me through thick and thin. You have been a good friend to me over the last ten years and I look forward to the many memories in the future. Finally, I'd like to thank my cat Arya who always cheer me up when we snuggle.

TABLE OF CONTENTS

LIST OF FIGURES	10
LIST OF TABLES.....	15
List OF ABBREVIATIONS	16
ABSTRACT.....	18
CHAPTER 1. INTRODUCTION	21
1.1 Mass Spectrometry.....	21
1.1.1 Principles	21
1.1.2 Ionization.....	22
1.1.2.1 Electrospray ionization	23
1.1.2.1.1 ESI Source.....	24
1.1.2.1.2 ESI Mechanism	26
1.1.2.1.3 Ion Evaporation Model (IEM).....	27
1.1.2.1.4 Charge Residue Model (CRM)	27
1.1.2.1.5 Chain Ejection Model (CEM)	28
1.1.3 Mass Analyzers.....	29
1.1.3.1 Quadrupole and Linear Quadrupole Ion Trap (LQIT).....	30
1.1.3.2 Time of Flight (TOF).....	32
1.2 Tandem Mass Spectrometry	33
1.2.1 Collision-induced Dissociation (CID).....	35
1.2.2 Dipolar Direct Current (DDC) Collision-induced Dissociation (CID).....	38
1.3 Gas-phase Ion/Ion Reactions	39
1.3.1 Instrumentation	40
1.3.2 Thermodynamics and Kinetics	42
1.3.3 Gas-phase Covalent Modifications.....	43
1.4 Conclusions.....	44
1.5 References.....	44
CHAPTER 2. EXPLORATION OF GAS-PHASE ION/ION REACTIONS OF CARBOHYDRATES	58
2.1 Introduction.....	58

2.2	Experimental	61
2.2.1	Materials	61
2.2.2	Isotopic ¹⁸ O Labeling at the Reducing End	62
2.2.3	Reductive Amination at the Reducing End	62
2.2.4	Synthesis of Fixed Charge Pyridinium-based Reagents	62
2.2.5	Mass Spectrometry	62
2.3	Results and discussions	63
2.3.1	Ion/ion reactions of Alkoxides, Formation of Ethers and Esters in Carbohydrates ..	63
2.3.2	Schiff Base Reactions of Carbohydrates	68
2.3.3	Metal Adduction to Carbohydrates via Gas-phase Ion/ion Reactions	71
2.4	Conclusion	73
2.5	References	74
CHAPTER 3. ION/ION CHARGE INVERSION/ATTACHMENT IN CONJUNCTION WITH DIPOLAR DC COLLISIONAL ACTIVATION AS A SELECTIVE SCREEN FOR SULFO- AND PHOSPHOPEPTIDES		94
3.1	Introduction	94
3.2	Experimental Section	97
3.2.1	Materials	97
3.2.2	Typsin Digestion	98
3.2.3	N-terminal Acetylation	98
3.2.4	Mass Spectrometry	98
3.2.5	Dipolar DC Dissociation Kinetics	99
3.2.6	Density Functional Theory Calculations	100
3.3	Results and Discussion	100
3.3.1	Density Functional Theory Calculations of Guanidinium Interaction	101
3.3.2	Complex Formation and DDC for Phosphopeptides vs. Unmodified Peptides	103
3.3.3	Complex Formation and DDC for Phosphopeptides vs. Sulfopeptides	105
3.3.4	DDC Dissociation kinetics	106
3.4	Conclusions	109
3.5	References	110
CHAPTER 4. INVESTIGATION OF HYALURONIC ACID		132

4.1	Introduction.....	132
4.2	Experimental Section.....	133
4.2.1	Materials.....	133
4.2.2	Digestion of Hyaluronic Acid.....	134
4.2.3	Mass spectrometry.....	134
4.2.4	Spectral Deconvolution.....	134
4.3	Results and Discussion.....	135
4.3.1	Electrospray of Single HA Polymer.....	135
4.3.2	Electrospray of HA Mixture.....	135
4.3.3	Proton Transfer of HA Anions.....	137
4.3.4	Odd-mers Present in HA Mixture.....	138
4.3.5	Charge-inversion of Proteins using HA.....	139
4.4	Conclusions.....	140
4.5	References.....	141
CHAPTER 5. INVESTIGATION OF MONOCLONAL ANTIBODIES.....		152
5.1	Introduction.....	152
5.2	Experimental.....	155
5.2.1	Materials.....	155
5.2.2	Mass spectrometry.....	156
5.2.3	Sample Preparation.....	156
5.2.4	Disulfide Cleavage Photochemistry Setup.....	157
5.2.5	Reduction and Alkylation of Disulfide Bonds.....	157
5.2.6	Circular Dichroism.....	157
5.3	Results and Discussions.....	158
5.3.1	Requirement for Sample Cleanup.....	158
5.3.2	Electrospray and DDC of mAbs.....	159
5.3.3	Parameters for DDC.....	163
5.3.4	Agitation and Analysis of mAbs.....	164
5.3.5	Thermal Denaturation.....	167
5.3.6	Photochemical Cleavage of disulfide bonds.....	170
5.4	Conclusions.....	171

5.5	References.....	172
	PUBLICATION.....	193

LIST OF FIGURES

- Figure 1.1 A schematic drawing showing a) general fissioning process of charged ESI droplet and the three accepted models of ionization: b) ion evaporation model (IEM), c) charge residue model (CRM), and d) chain ejection model (CEM). 55
- Figure 1.2 Mass spectrometers that has been modified for ion/ion reaction a) AB Sciex QTRAP 4000 (Sciex, Concord, Canada) and b) AB Sciex TripleTOF 5600 (Sciex, Concord, Canada). The 5600 has also been modified for q0 and q2 DDC. 56
- Figure 1.3 A generic energy diagram for a) ion/ion reaction and b) ion/molecule reaction involving proton transfer..... 57
- Figure 2.1 Product spectrum for a) ion/ion reaction between doubly deprotonated β -cyclodextrin, $[M-2H]^{2-}$, and tetramethylammonium, TMA. The structure of b) β -cyclodextrin and c) maltoheptaose. (Lightning bolt indicates ion subject to activation) 77
- Figure 2.2 Ion trap CID spectra of the electrostatic complex formed between tetramethylammonium (TMA) and a) β -cyclodextrin, b) maltoheptaose, c) maltoheptaose modified with 2-aminopyridine; diallyldimethylammonium and d) β -cyclodextrin, e) maltoheptaose, f) maltoheptaose modified with 2-aminopyridine. Methyl and allyl transfer products are denoted respectfully with red (●) and blue (●) dots. 78
- Figure 2.3 Nomenclature for carbohydrate fragment ions generated by tandem MS (Modified from Domon & Costello, 1988). 79
- Figure 2.4 Product ion spectra for ion/ion reactions between doubly-deprotonated β -cyclodextrin and a) 1-propionylpyridin-1-ium or c) 1-pivaloylpyridin-1-ium. Ion trap CID of the b) ethyl ester product and d) t-butyl ester product. 80
- Figure 2.5 Ion trap CID spectrum of t-butyl ester product formed with a) maltoheptaose, b) maltoheptaose modified with 2-amino pyridine at the reducing end, and c) ^{18}O reducing end labeled maltoheptaose (\diamond denoted addition of t-butyl ester group)..... 82
- Figure 2.6 Structure of PAMAM dendrimer, ethylenediamine core, generation 1.0 83
- Figure 2.7 Product ion spectrum of charge reduction ion/ion reactions between singly protonated 85
- Figure 2.8 Ion trap CID spectra of the electrostatic complex formed via ion/ion reaction between $[PAMAM\ G1+H]^+$ and a) $[Maltoheptaose-2H]^{2-}$, c) $[Maltoheptaose\ with\ 2-aminopyridine-2H]^{2-}$; or reactions between $[PAMAM\ G1+2H]^{2+}$ and b) $[Maltoheptaose-2H]^{2-}$, d) $[Maltoheptaose\ with\ 2-aminopyridine-2H]^{2-}$ 86
- Figure 2.9 Product spectrum of a) ion/ion reactions between doubly protonated PAMAM G1 and singly deprotonated ^{18}O -labeled maltoheptaose; b) collision activation of the electrostatic complex formed. 88
- Figure 2.10 Collisional ion trap CID of the Schiff base product peak obtained from activation of the electrostatic complex..... 89

Figure 2.11 Ion trap CID control spectra for a) [PAMAM G1+H] ⁺ , b) [Maltoheptaose-H] ⁻ , and c) [Maltoheptaose with 2-AP -H] ⁻	90
Figure 2.12 Ion trap CID spectra for a) [Maltoheptaose-H] ⁻ and b) [Maltoheptaose+Na] ⁺ (Filled diamonds indicates fragment containing Na ⁺ and hollow diamonds are water losses from C ions).	91
Figure 2.13 Ion trap CID spectra for electrostatic complexes formed between maltoheptaose and a) Na ⁺ , b) K ⁺ , c) Rb ⁺ , and d) Cs ⁺ (Filled diamonds indicates fragment containing the metal cation).	92
Figure 2.14 Comparison of cross-ring and glycosidic fragment peak areas as a percentage of all fragments present. b) Comparison of the types of cross-ring fragments that is present.....	93
Figure 3.1 (a) A generic energy diagram for a proton transfer ion/ion reaction involving a doubly-protonated reagent (blue) and a singly-deprotonated analyte (red). The reactants undergo a long-range attraction due to the Coulombic potential and, if they undergo an intimate collision, form a relatively long-lived complex. The complex can break up spontaneously to yield charged (yellow) and neutral (green) proton transfer products or the complex can be stabilized via collisions and/or emission. (b) The interaction strength between three basic groups and three deprotonated acids calculated via DFT. The model is a simplified version where only the interaction between positively charged basic groups and the negatively charged acidic groups are probed. The binding strength is the zero-point corrected energy difference between the complex and the sum of the products after proton transfer.	115
Figure 3.2 Nanoelectrospray of six peptide mixture containing three phosphopeptides in (a) negative mode and (b) positive mode. Charge-inversion ion/ion reaction of the anionic peptide mixture with [AAARAAARA+2H] ²⁺ (c) with no DDC applied, and (d) DDC voltage of 22 volts applied.....	116
Figure 3.3 (a) Negative mode nanoelectrospray of trypsin digested ubiquitin with phosphopeptides pSGGFL, pTGGFL, and pYGGFL spiked in and (b) post ion/ion reaction with DDC at 22 V applied.....	117
Figure 3.4 (a) Negative mode nanoelectrospray of a sulfopeptide, sYGGFL, two phosphopeptides, pTGGFL and pSGGFL, and three non-PTM peptides, YGGFL, GAIDDL, and NVVQIY. (b) Post-ion/ion reaction spectrum of the anionic peptide mixture with [AAARAAARA+2H] ²⁺ followed by (c) DDC using 22 V and (d) 25 V.	118
Figure 3.5 (a) Negative mode nanoelectrospray of a sulfopeptide, sYGGFL, two phosphopeptides, pTGGFL and pSGGFL, and three non-PTM peptides, YGGFL, GAIDDL, and GNRDADA. (b) Post-ion/ion reaction spectrum of the anionic peptide mixture with [HAHAHAA+2H] ²⁺ followed by (c) DDC at 19 V and (d) 22 V.	119
Figure 3.6 (a) The kinetic data for determining the dissociation rate of the peptide complex between [pYGGFL-H] ⁻ and [AAARAAARA+2H] ²⁺ . The natural log of the peak area of the complex over the peak area of the total ion current (TIC) is plotted against the activation time of DDC. (b) The complex dissociation rate of each peptide complex, k_{diss} , is plotted against the DDC voltage. The error bar is two standard deviations of the slope's fitting error in the kinetic data.....	120

Figure 3.7 (a) Kinetic data comparison between peptide complexes of AAARAAARA (\diamond) and RKRARKA (\square) for three phosphopeptides and a sulfopeptide. Kinetic data for AAARAAARA complexes are solid lines and dashed lines for RKRARKA complexes. (b) Kinetic data comparison of select peptides between AAARAAARA (\diamond) and Ac-AAARAAARA (\blacklozenge). The error bar is two standard deviations of the slope's fitting error in the kinetic data.	121
Figure 3.8 Optimized complex structure between methylguanidinium and acetate.....	122
Figure 3.9 Optimized complex structure between methylguanidinium and methylphosphate...	123
Figure 3.10 Optimized complex structure between methylguanidinium and methylsulfate.	124
Figure 3.11 Optimized complex structure between methylimidazole and methylphosphate.	125
Figure 3.12 Optimized complex structure between methylimidazole and methylsulfate.....	126
Figure 3.13 Optimized complex structure between methylamine and methylphosphate.	127
Figure 3.14 Optimized complex structure between methylamine and methylsulfate.....	128
Figure 3.15 Full spectrum of post charge-inversion ion/ion inversion reaction between $[AAARAAARA+2H]^{2+}$ and the six peptide mixture containing pSGGFL, pTGGFL, and pYGGFL.	129
Figure 3.16 Positive mode nESI spectrum of an ubiquitin tryptic digest containing pSGGFL, pTGGFL, and pYGGFL. No signs of phosphopeptides, either protonated or sodiated, were observed in the spectrum.	130
Figure 3.17 Spectra for dissociation kinetic study of the complex $[AAARAAARA+pYGGFL+H]^+$ at DDC voltage of 23 V and (a) 1200 ms, (b) 900 ms, (c) 600 ms, (d) 400 ms, and (e) 200 ms.....	131
Figure 4.1 Electrospray of a 6-mer HA using a) a voltage gradient of 5 V (QJet/Q0 to Q1) and 5 V (Q1 to q2); b) a voltage gradient of 2 V (QJet/Q0 to Q1) and 3 V (Q1 to q2) for ion optics.	143
Figure 4.2 a) Mass spectrum of HA mixture labeled 8k-15k MW and b) wide isolation window of the 'emerald city' region color coded by its unique regions: c) fully charged odd-mer HA, d) fully charged even-mer HA, and e) one charge less than max charge odd-mer HA.	144
Figure 4.3 Deconvoluted spectrum of a) narrow isolation window in the 'emerald city' spectrum containing HA13 and HA15 at max charge; post ion/ion reaction of ions within that isolation window with b) pyridine, c) 7,8-benzoquinoline, and d) 1,8-Bis(dimethylamino)naphthalene (Proton-sponge®).	145
Figure 4.4 Deconvoluted spectrum of a) 'emerald city' and b) post-proton transfer ion/ion reaction with Proton-sponge®. The odd HA-mers are noted in blue and the even-mers are noted in green.....	146
Figure 4.5 Mass spectrum of the a) post digested hyaluronic acid mixture and b) subsequent post-proton transfer ion/ion reaction reducing the charge of the majority of ions to 1- charge state.	147
Figure 4.6 a) Post ion/ion reaction between 8k-15k hyaluronic acid anionic mixture (m/z 200-1000) with 7+ ubiquitin. The labeled peaks are the charge of the ubiquitin anions after the	

reaction. b) A zoomed in of the 4- charge state of ubiquitin showing the presence of sodium adduction post ion/ion reaction. The 7+ ubiquitin was clean isolation of only the protonated species.	148
Figure 4.7 Charge-inversion ion/ion reaction spectra between 50 hyaluronic acid anions (m/z 200-1500) with a) 15+ cytochrome C and b) 24+ myoglobin.	149
Figure 4.8 . a) Pre-ion/ion reaction spectrum of isolated 7- and 8- HA from the HA mixture and post-ion/ion reaction spectrum using b)pyridine, c) 7,8-benzoquinoline, and d) 1,8-dimethylamino naphthalene (Proton-sponge®).	150
Figure 4.9 a) Pre-ion/ion reaction spectrum of isolated ‘emerald city’ from the HA mixture and post-ion/ion reaction spectrum using b) 1,8-dimethylamino naphthalene (Proton-sponge®).	151
Figure 5.1 a) A generic diagram of IgG1 with its two regions, disulfide bonds (red), and its approximate molecular weight labeled. The b) light chain and c) heavy chain of IgG with their various domains labeled as well each chain’s molecular weight.	177
Figure 5.2 nESI spectrum for a) 300x dilution of 123.23 mg/mL mAb sample in water, b) 50 uL of sample ran though PD MidiTrap G-25 followed by a 20x dilution in water, and c) q2DDC (50 ms, +/- 40V, q2RF 500) applied to the ions before injection into time-of-flight for mass analysis. The IgG ion’s charge states are label in red for monomer, orange for dimers, and green for trimers.	178
Figure 5.3 a) Mass spectrum of IgG in 1% acetic acid after filtered through PD Miditrap G-25 with q2 DDC applied. b) Reconstruction of denatured IgG mass spectrum from m/z region 3500 to 4500 using PeakView software.	179
Figure 5.4 Zoomed in region (m/z 3500-4500) of the denatured IgG spectrum where no DDC has been applied (blue) and q2 DDC has been applied (orange). The y-axis shows the absolute intensity of the two spectra where the only difference is whether DDC voltage was applied or not. The scan segment lengths are the same and the same nESI tip was used for both spectra.	180
Figure 5.5 Reconstructed mass spectrum of IgG (orange) and deglycoslated IgG using PNGase F (blue). The molecular weight difference between the two base peaks is 2878 Da corresponding to approximately two G0F glycan groups.	181
Figure 5.6 Butterfly spectrum of IgG in native solution condition before (blue) and after (orange) ejection of sample from the auto injector.	182
Figure 5.7 Butterfly spectrum of IgG in denatured solution condition before (blue) and after (orange) ejection of sample from the auto injector.	183
Figure 5.8 Butterfly spectrum of the MW of IgG reconstructed from the denatured condition mass spectrum before (blue) and after (orange) ejection of sample from the auto injector.	184
Figure 5.9 Circular dichroism (CD) of BSA from 30 °C to 70 °C in 10 °C steps with the mass spectrum of BSA at b) 30 °C, c) 50 °C, and d) 70 °C shown.	185
Figure 5.10 a) Circular dichroism (CD) of IgG from 30 °C to 70 °C in 10 °C steps with the mass spectrum of IgG at b) 30 °C and c) 70 °C shown.	186

Figure 5.11 a) DMS spectrum of BSA native (blue) and denature (red). The overall mass spectrum of the DMS spectrum for b) native BSA and d) denatured BSA as well as the DMS spectrum of individual charge states for c) native and e) denatured are shown. 187

Figure 5.12 Proposed reaction schematic of the photochemical disulfide bond cleavage reaction starting with a) radical initiation on the acetone followed by b) formation of alkyl hydroxyl radical which initiates the c) cleavage of disulfide bonds. 188

Figure 5.13 a) General schematic of the reaction cell used for the offline UV photoreaction where the sample is collected at the end of the tubing straight into the nESI tip. b) A generic structure for IgG1 showing four intermolecular disulfide bonds (labeled in red) that are broken after the UV photoreaction resulting in the light (25 kDa) and heavy (50 kDa) chain. 189

Figure 5.14 Mass spectra of IgG in 50/50 water/isopropanol with 2% acetone and 0.5 % formic acid a) before and b) after UV photochemistry. The peaks corresponding to the light chain and heavy chain are respectively labeled in green and red..... 190

Figure 5.15 Reconstruction of post UV photochemistry reaction IgG mass spectrum revealing molecular weight of a) light chain and b) heavy chain. 191

Figure 5.16 a) Mass spectrum of IgG post reduction and alkylation using *dithiothreitol (DTT)* and iodoacetamide (IAA). Reconstruction of above mass spectrum and the resulting molecular weight of b) light chain and c) heavy chain. 192

LIST OF TABLES

Table 1 Types of analyzers used in mass spectrometry	54
--	----

LIST OF ABBREVIATIONS

AC	Alternating Current
CD	Circular Dichroism
CEM	Chain Ejection Model
CID	Collision Induced Dissociation
CRM	Charge Residue Model
CV	Compensation Voltage
DC	Direct Current
DDC	Dipolar Direct Current
DMS	Differential Mobility Spectrometry
DTIMS	Drift Tube Ion Mobility Spectrometry
ECD	Electron Capture Dissociation
ESI	Electrospray Ionization
ETD	Electron Transfer Dissociation
FAIMS	High Field Asymmetric Waveform Ion Mobility Spectrometry
GC	Gas Chromatography
HPLC	High Performance Liquid Chromatography
IEM	Ion Evaporation Model
IMS	Ion Mobility Spectrometry
IRMPD	Infrared Multiphoton Photodissociation
IVR	Intramolecular Vibrational Energy Redistribution
LC	Liquid Chromatography
LQIT	Linear Quadrupole Ion Trap

MALDI	Matrix Assisted Laser Desorption Ionization
MS	Mass Spectrometry
MS/MS	Tandem Mass Spectrometry
MS _n N-Stage	Tandem Mass Spectrometry
MSAE	Mass-Selective Axial ejection
nESI	Nanoelectrospray Ionization
PFO	2,2,3,3,4,4,5,5,6,6,7,7,8,8,8-Pentadecafluoro-1-Octanol
Q	Quadrupole with RF/DC
q	RF only Quadrupole
RF	Radio Frequency
SEC	Size Exclusion Chromatography
SV	Separation Voltage
TEM	Transmission Electron Microscopy
TIMS	Trapped Ion Mobility Spectrometry
TOF	Time-of-Flight
TWIMS	Travelling Wave Ion Mobility Spectrometry
UV	Ultraviolet
UVPD	Ultraviolet Photodissociation

ABSTRACT

Mass spectrometry is a versatile, powerful analytical tool for chemical and biomolecule identification, quantitation, and structural analysis. Tandem mass spectrometry is key component in expanding the capabilities of mass spectrometry beyond just a molecular weight detector. Another key component is the discovery of electrospray ionization allowing not only liquid samples to be ionized but also generation of multiply charged ions enabling mass spectrometry analysis of large biomolecules. The fragmentation pathway of ion during tandem mass spectrometry is highly dependent on the nature of the ion as well as the form of dissociation technique employed. To-date, no single form of ion or dissociation method can provide all the structure information needed; therefore, it is common to use multiple forms of ions, different charge carrier or modifications, with a variety of other dissociation techniques to generate complimentary information. Practically, it is not always easy to generate the desired form of ion via ionization methods and is one of the limitations. Gas-phase ion/ion reactions provide an easy approach in manipulation of ions, either through changing the ion type or covalent modifications, in the gas-phase with the goal of enhancing the capabilities of mass spectrometers for either molecular weight or structural analysis. In this dissertation, studies of new gas-phase ion/ion chemistry for biomolecules such as carbohydrates and phospho/sulfopeptides were performed, and exploration into mass spectrometry analysis of IgGs is discussed.

Ion/ion reactions with carbohydrates were investigated with the goal of finding a charge-transfer or covalent modification reaction which can increase the structural information of carbohydrates upon tandem mass spectrometry. No luck was achieved with charge transfer ion/ion reactions which increased the overall fragmentation information in tandem mass spectrometry. Novel gas-phase covalent chemistry was discovered where alkoxides were found

to form ester and ethers. It was also discovered the aldehyde functional group at the reducing end of carbohydrates are susceptible to Schiff-base modifications. Schiff-base has been previously reported in peptides and this is the first time it has been discovered for carbohydrates.

In the next project a gas-phase approach for the rapid screening of polypeptide anions for phosphorylation or sulfonation based on binding strengths to guanidinium-containing reagent ions was developed. The approach relies on the generation of a complex via reaction of mixtures of deprotonated polypeptide anions with dicationic guanidinium-containing reagent ions and subsequent dipolar DC collisional activation of the complexes. The relative strengths of the electrostatic interactions of guanidinium with deprotonated acidic sites follows the order carboxylate < phosph(on)ate < sulf(on)ate. The differences between the binding strengths at these sites allows for the use of an appropriately selected dipolar DC amplitude to lead to significantly different dissociation rates for complexes derived from unmodified peptides versus phosphorylated and sulfated peptides. The difference in binding strengths between guanidinium and phosph(on)ate versus guanidinium and sulf(on)ate is sufficiently great to allow for the dissociation of a large fraction of phosphopeptide complexes with the dissociation of a much smaller fraction of sulfopeptide complexes. DFT calculations and experimental data with model peptides and with a mixture of tryptic peptides spiked with phosphopeptides are presented to illustrate and support this approach. Dissociation rate data are presented that demonstrate the differences in binding strengths for different anion charge-bearing sites and that reveal the DDC conditions most likely to provide the greatest discrimination between unmodified peptides, phosphopeptides, and sulfopeptides.

Hyaluronic acid, a linear carbohydrate polymer with repeating units of D-glucuronic acid and *N*-acetyl D-glucosamine, was found to exhibit unique properties in its electrospray ionization

mass spectrum that was never seen before. Electrospray of hyaluronic acid in aqueous solution in the negative polarity presented an incredibly intriguing mass spectrum, which we termed “emerald city” consisting of max charge or max charge-1 anions of hyaluronic acid. This is the first biomolecule observed to have the capability to deprotonate at every acid site that is possible. These set of highly charge anions exhibits unique characteristics upon use as a charge inversion reagent to charged invert multiply protonated proteins. A max of thirty-three protons was transferred when myoglobin 24+ was charge-inverted to a max charge state of 9- in the negative mode. Further research should be conducted to fully understand this phenomenal and its possible utilities.

Lastly, mass spectrometry analysis of monoclonal antibodies was performed. Monoclonal antibodies are 150 kDa sized protein complexes and is a major area of interest for pharmaceutical industry. Mass spectrometry analysis of big proteins is an emerging area for mass spectrometry and is quite different compared to small and medium molecule analysis on the mass spectrometer. Detailed in the last chapter are methods developed for sample cleanup of immunoglobulin G as well as the application of q2 DDC for removal of loosely bound adducts to achieve sharper peaks in the mass spectrum. Studies of protein denaturation was also conducted with methods such as circular dichroism and differential ion mobility also employed. And finally, a photochemical reaction setup was shown to cleave twelve out of sixteen total disulfide bonds in the immunoglobulin G within seconds compared to traditional solution phase reactions which can take hours.

CHAPTER 1. INTRODUCTION

1.1 Mass Spectrometry

Since the inception of the first mass spectrum by J.J. Thomson in 1912, [1] mass spectrometry has undergone countless improvement and development. Research in the past century has drastically improved the capabilities of what a mass spectrometer can do. Looking back in history, mass spectrometry was initially used by physicists for analysis of small particles and small molecule. Development of new ionization sources in the late 1980s has broadened the sample compatibility of mass spectrometers. As of this moment, mass spectrometry has been applied to biomolecules such as peptides/proteins, [2] lipids, [3] oligosaccharides, [4] and even virus. [5-7] Nowadays, mass spectrometry is a key and irreplaceable analytical tool widely used in areas like clinical, [8] pharmaceutical, [9] forensic, [10] academic, [11] and geochronological fields. [12] Compared to other analytical chemistry techniques, mass spectrometry is renowned for its high sensitivity, high selectivity, and fast analysis speed.

1.1.1 Principles

At its most basic core, mass spectrometry is the measurement of ionized molecules, or ions, in the gas-phase. It can be considered as a “molecular balance” which the mass-to-charge ratio (m/z) of ions are “weighted” and the molecular mass can be calculated from the charge. A mass spectrometer consists of three parts: an ionization source, the mass analyzer, and the detection system. The first step to mass spectrometric analysis is the production of gas-phase ions of the compound. The ionization source of a mass spectrometer determines what analytes can be ionized from the sample (e.g. small molecules, peptides/proteins, or macromolecular complexes, etc.) as well as their ion type (molecular ions, protonated/deprotonated, multiply

charges, etc.). In terms of a mass spectrometry experiment, choosing the right ionization source is critical to the success of the experiment. Each type of ionization source has a preference for specific types of molecules and selecting the wrong source can lead to decrease sensitivity. The mass analyzer determines how the m/z of the ions is measurement. The majority of mass analyzers used right now rely on either measure or manipulation of ion frequency or measurement of the ion travel time to measure their m/z . The mass analyzer also determines the accuracy, precision, range, and resolution of the measured ions and the resulting spectrum. Mass analyzer can be used independently or combined, which is referred to as a hybrid mass spectrometer. The detection and subsequent data collection system for mass spectrometers is also important to the instrument's figures of merit, such as sensitivity, resolution, and detection speed but will not be discussed in detail within this dissertation.

1.1.2 Ionization

Ionization is always the first step in mass spectrometry analysis. A variety of ionization techniques are used for mass spectrometry. A key consideration for the ionization process is the internal energy transfer process and the physico-chemical properties of the analyte that can be ionized. Based on the energy transfer level, ionization can be categorized as either “hard” or “soft.”

Electron ionization (EI), devised by Dempster and improved by Bleakney and Nier, is considered to be a hard ionization method. Commonly, electrons emitted from a heated filament are accelerated to 70 eV energy (1.4 Å wavelength) before interacting with neutral gas-phase molecules. After energy transfer and subsequent electronic excitations, an electron is expelled from the molecule resulting in a molecular ion ($M^{+\bullet}$). However, the molecular ion is not usually observed from EI as extensive fragmentations occur due to the energetic process of the ionization.

Molecular weight information is lost with EI but the large amount of fragment ions as well as its reproducibility make EI fragmentation database a good source for quick chemical identification.

Hard ionization methods are not conducive for the preservation of molecular weight information and limit one of the key usages of mass spectrometry which is molecular weight determination. Chemical ionization (CI) is a “soft” ionization method and produces ions with little excess energy during the ionization step; thus preserving the molecular species. Chemical ionization produces ion through a series of collisions between the neutral molecular ion to be analyze and primary ions present in the source. Analyte ions produces through these ion/molecular collisions result in an addition or abstraction of a proton ($[M+H]^+$ or $[M-H]^-$), depending on the process. Chemical ionization is a complementary technique to electron ionization and both were widely used for small molecule analysis. A variety of other ionization methods exists but only ionization methods related to this dissertation will be introduced in more detail.

1.1.2.1 Electrospray ionization

In 1989, Fenn et al. published results showing electrospray ionization (ESI) to ionize proteins molecules and able to generate multiply charge ions as well. [13, 14] The ability to ionize samples directly from liquid solution as well as the resulting multiply charged ions present in the mass spectrum was unprecedented and opened the door for biomolecule analysis research. ESI was welcomed by the entire mass spectrometry community and has since been one of the most used ionization methods for biomolecular research. In recognition of his contribution to large biomolecule analysis using mass spectrometry, John Fenn was awarded the 2002 Nobel Prize in chemistry along with Koichi Tanaka and Kurt Wüthrich.

Electrospray ionization was a revolution at the time it was introduced. Ionization methods prior to the introduction of ESI, such as EI, CI, or matrix assisted laser desorption ionization (MALDI), only produced singly charged ion species. The ability to ionize molecules with multiple charges, both cations and anions, paved the way for analysis of high molecular weight biomolecules which was a challenge back then due to the limited mass range of mass spectrometers. Many people recognized this aspect and ESI has since been used to analyze small molecules and peptides, [15] medium-sized polymers, [16] proteins, [13] large protein complexes, [17] and even viruses. [18] Electrospray ionization was the also first method providing the ability to ionize samples directly from solution and has since been used as the ionization interface for coupling between the MS and separation techniques such as liquid chromatography [15] and capillary electrophoresis. [19] LC/MS is one of the most used analytical techniques present and is widely used in a variety of fields such as drug development [20] and clinical disease screening.[21]

1.1.2.1.1 ESI Source

Electrospray ionization is generally operated by applying a high voltage, kilovolts, between the capillary and the inlet or curtain plate of the mass spectrometer. This voltage can be applied in a couple of ways: a voltage applied directly to the solution, voltage applied to the steel capillary, or a voltage applied to the inlet/curtain plate of the mass spectrometer. It doesn't matter how the voltage is applied as long there is a voltage gradient between the electrospray capillary and the mass spectrometer interface. The voltage applied will vary depending on the solvent composition of the solution. This onset voltage (V_{on}) for electrospray can be described by the following equation:

$$V_{on} \approx \sqrt{\frac{r_c \gamma \cos 49^\circ}{2\epsilon_0}} \cdot \ln \frac{4d}{r_c} \approx 1.9 \times 10^5 \cdot \sqrt{r_c \gamma} \cdot \ln \frac{4d}{r_c}$$

where ϵ_0 is the vacuum permittivity ($8.85 \times 10^{-12} \text{ F}\cdot\text{m}^{-1}$), r_c is the radius of the electrospray tip or capillary, d is the distance between the tip to the MS inlet, and γ is the solvent surface tension. For a set tip size and distance to the MS inlet, the solvent surface tension is directly related to the voltage needed for ESI. Solvents with high surface tension, water, will require a higher voltage compared to solvents with low surface tension, acetonitrile or methanol. Generally, a pure water solvent will require twice the voltage needed compared to a pure methanol solvent. A combination of solvents, such as 50/50 water/methanol are commonly used to decrease the voltage required for ESI sources. Electrospray ionization operates on flow rate of 1-20 $\mu\text{L}/\text{min}$, which is applied with a backing pressure such as a syringe pump, and a 100 μm tip diameter. [22] Voltages applied typically range between 2-6 kV. Methods such as a nebulizer gas [23] or heat [24, 25] have been used to aid the nebulization and desolvation of droplets from ESI. Several sprayer modifications such as pneumatically assisted electrospray, [26-28] ultrasonic nebulizer electrospray, [29, 30] electrosonic spray, [31] and nano-electrospray [32, 33] have been developed to expand the range of ESI applications. Nano-electrospray is now widely used and will be discussed.

Use of smaller tips for electrospray has been term nano-electrospray ionization (nESI). Compared to regular ESI, nESI have a very fine tip (1-5 μm), lower flow rate (20-50 nL/min), and much lower spray voltage are needed (1-2 kV). Nano-electrospray ionization produces much smaller initial droplets compared to ESI and does not require the use of a backing pressure or interface solutions for effective and continuous spray. The smaller droplets produced by nESI increases the sensitivity for non-surface-active compounds such as oligosaccharides and

glycoproteins. [34] Nano-ESI also has an increased tolerance to high aqueous solvents and salt contamination. [32, 34]

1.1.2.1.2 ESI Mechanism

The widely accepted general description of how ESI operates is described below and scheme is shown in Figure 1.1a. [35-38] The generation of an ion via ESI from the solution phase to the gas-phase can be best described by three major processes that occur. They are 1) production of charge droplets from the capillary; 2) droplet solvent evaporation leading to droplet size decrease; and 3) formation of ions from the final charged droplet. The starting point for ESI occurs when a high electric field is formed in the solution after a voltage is applied. The electric field facilitates a solvent polarization and charges of the same source as the voltage applied are pulled towards the liquid-air interface at the tip of the ESI source. At a certain voltage, the charges overcome the surface tension of the solution and form a pointed cone, termed Taylor cone after Sir Geoffrey Taylor. [39] At sufficient electric field strength, the coulombic repulsion of the charged ions in the Taylor cone region overcomes the surface tension derived forces and charged droplets are shot out of the tip of the Taylor cone. This is the initial stage of electrospray where charged droplets are formed from the tip.

The charge droplets evaporate, losing neutral particles, on its way to the mass spectrometer which can be accelerated through the use of curtain gas or heat. As the size of the droplet decrease, the charge density on the droplet surface increases. The droplet's size will eventually decrease to the point where the surface charge reaches the Rayleigh limit, where the number of charge, z_R , at that point can be described by the following equation:

$$z_R = \frac{8\pi}{e} \sqrt{\epsilon_0 \gamma R^3}$$

where e is the elementary charge, ϵ_0 is the vacuum permittivity, γ is the surface tension, and R is the droplet radius. At this point, “Coulomb explosion” or “Coulomb fission” occurs and the large droplet spits off smaller offspring/progeny droplets which holds 2% in mass and 15% in charge compared to the parent droplet. This process occurs repeatedly to generate smaller and smaller droplets which are eventually the source of ions detected by mass spectrometry.

Multiple theories for how ions are released from the final droplets have been proposed and supported by different experimental observations. The three widely accepted mechanism for how ions are created from droplets are: ion evaporation model (IEM), [40] charge residue model (CRM), [41, 42] and chain ejection model (CEM) [43, 44] While each of these models account for different scenarios of how ions are formed, the exact mechanistic model can be at times hard to tell and thus it is very important to consider all three models collectively. [45]

1.1.2.1.3 Ion Evaporation Model (IEM)

The Ion Evaporation Model (IEM), Figure 1.1b proposed by Iribarne and Thomson in 1976 [40] has been used to explain how small molecules are ionized with ESI. It operates on the principle that once the droplet reaches a diameter of 10 nm or less, the droplet surface electric field is strong enough to cause direct emission of ions prior to Rayleigh fission. This emission process is dependent upon the size and molecular weight of the ions and has been experimentally well supported for small inorganic and organic ions. [46-49] Ionization of large biomolecules such as peptides or proteins are not explained by IEM and must be achieved otherwise.

1.1.2.1.4 Charge Residue Model (CRM)

The Charge Residue Model, Figure 1.1c, was initially hypothesized by Dole et al. in 1968 [50] with a more detailed consideration as well as support for this model given by Schmelzeisen-Redeker et al in 1989. [51] The model proposes that analyte molecules stay in the droplet as

solvent evaporation and Rayleigh fission occurs. In the final droplets prior to naked ions forming, each individual droplet has one or a couple of analyte molecules per small droplet depending on the initial analyte concentration. As the solvent eventually evaporates from the final droplet, all the charge and salt condense upon the analyte and forms the ion. It is widely accepted that large molecules proceed through the CRM mechanism, such as proteins with molecular weight greater than 10 kDa. [33]

Based on CRM, the charge states of CRM-formed analytes are directly linked to the Rayleigh limit of the droplets as they undergoes the fission process. The de la Mora group [47] has confirmed this relationship by data analysis of experimental data and theoretical charge states calculated from the Rayleigh limit. Large protein ions formed through CRM will typically have salt adduction on them due to the condensation process as the droplet desolvates and this has been experimentally observed. [52] Reduction of salt adduction can be achieved via the addition of volatile salts such as ammonium acetate into the sample and is commonly used for ESI of large proteins. [53, 54]

1.1.2.1.5 Chain Ejection Model (CEM)

The chain ejection model (CEM), Figure 1.1d, was introduced by Konermann et al. in 2013 to describe the ionization process for unfolded proteins based on molecular dynamics simulations and experimental data. [45] While CRM can effectively describe the process of how native protein ions form, it was deemed insufficient for its ability to describe highly charged and unfolded protein ions. CEM proposes that unfolded protein molecules protrude directly from the charged droplet through a process similar to ion evaporation. Coulombic repulsion between the droplet's surface charges and the initially protruding highly charge unfolded protein chain will further escalate the extruding process and eject the entire protein chain out of the droplet.

Experimentally, CEM is supported by the difference in the mass spectra between native condition proteins, which ionizes via CRM, and denatured protein, which ionizes via CEM. [43, 44] The presence of highly charged denatured protein ion peaks having far less adduction than native protein ions confirms the two type of ions are formed via different methods and CRM can explain this difference whereas CEM cannot.

1.1.3 Mass Analyzers

Once gas-phase ions have been produced, they need to be separated according to their masses. The physical property of ions that is being measured by the mass analyzer is their mass-to-charge ratio (m/z) rather than their mass alone. Similarly with ionization sources, a great variety of mass analyzers also exist. All mass analyzers use some form of static or dynamic electric or magnetic fields to guide and separate ions. The differences in mass analyzer lie in the manner in which how such fields are used.

A variety of mass analyzers have been developed and commercialized, a table of mass analyzers commonly used in mass spectrometry is shown in Table 1.1. Each mass analyzer has its advantages and limitations which the user should be aware of. The most recent commercialized mass analyzer was the orbitrap in 2005, brought to the market by Thermo Fisher Scientific. Existing mass analyzers are continuously being improved upon and new mass analyzers are always in development. Mass spectrometers that have been modified for gas-phase ion/ion reactions such as the AB Sciex QTRAP 4000 (a hybrid triple quadrupole ion trap), Figure 1.2a, and AB Sciex TripleTOF 5600 (a hybrid quadrupole time-of-flight), Figure 1.2b, were used in this thesis and these types of mass analyzers will be discussed in brief detail.

1.1.3.1 Quadrupole and Linear Quadrupole Ion Trap (LQIT)

Quadrupole and quadrupole ion traps are robust mass analyzers that have been used for analysis of small to medium sized molecules. They have a resolving power of a couple thousand with a mass range of up to two to three thousand m/z on commercial instruments. Quadrupoles are easy to manufacture, flexible in its usage; thus, they are widely used in commercial instruments as either the core mass analyzer or as part of a hybrid mass analyzer.

Quadrupole mass analyzers, as the name suggests, are made up of four rods of circular or, ideally, hyperbolic sections. The four rods are perfectly parallel to each other. They operate on the principle using the stability of trajectories in oscillating electric fields to separate ions according to their m/z ratios. The initial principle of quadrupole was described by Paul and Steinweger [55] in 1953. A quadrupolar field is created by two out-of-phase RF waveforms applied to two pairs of opposing rods. Ions traveling through the quadrupole are subjected to the influence of the quadrupolar alternative electric field. The ion motion equations for a quadrupole can be described by the following equations that are used to plot a Mathieu stability diagram:

$$a_u = a_x = -a_y = \frac{8zeU}{m\Omega^2r_0^2}$$

$$q_u = q_x = -q_y = \frac{4zeU}{m\Omega^2r_0^2}$$

where z is the number of charges, e is the elementary charge, U is the potential for the applied DC voltage, V is the zero-to-peak RF voltage, m is the mass of the ion, Ω is the driving RF frequency, and r_0 is the effective radius between the electrodes. Ions are stable in the shaded region in the Mathieu stability diagram.

When a set of lens at the end of the quadrupole are applied with a DC potential that can effectively trap the ions in the z dimension of the quadrupole, this setup is considered a linear

quadrupole ion trap (LQIT). As the 3D quadrupole ion trap [56] is not used in the projects within this dissertation, only the linear ion trap will be introduced and discussed.

An ion trap is a device that uses an oscillating electric field to store ions. Ion trap operates by using an RF quadrupolar field that traps ions in two or three dimensions. Therefore, ion traps can be classified as either 3D or 2D ion traps. Historically, the first ion traps were 3D ion trap introduced by Paul and Steinwedel in 1960. [57] Compared to 3D ion traps, one great advantage linear ion traps have is more than 10-fold higher ion trapping capacity allowing the trap to contain more ions before space charge effects occur. Ions are also more efficiently trapped in a 2D ion trap compared to 3D ion traps.

Mass analysis with LQIT is performed by ejection of ions from the trap at varying m/z values. There are two common ways to eject ions out of an ion trap: boundary ejection and resonance ejection. [58] Boundary ejection is achieved by simply ramping the driving RF amplitude to make the ions reach an unstable q_u value on the Mathieu stability diagram. Resonance ejection uses a supplemental AC waveform applied on the rods that matches with the ion's secular frequency within the trap. The in resonance ion absorbs energy from the applied AC waveform, thereby increasing the ion's motion within the trap, and eventually resulting in ejection from the trap. Two selectively mass ejection of ions from LQITs have been developed using resonance ejection: mass selective axial ejection (MSAE) [59] and radial ejection. [60] MSAE was invented by Hager, from MDS Sciex, in 2002 and utilizes resonance ejection to push ions near the exit lens fringe fields which subsequently axially eject ions out. Radial ejection has been previously described [58] but commercial utilization of slits in the rods for radial ejection was first described by Senko and Schwartz from Thermo Finnigan in 2002. [60, 61]

1.1.3.2 Time of Flight (TOF)

The concept of time of flight (TOF) mass analyzers was described by Stephens in 1946. [62] Since then TOF has been developed into a high speed, high resolution, great mass accuracy, and an unlimited theoretical mass limit mass analyzer. The underlying principle for TOF mass analyzers is separation and measurement of ions over time. Ions are pulsed with a potential to give the ions a fixed total kinetic energy. The velocity differs between ions depending upon their m/z which in turn relates to the arrival time at the detector. The relationship between the m/z of ions and the arrival time is:

$$\frac{m}{z} = \left(\frac{2eV}{L^2} \right) t^2$$

where m is the mass of the ion, z is the number of charges, e is the elementary charge, V is the pulsing voltage, L is the length of the TOF ion path, and t is the arrival time. From the equation, the arrival time is directly tied to the m/z of the ion and with enough of a wait time and a sensitive detector any large ions can theoretically be detected. The resolution of TOF is directly linked to the path length and different geometries have been designed to increase the path length and resolution since the straight tube configuration. [63] Geometries such as V-shaped, [64] W-shaped, [65] and multi-turn shaped TOF mass analyzers have been developed. [66] Electrostatic reflectors called reflectrons are commonly used in any curved TOF geometry acting as an ion mirror to bounce ions back into the flight tube after reaching one end. Reflectrons can also correct the kinetic energy dispersion of ions leaving the source to increase the resolution of the mass spectrum at the expense of sensitivity and mass range limitation.

TOF is widely used in high mass ion detection, such as native mass spectrometry where large proteins are analyzed. [67] TOF is also commonly used in online LC/MS setups due to the rapid analysis time that TOFs have compared to other mass analyzers. TOFs generally have a

higher resolving power compared to quadrupoles or quadrupole ion traps, tens of thousands versus a couple thousand, and an instrument to use when higher resolution is needed. [68]

1.2 Tandem Mass Spectrometry

Tandem mass spectrometry (abbreviated MS/MS, or MSⁿ, where *n* is the number of sequential mass analysis steps) is any general method involving at least two or multiple stages of mass analysis for the purpose of structural elucidation. [69-71] Typically in the first stage of tandem MS the parent analyte ion is isolated before some form of activation method is employed to fragment the parent ion. The fragment ions can then be mass analyzed making it a MS/MS, or MS², experiment or further isolation and fragmentation can be employed making it a MSⁿ experiment, where *n* refers to the generation of ions analyzed. For example, isolation of an ion generated in an MS² experiment followed by subsequent fragmentation and mass analysis of the fragments would be considered a MS³ experiment.

Currently, there are two overarching ways to performed tandem MS: in space or in time. Tandem MS in space occurs when each stage of MSⁿ is performed in physically distinct regions. This is achieved through the coupling of multiple mass analyzers and funneling ions through each mass analyzer as a stage of tandem MS. A commonly used instrument that utilized the tandem in space method is a triple quadrupole mass analyzer. The triple quadrupole configuration, labeled as QqQ, employs the use of two quadrupole with RF/DC capabilities (labeled as Q) and a single RF only quadrupole (labeled as q) sandwiched in-between. Another configuration is the quadrupole time-of-flight (QqTOF) configuration swaps out the final quadrupole mass analyzer for a time-of-flight mass analyzer. Other instruments configurations, such as the combination of electric (E) and magnetic (D) sector mass analyzers, have also been used in the past but are not prominently used presently. In order to obtain high order MSⁿ spectra

using tandem MS in space multiple mass analyzers are needed to be combined. Practically the most amounts of mass analyzers linked up together are typically around three to four; thus, limiting the degree of MS^n that can be performed.

Tandem MS in time is performed in sequential time events within an ion trap storage device. Mass analyzers such as ion traps (3D or linear) or FT-ICR are commonly used for tandem MS in time experiments. Each sequential step of tandem MS is performed within the ion trap where ions are isolated, fragmented, and mass analyzed. All steps of the tandem MS are performed within a single mass analyzer allowing for far greater degree of MS^n experiments compared to tandem in space. The only limitation on how many n number of tandem stages which can be performed is limited on the number of ions present. Compared to beam type tandem MS experiments (in space), ion trap tandem MS experiments (in time) have a lower duty cycle and is not always compatible on chromatography time scales in an LC/MS setup.

For any tandem MS experiment, structural elucidation for the ion of interest is achieved through a fragmentation event. The ion that is being fragmented is called the precursor ion, and the fragments are called product ions. Three factors determine the fragmentation pattern or pathway of the precursor ion: the nature of the ion, the form of the ion, and the activation method applied. [72] Different types molecular species of ions fragment differently, a peptide will have different fragmentation patterns compared to a lipid or a carbohydrate, and this is the nature of the ion. Even with the same analyte, a difference in the type of ion (e.g. protonated, deprotonated, metallated, radical) will also influence the fragmentation pathway. Different types of activation methods employed (e.g. slow heating, fast heating, electron-based) also determines the resulting fragmentation pattern. To-date, there is no universal fragmentation method which can generate comprehensive structural information for any ions; therefore, comprehensive structural analysis

are typically performed using methods which provides complementary information. The most common method is utilizing different fragment methods [73] but alternative methods such as changing the type of ion, [74] the number of charges on the ion, [75] or chemical modification to change the nature of the ion [76] have also been used.

A plethora of activation methods has been developed for fragmenting ions and can generally be grouped into three major categories: collision-based (e.g. collision-induced dissociation (CID) [77] or surface-induced dissociation (SID) [78]), electron-based (e.g. electron capture dissociation (ECD) [79] or electron transfer dissociation (ETD) [80]), and photon-based (e.g. infrared multiple photodissociation (IRMPD) [81] or ultraviolet photodissociation (UVPD) [82]). The methods of activation as well as the activation time are important factors which determine the activation pathway as well as the resulting fragmentation patterns and should always be kept in-mind when comparing and contrasting. Not all of the above mentioned dissociation methods will be discussed within the confines of this thesis but methods pertinent to the research present in the following chapters will be discussed.

1.2.1 Collision-induced Dissociation (CID)

Collision-induced dissociation (CID) or also known as collision-activated dissociation (CAD) is the most widely used form of fragmentation method and is ubiquitous on all mass spectrometers. [35, 77] The process operates on the premise of converting an ion's translation energy into internal energy leading to chemical bond breakage. [83] This conversion process occurs via acceleration of target ions and collisions with neutral bath gas molecules, typically helium or nitrogen, leading to energy transfer and subsequent fragmentation. Several methods exist that activate ions through collisions but all of them can be separated into two categories: high- or low-energy collisions.

High-energy collisions occur on the order of keV energy and are only performed on electromagnetic or TOF mass spectrometers. In these instruments, ions are accelerated to keV energy through kV potentials before introduction into a collisional cell where single collisions are most likely to occur. Collisional activation performed via a potential acceleration is termed beam-type CID and can be performed for both high- and low-energy collisional activation methods. At keV of energy, the ion excitation and activation time scale occurs via vertical electronic transitions. [84] The energy is then redistributed in the form of vibrational energy where a bond cleavage may occur.

Low-energy collisional activation occurs on the order of a couple up to a hundred eV and is used in triple quadrupole, ion trap, ICR, or quadrupole-TOF hybrid type instruments. Low-energy CID can occur via beam type or resonance excitation in an ion trap. These types of activation methods are slower than high-energy beam type CID [85] and the excitation energy is mostly of vibrational nature. [86] The difference in how the excitation energy is deposited, vibrational or electronic, directly influences the fragmentation pathway. However, even activation methods that are both vibrational will differ based on the activation time scale. Low-energy beam type CID is a faster activation method compared to low energy resonance excitation CID and the resulting fragmentation pattern might differ. [85]

Ion trap CID is capable in both 3D as well as 2D linear ion trap mass spectrometers. Application of a supplemental AC signal that is in resonance with the fundamental secular frequency of the precursor ion accelerates the ion within the trap. This is termed as ‘resonance excitation.’ Increase of the AC voltage increases the amplitude of the ion’s harmonic oscillation in the trap and increases its maximum displacement from the trap’s center. Ions displaced from the center of the trap experiences higher order RF field heating, termed ‘RF-heating’. This effect

is a major contribution to the increase internal energy of the ion when collisions are probable. [85] Ion trap CID is a ‘slow-heating’ activation method where ions have time to redistribute energy and conformation during the 1-100 ms supplemental AC application time where hundreds of collisions can occur.

The secular frequency of ions within a quadrupole ion trap is defined by the following equation:

$$\omega_{u,n} = \left(n + \frac{1}{2}\beta_u \right) \Omega \quad 0 \leq n \leq \infty$$

where β is the stability related parameter, u is the axis of interest, Ω is the quadrupole RF drive frequency, and n is the frequency order. For the fundamental secular frequency n is equal to zero. The β_u is related to the Mathieu stability diagram parameters a_u and q_u and for when $q_r < 0.2$ and $q_z < 0.4$, the following approximation, known as the Dehmelt approximation, can be made:

$$\beta_u \approx \sqrt{a_u + \frac{q_u^2}{2}}$$

The precise value of β_u is defined by a continued fraction expression involving a_u and q_u which can be found in literature. [56]

What has so far been discussed is using resonance excitation ion trap CID for excitation of a single ion species using its fundamental secular frequency. It should be noted that in actual practice, depending on the voltage of the supplemental AC waveform applied, ions close to the frequency applied can also be excited and fragmented. Other ways to do a more broadband excitation is through the modulation of the driving quadrupole RF frequency or ramps in the excitation AC waveform frequency during the CID time step. [87, 88]

1.2.2 Dipolar Direct Current (DDC) Collision-induced Dissociation (CID)

Dipolar Direct Current (DDC) collision induced dissociation (CID) is a unique form of collisional activation method that is available in our lab but not widely available elsewhere. Tolmachev et al. have reported the use of dipolar DC pulses in a linear ion trap for activation purposes [89] and the McLuckey lab has since implemented this as well. [90-92] Unlike resonance excitation CID, DDC CID is a broadband excitation method applying heating to every ion in the trap. Application of a dipolar DC potential on opposing rods of a linear quadrupole ion trap will shift the entire ion population cloud off-center. All ions, precursor and product, will experience RF heating and collisional activation until the dipolar DC potential is switched off. DDC CID is still a slow heating process and follows the rules of resonance excitation CID [90, 91, 93] with the only difference being a broadband CID technique.

The approximate change in temperatures for an ion population exposed to DDC excitation is given by Tolmachev et al. as [89]:

$$\Delta T_K = \frac{m_g \Omega^2 r_0^2}{24k} \left(\frac{V_{DDC}}{V_{RF}} \right)^2$$

where m_g is the mass of the bath gas molecule, Ω is the RF drive frequency of the quadrupole ion trap, r_0 is the radius between the electrodes, k is the Boltzmann constant, V_{DDC} is the magnitude of DDC voltage applied, and V_{RF} is the zero-to-peak drive RF voltage. From the equation, it is clear that the change in temperature is not dependent upon the ion's m/z value and is entirely dependent upon the ratio of V_{DDC} to V_{RF} . The approximate average displacement r_e of ions from the center of the trap can also be expressed as:

$$r_e = \frac{r_0^3 \Omega^2 m V_{DDC}}{4e z V_{RF}^2}$$

While the approximate change in temperature of an ion is not dependent on its m/z value, the displacement of ions from the center of the trap is. This relationship introduces a high mass cutoff for DDC where ions of large m/z will be ejected from the trap. This limit can be approximated when r_e equals r_0 turning the above equation into:

$$\left(\frac{m}{z}\right)_{high} = \frac{4e}{r_0^2 \Omega^2} \frac{V_{RF}^2}{V_{DDC}}$$

Increase in the high mass cutoff for DDC requires higher driving RF amplitude compared to the DDC voltage applied but this also effects the overall average temperature change of ions which is the inverse of the relationship for the high mass cutoff.

Dipolar DC CID is an easy-to-use broadband collisional activation technique that provides uniform heating to an entire ion population. It is easier to use compared to resonance excitation CID where the frequency calculation is omitted and only tuning of the V_{RF} and V_{DDC} is required. Unlike other broadband collisional activation techniques such as beam-type CID, where the energy deposited is dependent upon the charge of the ion, DDC CID uniformly heats up the ions with no discrimination. It has been used for salt cluster removal as well as dissociation of loosely bound electron transfer products after electron transfer dissociation. [92, 94]

1.3 Gas-phase Ion/Ion Reactions

The advent of electrospray ionization brought about multiply charge ions in the gas-phase providing the opportunity for reactions of multiply charge ions of opposite polarity that was impossible with only singly charged ions. McLuckey et al. pioneered the research on oppositely charged ion/ion reactions in electrodynamic traps at Oak Ridge National Laboratory in the mid-1990s. [95, 96] Since then, Dr. Scott A. McLuckey has continued his research of ion/ion

resulting in a wide range of ion/ion reactions that have been discovered and researched: proton transfer, electron transfer, metal transfer, complex formations, and more recently covalent modifications. A key tenant of mass spectrometry as an analytical technique is its ability to provide molecular weight information, in the form of m/z and the ion's charge, as well as structural information, through the use of tandem MS. For tandem mass spectrometry, two main variables are crucial to how ions fragment: the nature of the ion as well as the dissociation method employed. To-date, no single ionization method or dissociation method provides an all-inclusive structure detail upon tandem MS and various combinations of ion types and activations method are to be employed. From a practical standpoint, this exploration is constrained by the ionization method as the most structurally informative fragments may not result from the ion type most readily formed by the at hand ionization method. Gas-phase ion/ion reactions provide an avenue for conversion of type as well as chemical modification to generate ion types that can provide more structurally information which cannot be easily generated from the ionization source.

1.3.1 Instrumentation

Gas-phase ion/ion reactions would not be possible without a) ability to generate ions of dual polarity and b) the existence of an environment allowing the physical and temporal overlap of oppositely charged ion in the mass spectrometer. Ion generation is typically achieved through the use of at least two ion sources, one for positive ions and one for negative ions, sequentially injected into the mass spectrometer and an ion trap is the ideal reaction vessel for ion/ion reactions due to the “tandem-in-time” nature of the device.

The 3D ion trap was the first ion trap system used for ion/ion reactions. [97] Since then, linear quadrupole ion trap has also been used for ion/ion reaction and have several distinct

advantages compared to 3D ion trap, namely greater trapping capacity, improved dynamic range, and enhanced efficiency in coupling to external ion sources, detectors, and other mass analyzers. [98] However, unlike 3D ion trap where the inherent operation mode of having the drive RF on the ring electrodes allows for trapping ions of both polarities [56] linear ion traps require minor modifications for storage of dual polarity ions. Conventional operation of linear ion traps applies a DC potential on containment lens to trap ions in the z-axis direction but is not amendable to bipolar storage of oppositely charged ions. Application of an AC waveform at sufficiently high frequency at the end-cap lenses enables the ability of trapping bipolar ions. [80, 99] In terms of how ion/ion reactions are performed, ions of one polar is first introduced into the ion trap and stored there before the opposite polarity ions are then ejected into the trap. The dual polarity ions are mutually stored in the trap for a certain amount of time, also known as the ‘reaction time’ for ion/ion reactions. After reaction, the ions can either be mass analyzed or transmitted to other mass analyzers for further analysis. This technique for ion/ion reactions is term “mutual storage mode.”

The second technique that can be used for ion/ion reaction is the “transmission mode” ion/ion reaction. [100-103] Unlike mutual storage mode where bipolar ions are trapped together, transmission mode ion/ion reactions are achieved by only trapping one polarity of ion in the ion trap and “washing” the opposing polarity of ions over them. These types of reactions have shown comparable efficiency to mutual storage reactions [102] with proton transfer as well as electron transfer ion/ion reaction performed this way. [100-102]

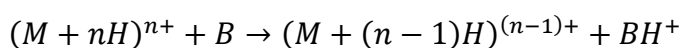
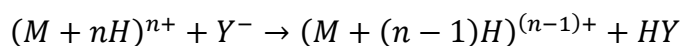
The instruments used in the following chapter for ion/ion reactions are modified QqQ and QqTOF systems from AB Sciex, as shown in Figure 1.2. Both set of instruments are modified for mutual storage ion/ion reaction mode in the higher pressure q2 collision cell. AC waveforms are

applied at the IQ2 and IQ3 lenses of q2 to trap bipolar ions. Ions are typically generated using dual nESI sources and sequentially injected into the mass spectrometer.

1.3.2 Thermodynamics and Kinetics

A brief overview of the thermodynamics and kinetics associated with ion/ion reactions will be performed here. More detailed discussions are available in literature. [104-108]

To better understand the thermodynamics of gas-phase ion/ion reactions it is important to also take a look at ion/molecule reactions. A generic proton transfer reaction for ion/ion and ion/molecule as well as generic energy diagrams, Figure 1.3, for the two reactions are shown:



where M is your analyte, Y⁻ is a deprotonated anion, and B is a strong neutral gaseous base. The entrance channel for the ion/ion reaction, Figure 1.3a, is dominated by long-range charge-dependent electrostatic interaction, while the exit channel is governed by shorter-range ion-dipole and ion-induced dipole forces. Compared to ion/molecule reaction, Figure 1.3b, the entrance channel is dominated by short-range polarization forces, similar to the exit channel for ion/ion reactions, while the exit channel is governed by long range electrostatic repulsion forces. Ion/ion reactions are an exothermic reaction, ~100 kcal/mol for any charge n, compared to ion/molecule reaction based on the qualitative shapes of the energy surfaces shown. Also, due to the nature of opposing charge, virtually any cation/anion combination in the gas-phase will collide and form some form of reaction which is not true for ion/molecule reactions.

A model that predicts the collisional rate, k_c , for ion/ion reactions as a function of the ions' charge, where a long-live collision complex is formed, is shown:

$$k_c = v\pi \left[\frac{Z_1 Z_2 e^2}{4\pi\epsilon_0\mu v^2} \right]^2$$

where v is the relative velocity of the bipolar ions, ϵ_0 is the vacuum permittivity, μ is the reduced mass of the two reactant, Z_1 and Z_2 are the charges on the ions, and e is the elementary charge. Based on this reaction rate equation, ion/ion reactions are charge-squared dependent. It should be noted that when ion/ion reactions of varying charges occur at the same time, due to the charge-squared dependence of the reaction rate, ions of higher charge will react much faster than lower charges. [107]

1.3.3 Gas-phase Covalent Modifications

Ion/ion reaction, such as proton transfer or metal transfer, can manipulate the charge of ion thereby changing its nature with the intent that different ion types can generate complimentary structural information. Another category of ion/ion reaction has since been developed allowing for gas-phase covalent modification of ions. Solution phase derivatization techniques are commonly used in mass spectrometry for manipulation of analytes such as peptides and proteins with the goal of facilitation of ionization, [109] quantification, [110, 111] and characterization. [112, 113] These type of ion/ion reactions typically proceed through a long-live stable collision complex where the reagent ion engages in a strong electrostatic interaction with the analyte ion. This strong interaction provides a long lifetime of the complex where reorganization and bonds can be broken and formed. A high energy barrier from this strong interaction is also present limiting the ease of proton transfer reactions and allowing for other reaction pathways to be preferred. To date, all reagent ions with the purpose of ion/ion covalent reactions are bi- [114-116] or trifunctional with strong, or “sticky,” sites, commonly sulfonate or fixed charge quaternary ammonium functions, present. Examples of gas-phase ion/ion covalent modification

reactions include: N-hydroxysuccinimide (NHS) esters and primary amine; [115] guanidine [117] and carboxylates; [118] Schiff base reactions; [114] and gas-phase oxidation of peptides with periodate or persulfate derivatives. [119, 120]

1.4 Conclusions

Mass spectrometry is a power analytical tool praised for its high sensitivity, high selectivity, analysis speed, and low sample requires. Development of tandem MS techniques increased the versatility of mass spectrometry for not only being able to determine molecular weight but also structure analysis. Ionization methods such as ESI ushered in biomolecules, such as peptides and proteins, for mass spectrometry analysis. ESI also paved the way for ion/ion reactions which have been used in various applications from spectra simplification or accurate molecular weight determination by proton transfer to biomolecule structural analysis by either charge transfer or covalent modification reactions.

1.5 References

- [1] J.J. Thomson, *Rays of Positive Electricity and Their Application to Chemical Analyses*, Longmans, Green and Company, 1913.
- [2] V.H. Wysocki, K.A. Resing, Q. Zhang, G. Cheng, Mass spectrometry of peptides and proteins, *Methods*, 35 (2005) 211-222.
- [3] Y.H. Rustam, G.E. Reid, Analytical Challenges and Recent Advances in Mass Spectrometry Based Lipidomics, *Anal Chem*, 90 (2018) 374-397.
- [4] M.J. Kailemia, L.R. Ruhaak, C.B. Lebrilla, I.J. Amster, Oligosaccharide analysis by mass spectrometry: a review of recent developments, *Anal Chem*, 86 (2014) 196-212.
- [5] K.M. Downard, B. Morrissey, A.B. Schwahn, Mass spectrometry analysis of the influenza virus, *Mass spectrometry reviews*, 28 (2009) 35-49.
- [6] G. Siuzdak, B. Bothner, M. Yeager, C. Brugidou, C.M. Fauquet, K. Hoey, C.-M. Change, Mass spectrometry and viral analysis, *Chemistry & Biology*, 3 (1996) 45-48.

- [7] S. Dominguez-Medina, S. Fostner, M. Defoort, M. Sansa, A.K. Stark, M.A. Halim, E. Vernhes, M. Gely, G. Jourdan, T. Alava, P. Boulanger, C. Masselon, S. Hentz, Neutral mass spectrometry of virus capsids above 100 megadaltons with nanomechanical resonators, *Science*, 362 (2018) 918-922.
- [8] P.J. Jannetto, R.L. Fitzgerald, Effective Use of Mass Spectrometry in the Clinical Laboratory, *Clin Chem*, 62 (2016) 92-98.
- [9] B.L. Ackermann, M.J. Berna, J.A. Eckstein, L.W. Ott, A.K. Chaudhary, Current applications of liquid chromatography/mass spectrometry in pharmaceutical discovery after a decade of innovation, *Annu Rev Anal Chem (Palo Alto Calif)*, 1 (2008) 357-396.
- [10] W.D. Hoffmann, G.P. Jackson, Forensic Mass Spectrometry, *Annu Rev Anal Chem (Palo Alto Calif)*, 8 (2015) 419-440.
- [11] M. Bantscheff, M. Schirle, G. Sweetman, J. Rick, B. Kuster, Quantitative mass spectrometry in proteomics: a critical review, *Analytical and bioanalytical chemistry*, 389 (2007) 1017-1031.
- [12] R.R. Parrish, Zircon U-Th-Pb Geochronology by Isotope Dilution -- Thermal Ionization Mass Spectrometry (ID-TIMS), *Reviews in Mineralogy and Geochemistry*, 53 (2003) 183-213.
- [13] J.B. Fenn, M. Mann, C.K. Meng, S.F. Wong, C.M. Whitehouse, Electrospray ionization for mass spectrometry of large biomolecules, *Science*, 246 (1989) 64-71.
- [14] J.B. Fenn, M. Mann, C.K. Meng, S.F. Wong, C.M. Whitehouse, Electrospray ionization-principles and practice, *Mass spectrometry reviews*, 9 (1990) 37-70.
- [15] C.M. Whitehouse, R.N. Dreyer, M. Yamashita, J.B. Fenn, Electrospray interface for liquid chromatographs and mass spectrometers, *Anal Chem*, 57 (1985) 675-679.
- [16] S.F. Wong, C.K. Meng, J.B. Fenn, Multiple charging in electrospray ionization of poly(ethylene glycols), *The Journal of Physical Chemistry*, 92 (1988) 546-550.
- [17] S.H. Lomeli, S. Yin, R.R. Ogorzalek Loo, J.A. Loo, Increasing charge while preserving noncovalent protein complexes for ESI-MS, *Journal of the American Society for Mass Spectrometry*, 20 (2009) 593-596.
- [18] B. Bothner, G. Siuzdak, Electrospray ionization of a whole virus: analyzing mass, structure, and viability, *Chembiochem*, 5 (2004) 258-260.
- [19] J.A. Olivares, N.T. Nguyen, C.R. Yonker, R.D. Smith, On-line mass spectrometric detection for capillary zone electrophoresis, *Analytical Chemistry*, 59 (2002) 1230-1232.

- [20] G. Loos, A. Van Schepdael, D. Cabooter, Quantitative mass spectrometry methods for pharmaceutical analysis, *Philos Trans A Math Phys Eng Sci*, 374 (2016).
- [21] C.S. Ho, C.W.K. Lam, M.H.M. Chan, R.C.K. Cheung, L.K. Law, L.C.W. Lit, K.F. Ng, M.W.M. Suen, H.L. Tai, Electrospray ionisation mass spectrometry: principles and clinical applications, *Clin Biochem Rev*, 24 (2003) 3-12.
- [22] G.J. Van Berkel, V. Kertesz, Using the electrochemistry of the electrospray ion source, *Anal Chem*, 79 (2007) 5510-5520.
- [23] A. Krueve, K. Herodes, I. Leito, Optimization of electrospray interface and quadrupole ion trap mass spectrometer parameters in pesticide liquid chromatography/electrospray ionization mass spectrometry analysis, *Rapid communications in mass spectrometry : RCM*, 24 (2010) 919-926.
- [24] B.L. Schwartz, K.J. Light-Wahl, R.D. Smith, Observation of noncovalent complexes to the avidin tetramer by electrospray ionization mass spectrometry, *Journal of the American Society for Mass Spectrometry*, 5 (1994) 201-204.
- [25] M.G. Ikonornou, P. Kebarle, A heated electrospray source for mass spectrometry of analytes from aqueous solutions, *Journal of the American Society for Mass Spectrometry*, 5 (1994) 791-799.
- [26] A.P. Bruins, T.R. Covey, J.D. Henion, Ion spray interface for combined liquid chromatography/atmospheric pressure ionization mass spectrometry, *Analytical Chemistry*, 59 (2002) 2642-2646.
- [27] M.G. Ikonomou, A.T. Blades, P. Kebarle, Electrospray-ion spray: a comparison of mechanisms and performance, *Analytical Chemistry*, 63 (2002) 1989-1998.
- [28] T.R. Covey, A.P. Bruins, J.D. Henion, Comparison of thermospray and ion spray mass spectrometry in an atmospheric pressure ion source, *Organic Mass Spectrometry*, 23 (1988) 178-186.
- [29] J.F. Banks, Jr., J.P. Quinn, C.M. Whitehouse, LC/ESI-MS determination of proteins using conventional liquid chromatography and ultrasonically assisted electrospray, *Anal Chem*, 66 (1994) 3688-3695.
- [30] J.F. Banks, Jr., S. Shen, C.M. Whitehouse, J.B. Fenn, Ultrasonically assisted electrospray ionization for LC/MS determination of nucleosides from a transfer RNA digest, *Anal Chem*, 66 (1994) 406-414.
- [31] Z. Takats, J.M. Wiseman, B. Gologan, R.G. Cooks, Electrosonic spray ionization. A gentle technique for generating folded proteins and protein complexes in the gas phase and for studying ion-molecule reactions at atmospheric pressure, *Anal Chem*, 76 (2004) 4050-4058.

- [32] M. Wilm, M. Mann, Analytical properties of the nanoelectrospray ion source, *Anal Chem*, 68 (1996) 1-8.
- [33] M. Wilm, Principles of electrospray ionization, *Mol Cell Proteomics*, 10 (2011) M111 009407.
- [34] M. Karas, U. Bahr, T. Dülcks, Nano-electrospray ionization mass spectrometry: addressing analytical problems beyond routine, *Fresenius' Journal of Analytical Chemistry*, 366 (2000) 669-676.
- [35] E. de Hoffmann, V. Stroobant, *Mass Spectrometry: Principles and Applications*, Wiley, 2013.
- [36] G. Siuzdak, An introduction to mass spectrometry ionization: An excerpt from *The Expanding Role of Mass Spectrometry in Biotechnology*, 2nd ed.; MCC Press: San Diego, 2005, *Journal of the Association for Laboratory Automation*, 9 (2004) 50-63.
- [37] A.T. Blades, M.G. Ikonomou, P. Kebarle, Mechanism of electrospray mass spectrometry. Electrospray as an electrolysis cell, *Analytical Chemistry*, 63 (2002) 2109-2114.
- [38] P. Kebarle, L. Tang, From ions in solution to ions in the gas phase - the mechanism of electrospray mass spectrometry, *Analytical Chemistry*, 65 (2008) 972A-986A.
- [39] G.I. Taylor, Disintegration of water drops in an electric field, *Proceedings of the Royal Society of London. Series A. Mathematical and Physical Sciences*, 280 (1964) 383-397.
- [40] J.V. Iribarne, On the evaporation of small ions from charged droplets, *The Journal of Chemical Physics*, 64 (1976).
- [41] M. Dole, R.L. Hines, L.L. Mack, R.C. Mobley, L.D. Ferguson, M.B. Alice, Gas Phase Macroions, *Macromolecules*, 1 (1968) 96-97.
- [42] A.T. Iavarone, E.R. Williams, Mechanism of charging and supercharging molecules in electrospray ionization, *Journal of the American Chemical Society*, 125 (2003) 2319-2327.
- [43] E. Ahadi, L. Konermann, Modeling the behavior of coarse-grained polymer chains in charged water droplets: implications for the mechanism of electrospray ionization, *J Phys Chem B*, 116 (2012) 104-112.
- [44] L. Konermann, A.D. Rodriguez, J. Liu, On the formation of highly charged gaseous ions from unfolded proteins by electrospray ionization, *Anal Chem*, 84 (2012) 6798-6804.
- [45] L. Konermann, E. Ahadi, A.D. Rodriguez, S. Vahidi, Unraveling the mechanism of electrospray ionization, *Anal Chem*, 85 (2013) 2-9.

- [46] R.B. Cole, Some tenets pertaining to electrospray ionization mass spectrometry, *Journal of Mass Spectrometry*, 35 (2000) 763-772.
- [47] J. Fernandez de la Mora, Electrospray ionization of large multiply charged species proceeds via Dole's charged residue mechanism, *Analytica Chimica Acta*, 406 (2000) 93-104.
- [48] P. Kebarle, A brief overview of the present status of the mechanisms involved in electrospray mass spectrometry, *Journal of Mass Spectrometry*, 35 (2000) 804-817.
- [49] Z. Olumee, J.H. Callahan, A. Vertes, Droplet Dynamics Changes in Electrostatic Sprays of Methanol-Water Mixtures, *The Journal of Physical Chemistry A*, 102 (1998) 9154-9160.
- [50] M. Dole, L.L. Mack, R.L. Hines, R.C. Mobley, L.D. Ferguson, M.B. Alice, Molecular Beams of Macroions, *The Journal of Chemical Physics*, 49 (1968) 2240-2249.
- [51] G. Schmelzeisen-Redeker, L. Bütfering, F.W. Röllgen, Desolvation of ions and molecules in thermospray mass spectrometry, *International Journal of Mass Spectrometry and Ion Processes*, 90 (1989) 139-150.
- [52] U.H. Verkerk, P. Kebarle, Ion-ion and ion-molecule reactions at the surface of proteins produced by nanospray. Information on the number of acidic residues and control of the number of ionized acidic and basic residues, *Journal of the American Society for Mass Spectrometry*, 16 (2005) 1325-1341.
- [53] T.-Y. Yen, M. Judith Charles, R.D. Voyksner, Processes that affect electrospray ionization-mass spectrometry of nucleobases and nucleosides, *Journal of the American Society for Mass Spectrometry*, 7 (1996) 1106-1108.
- [54] N. Felitsyn, M. Peschke, P. Kebarle, Origin and number of charges observed on multiply-protonated native proteins produced by ESI, *International journal of mass spectrometry*, 219 (2002) 39-62.
- [55] W. Paul, H. Steinwedel, Quadrupole mass filter, *Z. Naturforsch. A*, 8 (1953) 448.
- [56] R.E. March, An introduction to quadrupole ion trap mass spectrometry, *Journal of Mass Spectrometry*, 32 (1997) 351-369.
- [57] J.F.J. Todd, Ion trap mass spectrometer—past, present, and future (?), *Mass spectrometry reviews*, 10 (1991) 3-52.
- [58] D.J. Douglas, A.J. Frank, D. Mao, Linear ion traps in mass spectrometry, *Mass spectrometry reviews*, 24 (2005) 1-29.
- [59] F.A. Londry, J.W. Hager, Mass selective axial ion ejection from a linear quadrupole ion trap, *Journal of the American Society for Mass Spectrometry*, 14 (2003) 1130-1147.

- [60] J.C. Schwartz, M.W. Senko, J.E.P. Syka, A two-dimensional quadrupole ion trap mass spectrometer, *Journal of the American Society for Mass Spectrometry*, 13 (2002) 659-669.
- [61] M.W. Senko, J.C. Schwartz, Trapping Efficiency Measurements in a 2D Ion Trap Mass Spectrometer, in: *Proceedings of the 50th ASMS Conference*, 2002.
- [62] W. Stephens, A Pulsed Mass Spectrometer with Time Disaersion, *Phys. Rev.*, 69 (1946) 691.
- [63] M.M. Wolff, W.E. Stephens, A Pulsed Mass Spectrometer with Time Dispersion, *Review of Scientific Instruments*, 24 (1953) 616-617.
- [64] U. Boesl, Time-of-flight mass spectrometry: Introduction to the basics, *Mass spectrometry reviews*, 36 (2017) 86-109.
- [65] I.V. Chernushevich, S.I. Merenbloom, S. Liu, N. Bloomfield, A W-Geometry Ortho-TOF MS with High Resolution and Up to 100% Duty Cycle for MS/MS, *Journal of the American Society for Mass Spectrometry*, 28 (2017) 2143-2150.
- [66] M. Toyoda, Development of multi-turn time-of-flight mass spectrometers and their applications, *Eur J Mass Spectrom (Chichester)*, 16 (2010) 397-406.
- [67] A.C. Leney, A.J. Heck, Native Mass Spectrometry: What is in the Name?, *Journal of the American Society for Mass Spectrometry*, 28 (2017) 5-13.
- [68] S.A. McLuckey, J.M. Wells, Mass Analysis at the Advent of the 21st Century, *Chemical reviews*, 101 (2001) 571-606.
- [69] R.G. Cooks, *Metastable Ions*, Elsevier Scientific Publishing Company, 1973.
- [70] F.W. McLafferty, *Tandem mass spectrometry*, Wiley, 1983.
- [71] K.L. Busch, G.L. Glish, S.A. McLuckey, *Mass spectrometry/mass spectrometry: techniques and applications of Tandem mass spectrometry*, VCH, 1988.
- [72] M. Mentinova, D.M. Crizer, T. Baba, W.M. McGee, G.L. Glish, S.A. McLuckey, Cation recombination energy/coulomb repulsion effects in ETD/ECD as revealed by variation of charge per residue at fixed total charge, *Journal of the American Society for Mass Spectrometry*, 24 (2013) 1676-1689.
- [73] T.P. Cleland, C.J. DeHart, R.T. Fellers, A.J. VanNispen, J.B. Greer, R.D. LeDuc, W.R. Parker, P.M. Thomas, N.L. Kelleher, J.S. Brodbelt, High-Throughput Analysis of Intact Human Proteins Using UVPD and HCD on an Orbitrap Mass Spectrometer, *Journal of proteome research*, 16 (2017) 2072-2079.

- [74] D.J. Foreman, S.K. Betancourt, A.L. Pilo, S.A. McLuckey, Novel Peptide Ion Chemistry Associated with Gold (I) Cationization: Preferential Cleavage at Lysine Residues, *International journal of mass spectrometry*, 427 (2018) 114-122.
- [75] D.J. Foreman, E.T. Dziekonski, S.A. McLuckey, Maximizing Selective Cleavages at Aspartic Acid and Proline Residues for the Identification of Intact Proteins, *Journal of the American Society for Mass Spectrometry*, 30 (2019) 34-44.
- [76] A. Leitner, A review of the role of chemical modification methods in contemporary mass spectrometry-based proteomics research, *Anal Chim Acta*, 1000 (2018) 2-19.
- [77] J. Mitchell Wells, S.A. McLuckey, Collision-Induced Dissociation (CID) of Peptides and Proteins, in: *Biological Mass Spectrometry*, 2005, pp. 148-185.
- [78] A.L. McCormack, A. Somogyi, A.R. Dongre, V.H. Wysocki, Fragmentation of protonated peptides: surface-induced dissociation in conjunction with a quantum mechanical approach, *Anal Chem*, 65 (1993) 2859-2872.
- [79] R.A. Zubarev, N.L. Kelleher, F.W. McLafferty, Electron Capture Dissociation of Multiply Charged Protein Cations. A Nonergodic Process, *Journal of the American Chemical Society*, 120 (1998) 3265-3266.
- [80] J.E. Syka, J.J. Coon, M.J. Schroeder, J. Shabanowitz, D.F. Hunt, Peptide and protein sequence analysis by electron transfer dissociation mass spectrometry, *Proceedings of the National Academy of Sciences of the United States of America*, 101 (2004) 9528-9533.
- [81] M.C. Crowe, J.S. Brodbelt, Infrared multiphoton dissociation (IRMPD) and collisionally activated dissociation of peptides in a quadrupole ion trap with selective IRMPD of phosphopeptides, *Journal of the American Society for Mass Spectrometry*, 15 (2004) 1581-1592.
- [82] J.S. Brodbelt, Photodissociation mass spectrometry: new tools for characterization of biological molecules, *Chem Soc Rev*, 43 (2014) 2757-2783.
- [83] S.A. McLuckey, Principles of collisional activation in analytical mass spectrometry, *Journal of the American Society for Mass Spectrometry*, 3 (1992) 599-614.
- [84] H. Yamaoka, P. Đông, J. Durup, Energetics of the Collision-Induced Dissociations $C_2H_2^+ \rightarrow C_2H^+ + H$ and $C_2H_2^+ \rightarrow H^+ + C_2H$, *The Journal of Chemical Physics*, 51 (1969) 3465-3476.
- [85] S.A. McLuckey, D.E. Goeringer, SPECIAL FEATURE:TUTORIAL Slow Heating Methods in Tandem Mass Spectrometry, *Journal of Mass Spectrometry*, 32 (1997) 461-474.
- [86] R.N. Schwartz, Z.I. Slawsky, K.F. Herzfeld, Calculation of Vibrational Relaxation Times in Gases, *The Journal of Chemical Physics*, 20 (1952) 1591-1599.

- [87] S.A. McLuckey, D.E. Goeringer, G.L. Glish, Selective ion isolation/rejection over a broad mass range in the quadrupole ion trap, *Journal of the American Society for Mass Spectrometry*, 2 (1991) 11-21.
- [88] J.B. Plomley, R.E. March, R.S. Mercer, Tandem Mass Spectrometry of Polychlorodibenzo-p-Dioxin and Polychlorodibenzofuran in a Quadrupole Ion Trap. 1. Comparison of Single-Frequency, Secular Frequency Modulation, and Multifrequency Resonant Excitation Modes, *Analytical Chemistry*, 68 (1996) 2345-2352.
- [89] A.V. Tolmachev, A.N. Vilkov, B. Bogdanov, L. Pasa-Tolic, C.D. Masselon, R.D. Smith, Collisional activation of ions in RF ion traps and ion guides: the effective ion temperature treatment, *Journal of the American Society for Mass Spectrometry*, 15 (2004) 1616-1628.
- [90] B.M. Prentice, R.E. Santini, S.A. McLuckey, Adaptation of a 3-D quadrupole ion trap for dipolar DC collisional activation, *Journal of the American Society for Mass Spectrometry*, 22 (2011) 1486-1492.
- [91] I.K. Webb, F.A. Londry, S.A. McLuckey, Implementation of dipolar direct current (DDC) collision-induced dissociation in storage and transmission modes on a quadrupole/time-of-flight tandem mass spectrometer, *Rapid communications in mass spectrometry : RCM*, 25 (2011) 2500-2510.
- [92] I.K. Webb, Y. Gao, F.A. Londry, S.A. McLuckey, Trapping mode dipolar DC collisional activation in the RF-only ion guide of a linear ion trap/time-of-flight instrument for gaseous bio-ion declustering, *J Mass Spectrom*, 48 (2013) 1059-1065.
- [93] B.M. Prentice, S.A. McLuckey, Dipolar DC collisional activation in a "stretched" 3-D ion trap: the effect of higher order fields on rf-heating, *Journal of the American Society for Mass Spectrometry*, 23 (2012) 736-744.
- [94] S. Adhikari, E.T. Dziekonski, F.A. Londry, S.A. McLuckey, Dipolar DC induced collisional activation of non-dissociated electron-transfer products, *J Mass Spectrom*, 54 (2019) 459-465.
- [95] W.J. Herron, D.E. Goeringer, S.A. McLuckey, Ion-ion reactions in the gas phase: Proton transfer reactions of protonated pyridine with multiply charged oligonucleotide anions, *Journal of the American Society for Mass Spectrometry*, 6 (1995) 529-532.
- [96] W.J. Herron, D.E. Goeringer, S.A. McLuckey, Gas-phase electron transfer reactions from multiply-charged anions to rare gas cations, *Journal of the American Chemical Society*, 117 (1995) 11555-11562.
- [97] J.M. Wells, P.A. Chrisman, S.A. McLuckey, "Dueling" ESI: Instrumentation to study ion/ion reactions of electrospray-generated cations and anions, *Journal of the American Society for Mass Spectrometry*, 13 (2002) 614-622.

- [98] Y. Xia, S.A. McLuckey, Evolution of instrumentation for the study of gas-phase ion/ion chemistry via mass spectrometry, *Journal of the American Society for Mass Spectrometry*, 19 (2008) 173-189.
- [99] Y. Xia, J. Wu, S.A. McLuckey, F.A. Londry, J.W. Hager, Mutual storage mode ion/ion reactions in a hybrid linear ion trap, *Journal of the American Society for Mass Spectrometry*, 16 (2005) 71-81.
- [100] J. Wu, J.W. Hager, Y. Xia, F.A. Londry, S.A. McLuckey, Positive ion transmission mode ion/ion reactions in a hybrid linear ion trap, *Analytical chemistry*, 76 (2004) 5006-5015.
- [101] X. Liang, J.W. Hager, S.A. McLuckey, Transmission mode ion/ion electron-transfer dissociation in a linear ion trap, *Analytical chemistry*, 79 (2007) 3363-3370.
- [102] X. Liang, S.A. McLuckey, Transmission mode ion/ion proton transfer reactions in a linear ion trap, *Journal of the American Society for Mass Spectrometry*, 18 (2007) 882-890.
- [103] J.F. Emory, K.H. Hassell, F.A. Londry, S.A. McLuckey, Transmission mode ion/ion reactions in the radiofrequency-only ion guide of hybrid tandem mass spectrometers, *Rapid Communications in Mass Spectrometry: An International Journal Devoted to the Rapid Dissemination of Up-to-the-Minute Research in Mass Spectrometry*, 23 (2009) 409-418.
- [104] S.A. McLuckey, J.L. Stephenson, Ion/ion chemistry of high-mass multiply charged ions, *Mass spectrometry reviews*, 17 (1998) 369-407.
- [105] S.J. Pitteri, S.A. McLuckey, Recent developments in the ion/ion chemistry of high-mass multiply charged ions, *Mass spectrometry reviews*, 24 (2005) 931-958.
- [106] J.L. Stephenson, S.A. McLuckey, Ion/ion reactions in the gas phase: proton transfer reactions involving multiply-charged proteins, *Journal of the American Chemical Society*, 118 (1996) 7390-7397.
- [107] S.A. McLuckey, J.L. Stephenson, K.G. Asano, Ion/ion proton-transfer kinetics: implications for analysis of ions derived from electrospray of protein mixtures, *Analytical chemistry*, 70 (1998) 1198-1202.
- [108] B.M. Prentice, S.A. McLuckey, Gas-phase ion/ion reactions of peptides and proteins: acid/base, redox, and covalent chemistries, *Chem Commun (Camb)*, 49 (2013) 947-965.
- [109] W.-C. Yang, H. Mirzaei, X. Liu, F.E. Regnier, Enhancement of amino acid detection and quantification by electrospray ionization mass spectrometry, *Analytical Chemistry*, 78 (2006) 4702-4708.
- [110] S.P. Gygi, B. Rist, S.A. Gerber, F. Turecek, M.H. Gelb, R. Aebersold, Quantitative analysis of complex protein mixtures using isotope-coded affinity tags, *Nature biotechnology*, 17 (1999) 994.

- [111] P.L. Ross, Y.N. Huang, J.N. Marchese, B. Williamson, K. Parker, S. Hattan, N. Khainovski, S. Pillai, S. Dey, S. Daniels, Multiplexed protein quantitation in *Saccharomyces cerevisiae* using amine-reactive isobaric tagging reagents, *Molecular & cellular proteomics*, 3 (2004) 1154-1169.
- [112] R.L. Beardsley, L.A. Sharon, J.P. Reilly, Peptide de novo sequencing facilitated by a dual-labeling strategy, *Analytical chemistry*, 77 (2005) 6300-6309.
- [113] J.A. Madsen, J.S. Brodbelt, Simplifying fragmentation patterns of multiply charged peptides by N-terminal derivatization and electron transfer collision activated dissociation, *Analytical chemistry*, 81 (2009) 3645-3653.
- [114] H. Han, S.A. McLuckey, Selective covalent bond formation in polypeptide ions via gas-phase ion/ion reaction chemistry, *Journal of the American Chemical Society*, 131 (2009) 12884-12885.
- [115] M. Mentinova, S.A. McLuckey, Covalent modification of gaseous peptide ions with N-hydroxysuccinimide ester reagent ions, *Journal of the American Chemical Society*, 132 (2010) 18248-18257.
- [116] B.M. Prentice, J.D. Gilbert, J.R. Stutzman, W.P. Forrest, S.A. McLuckey, Gas-phase reactivity of carboxylic acid functional groups with carbodiimides, *Journal of the American Society for Mass Spectrometry*, 24 (2013) 30-37.
- [117] W.M. McGee, M. Mentinova, S.A. McLuckey, Gas-phase conjugation to arginine residues in polypeptide ions via N-hydroxysuccinimide ester-based reagent ions, *Journal of the American Chemical Society*, 134 (2012) 11412-11414.
- [118] Z. Peng, W.M. McGee, J. Bu, N.Z. Barefoot, S.A. McLuckey, Gas phase reactivity of carboxylates with N-hydroxysuccinimide esters, *Journal of the American Society for Mass Spectrometry*, 26 (2015) 174-180.
- [119] A.L. Pilo, J. Bu, S.A. McLuckey, Transformation of $[M + 2H](2+)$ Peptide Cations to $[M - H](+)$, $[M + H + O](+)$, and $M(+*)$ Cations via Ion/Ion Reactions: Reagent Anions Derived from Persulfate, *Journal of the American Society for Mass Spectrometry*, 26 (2015) 1103-1114.
- [120] A.L. Pilo, J. Bu, S.A. McLuckey, Gas-phase oxidation of neutral basic residues in polypeptide cations by periodate, *Journal of the American Society for Mass Spectrometry*, 27 (2016) 1979-1988.

Table 1 Types of analyzers used in mass spectrometry

Type of analyzer	Symbol	Principle of separation
Electric sector	E	Kinetic energy
Magnetic sector	B	Momentum
Quadrupole	Q	m/z (trajectory stability)
Ion trap	IT	m/z (resonance frequency)
Time-of-flight	TOF	Velocity (flight time)
Fourier transfer ion cyclotron resonance	FT-ICR	m/z (resonance frequency)
Fourier transfer orbitrap	FT-OT	m/z (resonance frequency)

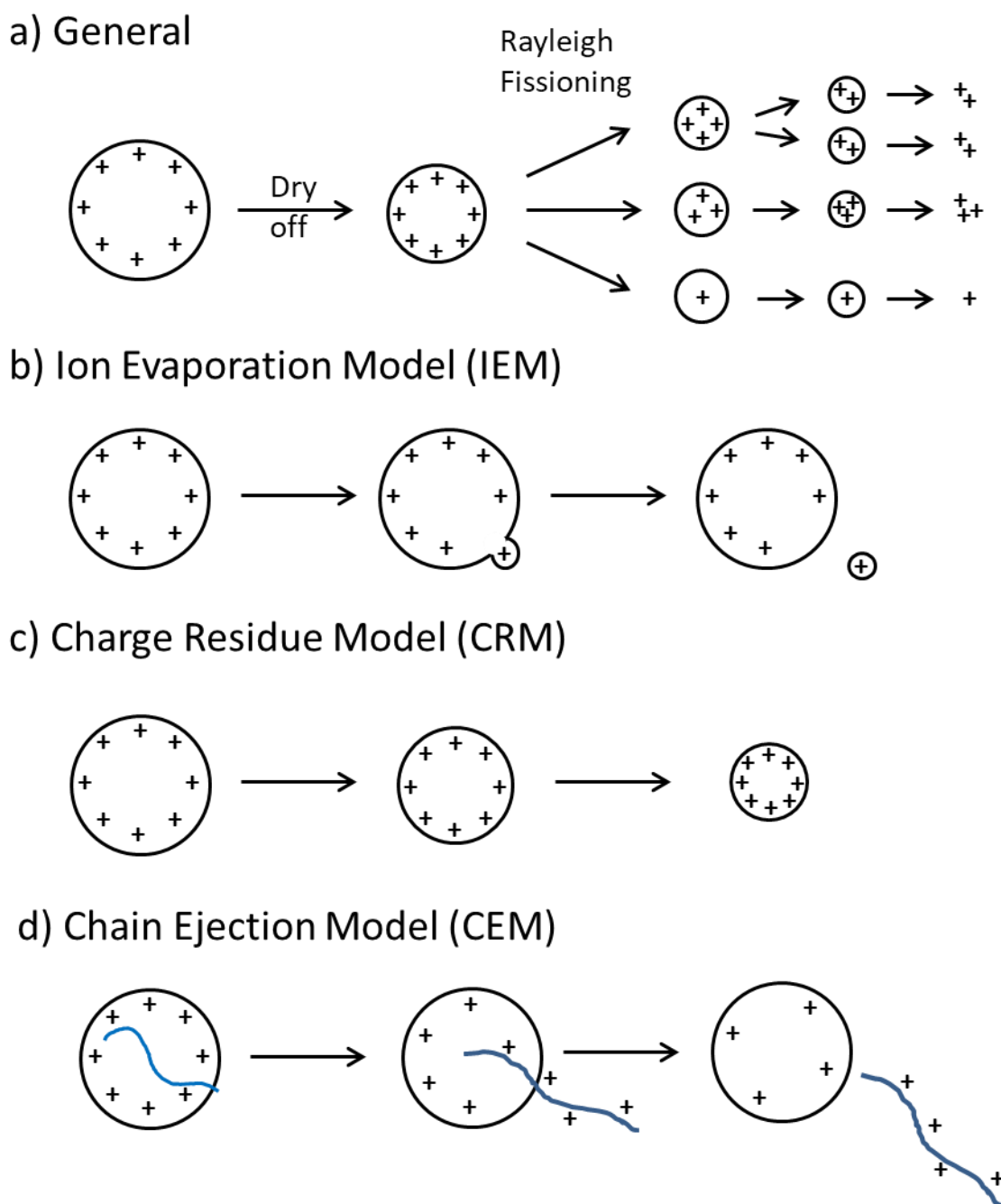


Figure 1.1 A schematic drawing showing a) general fissioning process of charged ESI droplet and the three accepted models of ionization: b) ion evaporation model (IEM), c) charge residue model (CRM), and d) chain ejection model (CEM).

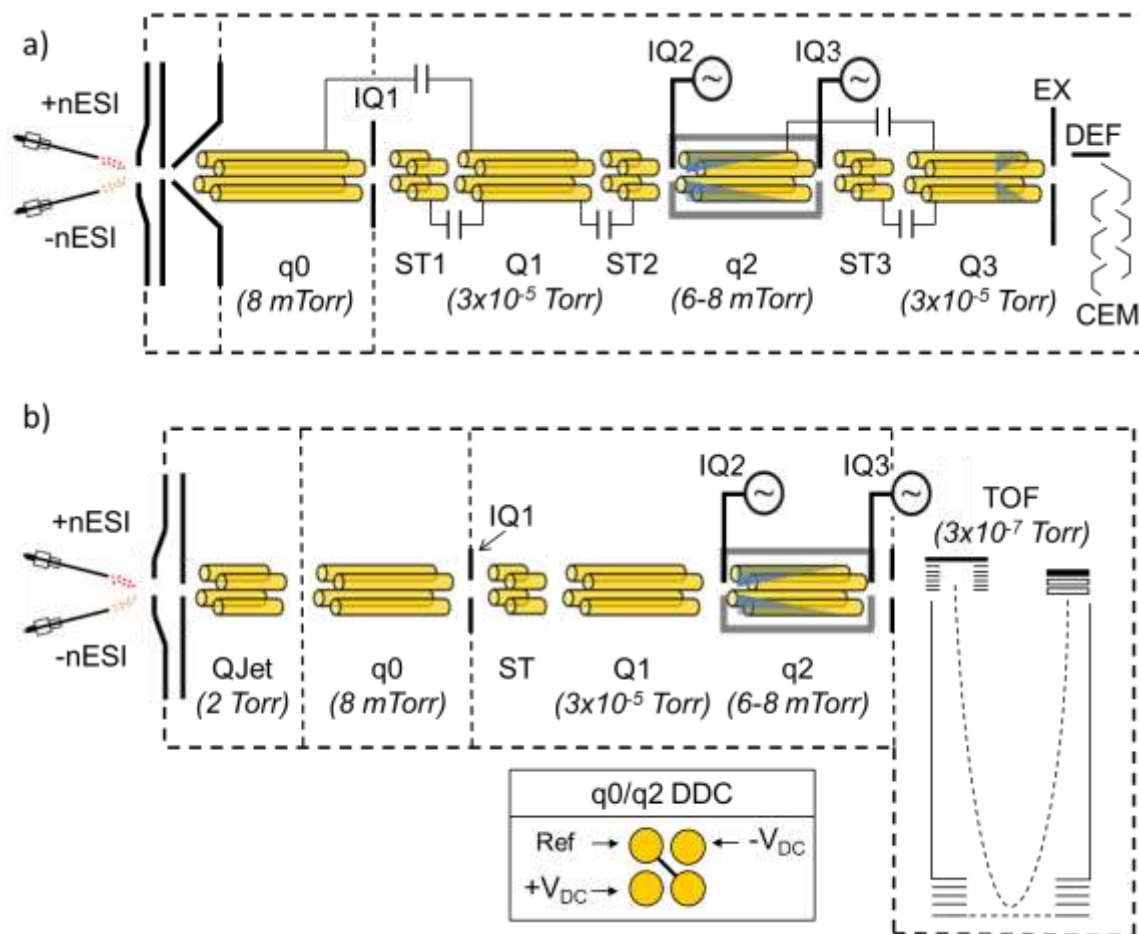
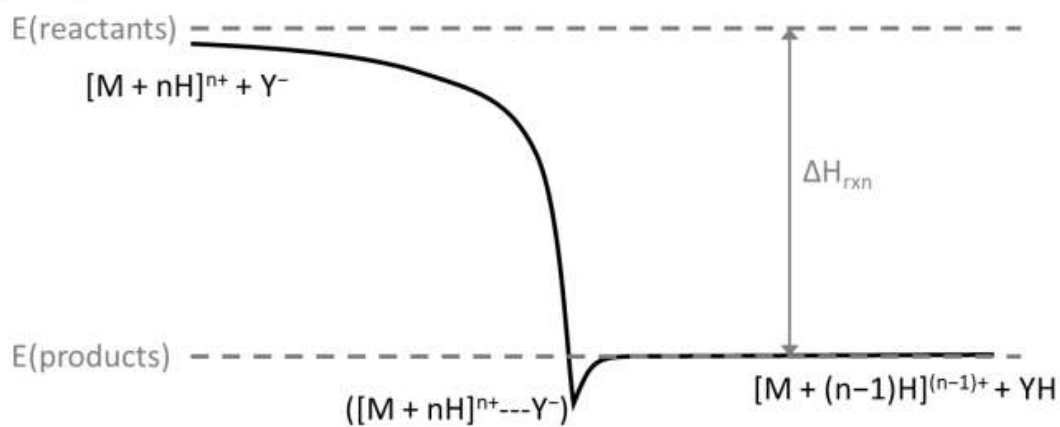


Figure 1.2 Mass spectrometers that has been modified for ion/ion reaction a) AB Sciex QTRAP 4000 (Sciex, Concord, Canada) and b) AB Sciex TripleTOF 5600 (Sciex, Concord, Canada). The 5600 has also been modified for q0 and q2 DDC.

a) ion/ion reaction



b) ion/molecule reaction

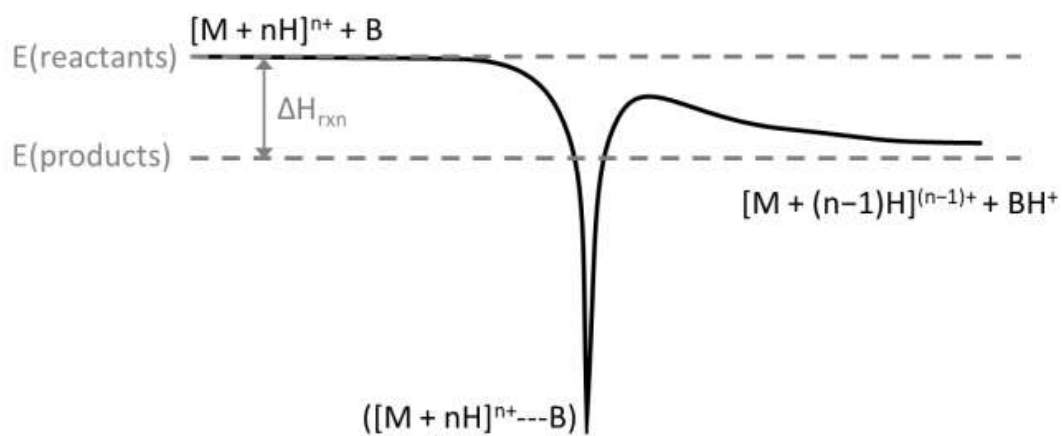


Figure 1.3 A generic energy diagram for a) ion/ion reaction and b) ion/molecule reaction involving proton transfer.

CHAPTER 2. EXPLORATION OF GAS-PHASE ION/ION REACTIONS OF CARBOHYDRATES

2.1 Introduction

Glycans, either alone or as glycoconjugates to proteins or lipids, play important roles in numerous biological functions that are crucial to the development and survival of an organism. These functions include aiding in the conformation and stability of proteins, acting as chemical markers for cell-to-cell recognition, and modulating biological processes such as immune system development and activation.[1, 2] Among the many tools available for the study of glycans (e.g., high performance liquid chromatography (HPLC), electrophoresis, and nuclear magnetic resonance (NMR)[3]) tandem mass spectrometry (MS^n) has emerged as a powerful technique due to its high speed, high sensitivity, and minimal sample requirement. While great strides have been made in the analysis of some bioanalytes, including peptides,[4] proteins,[5] and DNA,[6] using mass spectrometry, glycans have not enjoyed the same progress due to their complex nature. Unlike proteins and nucleic acids, which are linear in sequence, polysaccharide structures are complicated by the presence of cross-linking, branching, and isomeric conformations. Further complications arise for analysis of glycoconjugates as both the conjugate and its polysaccharide linkage site are also emphases of characterization; thereby, adding difficulties to an already complex problem.

Generation of structural information within the mass spectrometer is done through a variety of techniques to induce fragmentation of the analyte ion. Collision induced dissociation (CID) is the oldest and most widely used dissociation method. The two types of structural fragments generated are glycosidic and cross-ring cleavage fragments.[7] Glycosidic fragments break the glycosidic linkage between saccharide subunits thus providing information regarding

the generic monomeric substructure. Cross-ring fragments require breakage of two bonds within six member monosaccharide ring and can provide linkage information. Low energy CID of just oligosaccharides predominantly yields glycosidic fragments.[8] Further complication of CID mass spectra of glycans can occur via fucose migration,[9] internal monosaccharide loss,[10] and elimination of residues that are linked through labile bonds.[11, 12] Low energy CID of oligosaccharides ionized with transition metals, alkali metals, and alkali earth metals yields some cross-ring cleavages that are not present upon low energy CID of its protonated counterpart.[13] High energy CID of just oligosaccharides results in more cross-ring cleavages but is a fragmentation method not widely used because it is not available on many modern instruments.[14] Low energy CID of glycopeptides is similar to that of oligosaccharides as glycosidic bonds are primarily cleaved while minimum amino acid sequence information is obtained.[15]

Electron activated dissociation (ExD) methods such as electron capture dissociation (ECD)[16], electron transfer dissociation (ETD)[17], and electron detachment dissociation (EDD)[18] have recently been applied to glycan structure characterization.[19-21] These dissociation methods usually produce cross-ring cleavages that are not observed with low energy CID. Odd-electron species are often generated via electron activation methods facilitating homolytic-bond cleavage. This results in ring-opening and cross-ring cleavages which provide linkage-site and branching information. As a result, recent research into saccharides has shown an increased focus on the generation and chemistry of gas-phase radical ions.

Electron-capture dissociation and electron-transfer dissociation require multiple charges in the analyte as generating a radical ion results in charge reduction. However, it is difficult to multiply protonate oligosaccharides due to the lack of basic functional groups. Although it is

easier to generate multiply charged glycoconjugates, e.g., glycopeptides or glycoaminoglycans, the charge is not always located on the glycan portion. This can be problematic because charge and radical site locations determine the fragmentation processes that can occur.[22] Two methods of generating multiply charged analytes have been investigated: metal adduction and derivatization at the reducing terminus of oligosaccharides. Oligosaccharides have been adducted with various metals, including Mg^{2+} , Ca^{2+} , Mn^{2+} , Co^{2+} , and Cu^{2+} , to generate ions of the form $[M+metal]^{2+}$ upon electrospray ionization (ESI); the fragmentation pattern observed upon activation of the metalated oligosaccharide is highly dependent upon the choice of metal adduct as well as the degree of branching within the oligosaccharide.[23] Electron-capture dissociation of metal-adducted oligosaccharides yields cross-ring cleavages that provides complementary fragmentation behavior when used in conjunction with another fragmentation technique, e.g., infrared multiphoton dissociation (IRMPD).[8]

The discovery of radical mediated dissociation pathways for oligosaccharides favoring cross-ring cleavages has shifted the focus to radical directed dissociation methods. Recent work has shown activation, by photochemical or collisional processes, of a derivatized oligosaccharide generates a free radical; subsequent activation generates extensive fragmentation types including both glycosidic and cross-ring cleavages.[24, 25] These derivatization methods have the advantage of radical localization in addition to eliminating the need for multiple charges; however, their application is limited to non-conjugated oligosaccharides. Additionally, the method requires additional sample preparation to covalently modify the reducing terminus of the oligosaccharide to include the radical precursor. Sugar radicals have also been generated from CID of non-covalent complexes with *S*-nitroso thiy radical precursors; however, low radical cation abundance plus variability in reagent selection makes its application uncertain.[26]

The vast majority of glycan structural elucidation research revolves around solution-phase modifications, e.g. covalent or isotopic modification, and different fragmentation activation methods, e.g. ECD or ETD. Different types of gas-phase ion/ion chemistry have been demonstrated, described, and studied previously for a variety of biomolecules, such as peptides, proteins, and nucleotides, but little research have been shown for glycans. My research goal is to apply the unique technique of ion/ion chemistry we have at the McLuckey lab and use it for characterization of glycans. Gas-phase ion/ion reactions have the distinct advantage of 1) the lack of sample preparation; 2) easy implementation via dual spray nanoelectrospray ionization followed by ion/ion reactions; and 3) greater control over the reaction by accurately isolating reaction ions and varying the reaction time scale.

2.2 Experimental

2.2.1 Materials

CHROMASOLV[®] HPLC grade water, methanol, acetic acid, DMSO, acetic acid, β -cyclodextrin, 2-aminopyridine, tetramethylammonium acetate, pivalic anhydride, pyridine, dichloromethane, and 97% ¹⁸O water were purchased from Sigma–Aldrich (St. Louis, MO). Maltoheptaose was purchased from Carbosynth (Berkshire, GBR). All carbohydrate solutions for negative nanoelectrospray ionization were prepared at a concentration of 0.1 mg/mL and dissolved in water with 3% by volume NH₄OH. All positive reagents (except for those synthesized below) were subjected to positive nanoelectrospray ionization at a final concentration of 0.1 mg/mL in aqueous solution. CHROMASOLV[®] HPLC grade water, PAMAM dendrimer generation 1.0, and 97% ¹⁸O water were purchased from Sigma–Aldrich (St. Louis, MO). Maltoheptaose was purchased from Carbosynth (Berkshire, GBR). All carbohydrate solutions for negative nanoelectrospray ionization were prepared at a concentration of 0.1

mg/mL and dissolved in water with 3% by volume NH_4OH . All positive reagents were subjected to positive nanoelectrospray ionization at a final concentration of 0.1 mg/mL in aqueous solution.

2.2.2 Isotopic ^{18}O Labeling at the Reducing End

The catalyst solution was prepared by dissolving 2.7 mg of 2-aminopyridine in 1.0 mL of anhydrous methanol. Maltoheptaose (50 μg) was dissolved in 25 μL of H_2^{18}O (97%) with 2.5 μL of catalyst solution and 1 μL of acetic acid. The solution was incubated at 55 $^\circ\text{C}$ overnight. After completion of the reaction, the ^{18}O -labeled maltoheptaose was dried in a SpeedVacTM concentrator followed by reconstituting in water.

2.2.3 Reductive Amination at the Reducing End

200 nmol lyophilized maltoheptaose was mixed with 30 μL 0.5 M 2-aminopyridine in 70:30 DMSO:glacial acetic acid solution. 1 mg solid NaBH_3CN was then added. The solution was incubated at 70 $^\circ\text{C}$ for 2 hours before dried in a SpeedVacTM concentrator and reconstituted in water.

2.2.4 Synthesis of Fixed Charge Pyridinium-based Reagents

The two fixed charge pyridinium-based reagent, 1-propionylpyridin-1-ium and 1-pivaloylpyridin-1-ium, was synthesized by similar procedures. Pyridine was mixed with either pivalic (for the former reagent) or propionic (for the latter reagent) pivalic anhydride in a 1:1 ratio in dichloromethane. This mixture reacted at room temperature for three hours before directly used in nanoelectrospray ionization experiments.

2.2.5 Mass Spectrometry

All experiments were performed upon a QTRAP 4000 hybride triple quadrupole/linear ion trap (SCIEX[®], Concord, ON, Canada) modified for ion/ion reactions. Alternating

nanoelectrospray ionization allows for sequential injections of the analyte and reagent ion into the mass spectrometer. The analyte and reagent ions are isolated in Q1-mass filter prior to storage in q2, which has been modified to simultaneously store ions of opposite charges. Following a defined mutual reaction time of 500 to 1000 milliseconds in q2, the product ions are moved to Q3, a linear ion trap, where the ions of interest are mass-selected. Collisional-activated fragmentation in Q3 is achieved via resonance excitation. The product ions were mass analyzed by mass-selective axial ejection (MSAE). For analysis of ions higher than the original mass range mass extension is applied. The usual MSAE frequency of 310 kHz is ejecting ions at a q value of approximately 0.84 on the Mathieu stability diagram while scanning the ions within the trap. By lowering the MSAE frequency the ejection q value is lowered resulting in a higher mass range which can be scanned. The resulting spectrum is shifted by a multiplier based on the frequency set and need to be recalibrated post data collection.

2.3 Results and discussions

2.3.1 Ion/ion reactions of Alkoxides, Formation of Ethers and Esters in Carbohydrates

The dominate presence of hydroxyl groups on carbohydrates make them a point of focus for gas-phase covalent chemistry. Our research group has previously shown ion/ion reactions of “onium” reagents with carboxylate groups and here we demonstrate gas-phase alkoxide chemistry with carbohydrates.

Tetraalkyl ammonium reagents have been demonstrated to alkylate carboxylate anions in the gas-phase, effectively yielding ester products. It was hypothesized that a similar reaction might be possible with alkoxides as well. A demonstration of this gas-phase ion/ion reaction was first done with β -cyclodextrin (Figure 2.1b), a cyclic seven unit carbohydrate ring. In order for this reaction to work, a multiply charge anion needs to be generated and react with the positive

singly charged tetraalkyl ammonium cation. A solution of β -cyclodextrin containing 3% ammonium hydroxide by volume readily produces a doubly deprotonated anion when subjected to negative mode nanoelectrospray ionization (nESI). The dianion is first isolated via the Q1-mass filter before stored in q2 as described previously. The cation reagent, tetramethylammonium (TMA), is sequentially injected via positive mode nESI, isolated in Q1, and held in q2 to react with the previously stored dianion thereby forming an electrostatic complex (Figure 2.1a). The electrostatic complex can then be subjected to collisional activation in Q3 to drive the alkylation reaction. Following collisional activation, the resulting spectrum reveals that the β -cyclodextrin dianion was methylated, yielding a charge-reduced ether product (Figure 2.2a). The pathway following activation predominately alkylation favors the pathway with no other ions of appreciable abundance being observed. Alkylation of doubly deprotonated β -cyclodextrin with a different tetraalkyl ammonium cation, diallyldimethylammonium, yields similar results as methyl and allyl transfer products are the dominate peaks in the spectrum (Figure 2.2d). The cyclic nature of β -cyclodextrin requires that if carbohydrate fragments are seen from collisional activation a minimal of two bonds must be broken which might explain why the alkyl transfer pathways are much more favorable.

Other anionic carbohydrate systems were studied as well in order to see if this behavior is consistent for carbohydrate alkoxides in a broad sense. The model carbohydrate maltoheptaose (Figure 2.1c), a linear seven unit carbohydrate, was selected for further investigations. Similar to β -cyclodextrin, maltoheptaose was sprayed via negative mode nESI in a 3% ammonium hydroxide by volume solution and the dianion was isolated for further ion/ion reactions. Collisional activation of the electrostatic complex formed via ion/ion reactions with TMA and diallyldimethylammonium yielded a very different result compare to those of β -cyclodextrin

(Figure 2.2b and 2.2e). Unlike β -cyclodextrin, the dominate fragment was not the alkyl transfer peaks but rather various forms of glycosidic bond fragments from maltoheptaose. The nomenclature for oligosaccharide fragmentation used for mass spectrometry is shown in Figure 2.3.

Fragment ions that contain a non-reducing end are labeled with uppercase letters from the beginning of the alphabet (A, B, C) and those that contain the reducing end are labeled with the end of the alphabet (X, Y, Z); subscripts indicate the location of the fragment. A and X fragment ions are produced by breakage of two bonds across the glycosidic ring with the initial superscript indicating the locations of the breakage. B, C, Y, and Z are the glycosidic bond fragments. A hemiacetal exists at the reducing end of the oligosaccharide which can interchange to an open-ring form containing an aldehyde which is reducible; therefore, getting the name: reducing end. Collisional activation of the electrostatic maltoheptaose complexes show glycosidic bonds fragment, as noted by the signature 162 Da loss, which also appears in the control spectrum of $[M-H]^-$ for maltoheptaose. Due to the ubiquitous nature of the 162 Da losses in maltoheptaose, the resulting fragment could either be a C or Y ion. Using $H_2^{18}O$ to ^{18}O -label the reducing end hydroxyl's oxygen, the resulting fragments in the CID spectrum shows no 2 Da shifts in mass and is concluded to be C ions rather than Y ions. Looking back to the collisional activated complexes of doubly deprotonated maltoheptaose and cation reagents, a couple types of fragments are present: glycosidic bond fragments contain the cation reagent, unmodified glycosidic bond fragments, alkyl transfer products, and glycosidic fragments of alkyl transfer products. For TMA, relatively few methyl transfer products are formed and the vast major of fragment ions are glycosidic bond fragments with or without TMA electrostatically bound. More methyl and allyl transfer products are observed for diallyldimethylammonium with allyl transfer

products being slightly more abundant. This slight increase in abundance compared to methyl transfer could be attributed to the existence of resonance stabilization for allyl groups which is not present for methyl groups. Three glycosidic bond fragments are observed from the alkyl transfer products and unmodified glycosidic bond fragments are present as well.

The dramatic difference in the collisional activated spectra of the electrostatic complexes between β -cyclodextrin and maltoheptaose for alkyl cation reagents is thought to be attributed to the presence of the reducing end for maltoheptaose. The reducing end hydroxyl group is slightly more acidic compared to the other hydroxyls on the oligosaccharide due to the close presence of an oxygen atom on the ring causing an electron withdrawing effect on the reducing end hydroxyl. During negative mode ionization of the dianion it is very likely one of the negative charges resides at the reducing end. Reductive amination of the reducing end with 2-aminopyridine was performed using the procedure described previously. Collisional activation of the complex between the doubly deprotonated reductively aminated maltoheptaose and alkyl cations reagents generates spectra that are extremely similar to those of β -cyclodextrin (Figure 2.2c and 2.2f). The alkyl transfer products are the dominate peaks observed and no other side fragmentation occurs. The previously reasoning given for why no carbohydrate fragments are observed for β -cyclodextrin does not apply here for maltoheptaose as it is a linear oligosaccharide. Singly deprotonated reductively aminated maltoheptaose also fragments differently compared to the unmodified maltoheptaose as the most intense peaks are from cross-ring cleavages with relatively few glycosidic bond fragments. It can be concluded that the reducing end plays an undeniable role in how alkyl transfers occur as well as the fragmentation pathway of maltoheptaose.

Alkyl transfer to alkoxides are achieved via the use of tetraalkyl ammonium reagents but for the formation of esters from alkoxides the cationic reagent must be a more appealing target for nucleophilic attacks from alkoxides and not promote a pathway of proton transfer. As described in the synthesis section, 1-propionylpyridin-1-ium and 1-pivaloylpyridin-1-ium were synthesized and used as the cationic reagent (structures shown in Figure 2.4a and 2.4b). The reagent was designed so that the alkoxide anion would attack the carbonyl carbon of the pyridinium reagents resulting in the loss of pyridine and form an ester in that process. Again, this reaction was first demonstrated with β -cyclodextrin and 1-propionylpyridin-1-ium, the first reagent created (Figure 2.4a). No long-lived electrostatic complex is observed from the ion/ion reactions with 1-propionylpyridin-1-ium and an ethyl ester product is readily formed; however, collisional activation of the ethyl ester product results in an effective proton transfer charged reduced peak of β -cyclodextrin. It is theorized that an alpha hydrogen on the ethyl ester is involved in a rearrangement leading to an effective proton transfer reaction (Scheme 2.1). To remedy this issue 1-pivaloylpyridin-1-ium was synthesized such that all the alpha hydrogens are now methyl groups thereby blocking the pathway of an effective proton transfer reaction upon activation. Ion/ion reactions between doubly deprotonated maltoheptaose and 1-pivaloylpyridin-1-ium yield the desired tert-butyl ester product and following activation no proton transfer reaction happened; however, a tert-butyl carboxylic acid was lost (Figure 2.4c and 2.4d). The exact reason for why a carboxylic acid is lost is unknown and the exact location of where the hydrogen was abstract is still undetermined. Activation of the ester product generated from the reactions between 1-pivaloylpyridin-1-ium and maltoheptaose results in glycosidic bonds fragments that either contain the t-butyl ester product or does not (Figure 2.5a). The distribution of fragmentations that have or does not have the ester covalent modification indicates a range of

locations the modification is occurring along the carbohydrate chain. This also gives an indication to the variety of anionic charge locations that can occur. Determination of the exact type of fragments, C or Y, was achieved with ^{18}O -label maltoheptaose (Figure 2.5c). Comparison between the two spectra showed no shifts in peaks and therefore all the fragments are of the non-reducing end, C ions. Previous experiments with alkoxides have shown that the presence of the reducing end is unfavorable for alkyl transfer, subjecting the reducing end reductively aminated maltoheptaose to 1-pivaloylpyridin-1-ium gave similar results to those of β -cyclodextrin and is consistent with previous experiments (Figure 2.5b). The ^{18}O labeling experiment shows that the reducing end is not participating in the formation of esters and that the covalent attach is at the other anionic alkoxide site on maltoheptaose since the collision activation spectrum only show fragments of the non-reducing end; however, when the reducing end is non-existent no glycosidic bond fragments are generated. This directly indicates that the reducing end for maltoheptaose is directly involved in glycosidic bond fragmentation.

2.3.2 Schiff Base Reactions of Carbohydrates

Another functional group present for oligosaccharides is the hemiacetal located at the reducing end. The hemiacetal can undergo base-catalyzed ring opening event and generate an aldehyde which can be the target of covalent modification. It is common in solution phase to reductively aminate the reducing end with a chromophore to facilitate the detection of oligosaccharides in HPLC-UV as well as enhancing the signal of carbohydrates for mass spectrometry. Demonstration of this reaction is achieved within the gas-phase at a fraction of the time needed for this reaction to occur in solution.

Gas-phase Schiff base covalent chemistry has been shown via ion/ion charge inversion reactions between doubly deprotonated 4-formyl-1,3-benzene disulfonic acid (FBDSA) and a

lysine containing peptide. It is hypothesized that if the hemiacetal of the model oligosaccharide maltoheptaose can undergo ring open and form an aldehyde then a Schiff base reaction could be possible in the presence of primary amines. While the ring form of sugars is the most stable form, an equilibrium exists for the position of the reducing end hydroxyl group between the alpha and beta position. The intermediate of this equilibrium is the ring open form of the sugar ring and contains the aldehyde (Scheme 2.2). The reagent chosen for these set of experiments is the PAMAM dendrimer generation 1.0 which contains 8 primary amine groups thereby maximizing the chances that Schiff base reaction will occur should an aldehyde be present. The negative control analyte selected for these set of reactions is the maltoheptaose reductively aminated with 2-aminopyridine (2-AP) via solution phase chemistry.

Maltoheptaose and PAMAM G1 were reacted in both charge reduction and charge inversion ion/ion reaction experiments. Ion/ion reactions between $[\text{Maltoheptaose-2H}]^{2-}$ and $[\text{PAMAM G1+H}]^+$ readily generates the desired electrostatic complex although proton transfer products are the most abundant peak present (Figure 2.7a). Some amounts of glycosidic bond fragments, C ions, were seen during the ion/ion reaction step indicating either an excess of energy from the proton transfer step or a harsh transfer step between the quadrupoles. Only a tiny amount of the complex is observed during the charge inversion reaction with proton transfer from PAMAM G1 to maltoheptaose being more dominant (Figure 2.7b). Similar trends were also observed for maltoheptaose with 2-AP with charge reduction generating the most amount of complex and charge inversion giving the least amount (Figure 2.7c and 2.7d). No glycosidic bond cleavages are observed from the charge reduction ion/ion reaction sequence compared to non-modified maltoheptaose. The difference in amount of complex formed between charge reduction and charge inversion can be explained by the “stickiness” of charges that are present.

Alkoxides are relatively stickier compared to primary protonated amine groups thus having two alkoxides compared to two primary protonated amines will result in more electrostatic complexes formed.

Evidence of Schiff base chemistry is determined by the loss of water following activation of the electrostatic complexes formed from the ion/ion reactions. No water loss was observed upon activation of the charge reduction reaction complex and the signature 162 Da loss indicates glycosidic bond cleavages (Figure 2.8a). All seven glycosidic bond were cleaved and a deprotonated PAMAM G1 is left. No Schiff base and proton transfer reaction occurred but the extensiveness of the glycosidic bond cleavages as well as all the fragments containing PAMAM G1 reveal a strong electrostatic complex that is formed. A significant water loss peak appeared upon collisional activation of the charge inversion reaction complex along with the presence of a proton transfer reaction and PAMAM G1 fragments (Figure 2.8b). The dominate water loss peak strongly suggests a Schiff base reaction occurring as maltoheptaose and PAMAM G1 do not fragment water (Figure 2.11). The suggested schematic for how an aldehyde group is present in the gas phase is highly dependent upon a charge at present the reducing end (Scheme 2.3a). As the charge is likely to be on the reducing end hydroxyl since it the most acidic out of all the hydroxyls present the presence of an aldehyde should be prevalent in both the charge reduction and charge inversion reactions; however, no Schiff base reaction occurred for charge reduction but did happen for charge inversion. This phenomenal suggests that the presence of two anionic charge sites for charge reduction hinders the primary protonated amine from selectively interaction with the charge present at the reducing end and instead forms an ionic interaction with the other negative charge site.

With only one charge present, in this case the charge inversion reaction, protonated primary amines react exclusively at the reducing end anionic charge site and Schiff base reactions occur. It can also be concluded that compared to other alkoxides along the carbohydrate chain, the reducing end alkoxide is less favored. Confirmation of Schiff base chemistry is achieved by selective ^{18}O -labeling of the reducing end hydroxyl. The signature water loss that occurs via Schiff base chemistry should be originating from that hydroxyl group; therefore, a 20 Da loss would definitively confirm the location as well as the reaction actually occurring. Expected results was obtained from the ^{18}O -labeling maltoheptaose charge inversion ion/ion reaction experiments with PAMAM G1 as a 20 Da loss confirms Schiff base reaction (Figure 2.9). For the negative control experiments where the reducing end is blocked off no water loss is observed for the ion/ion reactions between PAMAM G1 and 2-AP modified maltoheptaose (Figure 2.8c and 2.8d). Only proton transfer reaction occurs. Further activation of the Schiff base product was conducted and only fragments of PAMAM G1 is observed as well as various water losses (Figure 2.10). The fragments are not all surprising as the lone charge resides on PAMAM G1 and location of charge often dictates fragmentation patterns. It is disappointing that no carbohydrate fragments were observed that provides extra structural information but that is likely due to the nature of PAMAM G1. With the right reagent more structural information of the carbohydrate can be achieved all with minimal time spent doing Schiff base chemistry in the solution which takes at least a couple of a hours while gas-phase Schiff base reaction takes only a couple hundred milliseconds.

2.3.3 Metal Adduction to Carbohydrates via Gas-phase Ion/ion Reactions

One of the ways to ionization and get cross-ring fragmentation of oligosaccharides is through metal adduction using cations such as Na^+ and Ca^+ . The primary fragments obtained via

metal adduction are cross-rings cleavages and are useful for providing linkage information. For [Maltoheptaose-H]⁺, the dominate fragment ions are glycosidic bond cleavages that provides monosaccharide composition details but lack linkage information. The introduction of alkali earth metal cations via ion/ion reactions to [Maltoheptaose-2H]²⁺ generates varying degrees of both glycosidic and cross-ring fragments which are relevant for structural characterization.

Carbohydrates do not ionization well in the positive mode, either by ESI or MALDI, and using metal adducts is a common tool to overcome that deficiency. It has been theorized previously that metal cations coordinate with the hydroxyl groups present on the carbohydrate thereby stabilizing the structure and opening the pathway to cross-ring cleavages. Negative ionization is not as commonly used as positive ionization for analysis of oligosaccharides but research done by David J. Harvey on fragmentation of negative ions from carbohydrates has shown reasons to work in the negative mode instead of positive mode. A common theme encounter with oligosaccharides in the negative mode is the lack of cross-ring fragments that are available. With model carbohydrate maltoheptaose the dominate fragments are glycosidic bond cleavages (Figure 2.11a). Sodium-adducted maltoheptaose in the positive mode yields far more cross-ring cleavages that are extremely useful for structural characterization (Figure 2.11b). It is hypothesized that the inclusion of metal cations in the negative mode will give similar cross-ring fragments but also maintain the glycosidic fragments that are present.

Doubly deprotonated maltoheptaose was reacted with various alkali earth metal cations in the gas phase. Cesium and rubidium can be readily ionization via nESI as individual cations but sodium and potassium were sprayed as metal-adduct polymers. Electrostatic complexes of the metal adducted maltoheptaose anions were easily formed upon ion/ion reactions and collisional activation reveals an interesting trend of the fragments (Figure 2.12). Cross-ring cleavages are

now much more prevalent compared to the singly deprotonated control spectrum affirming the suspicion that metal coordination in the negative mode has the same effect as in the positive mode. While cross-ring fragments increased, glycosidic cleavages are suppressed in the sodium adduct spectrum. This suppression is lessened as metal cation is potassium, rubidium, or cesium. This trend is better visualized in the charts in Figure 2.13. Cesium adducted anions give the best combination of both glycosidic and cross-ring fragments. It is unclear why cesium gives the most informative spectrum compare to other alkali earth metal cations but electron affinity and ionic radius are potential clues.

2.4 Conclusion

Carbohydrate alkoxides are shown to be viable targets for gas-phase covalent modification to ester and ethers. Alkyl transfer is most favorable if the reducing end is not present on the carbohydrate. Ester products are readily generated using the specially designed reagents and requires no additional activation after introduction of the oppositely charge reactants to each other; however, the presence of easily abstracted hydrogen atoms on the reagent can result in an end result of a proton transfer reaction. Reductively aminating the reducing end of maltoheptaose also reveals that the presence of the reducing is directly responsible for glycosidic bond cleavages of maltoheptaose. The reducing end alkoxide also does not tend to react with the reagents and is often lost during fragmentation. It is disappointing that modification of alkoxides on maltoheptaose did not change its fragmentation pattern to give more cross-ring fragments instead of the default glycosidic bond fragments.

Gas phase carbohydrate Schiff base reaction is demonstrated with maltoheptaose and PAMAM G1. The reaction is confirmed by isotopic labeling and a negative control experiment. The reaction is sensitive to the number of anionic charge sites on maltoheptaose since the

reducing end alkoxide is not as attractive compared to other anionic sites on the oligosaccharide as demonstrated with the charge reduction and charge inversion experiments. The lack of carbohydrate structural information after Schiff base reaction is attributed to PAMAM G1 and with a better reagent gas-phase Schiff base chemistry can be used to increase structural determination of carbohydrates.

Metal adducted anions successfully gave cross-ring cleavages that enhanced structural characterization of maltoheptaose. The ratio of glycosidic vs. cross-ring fragments is dependent upon the metal cation chosen with cesium giving the closest split of both glycosidic and cross-ring fragments. Glycoaminoglycans (GAGs) are a group of carbohydrate that contains an enormous amount of sulfates and ultimate goal of structural elucidation is to determine the location of those sulfates. GAGs are commonly analyzed in the negative mode but sulfates are readily lost upon fragmentation making structural elucidation difficult. Metals cations are known to stabilize sulfates and could potentially be a focus of future investigation.

2.5 References

- [1] A. Varki, Biological roles of oligosaccharides: all of the theories are correct, *Glycobiology*, 3 (1993) 97-130.
- [2] B.A. Cobb, D.L. Kasper, Coming of age: carbohydrates and immunity, *European journal of immunology*, 35 (2005) 352-356.
- [3] C.M. Szymanski, F.S. Michael, H.C. Jarrell, J. Li, M. Gilbert, S. Larocque, E. Vinogradov, J.R. Brisson, Detection of conserved N-linked glycans and phase-variable lipooligosaccharides and capsules from campylobacter cells by mass spectrometry and high resolution magic angle spinning NMR spectroscopy, *The Journal of biological chemistry*, 278 (2003) 24509-24520.
- [4] H. Steen, M. Mann, The ABC's (and XYZ's) of peptide sequencing, *Nature reviews. Molecular cell biology*, 5 (2004) 699-711.
- [5] J.R. Yates, C.I. Ruse, A. Nakorchevsky, Proteomics by mass spectrometry: approaches, advances, and applications, *Annual review of biomedical engineering*, 11 (2009) 49-79.

- [6] J.L. Beck, M.L. Colgrave, S.F. Ralph, M.M. Sheil, Electrospray ionization mass spectrometry of oligonucleotide complexes with drugs, metals, and proteins, *Mass spectrometry reviews*, 20 (2001) 61-87.
- [7] B. Domon, C. Costello, A systematic nomenclature for carbohydrate fragmentations in FAB-MS/MS spectra of glycoconjugates, *Glycoconjugate J*, 5 (1988) 397-409.
- [8] J.T. Adamson, K. Hakansson, Electron capture dissociation of oligosaccharides ionized with alkali, alkaline Earth, and transition metals, *Anal Chem*, 79 (2007) 2901-2910.
- [9] B. Ernst, D.R. Müller, W.J. Richter, False sugar sequence ions in electrospray tandem mass spectrometry of underivatized sialyl-Lewis-type oligosaccharides, *International Journal of Mass Spectrometry and Ion Processes*, 160 (1997) 283-290.
- [10] L.P. Brüll, W. Heerma, J. Thomas-Oates, J. Haverkamp, V. Kováčik, P. Kováč, Loss of internal 1 → 6 substituted monosaccharide residues from underivatized and per-O-methylated trisaccharides, *Journal of the American Society for Mass Spectrometry*, 8 (1997) 43-49.
- [11] J. Zhang, L. Lamotte, E.D. Dodds, C.B. Lebrilla, Atmospheric pressure MALDI Fourier transform mass spectrometry of labile oligosaccharides, *Anal Chem*, 77 (2005) 4429-4438.
- [12] D.J. Harvey, Structural determination of N-linked glycans by matrix-assisted laser desorption/ionization and electrospray ionization mass spectrometry, *Proteomics*, 5 (2005) 1774-1786.
- [13] D.J. Harvey, Ionization and collision-induced fragmentation of N-linked and related carbohydrates using divalent cations, *Journal of the American Society for Mass Spectrometry*, 12 (2001) 926-937.
- [14] D.J. Harvey, R.H. Bateman, M.R. Green, High-energy Collision-induced Fragmentation of Complex Oligosaccharides Ionized by Matrix-assisted Laser Desorption/Ionization Mass Spectrometry, *Journal of Mass Spectrometry*, 32 (1997) 167-187.
- [15] J.M. Hogan, S.J. Pitteri, P.A. Chrisman, S.A. McLuckey, Complementary structural information from a tryptic N-linked glycopeptide via electron transfer ion/ion reactions and collision-induced dissociation, *Journal of proteome research*, 4 (2005) 628-632.
- [16] R.A. Zubarev, N.L. Kelleher, F.W. McLafferty, Electron Capture Dissociation of Multiply Charged Protein Cations. A Nonergodic Process, *Journal of the American Chemical Society*, 120 (1998) 3265-3266.
- [17] J.E. Syka, J.J. Coon, M.J. Schroeder, J. Shabanowitz, D.F. Hunt, Peptide and protein sequence analysis by electron transfer dissociation mass spectrometry, *Proceedings of the National Academy of Sciences of the United States of America*, 101 (2004) 9528-9533.

- [18] B.A. Budnik, K.F. Haselmann, R.A. Zubarev, Electron detachment dissociation of peptide di-anions: an electron-hole recombination phenomenon, *Chemical Physics Letters*, 342 (2001) 299-302.
- [19] L. Han, C.E. Costello, Electron transfer dissociation of milk oligosaccharides, *Journal of the American Society for Mass Spectrometry*, 22 (2011) 997-1013.
- [20] J.J. Wolff, F.E. Leach, 3rd, T.N. Laremore, D.A. Kaplan, M.L. Easterling, R.J. Linhardt, I.J. Amster, Negative electron transfer dissociation of glycosaminoglycans, *Anal Chem*, 82 (2010) 3460-3466.
- [21] J.J. Wolff, L. Chi, R.J. Linhardt, I.J. Amster, Distinguishing glucuronic from iduronic acid in glycosaminoglycan tetrasaccharides by using electron detachment dissociation, *Anal Chem*, 79 (2007) 2015-2022.
- [22] F.W. McLafferty, F.e. Tureček, *Interpretation of mass spectra*, 4th ed., University Science Books, Mill Valley, Calif., 1993.
- [23] M.T. Cancilla, S.G. Penn, J.A. Carroll, C.B. Lebrilla, Coordination of Alkali Metals to Oligosaccharides Dictates Fragmentation Behavior in Matrix Assisted Laser Desorption Ionization/Fourier Transform Mass Spectrometry, *Journal of the American Chemical Society*, 118 (1996) 6736-6745.
- [24] J. Gao, D.A. Thomas, C.H. Sohn, J.L. Beauchamp, Biomimetic reagents for the selective free radical and acid-base chemistry of glycans: application to glycan structure determination by mass spectrometry, *Journal of the American Chemical Society*, 135 (2013) 10684-10692.
- [25] X. Zhang, R.R. Julian, Radical mediated dissection of oligosaccharides, *International journal of mass spectrometry*, 372 (2014) 22-28.
- [26] S. Osburn, S.J. Williams, R.A.J. O'Hair, Formation of sugar radical cations from collision-induced dissociation of non-covalent complexes with S-nitroso thiy radical precursors, *International journal of mass spectrometry*, 378 (2015) 95-106.

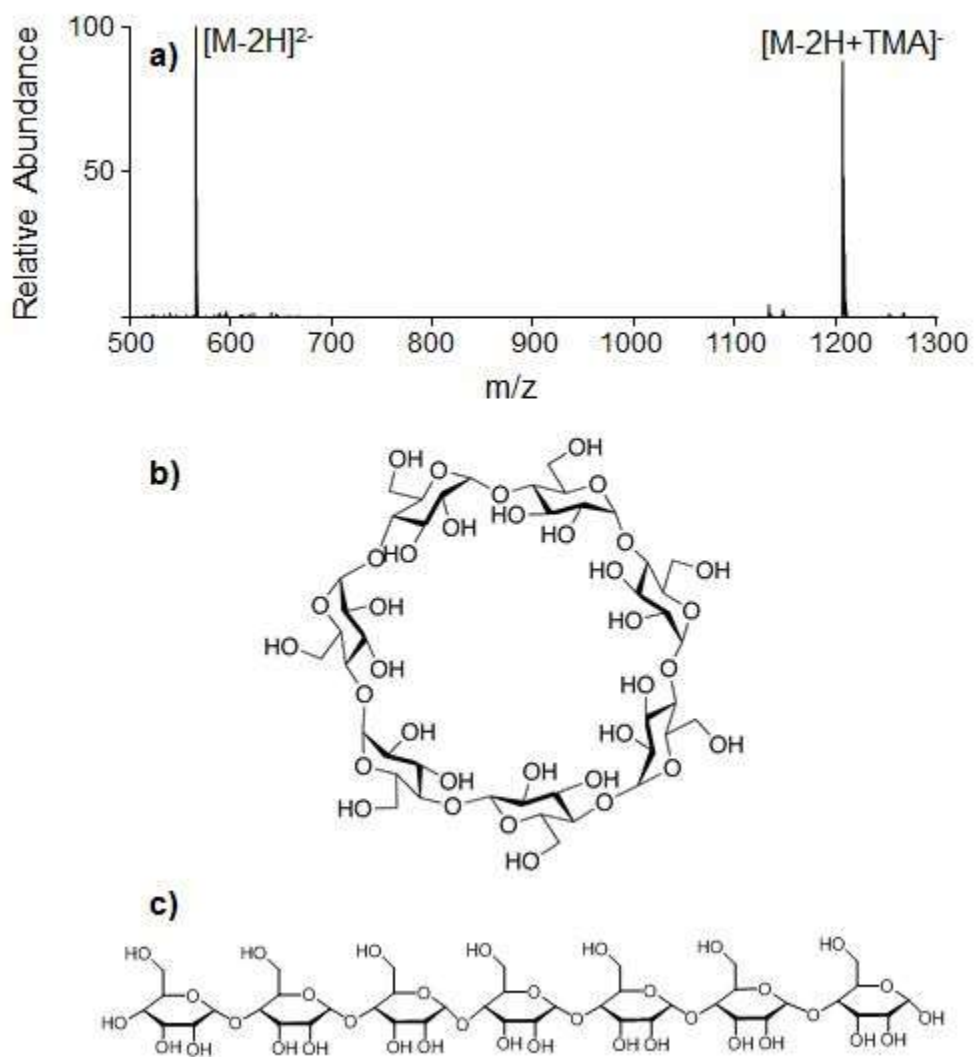


Figure 2.1 Product spectrum for a) ion/ion reaction between doubly deprotonated β -cyclodextrin, $[M-2H]^{2-}$, and tetramethylammonium, TMA. The structure of b) β -cyclodextrin and c) maltoheptaose. (Lightning bolt indicates ion subject to activation)

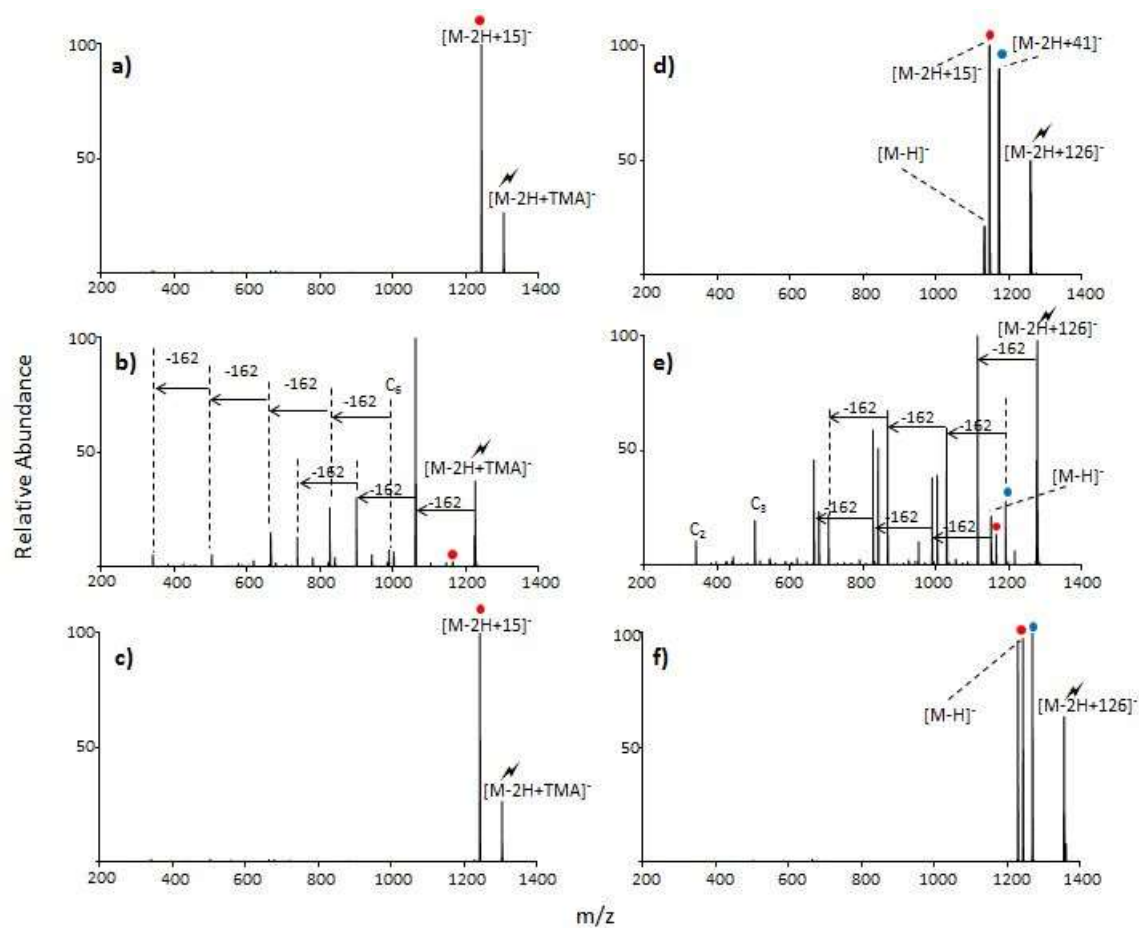


Figure 2.2 Ion trap CID spectra of the electrostatic complex formed between tetramethylammonium (TMA) and a) β -cyclodextrin, b) maltoheptaose, c) maltoheptaose modified with 2-aminopyridine; diallyldimethylammonium and d) β -cyclodextrin, e) maltoheptaose, f) maltoheptaose modified with 2-aminopyridine. Methyl and allyl transfer products are denoted respectfully with red (●) and blue (●) dots.

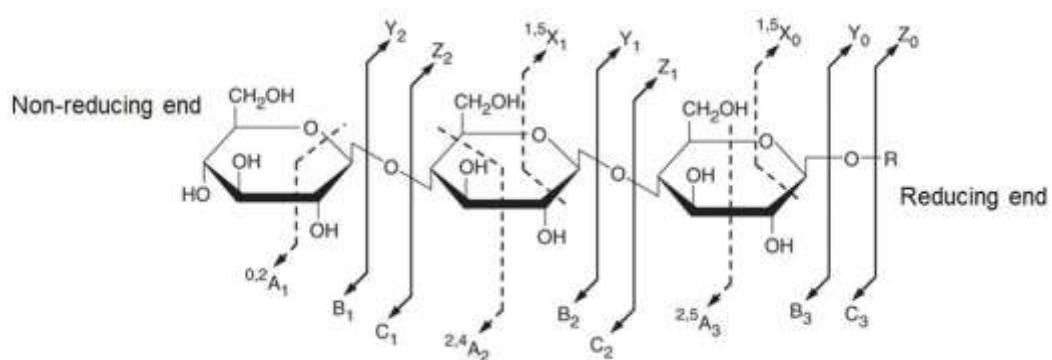


Figure 2.3 Nomenclature for carbohydrate fragment ions generated by tandem MS (Modified from Domon & Costello, 1988).

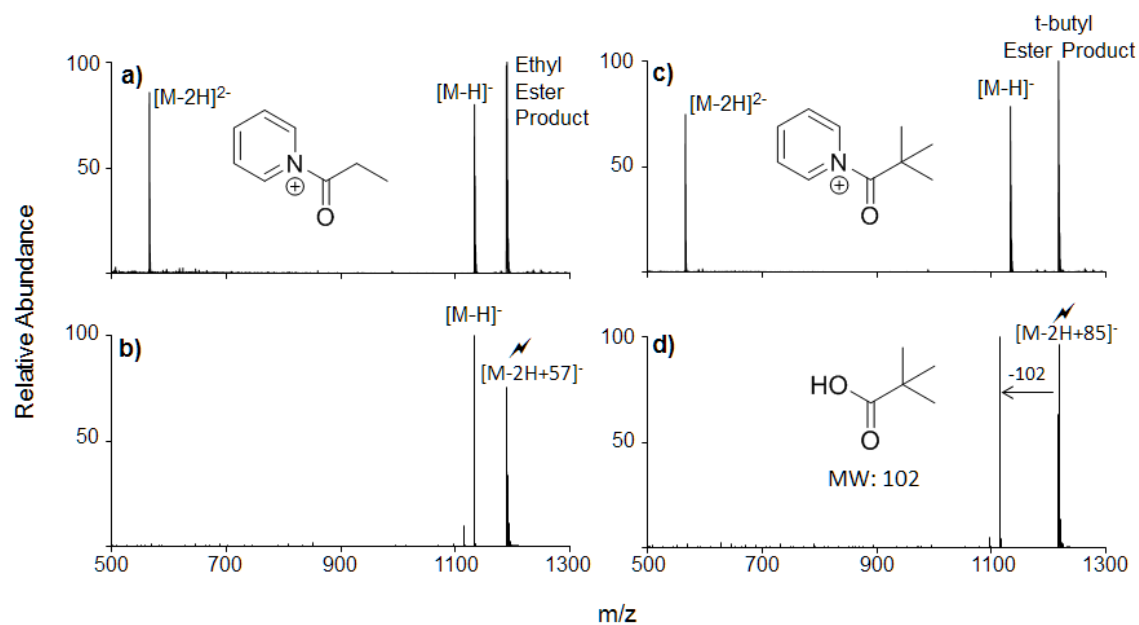
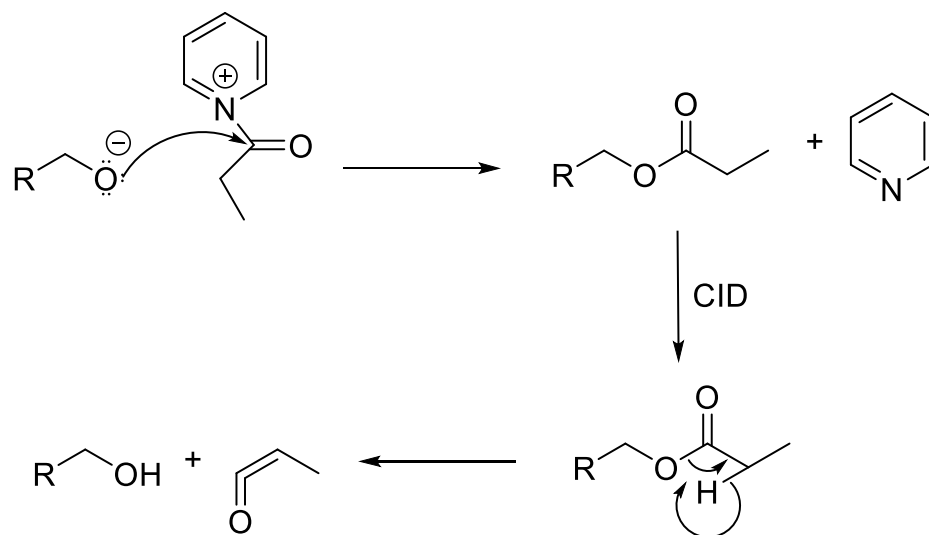


Figure 2.4 Product ion spectra for ion/ion reactions between doubly-deprotonated β -cyclodextrin and a) 1-propionylpyridin-1-ium or c) 1-pivaloylpyridin-1-ium. Ion trap CID of the b) ethyl ester product and d) t-butyl ester product.



Scheme 2.1 Proposed formation and dissociation of the ester product formed via ion/ion reactions between an alkoxide anion and 1-propionylpyridin-1-ium cation. CID activation leads to a 56 Da loss and the end result effectively being a proton transfer reaction.

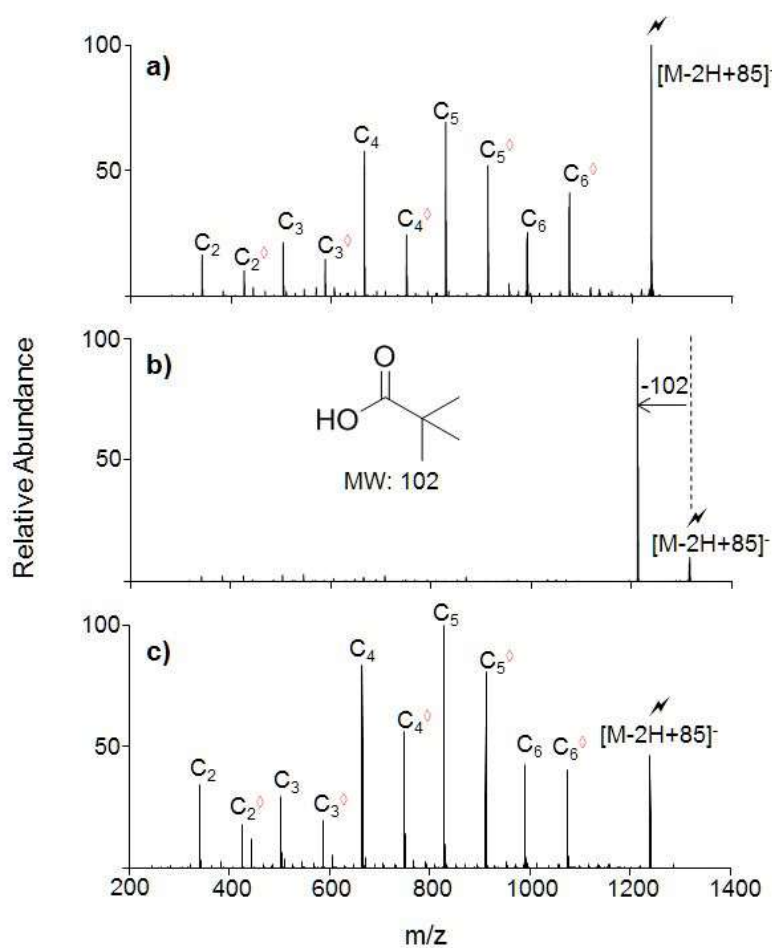


Figure 2.5 Ion trap CID spectrum of t-butyl ester product formed with a) maltoheptaose, b) maltoheptaose modified with 2-amino pyridine at the reducing end, and c) ^{18}O reducing end labeled maltoheptaose (\diamond denoted addition of t-butyl ester group).

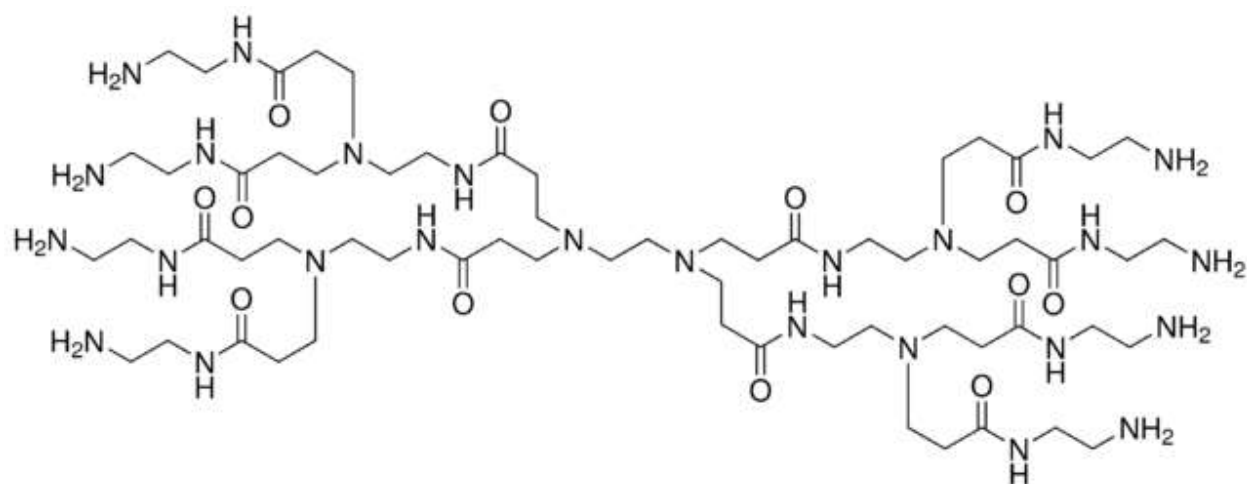
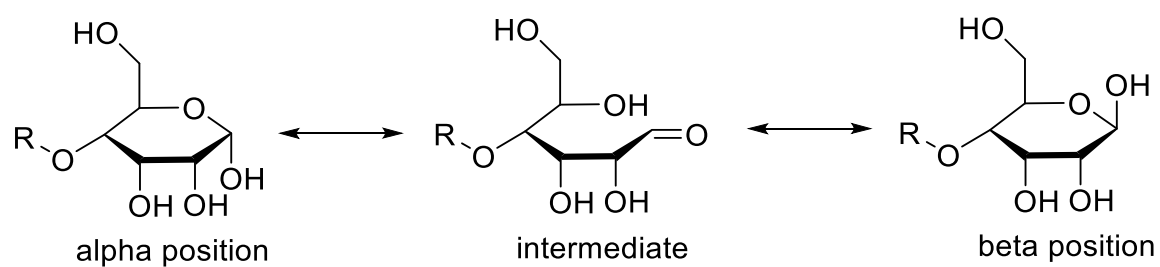


Figure 2.6 Structure of PAMAM dendrimer, ethylenediamine core, generation 1.0



Scheme 2.2 Equilibrium between the alpha and beta position of the hydroxyl group on the reducing end.

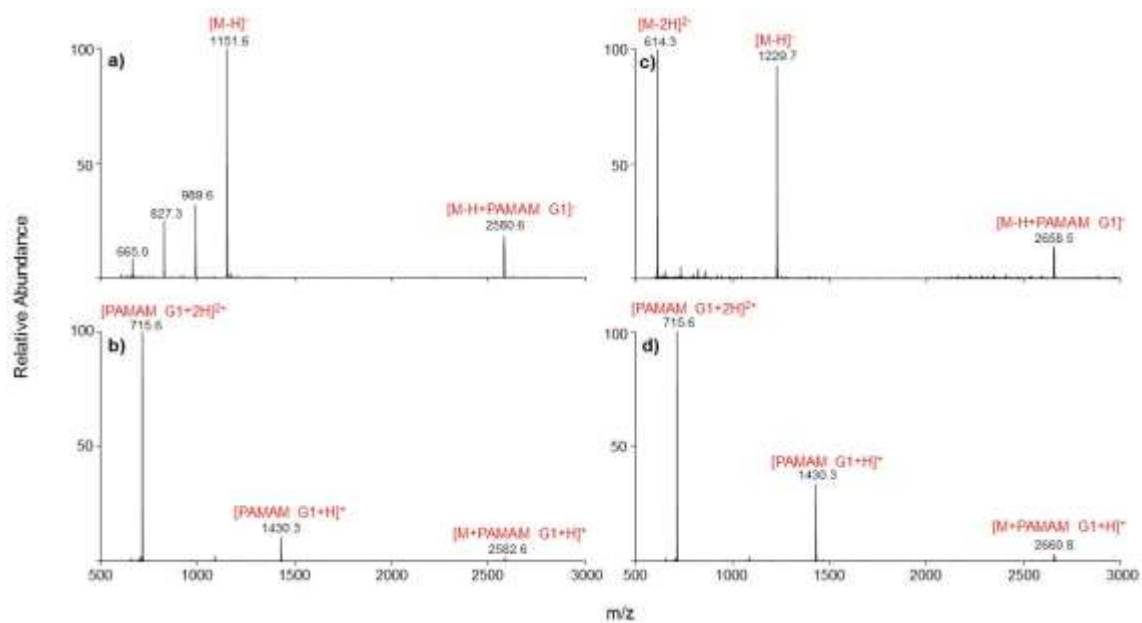


Figure 2.7 Product ion spectrum of charge reduction ion/ion reactions between singly protonated

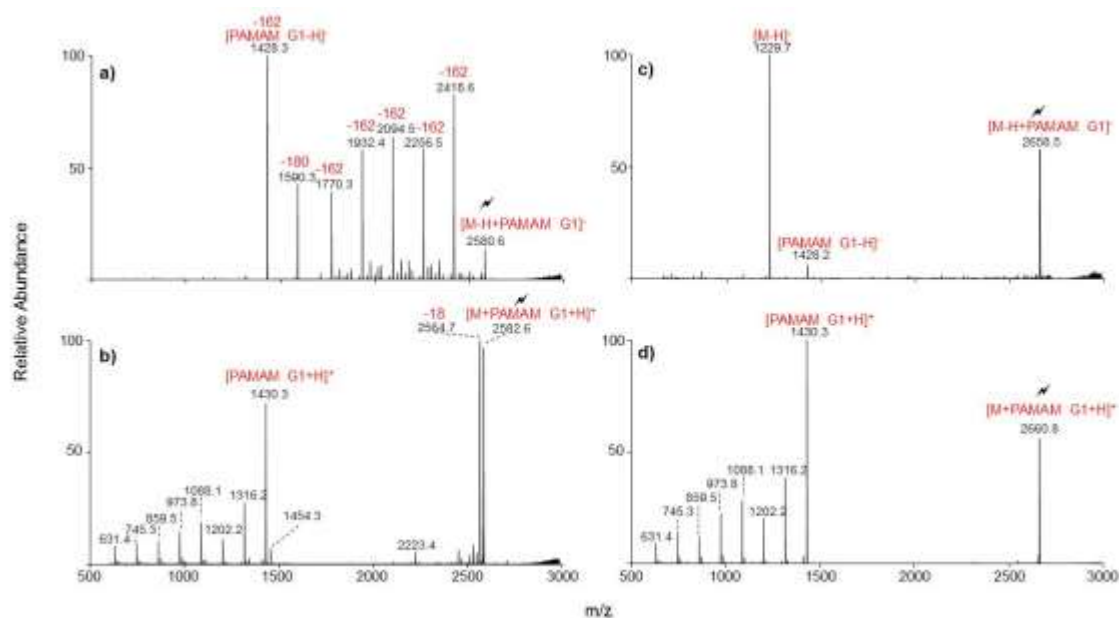
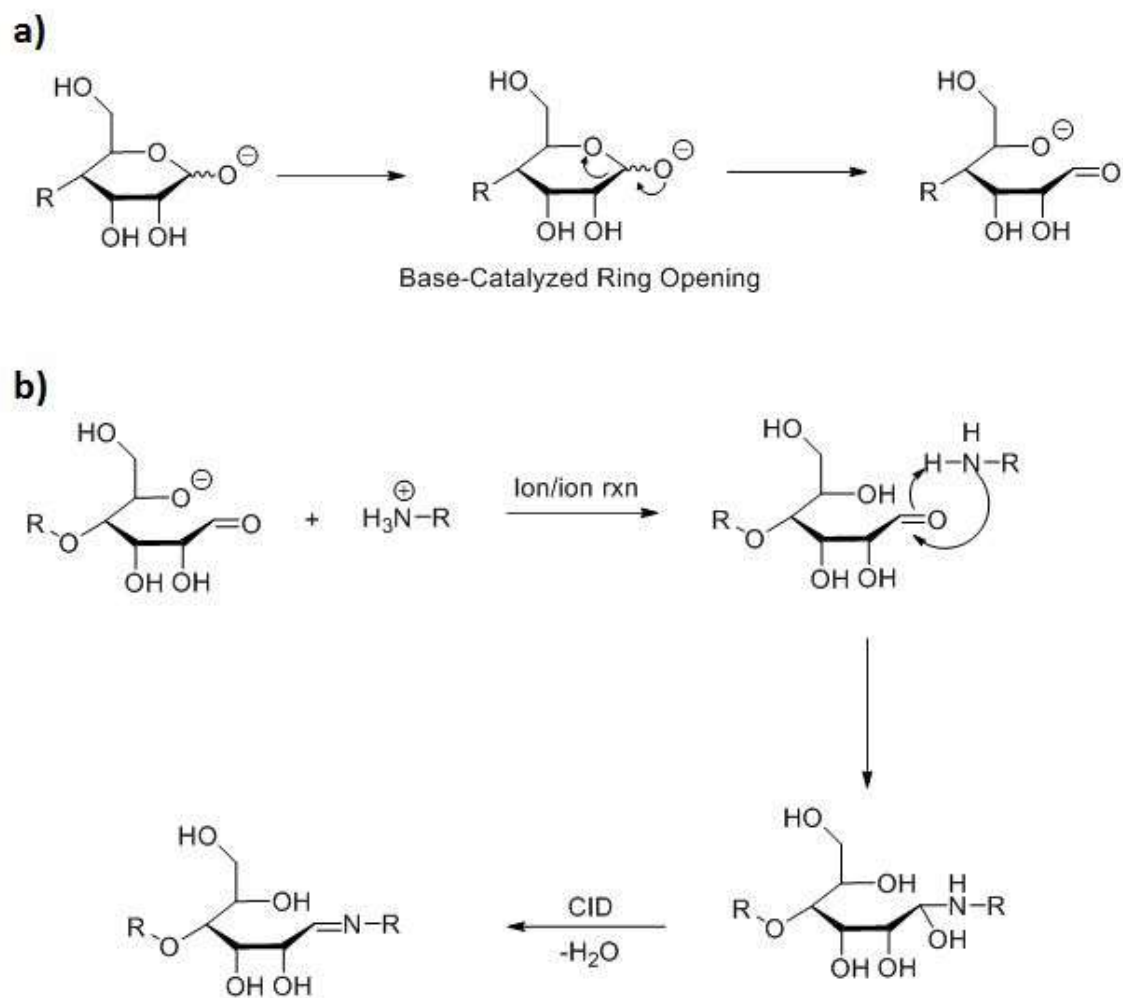


Figure 2.8 Ion trap CID spectra of the electrostatic complex formed via ion/ion reaction between $[\text{PAMAM G1+H}]^+$ and a) $[\text{Maltoheptaose-2H}]^{2-}$, c) $[\text{Maltoheptaose with 2-aminopyridine-2H}]^{2-}$; or reactions between $[\text{PAMAM G1+2H}]^{2+}$ and b) $[\text{Maltoheptaose-2H}]^{2-}$, d) $[\text{Maltoheptaose with 2-aminopyridine-2H}]^{2-}$.



Scheme 2.3 a) Formation of the aldehyde chemical group from the hemiacetal and b) summary of steps involved in the formation of a Schiff Base onto carbohydrates.

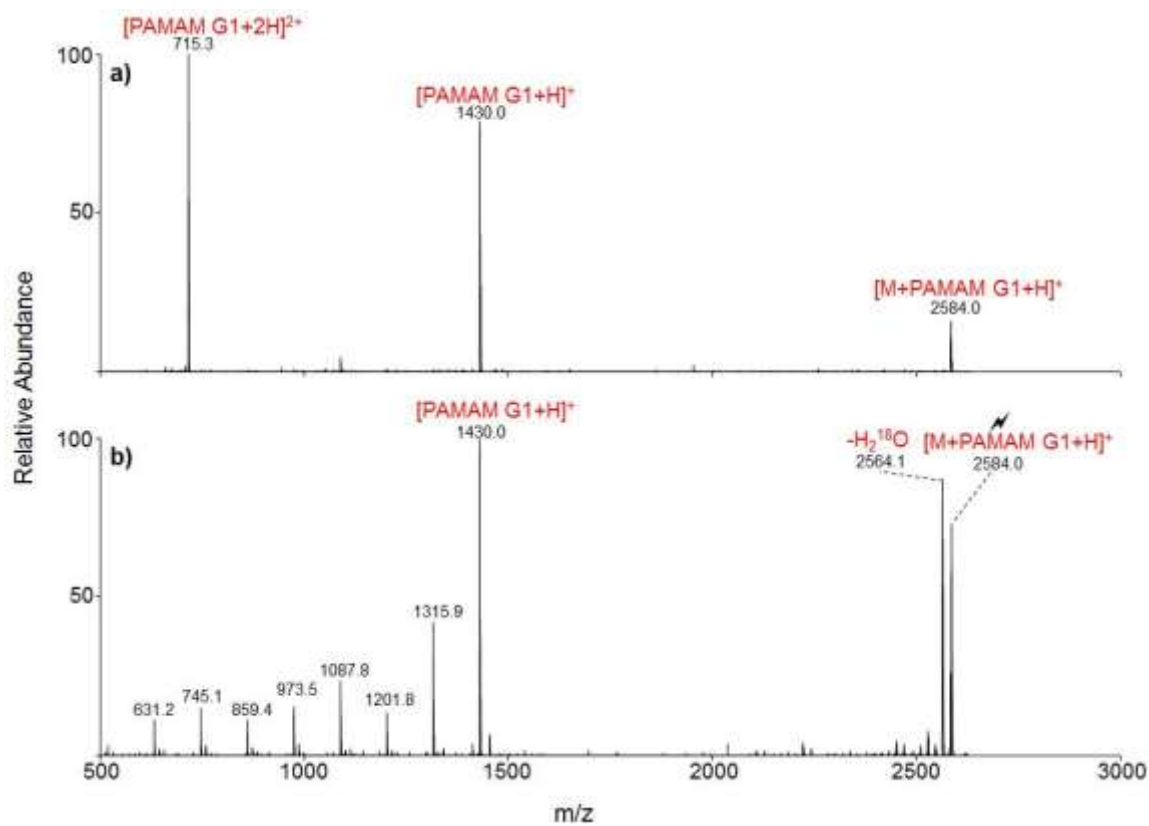


Figure 2.9 Product spectrum of a) ion/ion reactions between doubly protonated PAMAM G1 and singly deprotonated ^{18}O -labeled maltoheptaose; b) collision activation of the electrostatic complex formed.

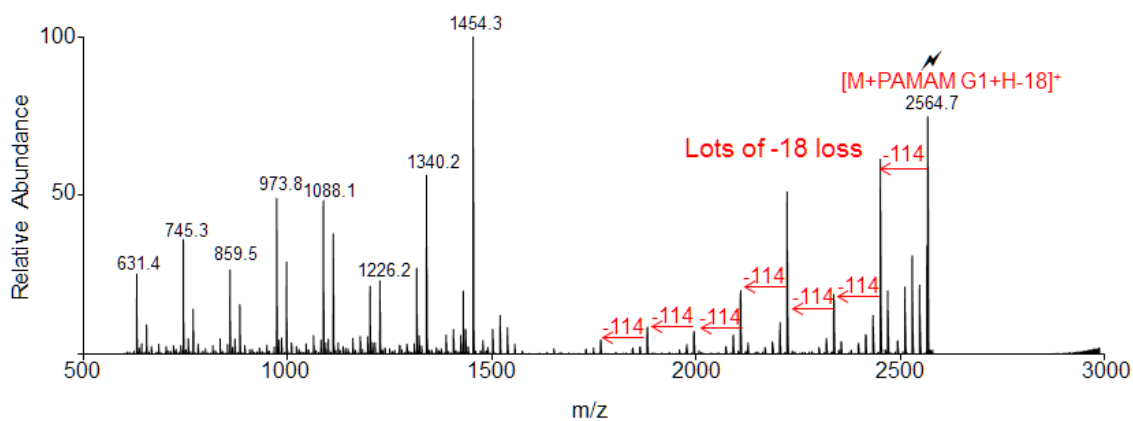


Figure 2.10 Collisional ion trap CID of the Schiff base product peak obtained from activation of the electrostatic complex.

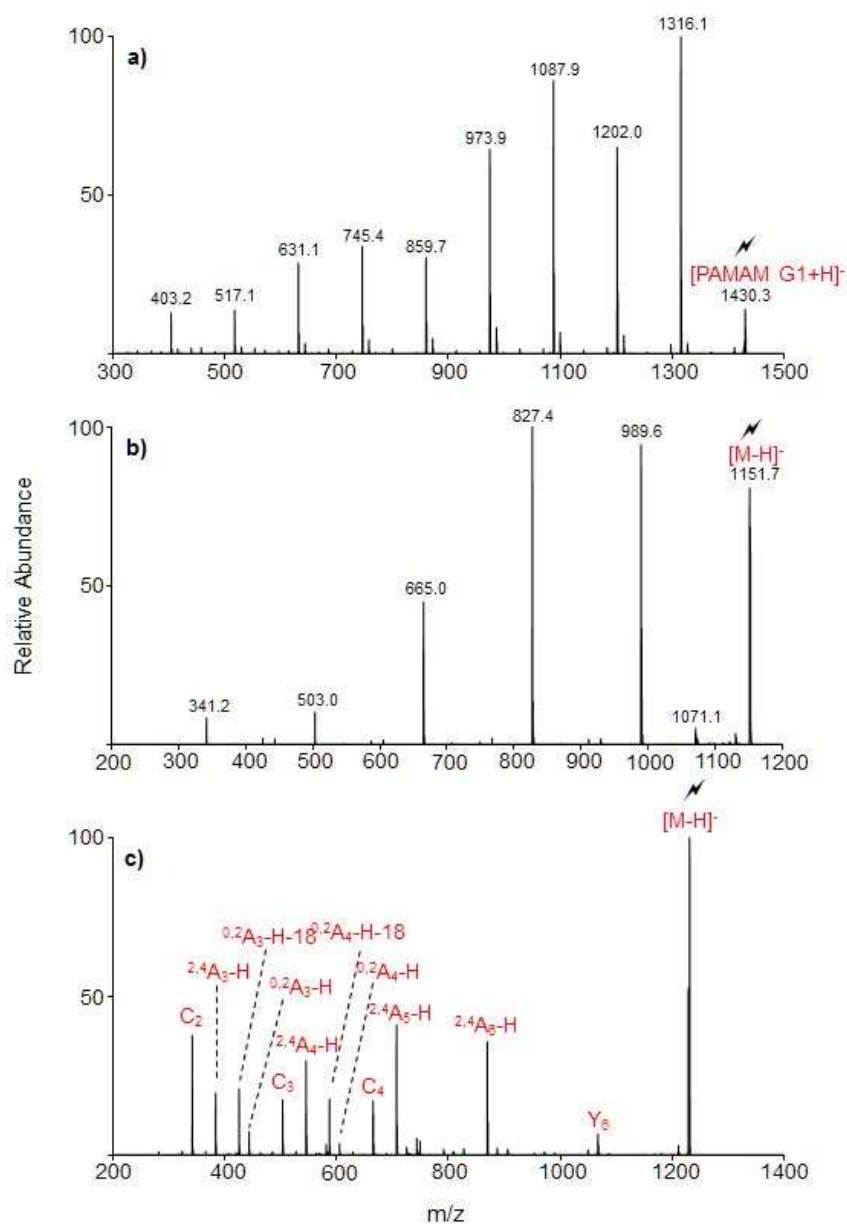


Figure 2.11 Ion trap CID control spectra for a) [PAMAM G1+H]⁺, b) [Maltoheptaose-H]⁻, and c) [Maltoheptaose with 2-AP-H]⁻.

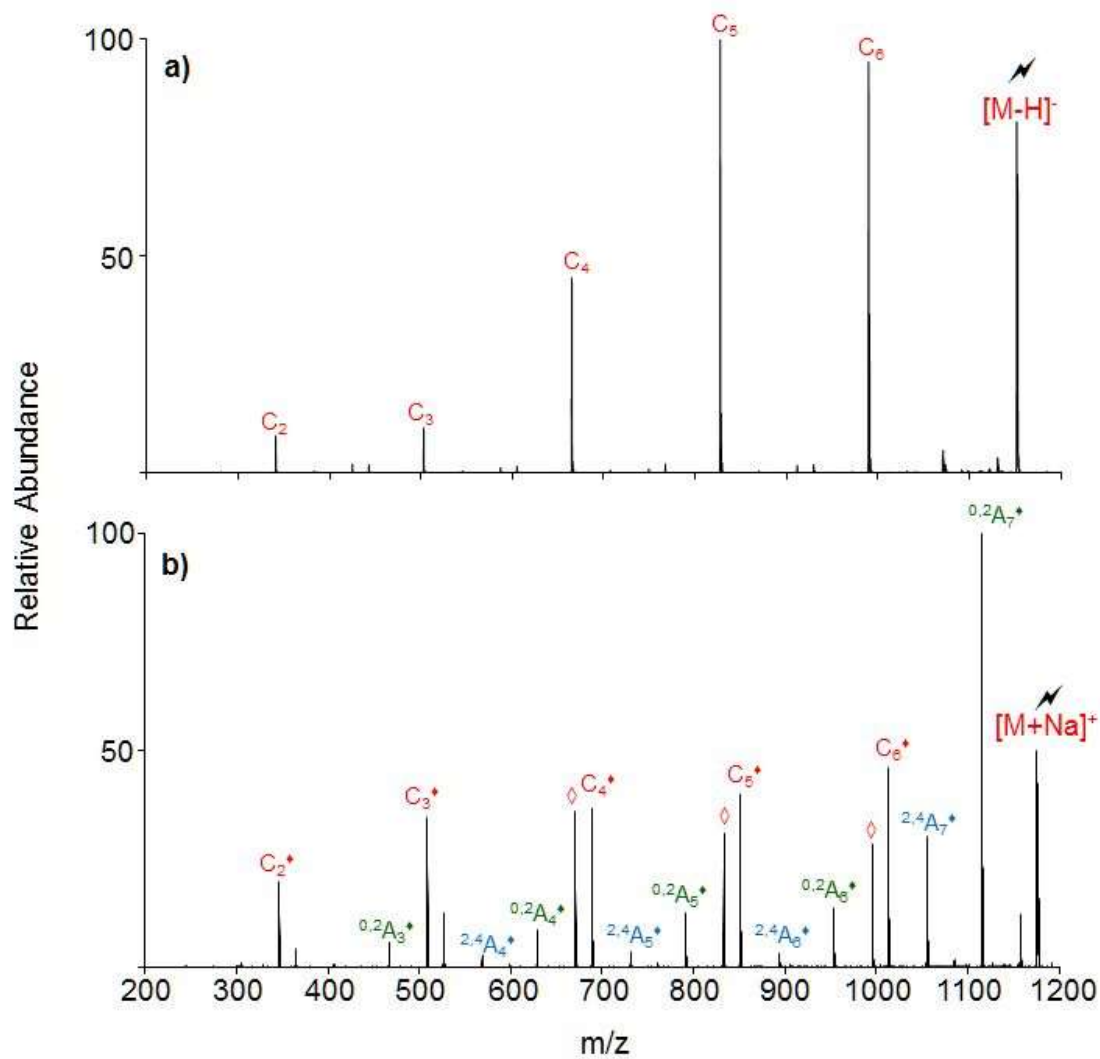


Figure 2.12 Ion trap CID spectra for a) [Maltoheptaose-H]⁻ and b) [Maltoheptaose+Na]⁺ (Filled diamonds indicates fragment containing Na⁺ and hollow diamonds are water losses from C ions).

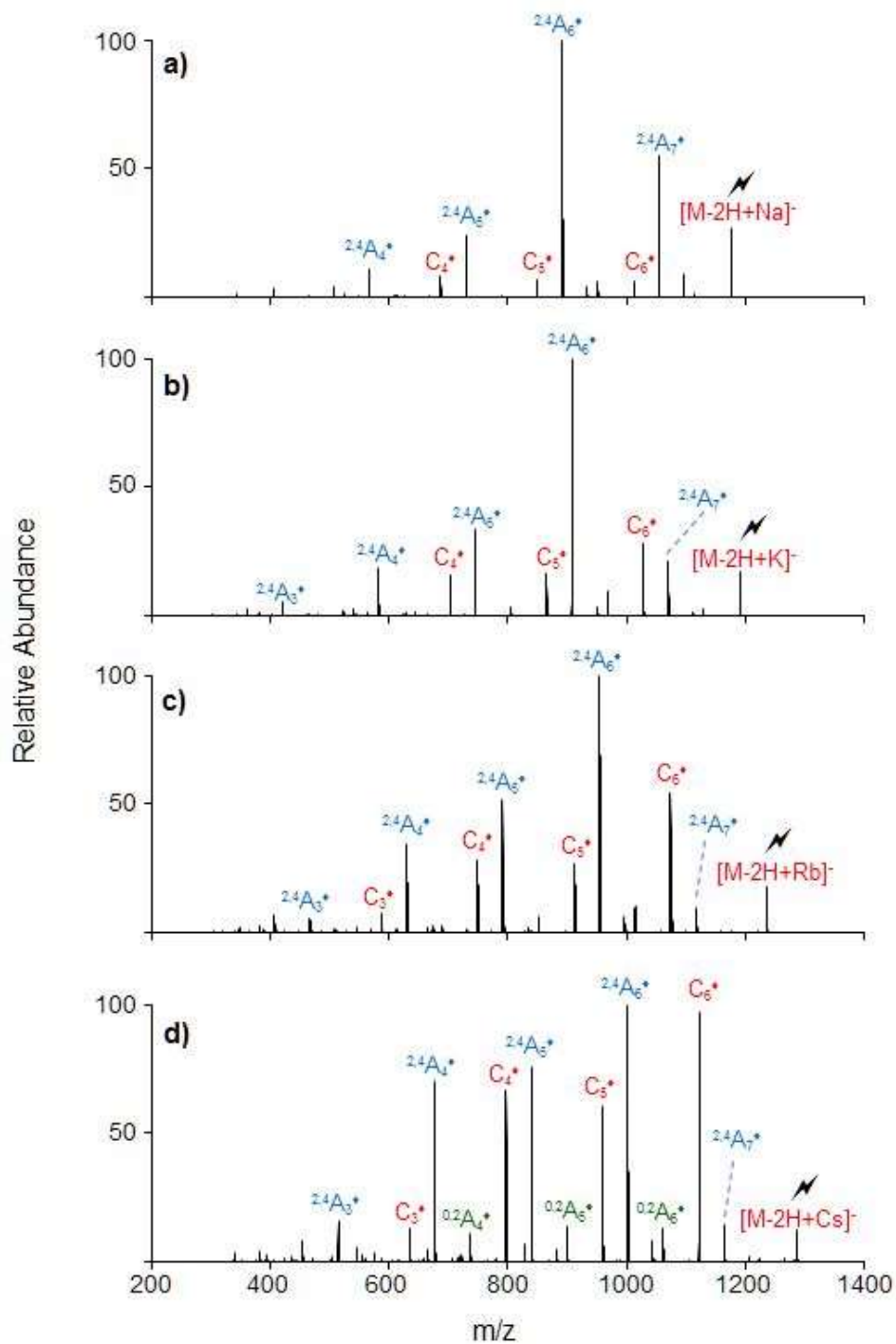


Figure 2.13 Ion trap CID spectra for electrostatic complexes formed between maltoheptaose and a) Na⁺, b) K⁺, c) Rb⁺, and d) Cs⁺ (Filled diamonds indicates fragment containing the metal cation).

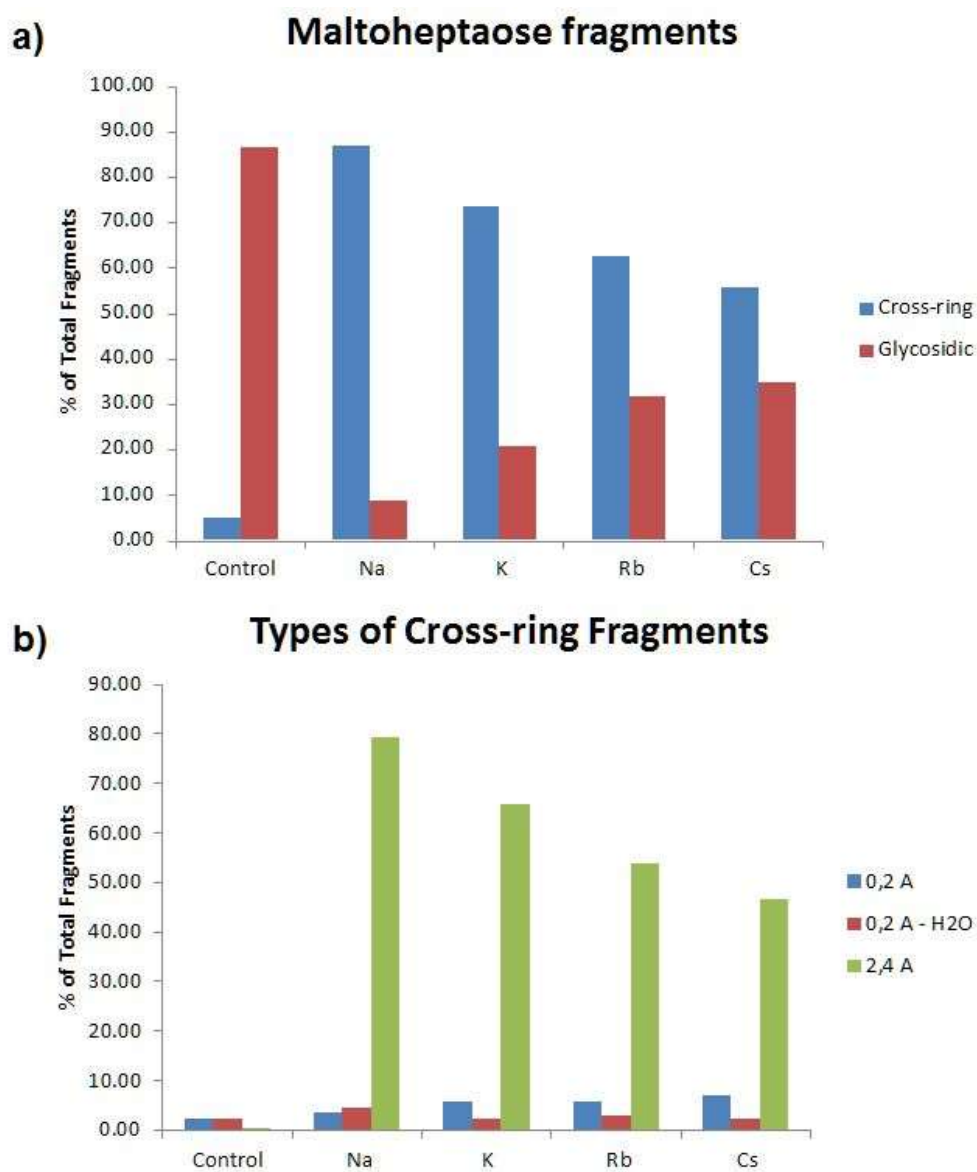


Figure 2.14 Comparison of cross-ring and glycosidic fragment peak areas as a percentage of all fragments present. b) Comparison of the types of cross-ring fragments that is present.

CHAPTER 3. ION/ION CHARGE INVERSION/ATTACHMENT IN CONJUNCTION WITH DIPOLAR DC COLLISIONAL ACTIVATION AS A SELECTIVE SCREEN FOR SULFO- AND PHOSHOPEPTIDES

A version of this chapter has been published in the International Journal of Mass Spectrometry Copyright © 2019 Elsevier B.V and approval has been granted to adapt that publication for this chapter.

3.1 Introduction

Protein post-translational modifications (PTMs) increase the functional diversity as well as the overall complexity of the proteome. Phosphorylation is one of the most abundant PTMs present in proteomes with as much as a third of eukaryotic proteins estimated to be phosphorylated. [1] Phosphorylation plays a central role in signaling and regulatory process and, as a result, phosphoproteomics is widely practiced. [2, 3] A common phosphoproteomics strategy involves a bottom-up work flow that relies on enrichment and/or separation using liquid chromatography and structural characterization via tandem mass spectrometry (MS/MS) techniques. [4] Enrichment prior to analysis is typically used, as phosphorylation is a low stoichiometry modification and must be separated from the high backgrounds of non-phosphorylated peptides. Enrichment strategies such as immobilized metal affinity chromatography (IMAC) and metal oxide affinity chromatography (MOAC) are common metal-based affinity chromatography methods. Evaluation of other affinity materials, such as amine-based species, is also being undertaken but traditional metal-based affinity chromatography remain dominant. [5]

Phosphopeptide analyses typically involve positive ionization in conjunction with MS/MS using one or more activation methods. Collision induced dissociation (CID) remains the

most popular activation method for peptide sequencing, based partly on its widespread availability, but is ill-suited for phosphopeptide analysis due to the lability of the phosphate bond, which often leads to loss of the PTM. [6] This is particularly problematic with ion trap CID and somewhat less so with beam-type CID and higher energy collisional activation (HCD), the latter of which tend to lead to greater contributions from amide bond cleavages. [7] Electron-based activation methods, such as electron transfer dissociation (ETD) and electron capture dissociation (ECD) preserve PTMs on peptides while cleaving the N-C α bond to form c- and z-type ions allowing determination of the PTM location. [8, 9] Negative mode ESI holds potential for phosphopeptide analysis as the presence of the acidic phosphate group facilitates efficient ionization in the negative mode. [10] However, similar issues with slow heating methods, such as ion trap CID, prevail in the negative mode where the PTMs are first lost upon dissociation. Alternative activation strategies for negative mode structure determination of phosphopeptides, such as negative electron transfer dissociation (nETD) and electron detachment dissociation (EDD), have since been described and applied. [11, 12]

Sulfonation is another PTM that appears in the proteome, although at a lesser abundance compared to phosphorylation and is less extensively studied. Sulfonation primarily appears at tyrosine whereas phosphorylation primarily occurs at tyrosine, serine, and threonine. Tyrosine sulfonation is present in secretory and transmembrane proteins and has been shown to play a role in modulating extracellular protein-protein interactions for a variety of physiological and pathogenic responses. [13, 14] Sulfoproteomics research is hampered by the lack of an effective enrichment method and difficulties in distinguishing sulfopeptides from phosphopeptides in the mass spectrometer. Metal based IMAC methods have been applied for enrichment of sulfopeptides but lack the specificity that has been shown for phosphopeptides. [15] Application

of novel antibodies for sulfopeptide enrichment has shown remarkable specificity for sulfotyrosine peptides and discrimination from phosphopeptides as well as sulfated glycans. [16] However, antibody enrichment has not been broadly adapted due to costs and concerns about their structural stability. Weak anion exchange chromatography has also been used for enrichment of sulfopeptides but modifications at the primary amines are required for better specificity. [17, 18]

The mass changes associated with sulfonation and phosphorylation are isobaric with the mass difference being only 9.5 mDa. Unless equipped with high resolution/high mass measurement accuracy mass spectrometers, such as an Orbitrap or FT-ICR, it can be challenging to distinguish between a given peptide that is either phosphorylated or sulfonated on the basis of mass. Both forms of modified peptide fragment similarly using low energy CID where major isobaric neutral losses occur (i.e., nominal losses of 80 Da (SO_3 or HPO_3) or -98 Da (H_2SO_4 or H_3PO_4)). While research has been done in comparing the spectra of ions derived from sulfopeptides and phosphopeptides under a variety of activation conditions, unless there is a comprehensive spectral library of sulfopeptides vs. phosphopeptides it remains challenging to distinguish a sulfopeptide from a phosphopeptide on the basis of fragmentation. [19]

We have investigated gas-phase charge inversion reactions via ion/ion chemistry as means for addressing measurement challenges in mass spectrometry. For example, we demonstrated charge-inversion reactions applied to ions derived from precipitated blood plasma to result in a 200-fold improvement in signal-to-noise ratio due to a significant reduction in chemical noise. [20] Charge-inversion has also been used to separate isomeric phosphatidylethanolamine and phosphatidylcholine lipids [21] as well as to facilitate location of double bonds in unsaturated fatty acids. [22] Here we present another gas-phase ion/ion charge-

inversion technique that allows for the distinction of phospho- and sulfopeptides from unmodified peptides as well as from each other. Research has demonstrated a relatively strong noncovalent interaction between guanidinium and phosphate and sulfate groups in both solution and in the gas phase. [23-26] Histidine interactions with acidic sites have also been studied and found to be somewhat weaker than those of guanidinium. [27] We seek to exploit the differences in the strengths of electrostatic interactions between guanidinium and deprotonated acidic sites (i.e., carboxylate vs. phosph(on)ate vs. sulf(on)ate) in the context of ion/ion reactions. Ion/ion reactions are induced between singly-charged peptide anion mixtures and a guanidinium containing peptide dication. The resulting cationic peptide complex is then subjected to a broadband collisional activation using dipolar DC (DDC). [28] The binding strength between the two peptides in the long-lived complex is dependent upon specific functional group interactions such that the complex stabilities are composition-dependent. This allows DDC to serve as an ‘energy filter’ to assist in the distinction of the functional groups involved in binding. We demonstrate this approach with model phosphopeptides and a sulfopeptide in both a simple mixture and a more complex mixture of tryptic ubiquitin peptides spiked with a phosphopeptide.

3.2 Experimental Section.

3.2.1 Materials.

Peptides YGGFL, GAIDDL, NVVQIY, pSGGFL, pTGGFL, pYGGFL, and sYGGFL were custom synthesized by Biomatik (Wilmington, DE, USA). The custom peptides AAARAAARA, and RKRARKA were synthesized by NeoBioLab (Cambridge, MA, USA). Water, Optima™ LC/MS Grade, was purchased from Fisher Scientific (Pittsburgh, PA, USA). Ubiquitin from bovine erythrocytes and trypsin from bovine pancreas were purchased from Sigma-Aldrich (St. Louis, MO, USA). All solutions for nanoelectrospray (nESI), using

capillaries pulled to tip diameter 3-4 μm , were prepared in an aqueous solution at an initial concentration of ~ 1 mg/ml and diluted to desired concentration before use. The final concentration of each peptide in the peptide mixtures in aqueous solution is between 3 μM and 30 μM .

3.2.2 Trypsin Digestion.

Approximately 1 mg of ubiquitin was dissolved in 500 μL of 50 mM NH_4HCO_3 . A trypsin solution of 1 mg/mL was added to the protein solution at a 1:40 mass ratio. The solution was incubated at 37 $^\circ\text{C}$ for 12 hours before evaporated to dryness using a vacuum centrifuge. The resulting product was reconstituted in 500 μL water.

3.2.3 N-terminal Acetylation.

Approximately 0.5 mg of peptide was dissolved in 250 μL water before 15 μL of 5 mM pH 6-7 borate buffer and 20 μL of acetic anhydride were added. The solution was left at room temperature and allowed to react for 2 hours before quenching the reaction with 2 μL glacial acetic acid. The resulting solution was evaporated to dryness using a vacuum centrifuge before being reconstituted in 500 μL water.

3.2.4 Mass Spectrometry.

All experiments were performed on a TripleTOF 5600 mass spectrometer (SCIEX, Concord, ON, Canada) modified for ion/ion reactions and dipolar DC (DDC), in analogy with a previously described Q-TOF instrument. [29, 30] Both reagent and analyte ions were formed via nano-electrospray emitters placed before the inlet aperture of the atmosphere vacuum interface. Cations and anions were formed alternately by pulsing the respective electrospray emitters. [31] For ion/ion reactions, the doubly protonated reagent was isolated by Q1 and accumulated in the

q2 reaction cell before the negatively charged analyte ions were generated and introduced into q2. The oppositely charged ions were allowed to react within q2 for 20 ms. After mutual storage, a ramped ion trap resonance ejection scan was performed to eject remaining reagent and proton transfer products thereby leaving only the complex ions within q2. In the experiments associated with Figures 3.2-3.4, a subsequent dipolar DC (DDC) excitation at a fixed amplitude was applied for 200 ms when the q2 RF voltage is set to be 250 m/z at a q value of 0.908 (i.e., low-mass cutoff = m/z 250) for broadband activation of the isolated complexes

3.2.5 Dipolar DC Dissociation Kinetics

The rates of complex ion dissociation follow pseudo first order kinetics under DDC conditions, as indicated in Equation 1. [28, 32-34]

$$[M]_t = e^{-k_{diss}t} \quad (1)$$

where $[M]_t$ is the molar fraction of the complex at time t , and k_{diss} is the pseudo-dissociation rate of the ion. The molar fraction of the complex is calculated as the ratio of complex ion's abundance over the abundance of all ions present. Complex ion dissociation kinetics were determined at a fixed RF amplitude (low-mass cutoff = m/z 250) as a function of dipolar DC amplitude. For a given DC and RF amplitude, the dissociation rate for a complex ion is determined from fitting the data to Equation 2:

$$\ln\left(\frac{[M]_t}{[M]_t + [Fragment]_t}\right) = -k_{diss}t \quad (2)$$

In all cases, the dominant fragment ion generated from DDC collisional activation of the complexes in this work was the protonated reagent. Error bars for k_{diss} correspond to the standard deviation from the linear fitting to Equation 2.

3.2.6 Density Functional Theory Calculations.

All optimizations and zero-point corrected energies (ZPE) were performed using the Gaussian 09 package [35] at the B3LYP/6-311++G(2d,p) level of theory. As the molecules are small, all structures were directly optimized in Gaussian 09. The anions and cations as well as their respective neutral forms were individually optimized for structure. The complex structure is a combination of the optimized anions and cations further subjected to optimizations.

3.3 Results and Discussion

The general approach for screening of mixtures of anionic peptides with carboxylate, phosph(on)ate, or sulf(on)ate charge bearing sites is summarized in Scheme 3.1.

The approach is based on reacting primarily singly-charged peptide anions with a doubly-charged cationic reagent that contains at least one arginine residue or, in this work, two protonated arginine residues. Of all the basic residues of the common amino acids, arginine has the highest proton affinity [36, 37] and engages in the strongest electrostatic interactions with anionic sites. Reagent dications with arginine residues are therefore more likely to react with anions to yield a complex ion, rather than undergo proton transfer. It is also advantageous for the reagent cation to be relatively large, which increases the cross-section for intimate collision. The first step of the process is therefore intended to generate singly positively charged complexes comprised of the analyte anions attached to the doubly protonated reagent. The most weakly-bound complexes can be preferentially fragmented by the judicious choice of dipolar DC amplitude while the more strongly-bound complexes survive. Provided there is a sufficiently large difference between the binding strengths associated with the different anionic charge sites, the dipolar DC conditions can be used to distinguish between the types of anionic peptides. We show below that, according to DFT calculation, complex stability based on the electrostatic

interaction between a guanidinium moiety (e.g., a protonated arginine residue) and a deprotonated site increase in the order carboxylate<phosph(on)ate<sulf(on)ate. We then demonstrate that dipolar DC conditions can be established that are able to distinguish phospho- and sulfopeptides from unmodified peptides and from one another.

3.3.1 Density Functional Theory Calculations of Guanidinium Interaction.

The key characteristic of interest here is the gas-phase binding strength between the negatively charged peptide analytes and the positively charged dicationic reagent. Acid-base chemistry generally dominates in electrospray ionization such that excess protons are localized on the most basic sites of a peptide, such as the N-terminus or lysine, arginine, and histidine side-chains, in positive ion mode and at acidic sites, such as the C-terminus or aspartic, and glutamic acid side-chains, in negative ion mode. That logic can be further extended in the presence of PTMs such as phosphorylation and sulfonation. Phosphate and sulfate groups have a lower pKa values than carboxylate groups, which makes them more likely to be the charge site when ionized in the negative mode. Hence, a carboxylate group is likely to be the moiety involved in the interaction with a cationic reagent for unmodified peptides whereas for the phosphopeptides and sulfopeptides the charge site will be at the phosphate or sulfate groups, respectively. Density functional calculations were used to quantify the binding strength between the different types of negatively charged (i.e. carboxylate, sulfonate, phosphonate) and positively charged (i.e. primary amine, imidazole, guanidinium) chemical groups in the context of ion/ion reactions. A generic Brauman-type energy diagram (i.e., reactants shown from the left, products shown on the right, intermediate shown in the middle) for doubly protonated reagent and a singly deprotonated analyte proceeding via a long-lived complex is shown in Figure 3.1(a). A more detailed analysis of energy surfaces for ion/ion reactions has been previously discussed. [34] In this case, reactions

that proceed through a relatively long-lived intermediate (i.e., a complex) are of particular interest. (Proton transfer at a crossing point without formation of a complex is possible at large impact parameters and is minimized when the physical cross-sections of the reactants are large. [34]) Complex formation is always thermodynamically favorable in this type of reaction by roughly 100 kcal/mol per pair of opposite charges. The lowest energy exit channel from the complex involves proton transfer to lead to a singly protonated product and a neutral product. The barrier to proton transfer from the complex is largely determined by the strength of the electrostatic interaction between the relevant protonated and deprotonated sites. The calculated energy barriers for proton transfer from a basic group cation to each of the three anionic groups of interest are listed in the table of Figure 3.1(b). The energies calculated via DFT shown in the table are the difference between the zero-point corrected energies (ZPE) of the complex and the sum of the two neutrals after proton transfer has occurred. (Reverse critical energies for proton transfer reactions are typically small and are expected to largely cancel so that the calculated values here are expected to be suitable for comparisons.) The calculations clearly show that interaction strength between guanidinium and the various negative charge sites follow the order sulf(on)ate>phosph(on)ate>carboxylate. For a given anionic site, the binding strengths for the cationic sites follows the order guanidinium>imidazole>primary amine. The energy-minimized structures of the complexes formed between the various cations and anions are provided in Figures 3.7-3.13. (Protonated imidazole/carboxylate and protonated methylamine/carboxylate complexes were not found to be lower in energy than the proton transfer products and are therefore not shown in Supplemental Information.)

3.3.2 Complex Formation and DDC for Phosphopeptides vs. Unmodified Peptides.

Model phosphopeptides, pSGGFL, pTGGFL, and pYGGFL, as well as a variety of other small model peptides of similar size, YGGFL, GAIDDL, and NVVQIY, were used to evaluate the relative stabilities of complexes formed with a doubly protonated reagent with two arginine residues. Mass spectra of this peptide mixture in both positive mode and negative mode nESI are shown in Figures 3.2(a) and (b), respectively. In the positive mode spectrum, signals from the phosphopeptides are essentially absent as only the protonated and sodiated versions of unmodified peptides are present. In contrast, the three phosphopeptides give rise to strong signals in the negative ion mode. Ion/ion reaction between the negatively charged peptides and doubly-protonated AAARAAARA formed a long-lived stable complex with 1+ charge that was detected in the positive mode, as shown in Figure 3.2(c). (Residual reagent cations as well as singly-protonated AAARAAARA generated via proton transfer were ejected by a resonance ejection ramp prior to mass analysis in generating Figure 3.2(c). The complete spectrum prior to the voltage sweep is shown in Figure 3.14.) It is clear from a comparison of the relative abundances of the peptide anions (Figure 3.2(a)) with the relative abundances of the complexes observed in Figure 3.2(c) that the relative propensities for stable complex formation are peptide anion dependent. Stable complex formation competes with proton transfer at a crossing on the energy surface (without complex formation) and proton transfer via break-up of an initially formed complex. [33] The likelihood for the initial formation of a long-lived complex increases with the physical sizes of the reactants (i.e., a larger analyte anion and a larger reagent increase the relative likelihood for a ‘sticky’ collision between the reactants). The relative likelihood for the survival of the initially formed complex, which leads to the observation of a stable complex, is related, in part, to the binding strength in the complex. The factors of peptide anion size and the strengths of the interactions in the complex largely determine the changes in relative abundances

in Figures 3.2(a) and 3.2(c). Based on the calculations discussed above, the binding strengths of the phosphopeptide complexes are expected to be significantly greater than those involving unmodified peptides. The selective dissociation of the more weakly-bound complexes can be effected via dipolar DDC collisional activation. DDC is a broad-band collisional activation technique that provides a roughly uniform degree of excitation across a wide range of masses. [27, 31, 32] As shown in Figure 3.2(d), a DDC amplitude of 22 V applied for 200 ms leads to the dissociation of essentially all of the complexes comprised of the unmodified peptides while prominent signals from the phosphopeptide-containing complexes remain. The resulting spectrum provides an illustration for how phosphopeptide anions can be distinguished from unmodified peptide anion via ion/ion complex formation and DDC collisional activation.

Application of this approach to a more complex sample containing phosphopeptides was also performed. Peptides derived from tryptic digestion of ubiquitin along with phosphopeptides spiked into solution were subjected to analysis. In the positive mode (see Figure 3.15), very little indication of the presence of the phosphopeptides is apparent while prominent signals are present in the negative mode spectrum (Figure 3.3(a)). Applying the charge inversion DDC process to the mixture highlights the phosphopeptide anions (Figure 3.3(b)). It is worthy of note that doubly- and triply-deprotonated TITLEVEPSDTIENVK ions, one of the ubiquitin tryptic peptides, are prominent in Figure 3.3(a). The doubly-deprotonated ion would be neutralized as a result of complex formation and the triply-deprotonated species would form a negatively charged complex. Therefore, evidence for this peptide would not be expected via a single ion/ion reaction. However, there are several pathways for generating cations with this peptide via two ion/ion reactions, such as a single proton transfer to the di-anion followed by reagent cation

attachment. However, there is no evidence that any TITLEVEPSDTIENVK-containing cations survived the DDC experiment associated with Figure 3.3(b).

3.3.3 Complex Formation and DDC for Phosphopeptides vs. Sulfopeptides.

Substituting sYGGFL for pYGGFL in the model peptide mixture of Figure 3.2 and repeating the ion/ion reaction experiment showed that the reagent cation formed a stable complex with the sulfopeptide in analogy with the phosphopeptides (see Figure 3.4(a)). Application of 22 V DDC, as above, resulted in the survival of only the phosphopeptide and sulfopeptide complexes. Application of 25 V DDC for the same time (200 ms) resulted in the disappearance of almost all of the phosphopeptide complexes while retaining a significant fraction of the sulfopeptide containing complexes. This result is consistent with the expectation that the stronger binding for sulf(on)ate relative to phosph(on)ate to guanidinium, as predicted by the DFT calculations, leads to more stable electrostatic complexes. The differences in binding strengths for the three anionic sites discussed here suggests that the amplitude of DDC applied to complexes generated in reaction with guanidinium-containing reagents can be used to distinguish between unmodified peptides and modified peptides at intermediate values and between phosphopeptides and sulfopeptides at higher DDC values.

3.3.4 Effect of Histidine Residue

From Figure 3.1 it was found that the imidazole chemical group has a similar large binding strength energy difference between phosphate and sulfate in comparison to guanidinium. The initial energy step difference between carboxylate and phosphate as well as the binding energy between imidazole and phosphate is a source of concern for the effective differentiation between carboxylates and phosphates. Evaluation of histidine in its effectiveness for phospho- and sulfopeptide differentiation was performed with the doubly charged $[\text{HAHAHAA}+2\text{H}]^{2+}$

peptide reagent, shown in Figure 3.5. The post ion/ion reaction spectrum, Figure 3.5b, illustrates similar effects of HAHAAHAA with sulfopeptide sYGGFL where the complex formed after ion/ion reaction is extremely high in abundance compared to AAARAAARA. The abundance of complex for the phosphopeptides, pTGGFL and pSGGFL, are lower compared to AAARAAA. This could well be due to the lower potential energy barrier between phosphate and imidazole from the calculations resulting in not all products forms are in the complex state and some proton transfer could occur, either from the initial ion/ion reaction step or subsequent proton transfer after complex formation. Activation of the resulting complexes with DDC at 19 V removed all traces of non-PTM complexes which is lower compared to AAARAAARA and is as expected based on the DFT calculations. Subsequent DDC activation at 21 V removed the phosphopeptide complexes leaving only the sulfopeptide complex intact, which is lower than the energy needed for AAARAAARA and is in accordance with calculations. Based on these set of results, imidazole containing peptide reagents have a fair strong affinity for sulfopeptides but the similar energy differences between carboxylates and phosphate make them as not selective for phosphopeptides. Also, the energy difference required for DDC to differentiate sulfopeptides from phosphopeptides is not as big compared to AAARAAARA which would be preferred to effectively differentiate the two based on binding strength energy.

3.3.5 DDC Dissociation kinetics

Differences in complex dissociation rates form the basis for the use of DDC to discriminate between different classes of anions (i.e., carboxylate, phosph(on)ate, sulf(on)ate). In order to evaluate reagents and conditions for optimal discrimination between anion classes, it is instructive to determine complex ion dissociation rates over a range of conditions. Figure 3.5(a) shows a series of kinetic plots at various DDC amplitudes for the complex formed from

deprotonated pYGGFL and doubly-protonated AAARAAARA. Examples of the kinetic spectra collected at 23 V DDC across various activation times are shown in Figure 3.16. Figure 3.5(b) summarizes the dissociation rates of the complexes formed from ion/ion reaction between doubly protonated AAARAAARA and deprotonated YGGFL, GAIDDL, pTGGFL, pSGGFL, pYGGFL, and sYGGFL. It is clear that the complexes of the unmodified peptides YGGFL and GAIDDL fragment at the lowest DDC amplitudes, which is consistent with the DFT calculations that show relatively weak interaction between guanidinium and carboxylate. With three acidic sites in GAIDDL, the opportunity for additional interactions in the complex likely underlies the requirement for higher DDC voltages to achieve dissociation rates similar to the complex with YGGFL. The complexes derived from three phosphopeptides show similar dissociation kinetics while the sulfopeptide complex requires significantly higher DDC voltages. Figure 3.5(b) shows why a DDC amplitude of 22 V is effective in destroying the complexes comprised of the unmodified peptides while the complexes of the modified peptides largely survive. Likewise, a DDC amplitude of 25 V is effective in destroying the complexes of the unmodified and phosphorylated peptides while the sulfopeptide complex remains intact.

The rate data of Figure 3.6 illustrate how the measurement of DDC kinetics can be used to evaluate the discriminatory value of a reagent cation. Figure 3.6(a), for example, summarizes the dissociation rate data obtained using doubly protonated RKRARKA as the reagent for deprotonated pYGGFL, pTGGFL, pSGGFL, and sYGGFL. For comparison, the rate data for the doubly-protonated AAARAAARA reagent are also provided. The more basic reagent (i.e., RKRARKA) leads to more stable complexes for all of the peptides, as reflected by the shift of the rate data to the right on the DDC amplitude scale. In the case of the phosphopeptides, the stability order changed from the pYGGFL/AAARAAARA complex being the most stable of the

three AAARAAARA complexes to being the least stable of the peptide/RKRARKA complexes. This observation highlights the importance of the additional interactions that are introduced by the incorporation of another arginine residue and two lysine residues. The sulfopeptide/RKRARKA complex was found to be significantly more stable than those of all of the phosphopeptides. However, the separation between the phosphopeptides and the sulfopeptide on the DDC scales was narrower with the RKRARKA reagent than with the AAARAAARA reagent. Overall, therefore, doubly-protonated AAARAAARA appears to be a more discriminatory reagent cation for phospho- versus sulfopeptides.

The comparison of Figure 3.6(a) suggests that interactions beyond those of a single guanidinium cation with a deprotonated acidic site can have a measureable effect on complex stability and can impact the discriminatory value of a doubly-protonated reagent for distinguishing between unmodified peptides and phospho- and sulfopeptides. Figure 3.6(b) compares DDC rate data for doubly-protonated AAARAAARA and N-terminally acetylated AAARAAARA to determine a possible role for the N-terminus in stabilizing the complexes with deprotonated pYGGFL, pSGGFL, and sYGGFL. Interestingly, neither of the tyrosine-containing peptide complexes showed a significant change in dissociation kinetics when the reagent peptide was N-terminally acetylated while the pSGGFL complex was observed to be less stable. This result suggests that the serine residue of pSGGFL interacts with the N-terminus in complexes with AAARAAARA more strongly than the tyrosine residues of pYGGFL and sYGGFL. It is beyond the scope of this work to examine all of the possible interactions that might take place in a complex formed between reagent and analyte polypeptides. In any case, in order to maximize the contribution from the targeted guanidinium/deprotonated acid interaction to the overall binding strength of the complex, it is desirable to minimize the possibility for other strong non-

covalent interactions. Along these lines, competition between fragmentation of covalent bonds and cleavage of the phosphate-guanidinium bond in some peptide complexes has been noted under low energy collision conditions, [26, 38] as has intermolecular phosphate transfer between complex components [39,40]. No evidence for such processes for either the phospho- or sulfo-peptides was observed in the DDC step in this work but these possibilities should be recognized when examining other reagent/peptide combinations.

3.4 Conclusions

This work provides proof-of-concept for an ion/ion reaction approach to distinguishing between unmodified, phosphorylated, and sulfated peptides. The basis for discrimination is the relative strengths of interaction between guanidinium and carboxylate, phosph(on)ate, and sulf(on)ate in the gas phase. The relative strengths of the electrostatic interactions between guanidinium and conjugate bases of the relevant acidic sites, determined by DFT calculations and supported experimentally, increase in the order carboxylate < phosph(on)ate < sulf(on)ate. The interaction is generated by reacting a doubly protonated reagent peptide with at least two arginine residues with singly deprotonated peptides in the gas phase to form a long-lived complex. The relative stabilities of the complexes are probed via dipolar DC (DDC) collisional activation, a broad-band collisional excitation technique. With an appropriately selected DDC amplitude and time, it was shown to be possible to fragment a large majority of complexes comprised of unmodified peptide anions while retaining large fractions of complexes comprised of phosphopeptides and sulfopeptides. Likewise, at a higher DDC amplitude, it was possible to fragment a large majority of phosphopeptide complexes while preserving a large fraction of the sulfopeptide complexes. The discriminatory value of the reagent and DDC conditions is readily apparent from dissociation kinetics experiments that provide dissociation rates as a function of

DDC amplitude for a fixed RF amplitude. Such data point to DDC conditions that provide the greatest degree of discrimination between anion types and are useful in evaluating reagent cations used to generate complexes. The results shown here highlight the roles that non-covalent interactions other than the guanidinium-anion interaction can affect complex ion stabilities. To maximize the role of the guanidinium interaction and to avoid other interactions that may vary with the analyte ion sequence/composition, it is desirable to minimize the presence of polar groups other than the arginine residues.

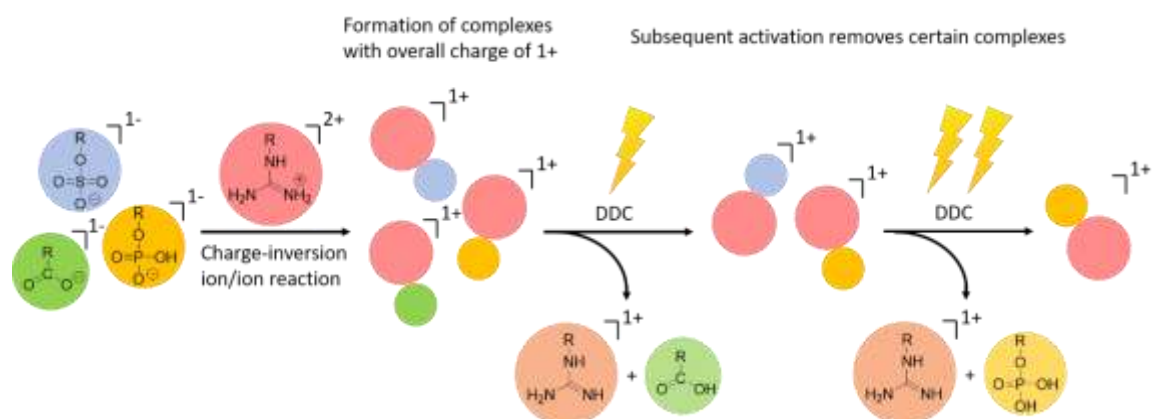
3.5 References

- [1] P. Cohen, The regulation of protein function by multisite phosphorylation – a 25 year update, *Trends in Biochemical Sciences*, 25 (2000) 596-601.
- [2] J.A. Ubersax, J.E. Ferrell, Jr., Mechanisms of specificity in protein phosphorylation, *Nature reviews. Molecular cell biology*, 8 (2007) 530-541.
- [3] P. Cohen, The origins of protein phosphorylation, *Nat Cell Biol*, 4 (2002) E127-130.
- [4] N.M. Riley, J.J. Coon, Phosphoproteomics in the Age of Rapid and Deep Proteome Profiling, *Anal Chem*, 88 (2016) 74-94.
- [5] Z.G. Wang, N. Lv, W.Z. Bi, J.L. Zhang, J.Z. Ni, Development of the affinity materials for phosphorylated proteins/peptides enrichment in phosphoproteomics analysis, *ACS Appl Mater Interfaces*, 7 (2015) 8377-8392.
- [6] J.S. Brodbelt, Ion Activation Methods for Peptides and Proteins, *Anal Chem*, 88 (2016) 30-51.
- [7] M.P. Jedrychowski, E.L. Huttlin, W. Haas, M.E. Sowa, R. Rad, S.P. Gygi, Evaluation of HCD- and CID-type fragmentation within their respective detection platforms for murine phosphoproteomics, *Mol Cell Proteomics*, 10 (2011) M111 009910.
- [8] A. Chi, C. Huttenhower, L.Y. Geer, J.J. Coon, J.E. Syka, D.L. Bai, J. Shabanowitz, D.J. Burke, O.G. Troyanskaya, D.F. Hunt, Analysis of phosphorylation sites on proteins from *Saccharomyces cerevisiae* by electron transfer dissociation (ETD) mass spectrometry, *Proceedings of the National Academy of Sciences of the United States of America*, 104 (2007) 2193-2198.

- [9] A. Stensballe, O.N. Jensen, J.V. Olsen, K.F. Haselmann, R.A. Zubarev, Electron capture dissociation of singly and multiply phosphorylated peptides, *Rapid communications in mass spectrometry : RCM*, 14 (2000) 1793-1800.
- [10] J.W. Flora, D.C. Muddiman, Selective, sensitive, and rapid phosphopeptide identification in enzymatic digests using ESI-FTICR-MS with infrared multiphoton dissociation, *Anal. Chem.* 73 (2001) 3305-3311.
- [11] B.A. Budnik, K.F. Haselmann, R.A. Zubarev, Electron detachment dissociation of peptide di-anions: an electron-hole recombination phenomenon, *Chemical Physics Letters*, 342 (2001) 299-302.
- [12] J.J. Coon, J. Shabanowitz, D.F. Hunt, J.E. Syka, Electron transfer dissociation of peptide anions, *J Am Soc Mass Spectrom*, 16 (2005) 880-882.
- [13] K.L. Moore, Protein tyrosine sulfation: a critical posttranslation modification in plants and animals, *Proceedings of the National Academy of Sciences of the United States of America*, 106 (2009) 14741-14742.
- [14] Y.S. Yang, C.C. Wang, B.H. Chen, Y.H. Hou, K.S. Hung, Y.C. Mao, Tyrosine sulfation as a protein post-translational modification, *Molecules*, 20 (2015) 2138-2164.
- [15] G. Demesa Balderrama, E.P. Meneses, L. Hernandez Orihuela, O. Villa Hernandez, R. Castro Franco, V. Pando Robles, C.V. Ferreira Batista, Analysis of sulfated peptides from the skin secretion of the *Pachymedusa dacinicolor* frog using IMAC-Ga enrichment and high-resolution mass spectrometry, *Rapid communications in mass spectrometry : RCM*, 25 (2011) 1017-1027.
- [16] A.J. Hoffhines, E. Damoc, K.G. Bridges, J.A. Leary, K.L. Moore, Detection and purification of tyrosine-sulfated proteins using a novel anti-sulfotyrosine monoclonal antibody, *The Journal of biological chemistry*, 281 (2006) 37877-37887.
- [17] Y. Amano, H. Shinohara, Y. Sakagami, Y. Matsubayashi, Ion-selective enrichment of tyrosine-sulfated peptides from complex protein digests, *Anal Biochem*, 346 (2005) 124-131.
- [18] M.R. Robinson, J.S. Brodbelt, Integrating Weak Anion Exchange and Ultraviolet Photodissociation Mass Spectrometry with Strategic Modulation of Peptide Basicity for the Enrichment of Sulfopeptides, *Anal Chem*, 88 (2016) 11037-11045.
- [19] G. Chen, Y. Zhang, J.C. Trinidad, C. Dann, 3rd, Distinguishing Sulfotyrosine Containing Peptides from their Phosphotyrosine Counterparts Using Mass Spectrometry, *J Am Soc Mass Spectrom*, 29 (2018) 455-462.

- [20] K.M. Hassell, Y. LeBlanc, S.A. McLuckey, Conversion of multiple analyte cation types to a single analyte anion type via ion/ion charge inversion, *The Analyst*, 134 (2009) 2262-2266.
- [21] S. Rojas-Betansourt, J.R. Stutzman, S.J. Blanksby, S.A. McLuckey, Gas-phase chemical separation of phosphatidylcholine and phosphatidylethanolamine cations via charge inversion ion/ion chemistry, *Anal. Chem.* 87 (2015) 11255-11262.
- [22] C.E. Randolph, D.J. Foreman, S.K. Betancourt, S.J. Blanksby, S.A. McLuckey, Gas-Phase Ion/Ion Reactions Involving Tris-Phenanthroline Alkaline Earth Metal Complexes as Charge Inversion Reagents for the Identification of Fatty Acids, *Anal Chem*, 90 (2018) 12861-12869.
- [23] K.A. Schug, W. Lindner, Noncovalent binding between guanidinium and anionic groups: focus on biological- and synthetic-based arginine/guanidinium interactions with phosph[on]ate and sulf[on]ate residues, *Chem Rev*, 105 (2005) 67-114.
- [24] S.N. Jackson, H.Y. Wang, A. Yergey, A.S. Woods, Phosphate stabilization of intermolecular interactions, *J Proteome Res*, 5 (2006) 122-126.
- [25] A.L. Patrick, N.C. Polfer, H₂SO₄ and SO₃ transfer reactions in a sulfopeptide-basic peptide complex, *Anal Chem*, 87 (2015) 9551-9554.
- [26] A.S. Woods, S.C. Moyer, S.N. Jackson, Amazing stability of phosphate-quaternary amine interactions, *J Proteome Res*, 7 (2008) 3423-3427.
- [27] L. Muller, S.N. Jackson, A.S. Woods, Histidine, the less interactive cousin of arginine, *Eur. J. Mass Spectrom.* 25 (2019) 212-218.
- [28] A.V. Tomachev, A.N. Vilkov, B. Bogdanov, L. Pasa-Tolic, C.D. Masselon, R.D. Smith, Collisional activation of ions in RF ion traps and ion guides: the effective ion temperature treatment, *J. Am. Soc. Mass Spectrom.* 15 (2004) 1616-1628.
- [29] Y. Xia, P.A. Chrisman, D.E. Erickson, J. Liu, X. Liang, F.A. Loundry, M.J. Yang, S.A. McLuckey, Implementation of ion/ion reaction in a quadrupole/time-of-flight tandem mass spectrometer, *Anal. Chem.* 78 (2006) 4146-4154.
- [30] I.K. Webb, F.A. Loundry, S.A. McLuckey, Implementation of dipolar direct current (DDC) collision-induced dissociation in storage and transmission modes on a quadrupole/time-of-flight tandem mass spectrometer, *Rapid communications in mass spectrometry : RCM*, 25 (2011) 2500-2510.
- [31] Y. Xia, X. Liang, S.A. McLuckey, Pulsed dual electrospray ionization for ion/ion reactions, *J. Am. Soc. Mass Spectrom.* 16 (2005) 1750-1756.

- [32] B.M. Prentice, R.E. Santini, S.A. McLuckey, Adaptation of a 3-D quadrupole iontrap for dipolar DC collisional activation, *J. Am. Soc. Mass Spectrom.* 22 (2011) 1486-1492.
- [33] B.S. Prentice, S.A. McLuckey, Dipolar DC collisional activation in a "stretched" 3-D ion trap: the effect of higher order fields on RF-heating, *J. Am. Soc. Mass Spectrom.* 23 (2012) 736-744.
- [34] J. Bu, C.M. Fisher, J.D. Gilbert, B.M. Prentice, S.A. McLuckey, Selective Covalent Chemistry via Gas-Phase Ion/ion Reactions: An Exploration of the Energy Surfaces Associated with N-Hydroxysuccinimide Ester Reagents and Primary Amines and Guanidine Groups, *J Am Soc Mass Spectrom.* 27 (2016) 1089-1098.
- [35] M.J. Frisch, G.W. Trucks, M.J. Frisch, G.W. Trucks, H.B. Schlegel, G.E. Scuseria, M.A. Robb, J.R. Cheeseman, G. Scalmani, V. Barone, B. Mennucci, G.A. Petersson, H. Nakatsuji, M. Caricato, X. Li, H.P. Hratchian, A.F. Izmaylov, J. Bloino, G. Zheng, J.L. Sonnenberg, M. Hada, M. Ehara, K. Toyota, R. Fukuda, J. Hasegawa, M. Ishida, T. Nakajima, Y. Honda, O. Kitao, H. Nakai, T. Vreven, J.A. Montgomery Jr., J.E. Peralta, F. Ogliaro, M. Bearpark, J.J. Heyd, E. Brothers, K.N. Kudin, V.N. Staroverov, R. Kobayashi, J. Normand, K. Raghavachari, A. Rendell, J.C. Burant, S.S. Iyengar, J. Tomasi, M. Cossi, N. Rega, J.M. Millam, M. Klene, J.E. Knox, J.B. Cross, V. Bakken, C. Adamo, J. Jaramillo, R. Gomperts, R.E. Stratmann, O. Yazyev, A.J. Austin, R. Cammi, C. Pomelli, J.W. Ochterski, R.L. Martin, K. Morokuma, V.G. Zakrzewski, G.A. Voth, P. Salvador, J.J. Dannenberg, S. Dapprich, A.D. Daniels, O. Farkas, J.B. Foresman, J.V. Ortiz, J. Cioslowski, D.J. Fox, Gaussian 09, Revision A.02, Gaussian, Inc., Wallingford, CT, 2009.
- [36] A.G. Harrison, The gas-phase basicities and proton affinities of amino acids and peptides, *Mass Spectrom. Rev.* 16 (1997) 201-217.
- [37] C. Bleiholder, S. Suhai, B. Paizs, Revising the proton affinity scale of the naturally occurring amino acids, *J. Am. Soc. Mass Spectrom.* 17 (2006) 1275-1281.
- [38] J. Laskin, Z. Yang, A.S. Woods, Competition between covalent and noncovalent bond cleavages in dissociation of phosphopeptide-amine complexes, *Phys. Chem. Chem. Phys.* 13 (2011) 6936-6946.
- [39] A.M. Palumbo, G.E. Reid, Evaluation of gas-phase rearrangement and competing fragmentation reactions on protein phosphorylation site assignment using collision induced dissociation MS/MS and MS³, *Anal. Chem.* 80(2008) 9735-9747.
- [40] M.-B. Gonzalez-Sanchez, F. Lanucara, G.E. Hardman, C.E. Eyers, Gas-phase intermolecular phosphate transfer within a phosphohistidine phosphopeptide dimer, *Int. J. Mass Spectrom.* 367 (2014) 28-34.



Scheme 3.1 Schematic depiction of the use of a guanidinium-containing dicationic reagent and dipolar DC collisional activation for the discrimination between carboxylate, phosph(on)ate, and sulf(on)ate containing peptide anions.

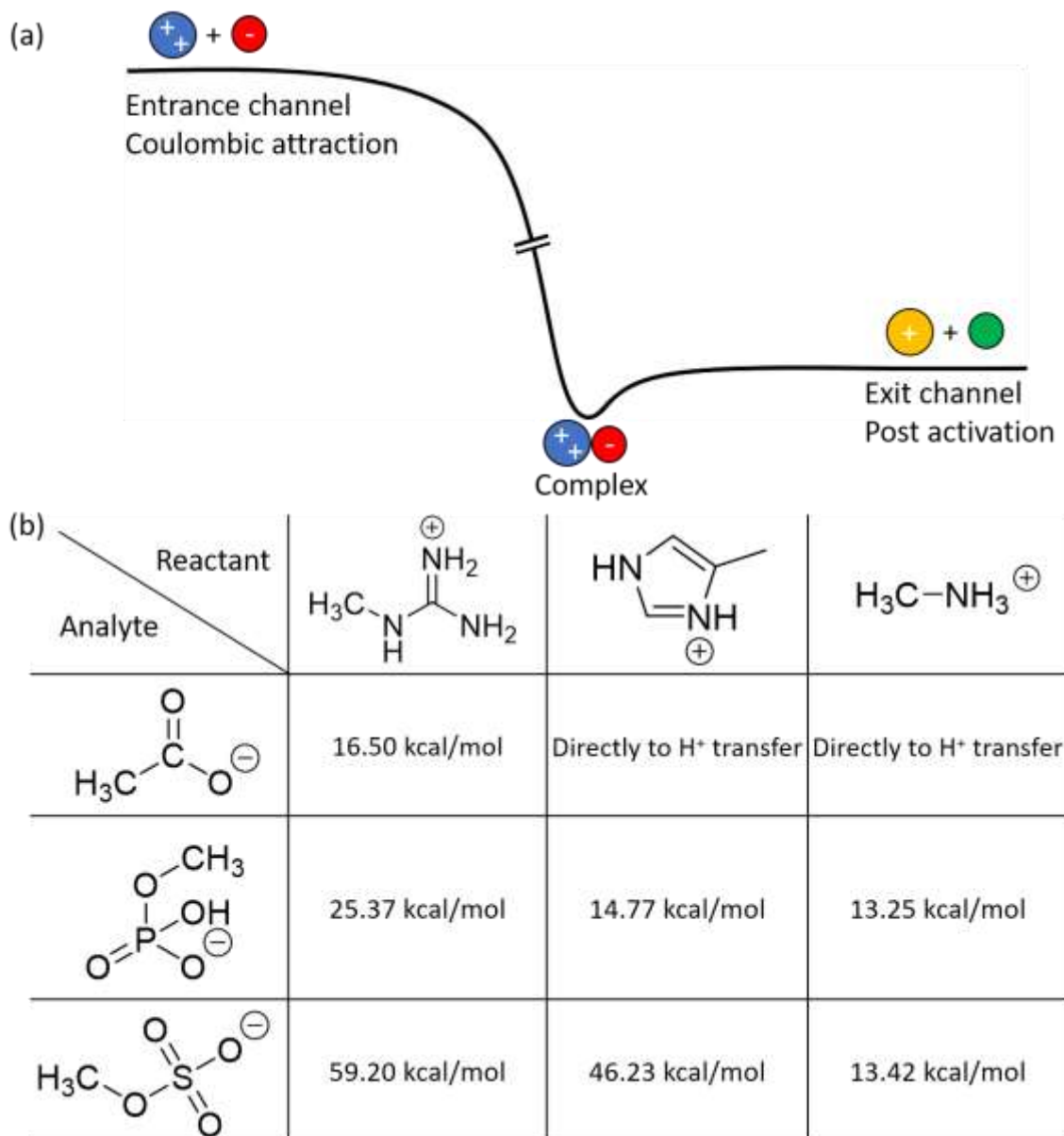


Figure 3.1 (a) A generic energy diagram for a proton transfer ion/ion reaction involving a doubly-protonated reagent (blue) and a singly-deprotonated analyte (red). The reactants undergo a long-range attraction due to the Coulombic potential and, if they undergo an intimate collision, form a relatively long-lived complex. The complex can break up spontaneously to yield charged (yellow) and neutral (green) proton transfer products or the complex can be stabilized via collisions and/or emission. (b) The interaction strength between three basic groups and three deprotonated acids calculated via DFT. The model is a simplified version where only the interaction between positively charged basic groups and the negatively charged acidic groups are probed. The binding strength is the zero-point corrected energy difference between the complex and the sum of the products after proton transfer.

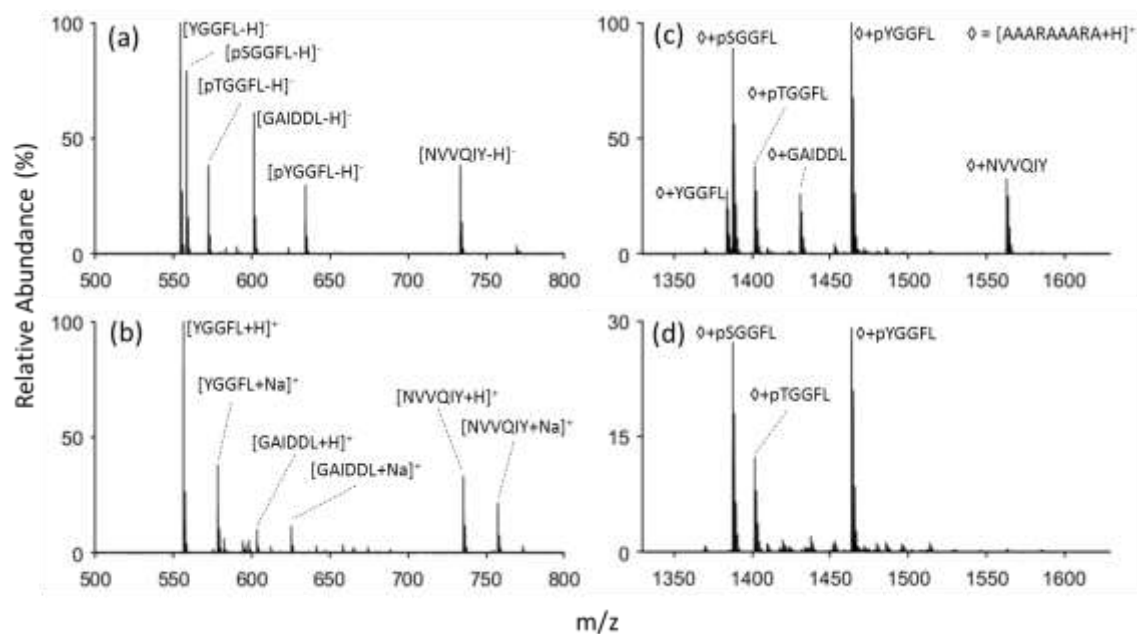


Figure 3.2 Nano-electrospray of six peptide mixture containing three phosphopeptides in (a) negative mode and (b) positive mode. Charge-inversion ion/ion reaction of the anionic peptide mixture with $[AAARAAARA+2H]^{2+}$ (c) with no DDC applied, and (d) DDC voltage of 22 volts applied.

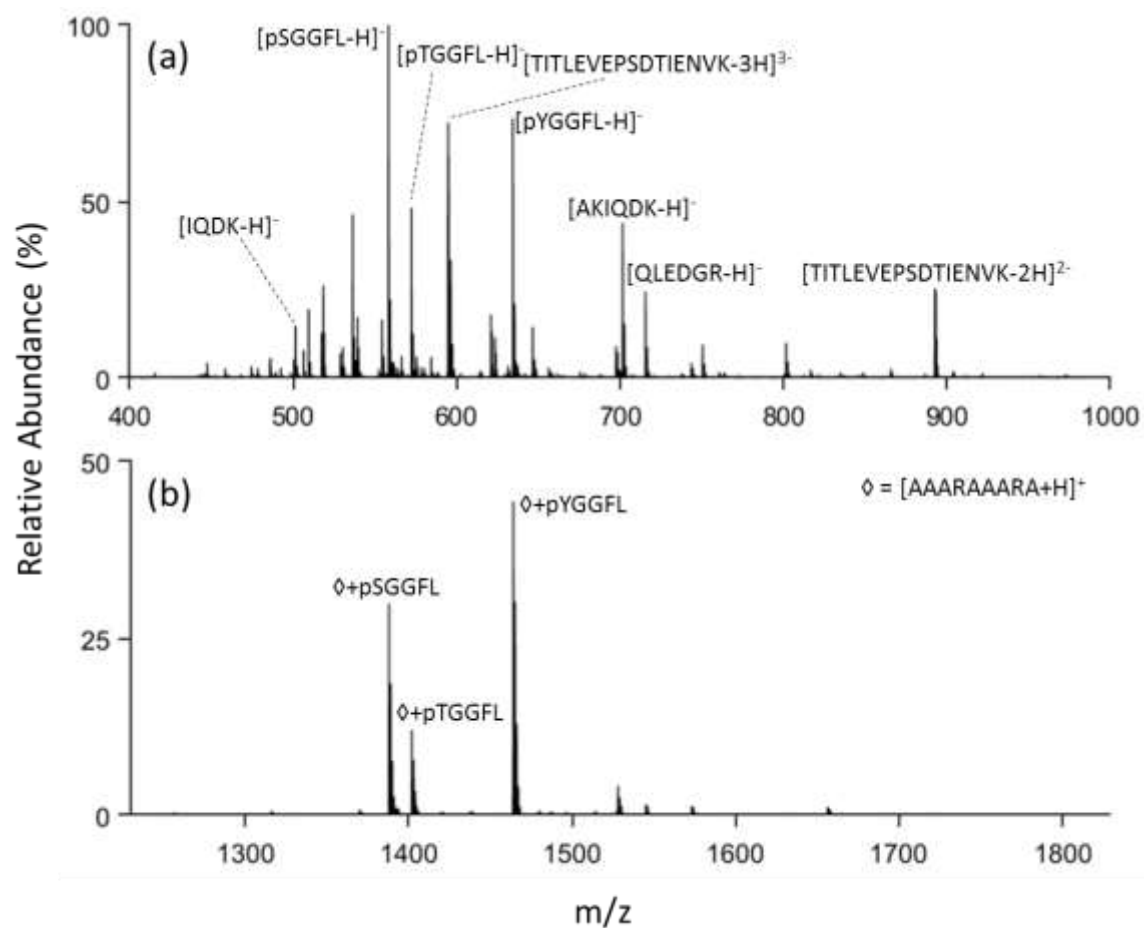


Figure 3.3 (a) Negative mode nanoelectrospray of trypsin digested ubiquitin with phosphopeptides pSGGFL, pTGGFL, and pYGGFL spiked in and (b) post ion/ion reaction with DDC at 22 V applied.

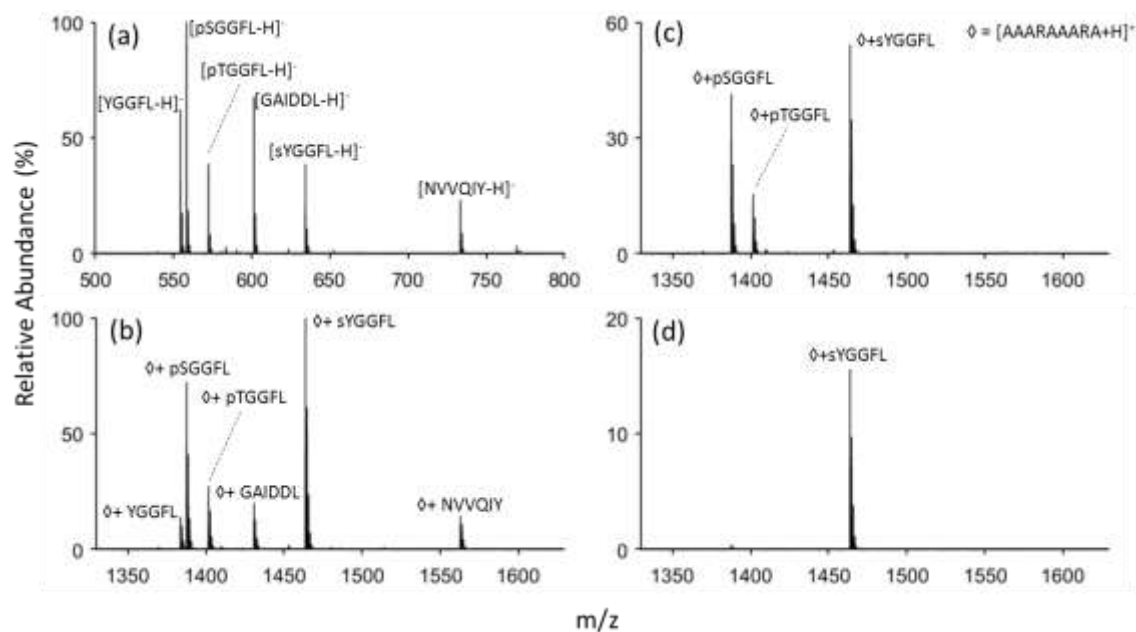


Figure 3.4 (a) Negative mode nanoelectrospray of a sulfopeptide, sYGGFL, two phosphopeptides, pTGGFL and pSGGFL, and three non-PTM peptides, YGGFL, GAIDDL, and NVVQIY. (b) Post-ion/ion reaction spectrum of the anionic peptide mixture with $[AAARAAARA+2H]^{2+}$ followed by (c) DDC using 22 V and (d) 25 V.

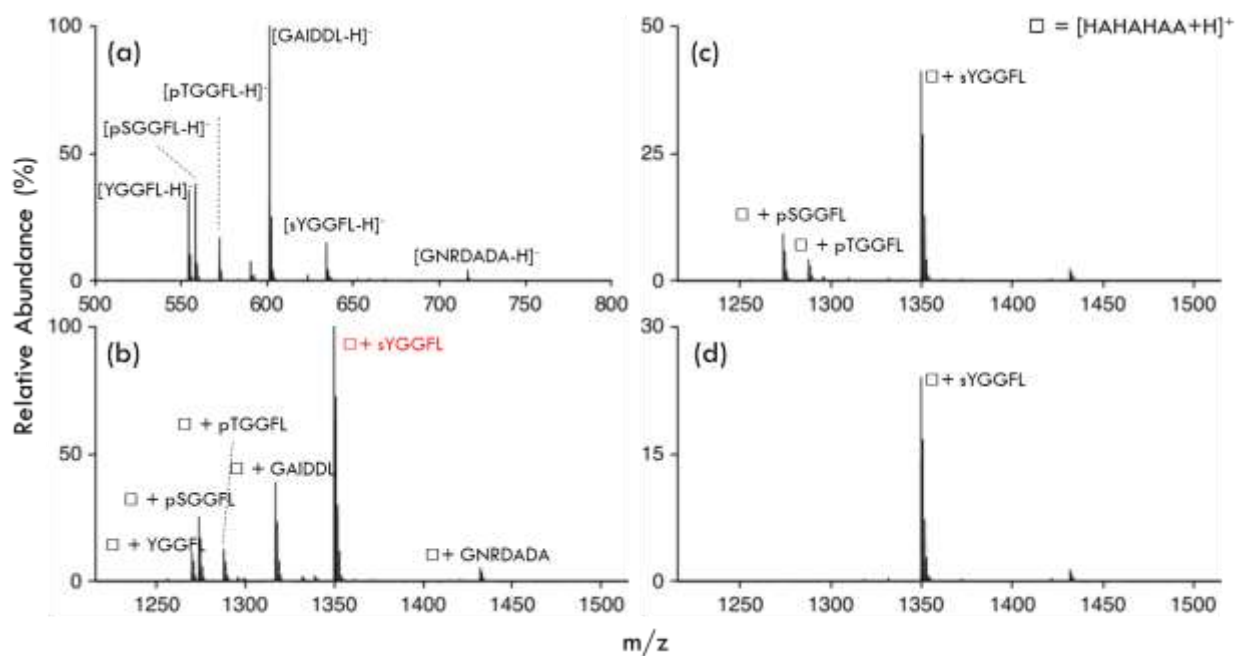


Figure 3.5 (a) Negative mode nanoelectrospray of a sulfopeptide, sYGGFL, two phosphopeptides, pTGGFL and pSGGFL, and three non-PTM peptides, YGGFL, GAIDDL, and GNRDADA. (b) Post-ion/ion reaction spectrum of the anionic peptide mixture with $[\text{HAHAHAA}+2\text{H}]^{2+}$ followed by (c) DDC at 19 V and (d) 22 V.

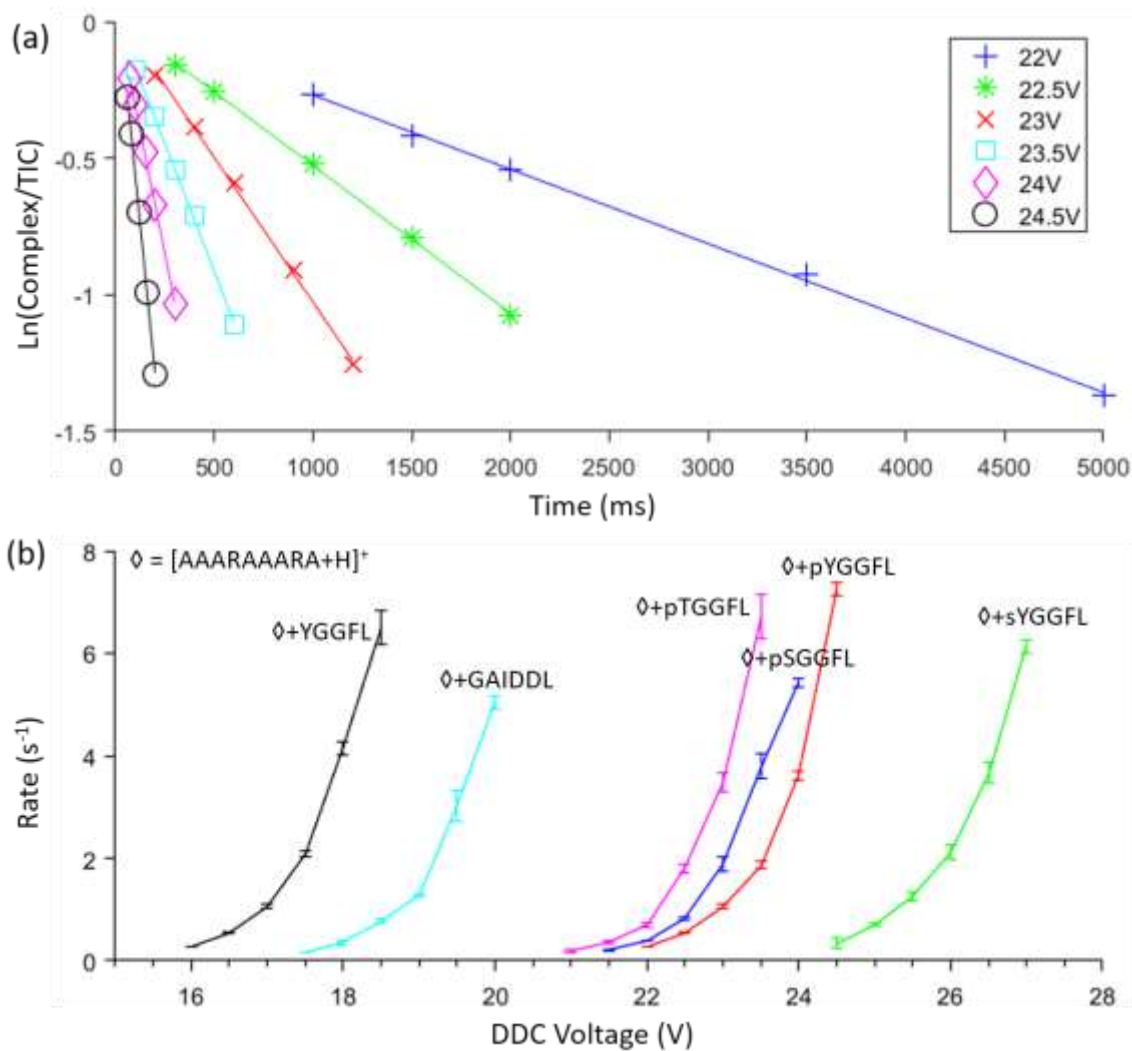


Figure 3.6 (a) The kinetic data for determining the dissociation rate of the peptide complex between $[\text{pYGGFL-H}]^-$ and $[\text{AAARAAARA}+2\text{H}]^{2+}$. The natural log of the peak area of the complex over the peak area of the total ion current (TIC) is plotted against the activation time of DDC. (b) The complex dissociation rate of each peptide complex, k_{diss} , is plotted against the DDC voltage. The error bar is two standard deviations of the slope's fitting error in the kinetic data.

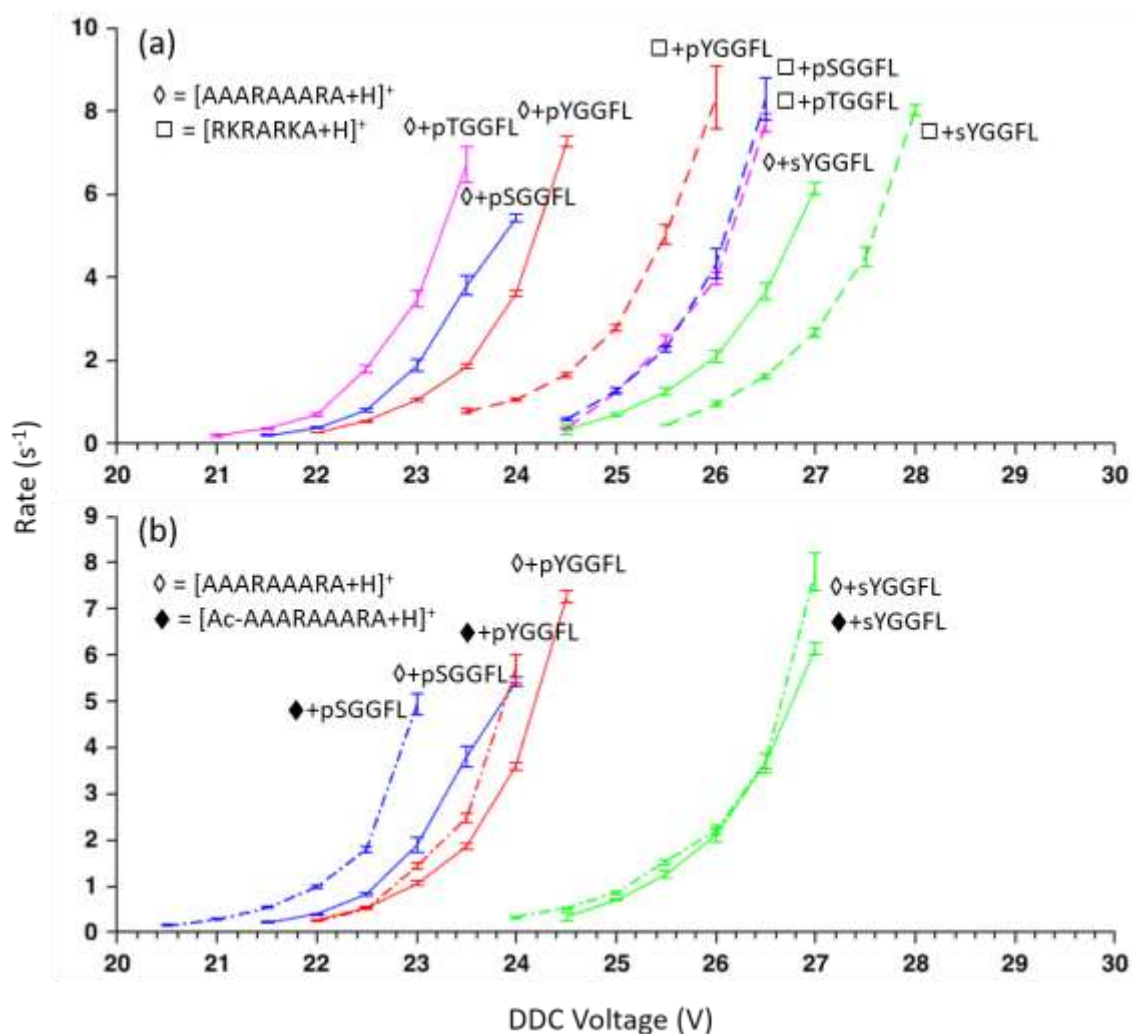


Figure 3.7 (a) Kinetic data comparison between peptide complexes of AAARAAARA (◇) and RKRARKA (□) for three phosphopeptides and a sulfopeptide. Kinetic data for AAARAAARA complexes are solid lines and dashed lines for RKRARKA complexes. (b) Kinetic data comparison of select peptides between AAARAAARA (◇) and Ac-AAARAAARA (◆). The error bar is two standard deviations of the slope's fitting error in the kinetic data.

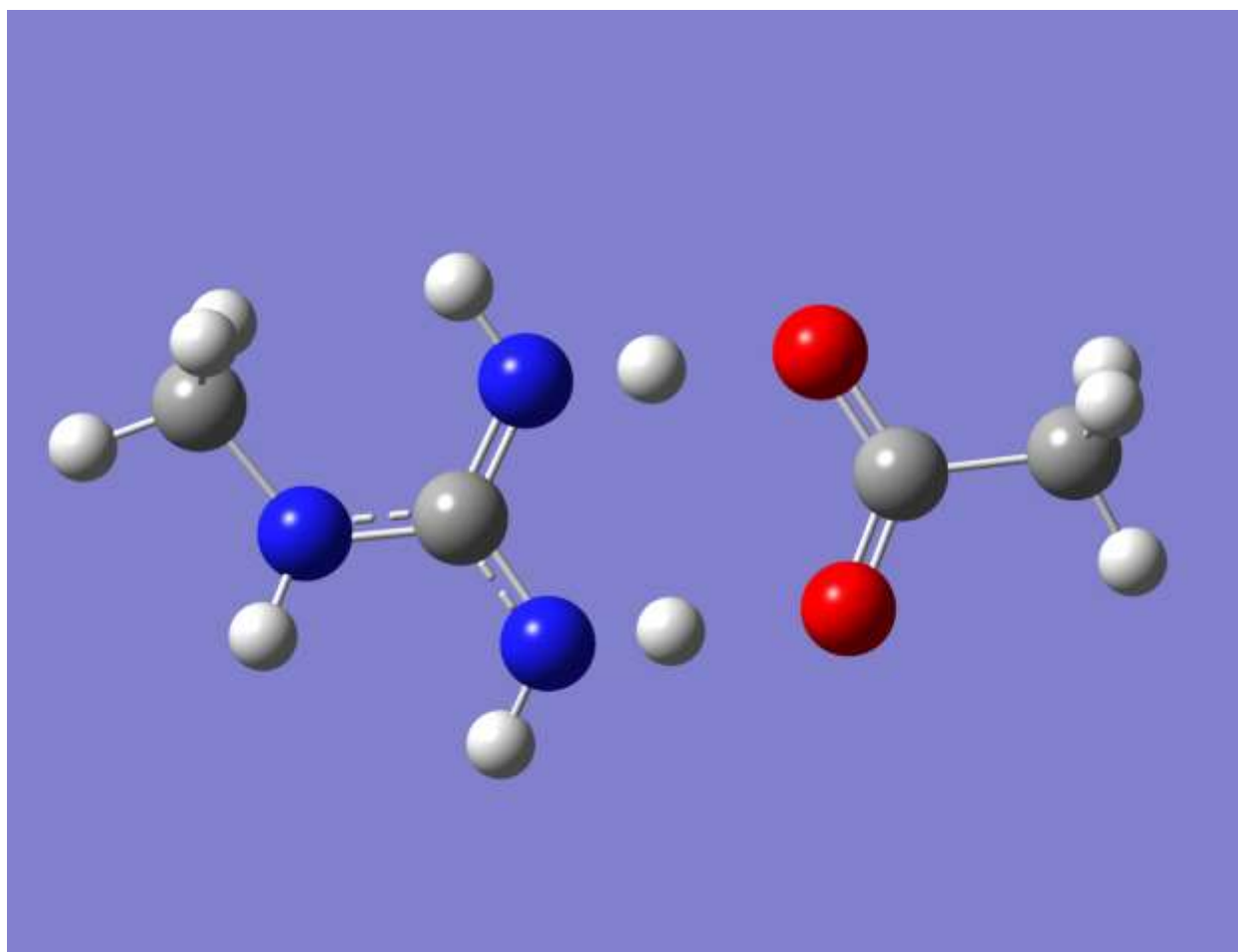


Figure 3.8 Optimized complex structure between methylguanidinium and acetate

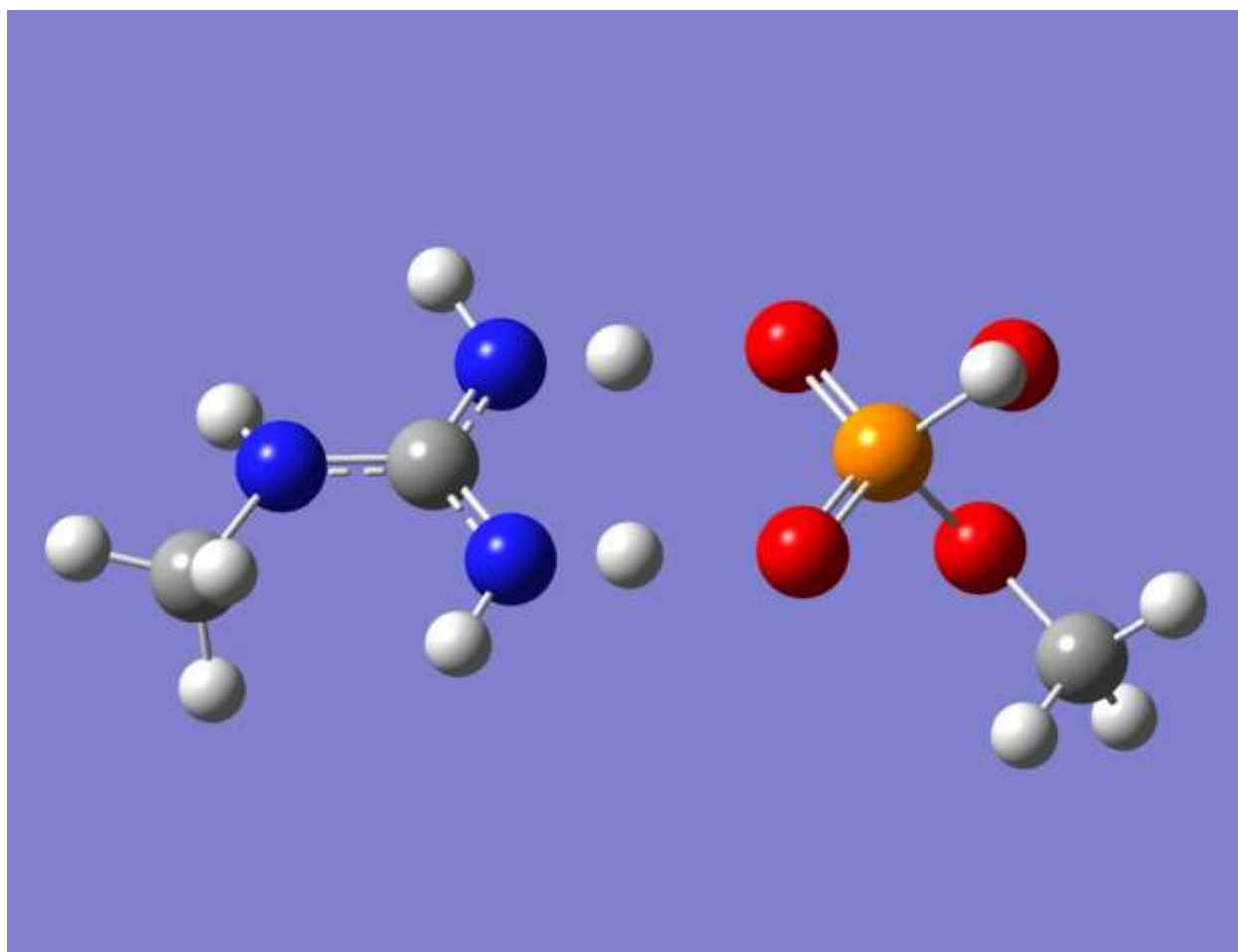


Figure 3.9 Optimized complex structure between methylguanidinium and methylphosphate.

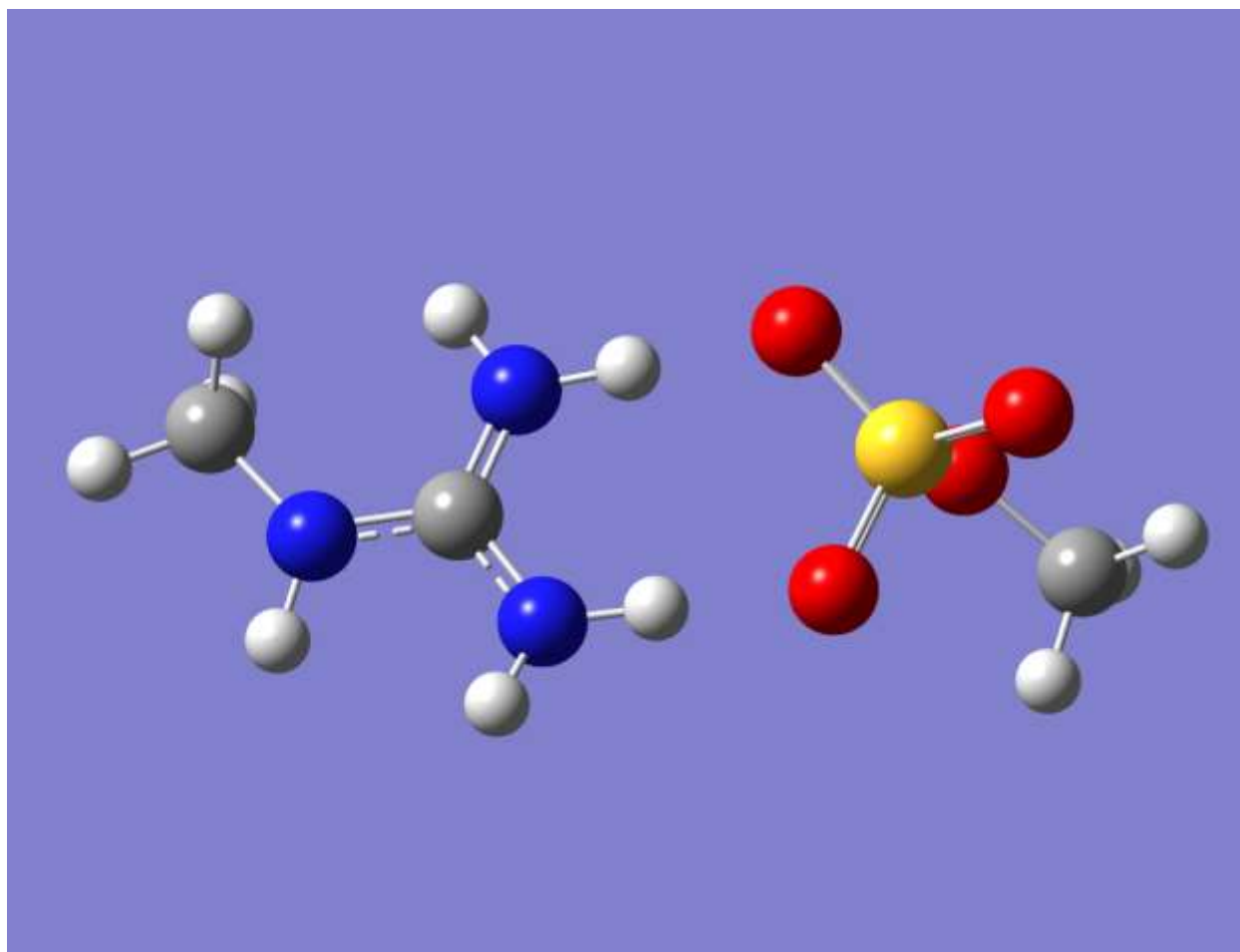


Figure 3.10 Optimized complex structure between methylguanidinium and methylsulfate.

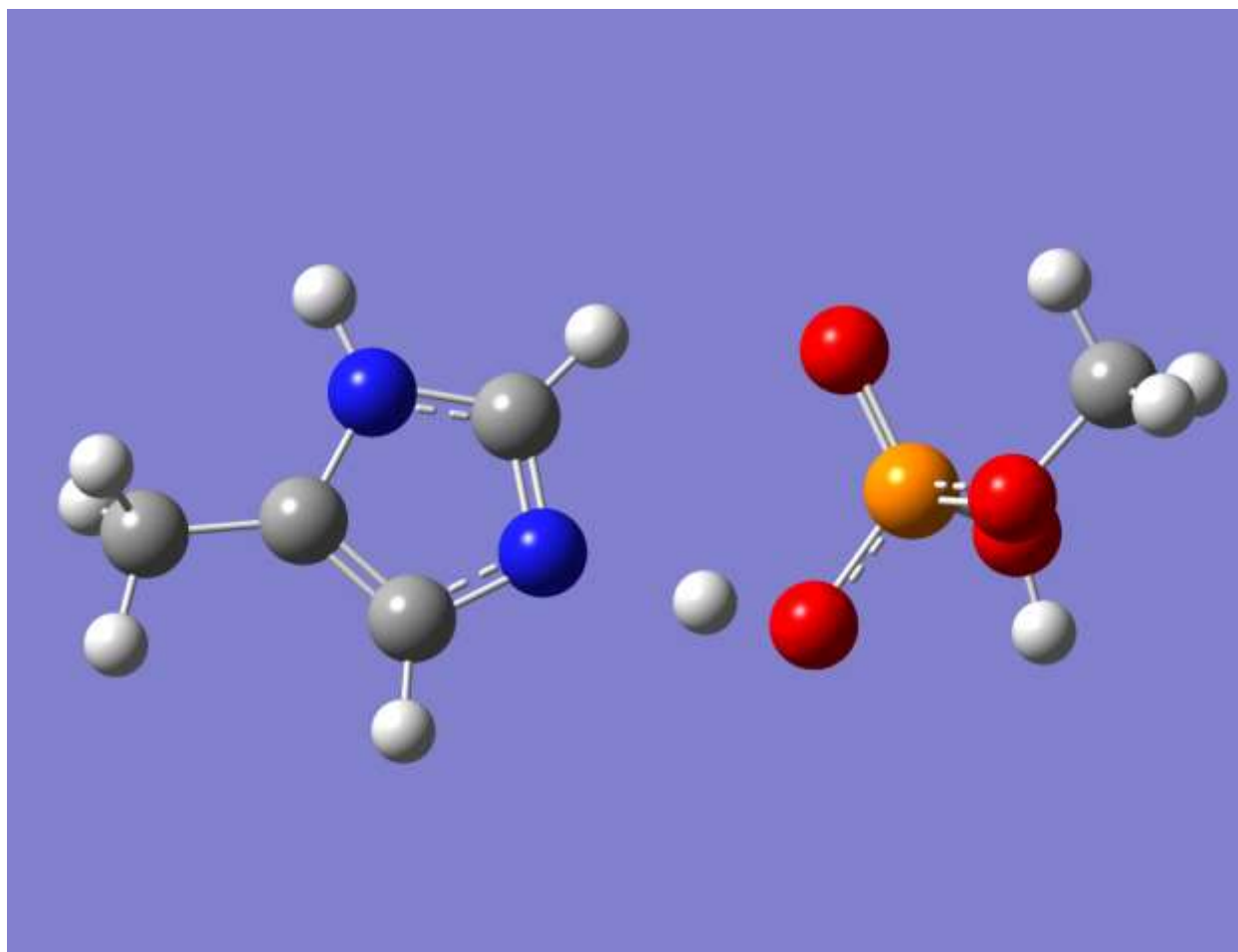


Figure 3.11 Optimized complex structure between methylimidazole and methylphosphate.

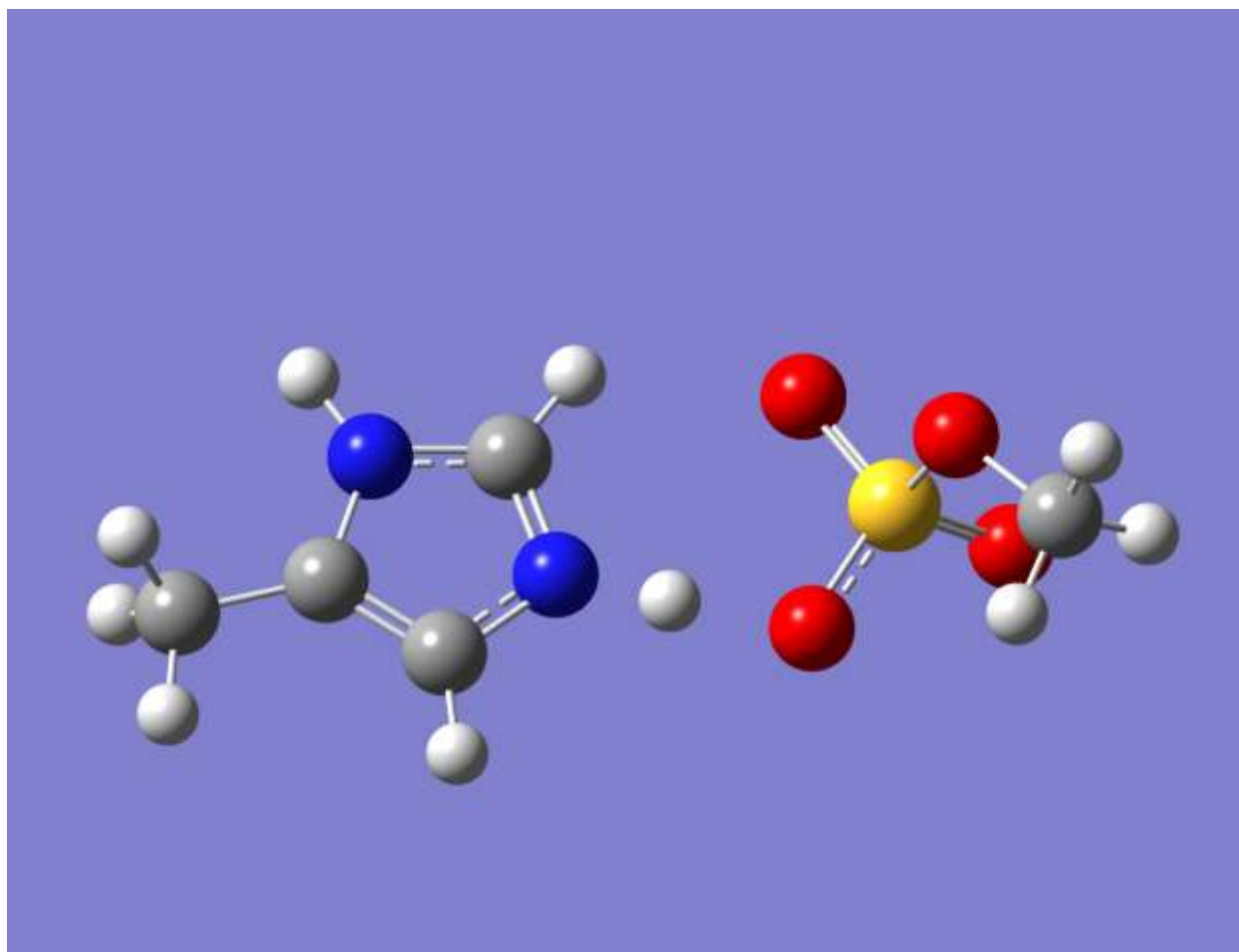


Figure 3.12 Optimized complex structure between methylimidazole and methylsulfate.

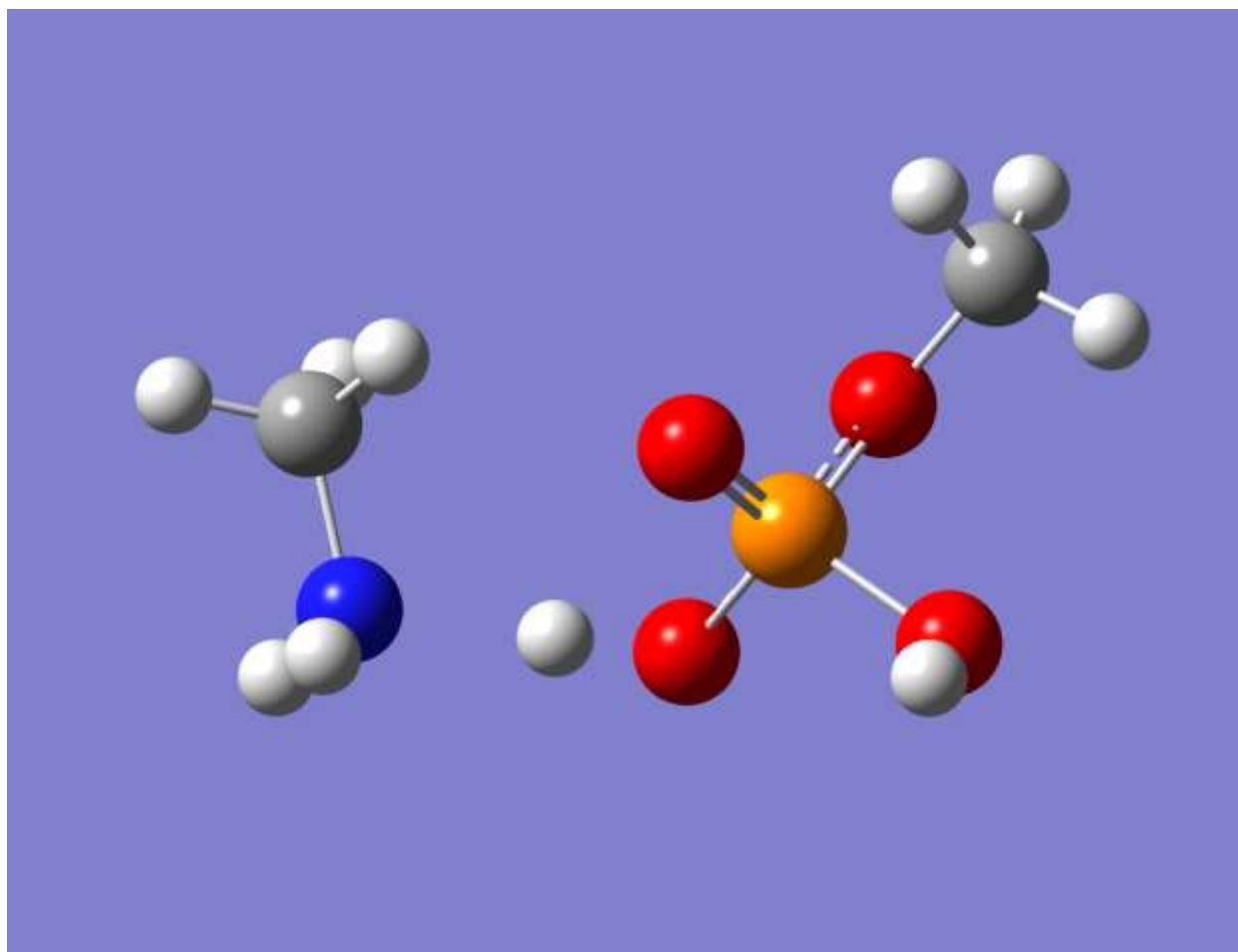


Figure 3.13 Optimized complex structure between methylamine and methylphosphate.

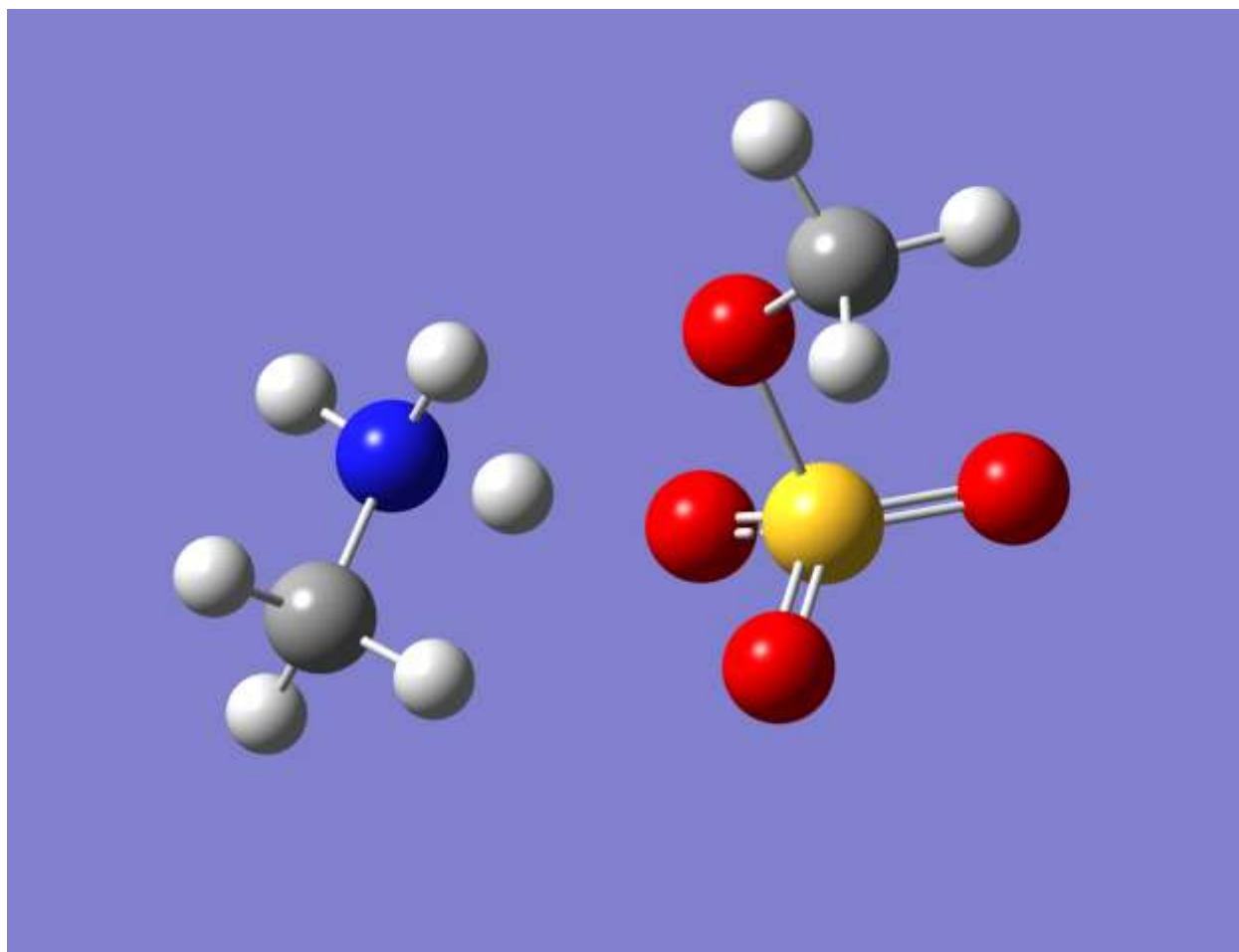


Figure 3.14 Optimized complex structure between methylamine and methylsulfate.

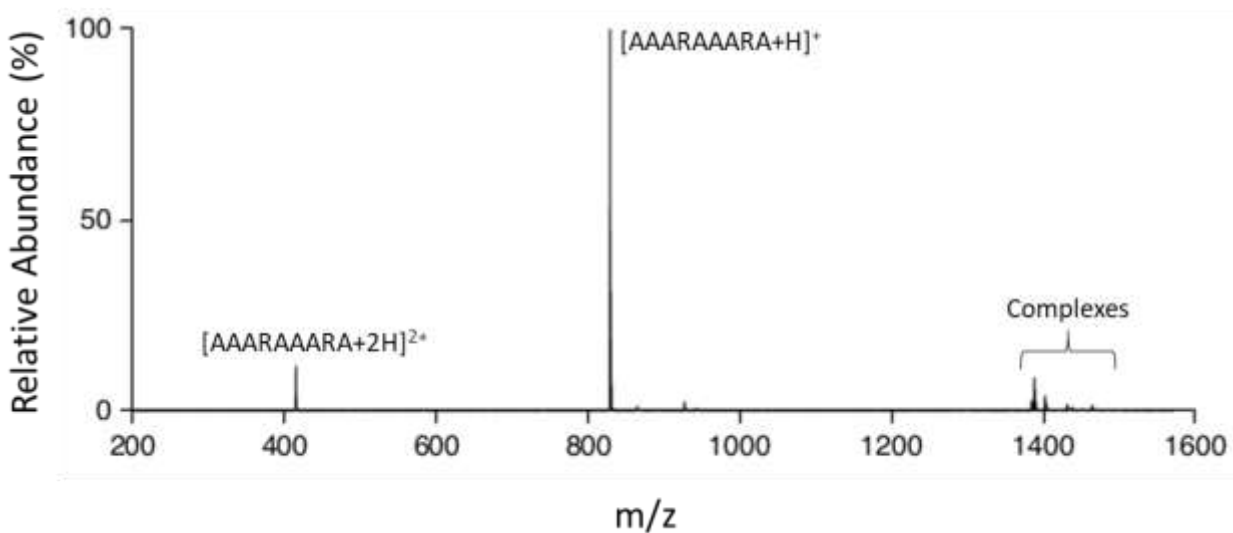


Figure 3.15 Full spectrum of post charge-inversion ion/ion inversion reaction between $[AAARAAARA+2H]^{2+}$ and the six peptide mixture containing pSGGFL, pTGGFL, and pYGGFL.

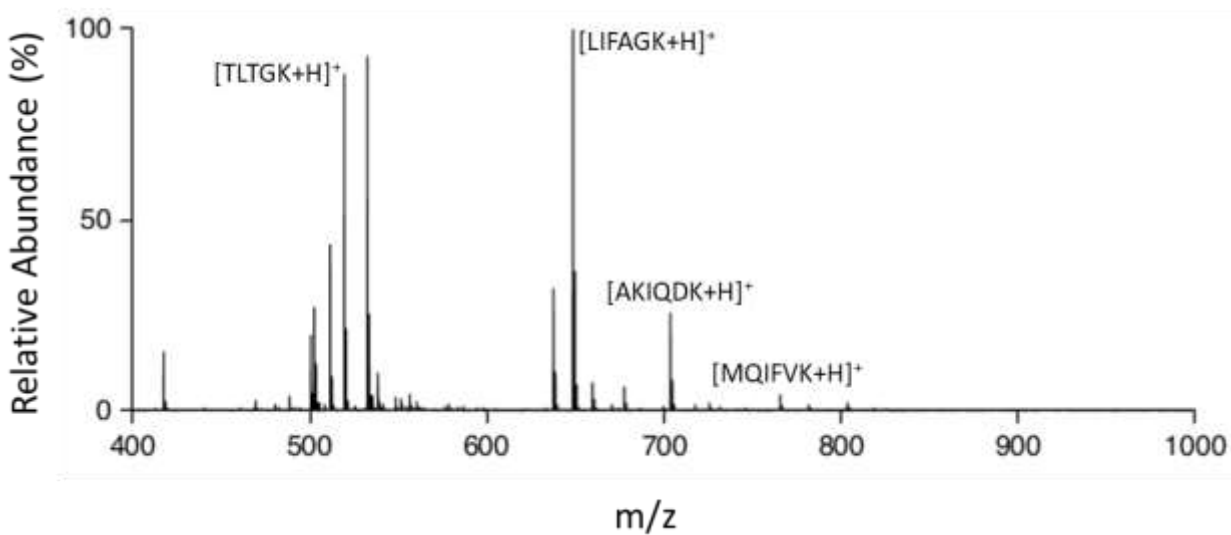


Figure 3.16 Positive mode nESI spectrum of an ubiquitin tryptic digest containing pSGGFL, pTGGFL, and pYGGFL. No signs of phosphopeptides, either protonated or sodiated, were observed in the spectrum.

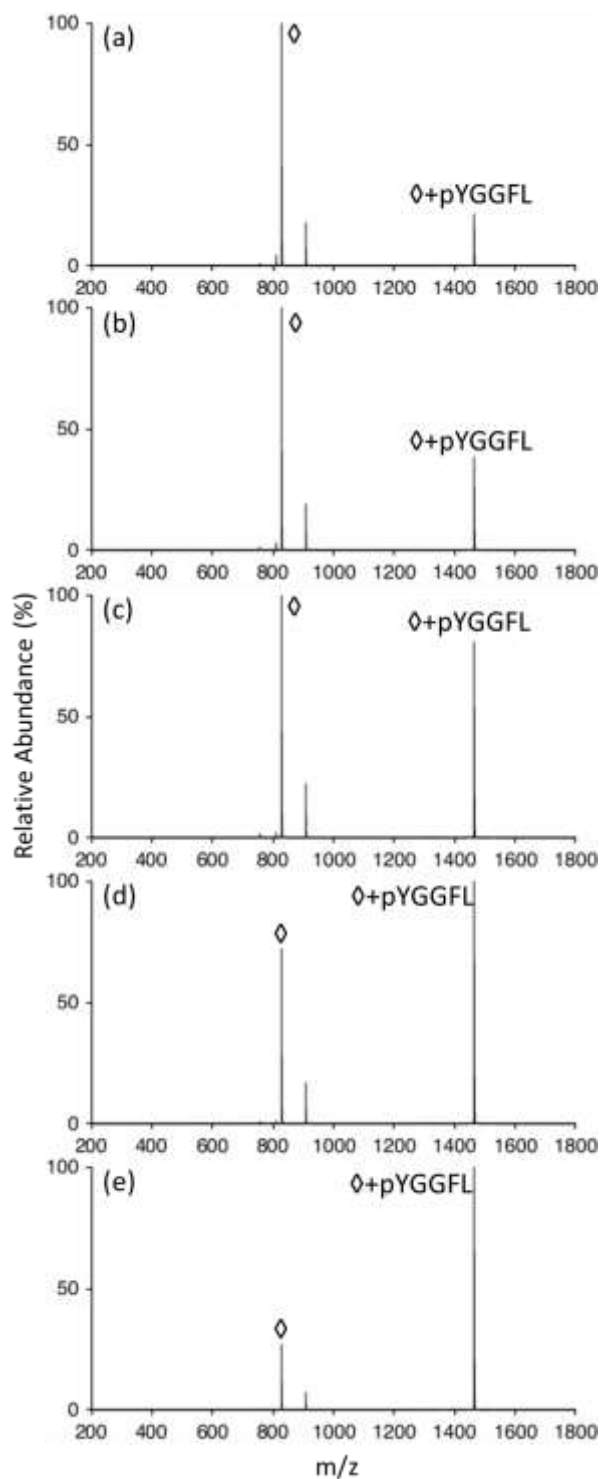


Figure 3.17 Spectra for dissociation kinetic study of the complex $[AAARAAARA+pYGGFL+H]^+$ at DDC voltage of 23 V and (a) 1200 ms, (b) 900 ms, (c) 600 ms, (d) 400 ms, and (e) 200 ms.

CHAPTER 4. INVESTIGATION OF HYALURONIC ACID

4.1 Introduction

Hyaluronic acid (HA) is a naturally occurring linear polysaccharide with repeating disaccharide units consisting of D-glucuronic acid (GlcA) and *N*-acetyl-D-glucosamine (GlcNAc) linked by a β -1,4 linkage. HA is a class of glycosaminoglycans (GAGs) but is quite distinct compared to other GAGs, such as heparin, due to its molecular weight, which can go up in the ranges of MDa, as well as the lack of sulphate groups present. The average adult human has about 12-15 g of HA with over half it present in the skin. At physiological pH, the D-glucuronic acid is deprotonated resulting in a negatively charged polymer that combines with the most prevalent extracellular cation Na^+ to form sodium hyaluronate, often referred to as hyaluronan. A number of biomedical applications have been found for HA such as cancer [27, 28], surgery [29], wound healing [30, 31], and drug delivery [32-34].

The chemical structural of HA was essentially solved in 1954 and characterization of HA is primarily done to determine the molecular weight (MW) of the polymer. The most common way to determine the average molecular weight of HA is using size exclusion chromatography coupled with a refractive index (conventional SEC) or multi-angle laser light scattering detector (SEC-MALLS). Conventional SEC has been the most preferred technique for HA MW analysis due to cost, robust sample tolerance, and ease of use compared to SEC-MALLS, the more accurate SEC method. Both SEC methods still experience a variance in MW determination for similar samples, more so with conventional SEC than SEC-MALLS, which has been a focus of research [35]. Electrospray ionization mass spectrometry (ESI-MS) [36] and matrix-assisted laser desorption ionization mass spectrometry (MALDI-MS) [37] have been the most favorable approaches for analysis of HA via mass spectrometry. Characterization of HA oligomers derived

from digestion with hyaluronidase via ESI-MS are typically performed with a HPLC separation step prior to mass analysis and has been previously reported [38, 39]. MALDI-MS has been used to analyze HA oligomers of sizes up to 15 kDa [40] which is much higher than the 8-9 kDa seen with ESI-MS [36] but the ionization energy of MALDI is sufficiently energetic to damage the analyte compared to ESI, a much lower energy ionization method.

Here we report analysis of a HA mixture via direct infusion nano-electrospray ionization mass spectrometry (nESI-MS). We report an interesting phenomenon observed in the HA spectrum upon ionization of HA in water. Application of negative mode proton transfer using three reagents was used to determine the fragility of highly charged HA anions upon proton transfer reaction. The aim of this work is to discuss a unique phenomenon observed upon electrospray ionization of HA as well as demonstrating the advantages of gas-phase ion/ion proton-transfer reactions for analysis of complex mixtures.

4.2 Experimental Section

4.2.1 Materials.

Low molecular weight sodium hyaluronate (8k-15k MW), pyridine, 7,8-benzoquinoline, 1,8-dimethylamino naphthalene (Proton-sponge®), and hyaluronidase from bovine testes was purchased from Sigma-Aldrich (St. Louis, MO, USA). Water (Optima™ LC/MS Grade), methanol (Optima™ Grade), acetonitrile (Optima™ Grade), and glacial acetic acid (HPLC Grade) was purchased from Fisher Scientific (Pittsburgh, PA, USA). Sodium hyaluronate was dissolved in water at a concentration of 1 mg/mL before diluted to desired concentration. Pyridine and 7,8-benzoquinoline were dissolved at 1 mg/mL concentration in acetonitrile with 1% acetic acid. Proton-sponge® was dissolved at 1 mg/mL concentration in a water:methanol:acetic acid (79.5:19.5:1) solution.

4.2.2 Digestion of Hyaluronic Acid

3.4 mg of hyaluronic acid (8k-15k) was dissolved in 1 mL of water before 100 μ L of a 10 mg/mL hyaluronidase solution was added. The solution was then incubated in a 37 $^{\circ}$ C water bath for 4 hours before removed and analyzed by mass spectrometry.

4.2.3 Mass spectrometry

All experiments were performed on a TripleTOF 5600 mass spectrometer (SCIEX, Concord, ON, Canada), previously modified for ion/ion reactions and dipolar direct current (DDC). Nano electrospray ionization (nESI) was used as the ionization method with borosilicate capillaries pulled using a P-88 micropipette puller (Sutter Instrument, Novato, CA, USA) to a tip diameter of 3-4 μ m. A home-built dual source was used for alternating nESI ionization in order to generate ions of opposite polarity. Ions of one polarity is first generated and guided through an RF-only ion guide (q0), an RF/DC mass resolving quad (Q1), and then stored in an RF-only high-pressure collision cell (q2). Ions of the opposite polarity are then injected through the quadrupoles and into q2. An AC waveform is applied at plates on the ends of q2 to trap the ions and allow time for reaction. The final ion products are injected into the time-of-flight (TOF) mass analyzer for analysis.

4.2.4 Spectral Deconvolution

All deconvolution was done by hand using Microsoft Excel. All peaks above six times the baseline noise was identified and deconvoluted. The intensity assigned to each ion of varying charge state is the sum of the peak height of all its isotopic peaks. The final intensity of each zero-charge state peak in the deconvoluted spectrum is the sum of all the intensities from all its varying charge states identified in the spectrum.

4.3 Results and Discussion

4.3.1 Electrospray of Single HA Polymer.

The electrospray condition for hyaluronic acid was first tested using a pure HA6 sample. It was first noticed that upon electrospray of HA6 (MW 1155 Da) the dominate peak in the spectrum, Figure 4.1a, was the fully deprotonated ion where all acid sites that can be deprotonated are deprotonated, giving HA6 a max charge of 3-. A small amount of the C₅ fragment ion was also observed within the spectrum. In Figure 4.1a, the ion optics were set at the default voltage gradients, commonly used for electrospray of peptides and proteins, where the voltage difference between QJet/q0, Q1, and q2 are respectively 5 V. Softening the transfer conditions such that the voltage gradient from QJet/q0 to Q1 is 2V and Q1 to q2 is 3 V eliminated the presence of the C₅ fragment ion, Figure 4.1b. Compared to peptides and proteins, HA appear to be a more fragile compound based on the required ion optics condition to avoid fragmentation.

4.3.2 Electrospray of HA Mixture.

Using the optimized electrospray condition obtained from HA6, a low molecular weight HA mixture (MW 8k-15k Da) was analyzed. The resulting spectrum revealed a very interesting distribution shape of ions present within the spectrum, Figure 4.2a. The majority of signal for HA was primarily in the range of 300 to 600 m/z. The most interesting feature centers in the m/z 380 region where a huge spike in signal is present and is flanked by two almost symmetric features in both lower and higher m/z, we have termed this region ‘emerald city.’ A wide isolation of the ‘emerald city’ region was applied to remove some of the overlapping ion peaks and signal in the m/z 400-550 region giving rise to an extremely clean ‘emerald city’ spectrum, Figure 4.2b.

There are three distributions present in the “emerald city” region: left, center, and right. The center portion (Figure 4.2d) consists of hyaluronic acid polymers containing equal numbers of the GlcA and GlcNAc monomers, otherwise known as the fully intact HA polymers consists of an even number of sugar units. All of these HA anions are at full charge, meaning all the carboxylic acid groups present on the GlcA units are deprotonated. Each set of peaks are of a different HA polymer and its max set of charges. As HA gets bigger and more charge, its m/z value steady decreases from its previous one unit less, one charge less HA polymer as shown in the center distribution of “emerald city.” The m/z spacing between each highly charge HA ion steadily decreases as size and charge increases resulting in a final region where the ions are unresolved.

The left distribution contains HA ions where an extra GlcA unit is present in the sequence resulting in an odd number of sugar units present within the oligomer, Figure 4.2c. Similar to the center region, all of the ions have charge equal to the number of GlcA unit present and is fully charged. For these set of HA oligomers, as the mass and charge increases, the HA ion’s m/z gradually increases as well; thus, ions with the lowest MW and charge on in the lower m/z range and vice versa for the HA of higher MW and charge. The right side of ‘emerald city’ is another distribution of HA where the identity of HA is similar to the left side where an extra GlcA unit is present and the overall number of sugar units are odd numbered, Figure 4.2e. Unlike the left and center region, these HA anions are one charge off from being fully charged. Similar to the center portion of ‘emerald city,’ as the distribution of ions are increasing in charge and size their m/z value decreases. For all HA ions in the ‘emerald city’ region as HA increases in size the overall signal decrease.

4.3.3 Proton Transfer of HA Anions.

As hyaluronic acid has been demonstrated to be a fragile compound compared to peptides and proteins, it is uncertain if proton transfer reaction will cause fragmentation leading to misinterpretation of the original HA ions' molecular weight information. Isolation of a region containing 7- and 8- HA anions from the emerald city distribution and subsequent ion/ion reactions with three negative mode proton transfer reagents, each with different gas-phase proton affinities, was performed to assess proton transfer reactions of HA. Figure 4.3 compares the deconvoluted negative product ion spectra (mass spectra shown in Figure 4.8) resulting from the reaction of select HA ions isolated from the emerald city distribution with a) protonated pyridine (m/z 80), b) protonated 7,8-benzoquinoline (m/z 180), and c) protonated 1,8-bis(dimethylamino)naphthalene (m/z 215), also known as 'Proton-sponge®.' The proton affinities of these compounds are 930 kJ/mol, 961 kJ/mol, and 1028 kJ/mol respectively. As the reaction enthalpy for proton transfer is related to the proton affinity of the reagent and the analyte, proton transfer reagents with a higher proton affinity minimizes the overall reaction exothermicity. Comparison between the deconvoluted spectra of the pre-proton transfer and post-proton transfer shows a very similar spectrum but a discernable increase in smaller HA sizes are observed for all three proton transfer reagents. There is also no significant difference observed in the abundance of the HA fragment ions with increasing proton affinity of the reagent ion. Proton hydrate would be the 'softest' proton transfer reagent but instrument conditions do not allow for observation of protonated water hydrates. No signs of reagent adduction are also observed. The lack of adduct ion present on hyaluronic acid post-ion/ion reaction indicates that no long-lived complex was formed during the ion/ion reaction process but does not confirm that all proton transfer reaction occurred exclusively via proton-hopping.

Proton transfer reaction was further conducted for the entire population of HA anions in the ‘emerald city’ distribution using proton sponge. While no significant difference was observed between the three reagents the selection of proton-sponge was made based on the experimental conditions needed for ion/ion reactions where a larger m/z reagent is more suitable. The pre- and post-ion/ion reaction deconvoluted spectra are shown in Figure 4.4 (mass spectra shown in Figure 4.9). With sufficient enough resolution, the closely spaced ions with charges up to 21 can be identified and deconvoluted; however, for ions of even higher charge or overlapping peaks which is observed in the central region of ‘emerald city,’ proton transfer is a method to decongest overcrowded peaks within a narrow m/z range and spread the signal out over a wider m/z thereby improving overall peak capacity of the mass spectrometer. This is observed in the deconvoluted spectra where a couple of ions not previously detected are now observable.

4.3.4 Odd-mers Present in HA Mixture

It is interesting that we observed a significant amount of odd HA-mers within the spectrum as HA oligomers are typically consisting of even number of carbohydrate units. It has been previously reported that odd-mer HA was observed from upon digestions and separation of HA followed by ESI-MS analysis [41]. Further research showed that the abundance of the odd-mer HA is directly influence via the cone voltage for the mass spectrometer and these fragments are due to in-source fragmentation [38]. Variation of the orifice and curtain plate voltage on our instrument as well as the subsequent ion optics transfer conditions did not show a significant impact on the abundance of the highly charge odd-mers present. The distinct distribution persisted until the voltage gradients were too shallow such that signal could not be acquired. While we are suspicious that these highly charged odd-mers might due to an electrospray phenomenon for high molecular weight HA, we lack the ability to isolate a single large HA

oligomer prior to ESI for specific tuning of the instrument. Another avenue to confirm if these odd-mers are coming from either the solution or electrospray process is via digestion of the large HA MW mixture. If approximately equal amounts of odd and even unit HA oligomers are observed after the digestion process, then it can be certain that what we have observed is not a result from the electrospray process. Digestion of the large HA MW mixture using the enzyme hyaluronidase and subsequent electrospray ionization revealed predominately even units of HA oligomers, shown in Figure 4.5, with only minor components of odd HA units present. Based on this result it is highly probable that the observed odd-mers of HA from the higher MW HA mixture is due to an electrospray phenomenon that only occurs with HA of sufficient size and charge. The premise of this paper is presenting the phenomenology of a HA anionic mixture spectrum and the ability to do negative mode proton transfer on this mixture. The nature of these odd-mers originating from high MW HA will be discussed in the future.

4.3.5 Charge-inversion of Proteins using HA

What initially was an attempt to proton transfer hyaluronic acid anions revealed some very interesting ion/ion chemistry which has not been previously observed. Previous proton transfer of HA anions was performed with a single charge protonated reagent. A singly charged reagent is typically selected because it allows more control over the reaction kinetics as well as the resulting spectrum is very simple after ion/ion reactions. The analyte loses a charge and the reagent is neutralized leaving no trace of it in the spectrum. Due to the highly charged and congested nature of hyaluronic acid, a multiply charged proton transfer reagent was selected and tested. Ion/ion reaction between the hyaluronic acid anion mixture with a 7+ charge of ubiquitin yield some unexpected results, shown in Figure 4.6a. Instead of seeing lower charged hyaluronic acid anions or protein-HA complex anions, negatively charged ubiquitin ions were observed

instead. From Figure 4.6a, the max charge of ubiquitin anions observed is 6- and means a max of 13 protons were transferred off from ubiquitin. A closer look at the 4- peak of ubiquitin, Figure 4.6b, reveals the presence of sodium adduction which can only occur when a long-term complex is formed between the cation and anions; however, no signs of the complexes were observed in the spectrum. This type of experiment was repeated with higher charged HA at 50 kDa and cytochrome C 15+ charge state as well as myoglobin 24+ charge state. The results of those charge inversion experiments are presented in Figures 4.7. Similar to ubiquitin, a max number of 22 protons were removed from cytochrome C and as much as 33 protons were removed from myoglobin. This appears to be a general phenomenon regarding how HA anions interact with protein cations and this type of charge-inversion reaction is the first of its kind. Previously charge inversion reactions typically are 1+ to 1- using a 2- anionic reagent or vice-versa if charge inverting a 1- to a 1+. A charge inversion reaction where a multiply protonated protein cation is charge inverted to a multiple deprotonated anion is the first of its kind. It is speculated that these highly charged hyaluronic acid anions have a tremendous affinity for protons and upon formation of a complex, multiple charge carriers, protons or sodium, are transferred over in a short period of time. This results in two highly charged anions in close proximity which are then ejected apart from each other due to coulombic repulsion, leading to no signs of complexes in the spectrum. Further investigation of hyaluronic acid and similar polymers should be conducted to study and understand this phenomenon.

4.4 Conclusions

Hyaluronic acid was observed to be fully deprotonated or close to upon electrospray ionization which is not commonly seen in peptides and protein. The resulting spectrum from the highly charged hyaluronic acid anions generated an interesting mass spectrum which we dubbed

‘emerald city.’ It was found that these highly charged hyaluronic acid anions are fragile and sensitive to electrospray and ion optic transfer conditions. Negative mode proton transfer reaction with three different proton transfer reagents all showed slight amounts of fragmentation even with proton-sponge, a low exothermicity reagent for proton transfer reaction. Application of negative mode proton transfer to the ‘emerald city’ hyaluronic acid anion mixture allowed for identification of previously unknown hyaluronic acid anions present.

4.5 References

- [1] M.K. Cowman, H.G. Lee, K.L. Schwertfeger, J.B. McCarthy, E.A. Turley, The Content and Size of Hyaluronan in Biological Fluids and Tissues, *Front Immunol*, 6 (2015) 261.
- [2] M.S. Karbownik, J.Z. Nowak, Hyaluronan: Towards novel anti-cancer therapeutics, *Pharmacological Reports*, 65 (2013) 1056-1074.
- [3] M.E. Edmonds, A.V. Foster, Diabetic foot ulcers, *BMJ*, 332 (2006) 407-410.
- [4] R. Moseley, M. Walker, R.J. Waddington, W.Y.J. Chen, Comparison of the antioxidant properties of wound dressing materials—carboxymethylcellulose, hyaluronan benzyl ester and hyaluronan, towards polymorphonuclear leukocyte-derived reactive oxygen species, *Biomaterials*, 24 (2003) 1549-1557.
- [5] G.D. Mogosanu, A.M. Grumezescu, Natural and synthetic polymers for wounds and burns dressing, *Int J Pharm*, 463 (2014) 127-136.
- [6] E. Esposito, E. Menegatti, R. Cortesi, Hyaluronan-based microspheres as tools for drug delivery: a comparative study, *Int J Pharm*, 288 (2005) 35-49.
- [7] S. Vasiliu, M. Popa, M. Rinaudo, Polyelectrolyte capsules made of two biocompatible natural polymers, *European Polymer Journal*, 41 (2005) 923-932.
- [8] Y.H. Yun, D.J. Goetz, P. Yellen, W. Chen, Hyaluronan microspheres for sustained gene delivery and site-specific targeting, *Biomaterials*, 25 (2004) 147-157.
- [9] S. Shanmuga Doss, N.P. Bhatt, G. Jayaraman, Improving the accuracy of hyaluronic acid molecular weight estimation by conventional size exclusion chromatography, *J Chromatogr B Analyt Technol Biomed Life Sci*, 1060 (2017) 255-261.
- [10] N. Volpi, On-line HPLC/ESI-MS separation and characterization of hyaluronan oligosaccharides from 2-mers to 40-mers, *Anal Chem*, 79 (2007) 6390-6397.

- [11] D.Y. Kang, W.S. Kim, I.S. Heo, Y.H. Park, S. Lee, Extraction of hyaluronic acid (HA) from rooster comb and characterization using flow field-flow fractionation (FIFFF) coupled with multiangle light scattering (MALS), *J Sep Sci*, 33 (2010) 3530-3536.
- [12] B.S. Prebyl, C. Kaczmarek, A.A. Tuinman, D.C. Baker, Characterizing the electrospray-ionization mass spectral fragmentation pattern of enzymatically derived hyaluronic acid oligomers, *Carbohydr Res*, 338 (2003) 1381-1387.
- [13] A. Tawada, T. Masa, Y. Oonuki, A. Watanabe, Y. Matsuzaki, A. Asari, Large-scale preparation, purification, and characterization of hyaluronan oligosaccharides from 4-mers to 52-mers, *Glycobiology*, 12 (2002) 421-426.
- [14] B. Yeung, D. Marecak, Molecular weight determination of hyaluronic acid by gel filtration chromatography coupled to matrix-assisted laser desorption ionization mass spectrometry, *J Chromatogr A*, 852 (1999) 573-581.
- [15] K.N. Price, A. Tuinman, D.C. Baker, C. Chisena, R.L. Cysyk, Isolation and characterization by electrospray-ionization mass spectrometry and high-performance anion-exchange chromatography of oligosaccharides derived from hyaluronic acid by hyaluronate lyase digestion: Observation of some heretofore unobserved oligosaccharides that contain an odd number of units, *Carbohydrate Research*, 303 (1997) 303-311.

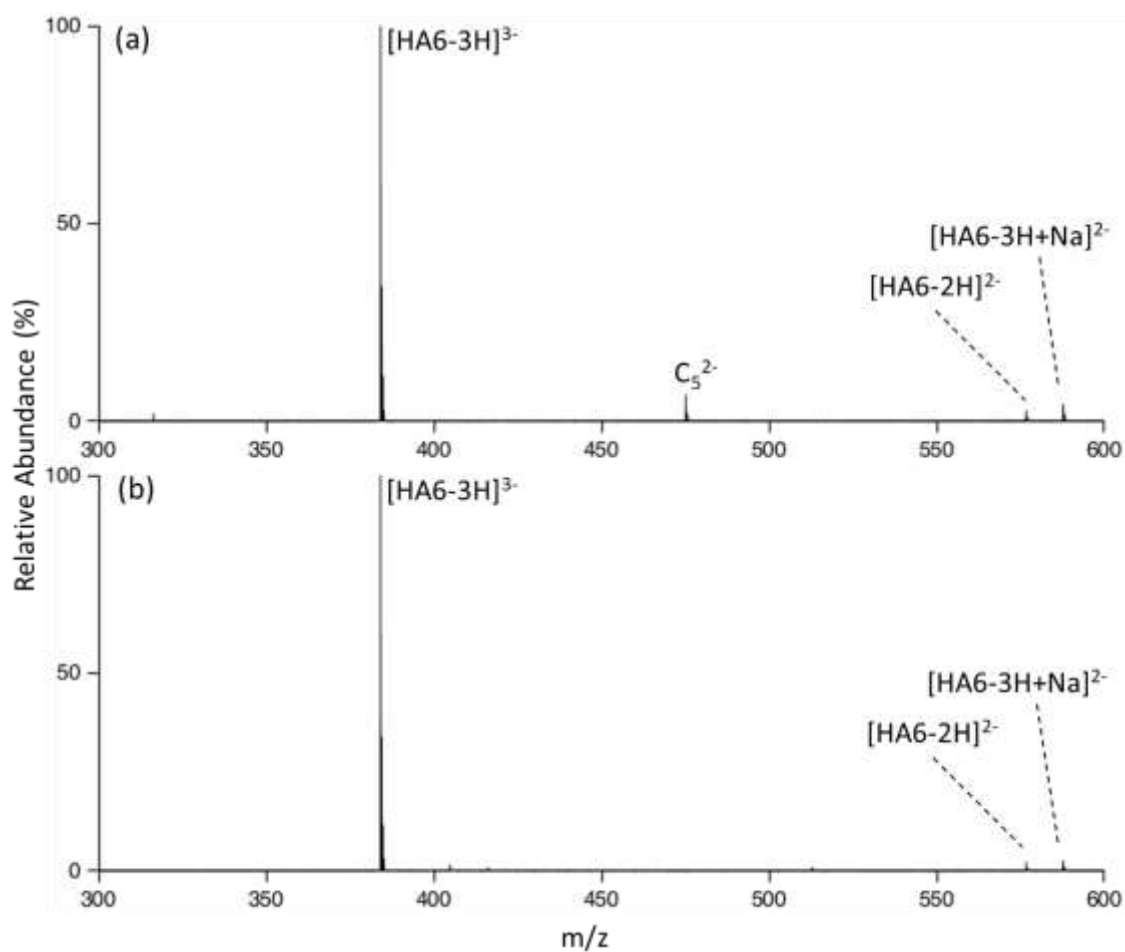


Figure 4.1 Electrospray of a 6-mer HA using a) a voltage gradient of 5 V (QJet/Q0 to Q1) and 5 V (Q1 to q2); b) a voltage gradient of 2 V (QJet/Q0 to Q1) and 3 V (Q1 to q2) for ion optics.

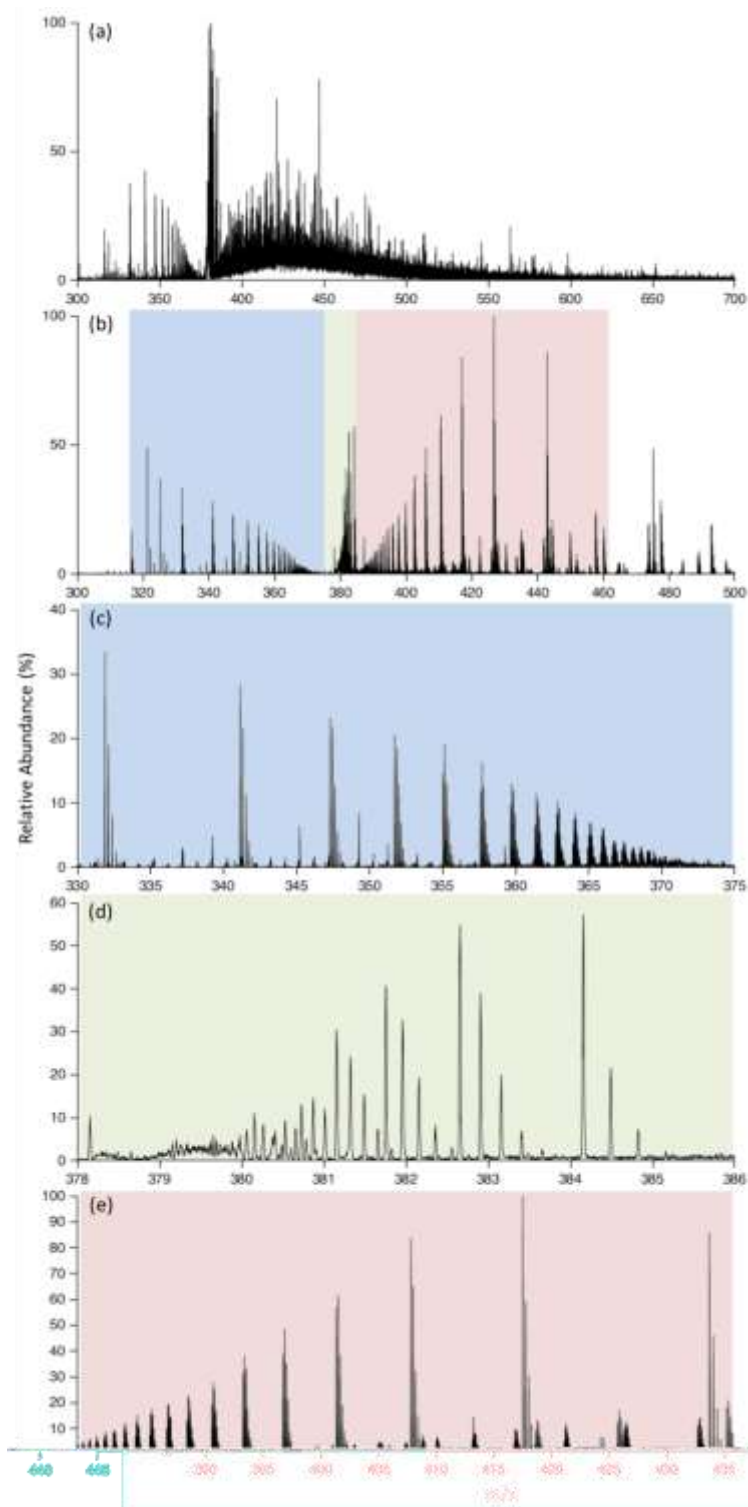


Figure 4.2 a) Mass spectrum of HA mixture labeled 8k-15k MW and b) wide isolation window of the ‘emerald city’ region color coded by its unique regions: c) fully charged odd-mer HA, d) fully charged even-mer HA, and e) one charge less than max charge odd-mer HA.

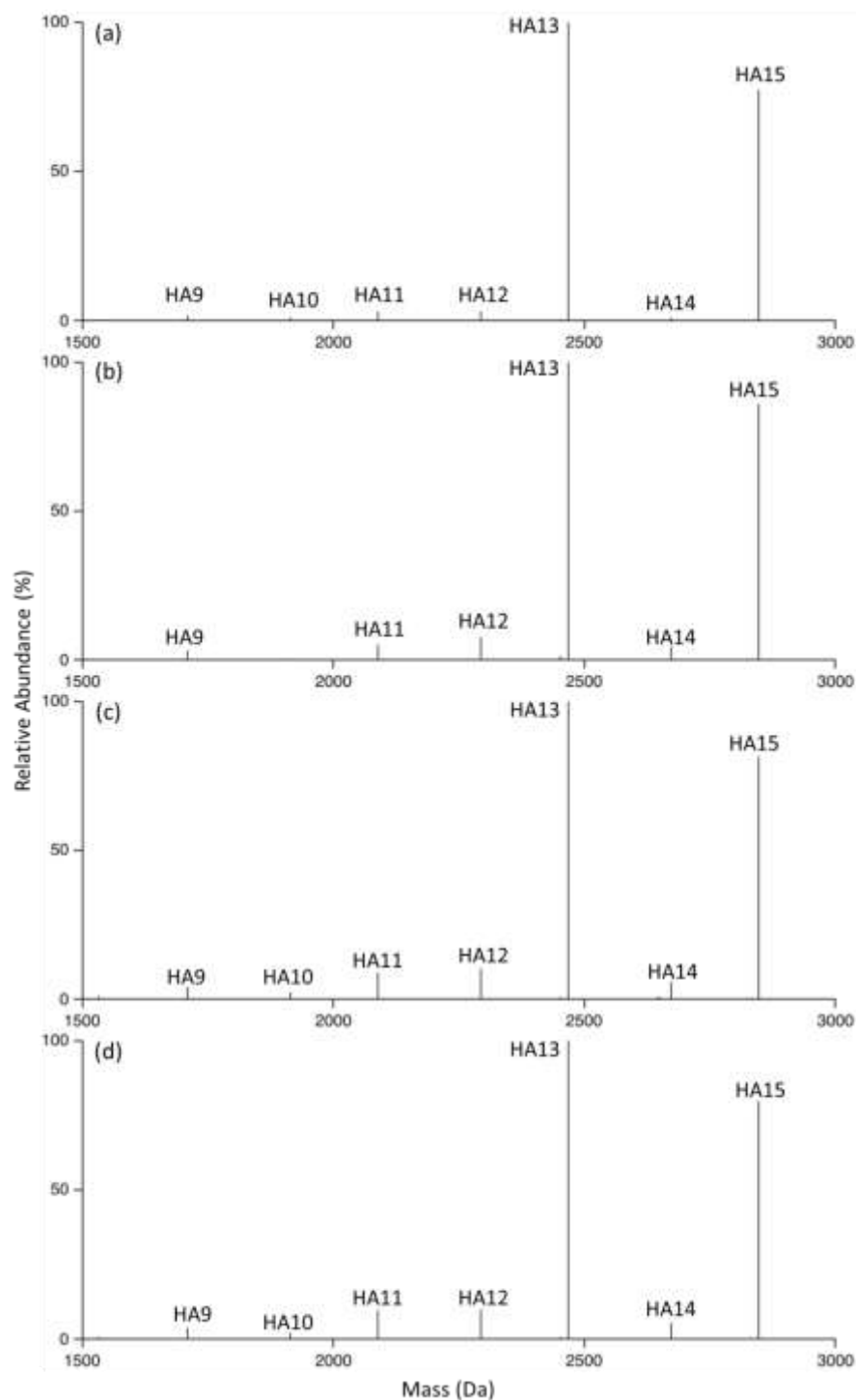


Figure 4.3 Deconvoluted spectrum of a) narrow isolation window in the ‘emerald city’ spectrum containing HA13 and HA15 at max charge; post ion/ion reaction of ions within that isolation window with b) pyridine, c) 7,8-benzoquinoline, and d) 1,8-Bis(dimethylamino)naphthalene (Proton-sponge®).

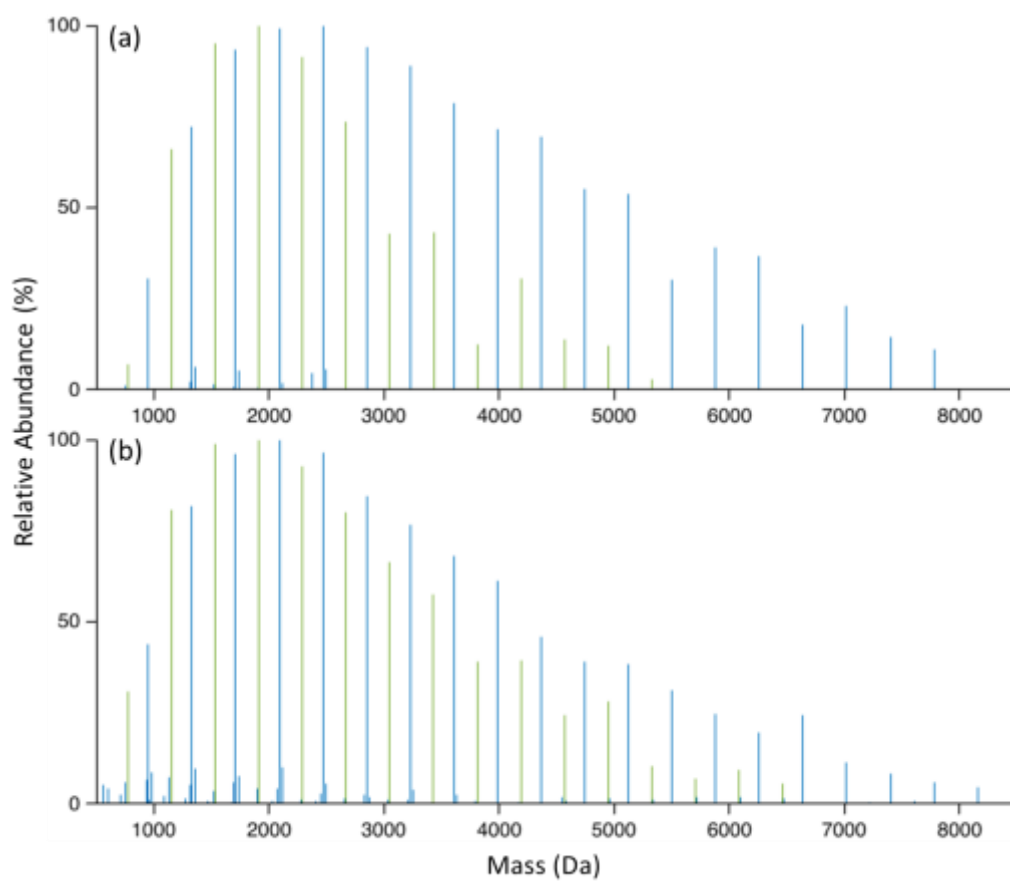


Figure 4.4 Deconvoluted spectrum of a) ‘emerald city’ and b) post-proton transfer ion/ion reaction with Proton-sponge®. The odd HA-mers are noted in blue and the even-mers are noted in green.

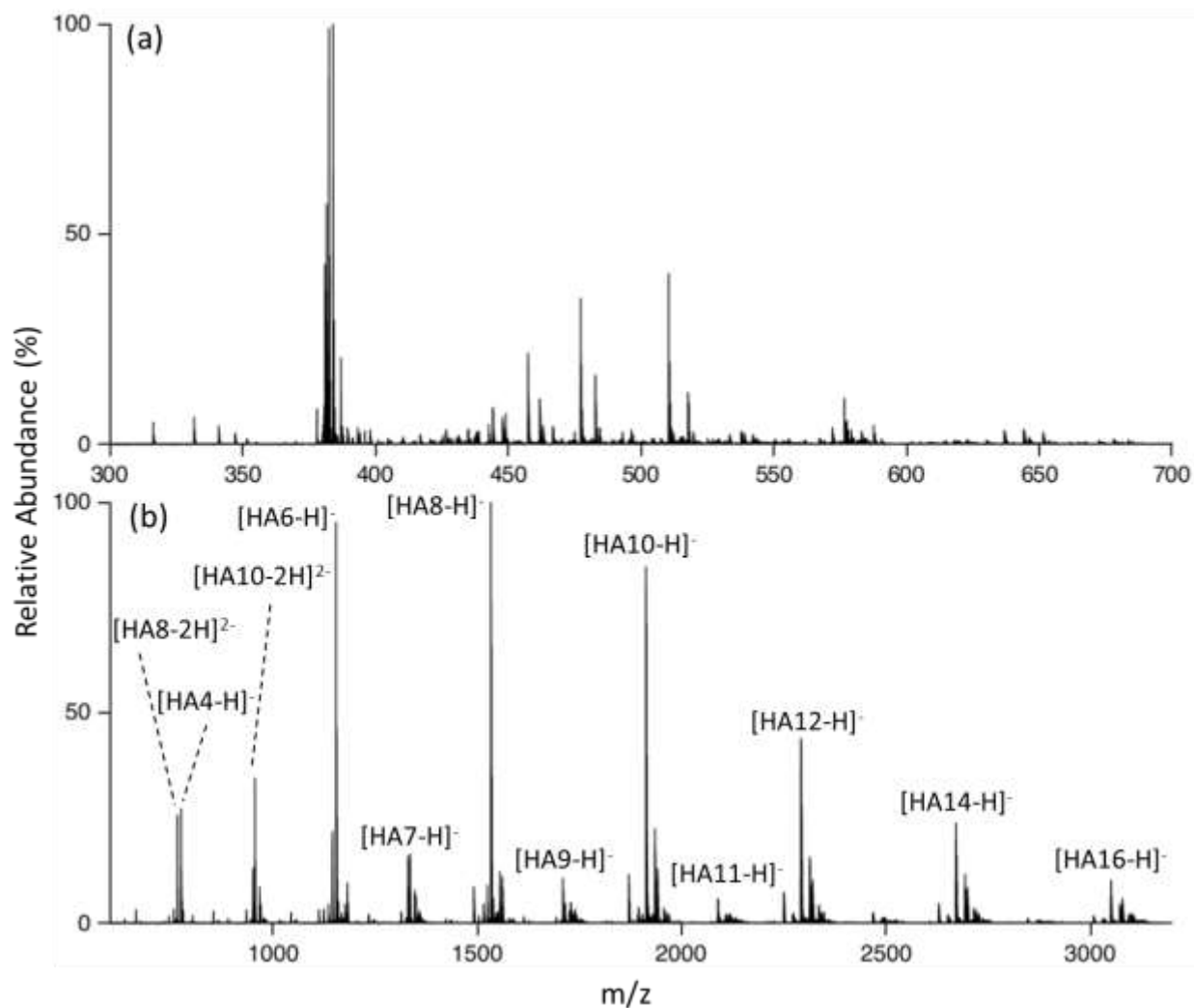


Figure 4.5 Mass spectrum of the a) post digested hyaluronic acid mixture and b) subsequent post-proton transfer ion/ion reaction reducing the charge of the majority of ions to 1- charge state.

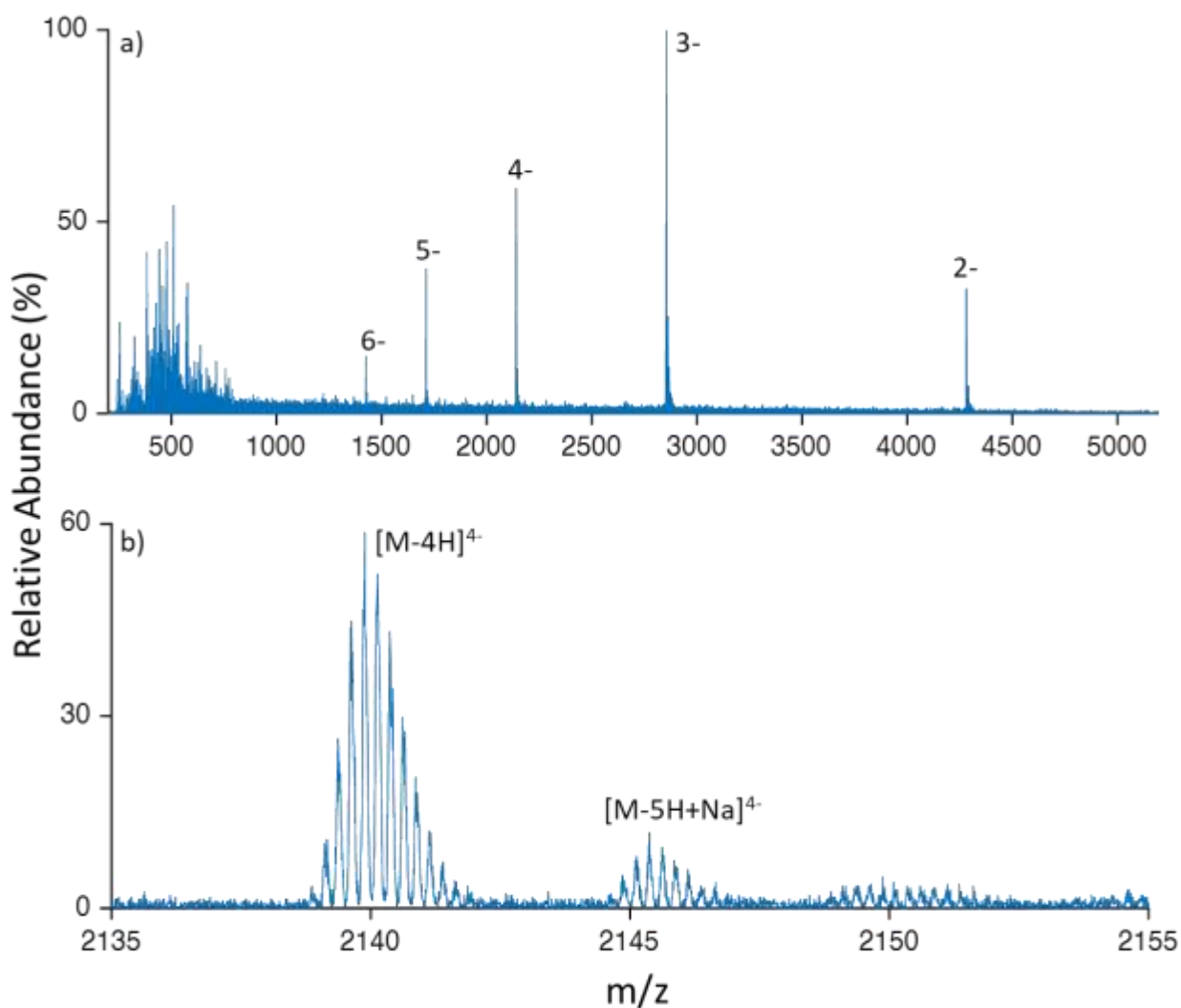


Figure 4.6 a) Post ion/ion reaction between 8k-15k hyaluronic acid anionic mixture (m/z 200-1000) with 7+ ubiquitin. The labeled peaks are the charge of the ubiquitin anions after the reaction. b) A zoomed in of the 4- charge state of ubiquitin showing the presence of sodium adduction post ion/ion reaction. The 7+ ubiquitin was clean isolation of only the protonated species.

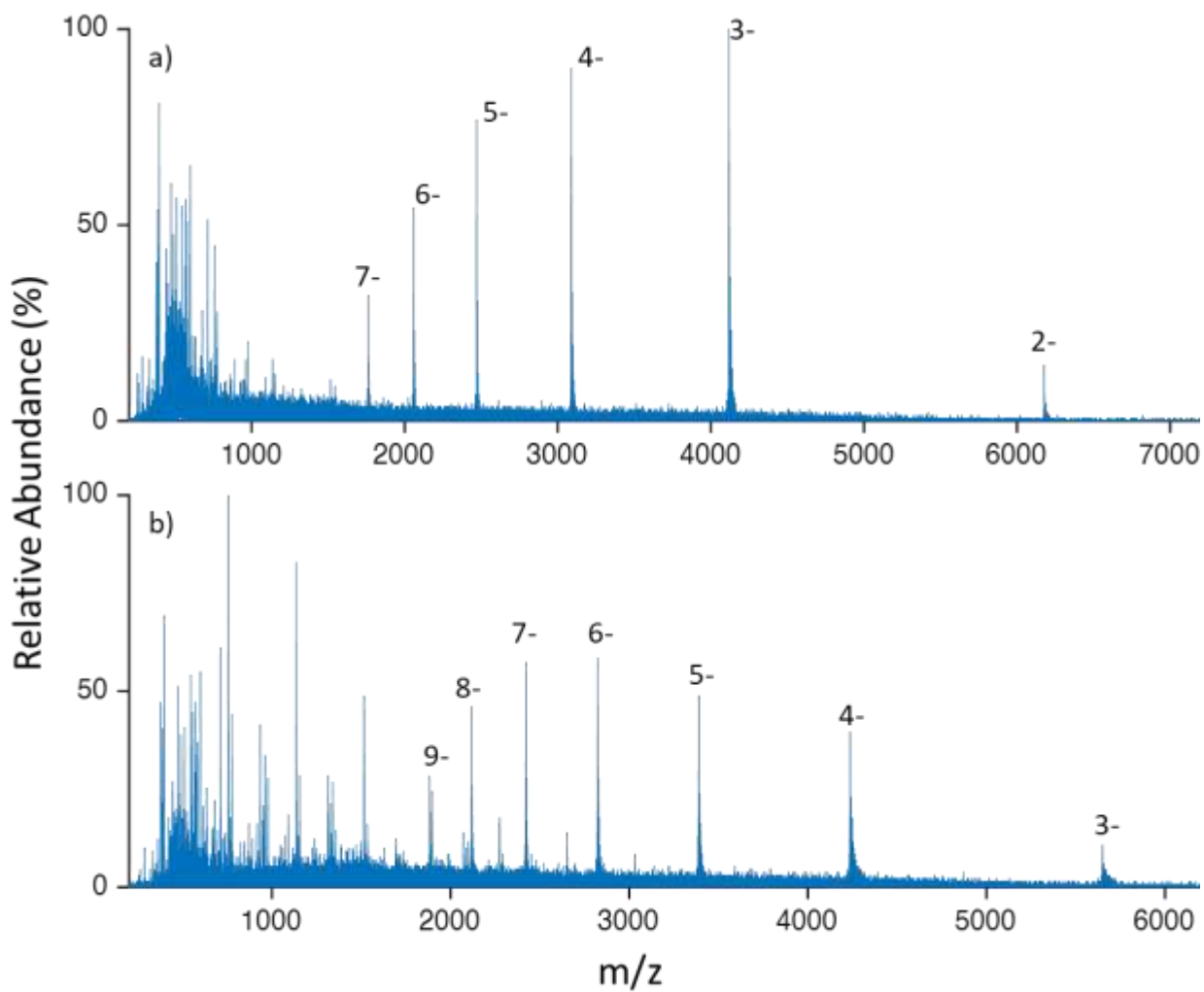


Figure 4.7 Charge-inversion ion/ion reaction spectra between 50 hyaluronic acid anions (m/z 200-1500) with a) 15+ cytochrome C and b) 24+ myoglobin.

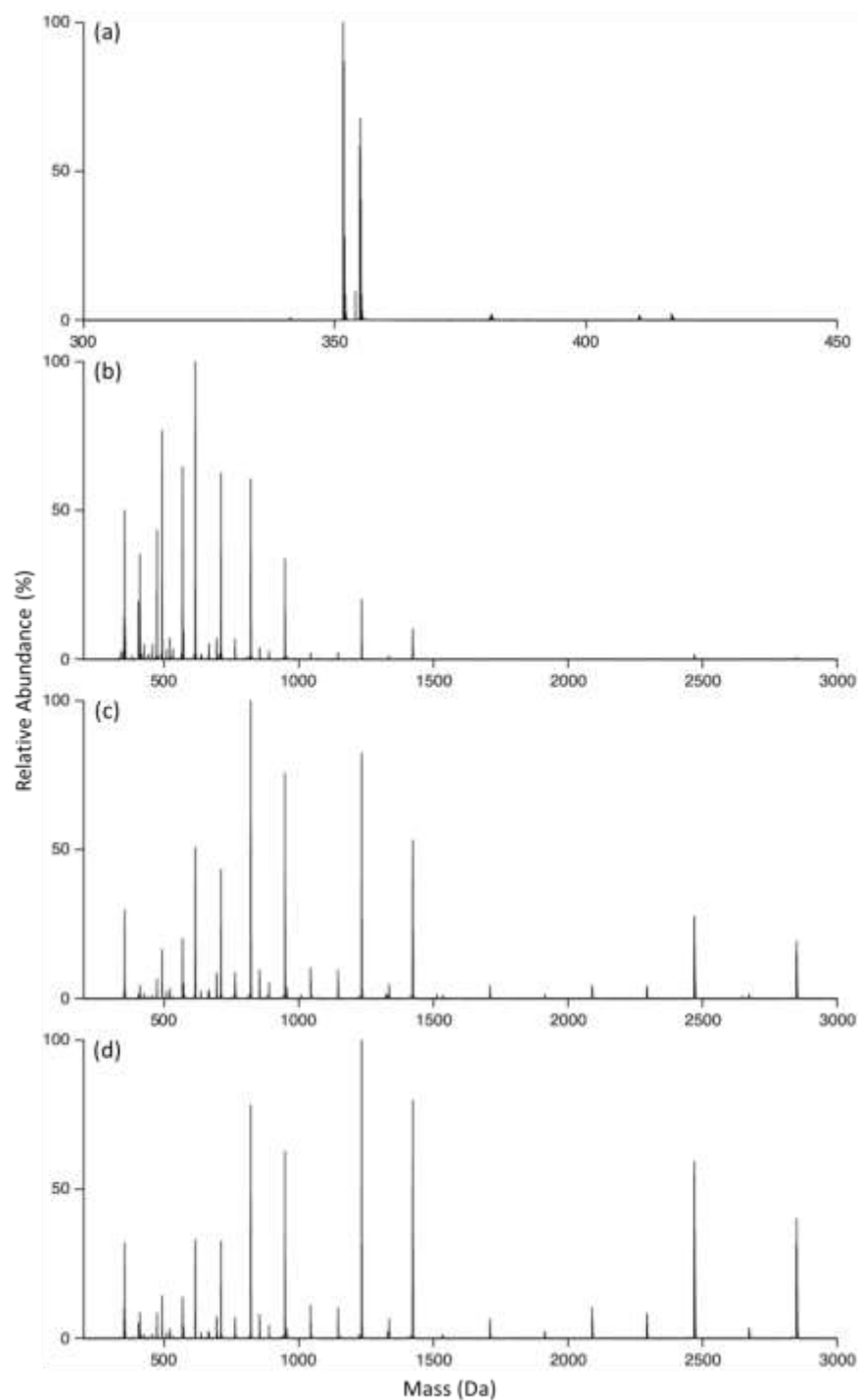


Figure 4.8 . a) Pre-ion/ion reaction spectrum of isolated 7- and 8- HA from the HA mixture and post-ion/ion reaction spectrum using b)pyridine, c) 7,8-benzoquinoline, and d) 1,8-dimethylamino naphthalene (Proton-sponge®).

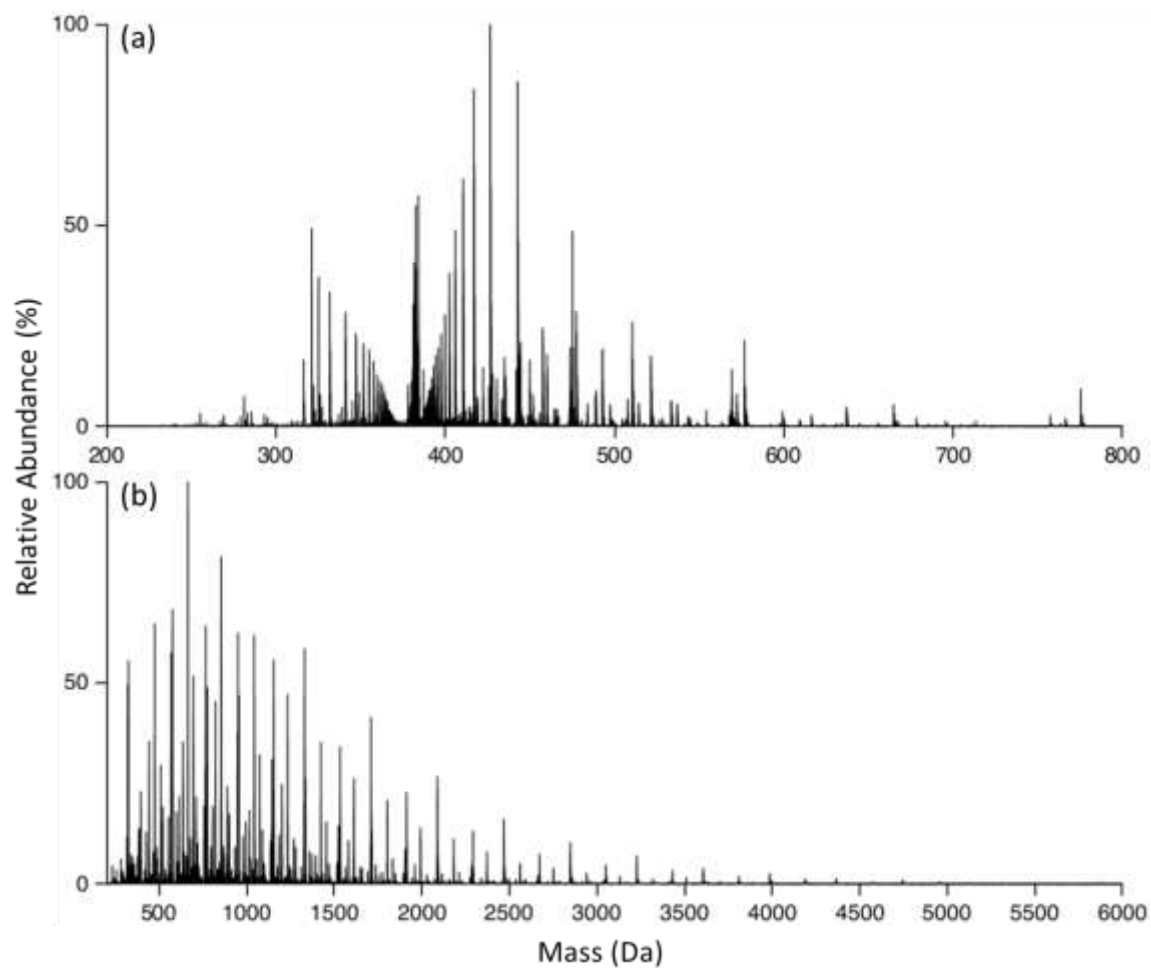


Figure 4.9 a) Pre-ion/ion reaction spectrum of isolated 'emerald city' from the HA mixture and post-ion/ion reaction spectrum using b) 1,8-dimethylamino naphthalene (Proton-sponge®).

CHAPTER 5. INVESTIGATION OF MONOCLONAL ANTIBODIES

5.1 Introduction

Monoclonal antibodies (mAbs) are a growing class of therapeutic protein candidates undergoing clinical development.[42] Currently, over 70 mAbs are commercially available after approval by the Food and Drug Administration (FDA) and just recently in 2018 twelve mAbs have been approved out of 59 total new drugs.[2, 3] They are used to treat a wide range of diseases such as cancer, autoimmune diseases, cardiovascular diseases, inflammatory diseases, and neurological diseases. [4-10] Unlike classical small molecule drugs, which still make up over ninety percent of drugs on the market today, large molecules such as mAbs, also known as biologics or biopharmaceuticals, are protein molecules composing of more than 1,300 amino acids and have an average molecular weight of 150 kDa. The increased size introduces extra complexities not only in the synthesis process but also structural properties and characterization.

The most common form of mAbs used as biotherapeutics are variants of immunoglobulin G (IgG), based on human or mouse IgG. As shown in Figure 5.1, IgGs are composed of four polypeptide chains (two ~25 kDa light and two ~50kDa heavy) totaling around 150 kDa in mass. The tertiary and quaternary structure of the protein is defined by the intra- and intermolecular disulfide bonds linking together the four polypeptide chains forming an overall Y-like shape, Figure 5.1a. Variations in the number of disulfide bonds as well as their location are aspects of various IgGs subclasses. The heavy and light chains are composed of different regions and domains. The light chain is composed of two domains, Figure 5.1b: a variable domain (VL) and a constant domain (CL). The heavy chain is similar such that it has a total of four domains with three constants (CH1, CH2, and CH3) and one variable (VH), Figure 5.1c. The domains are

paired up symmetrically, as shown in Figure 5.1a, and form various regions termed Fab and Fc. The Fab region contains the two variable domains, VL and VH, which make up the antigen binding site. The Fc region contains two highly conserved N-glycosylation sites. The connection between the Fab and Fc region is called the hinge region. This region is an area of major difference when looking at the various subgroups of IgG. The number of disulfide bonds can vary from 2, for IgG1, to 11, for IgG3. While the inter-chain disulfide bonds vary, the intra-chain disulfide bonds, a total of 12, are constant for the four classical IgG subclasses. Other forms of variation do occur such as methionine oxidation, deamidation of glutamine to glutamic acid, formation of pyroGlu, and etc. IgGs are complex structures that require sophisticated analytical tools to validate their quality throughout the manufacture process as well as transport. Mass spectrometry (MS) is a key analytical technique that can be used for molecular quality control of IgGs on a molecular level. The challenge to characterize IgGs using mass spectrometry is an ongoing research and development progress.

Several approaches are available for the MS analysis of large proteins such as IgGs. There are three well known proteomics methods used for primary structure characterization with the most common technique called bottom-up.[11] In bottom-up, tryptic digestion of the IgG is applied via the use of the trypsin enzyme that cleaves at the C-terminal end of lysine (K) and arginine (R) reducing intact IgG into shorter peptides (0.5-2 kDa). The resulting peptide mixture is analyzed typically via reverse phase HPLC followed by tandem MS for sequence analysis. The individual peptides are then assembled back together using computer software to get the full protein sequence which can be difficult and imperfect. Bottom-up can also introduce artificial post-translation modifications (PTMs) into the peptide sequence, such as deamidation,[12] due to the basic solution conditions needed for trypsin digestion. Top-down proteomics is another

method which approaches structure characterization from the opposite spectrum compared to bottom-up.[13] Proteins are analyzed in its entirety and no enzymatic digestion is performed prior to mass spectrometry analysis. This method preserves the overall tertiary and quaternary structure of proteins, should they be examine in their native state, which is valuable information, and saves time and effort to assemble the sequence back together. However, full sequence coverage obtained via tandem MS is technically challenging for top-down and overall lower compared to bottom-up.[reference] If disulfide bonds are also present in the protein, the overall sequence coverage can be drastically low. Top-down MS/MS can frequently obtain labile PTMs, such as glycosylation or phosphorylation, upon classical methods of fragmentation.[14, 15] Research into alternative fragmentation methods such as UVPD have shown an increase in sequence coverage of big proteins [16] compared to typical low energy collisional induced dissociation (CID) or higher-energy collision dissociation (HCD), specific to Thermo instruments, but the sequence coverage for large proteins such as IgG is not anywhere close to 100% and requires multiple fragmentation methods.[17] A compromising approach between bottom-up, full digestions of the protein, and top-down, no digestion at all, is the use of specific enzymes that breaks apart the protein into >10 kDa protein subunits for analysis termed middle-down. [58] For IgG, a popular enzyme used is IdeS, from *Streptococcus pyogenes*, which cleaves the heavy chain below the hinge region.[18] After reduction of disulfide bonds, three 25 kDa proteins are generated, namely, Lc (light chain), Fd (CH2 and CH3 of heavy chain, and Fc/2 (VH and CH1 of heavy chain). Mass spectrometry methods for analysis of proteins at these molecular weights is much more developed and easier to implement than 100+ Dka proteins with 100% sequence coverage achieved on carbonic anhydrase (29 kDa) using top-down proteomics. [19] For IgG, middle-down analysis using 193 nm ultraviolet photodissociation (UVPD) as the

activation method gave up to 80% sequence coverage. [16, 20] The brief explanation of methods described above is mass spectrometry techniques that have been researched and developed for proteomics. One aspect that has not been discussed are the uses of separation methods, such as reverse phase HPLC or size exclusion chromatography (SEC), to separate the complex mixture as well as its role in sample cleanup prior to MS analysis. LC/MS is a huge and important aspect for modern-day mass spectrometry applications but specific discussion of LC is not pertinent to the topic at hand.

As part of the Eli Lilly injectable collaboration program, access to pharmaceutical grade monoclonal antibodies was provided. Within this chapter, details of all the analysis performed IgG samples obtained from Eli Lilly as well as the methods involved are provided and explained.

5.2 Experimental

5.2.1 Materials.

Samples of monoclonal antibodies provided by Eli Lilly were obtained from the Michael Ladish and Pavlos Vlachos group here at Purdue University. The monoclonal antibodies are provided in either a concentration of 25 mg/mL (standard sample), 123.2 mg/L (low viscosity sample), and 192.5 mg/mL (high viscosity sample). The exact composition of the solution was not provided by Eli Lilly other than the concentration. Optima LC/MS grade water, glacial acetic acid, and isopropanol were purchased from Fisher Scientific (Pittsburgh, PA). Acetic acid was diluted to 1% in water before use. PD MidiTrap G-25 columns produced by GE Healthcare Life Sciences, dithiothreitol (DTT), iodoacetamide (IAA), ammonium bicarbonate, urea, and acetone were purchased from Sigma-Aldrich (St. Louis, MO).

5.2.2 Mass spectrometry.

Analysis of monoclonal antibodies was performed on a SCIEX TripleTOF 5600 (SCIEX, Concord, ON, Canada), a hybrid quadrupole/time-of-flight (TOF) mass spectrometer, previously modified for ion/ion reactions and dipolar direct current (DDC) implemented on the q0 and q2 quadrupoles. [21] A nano-electrospray spray ionization source was made from borosilicate glass pulled to have an average tip diameter of 3-5 μm . Ions were injected into the mass spectrometer, isolated in Q1 via transition mode if needed, and stored in q2 before injected into the time-of-flight for mass analysis. When DDC is applied to the ion population in q2, there is a 5 ms ramp-up and 5 ms ramp-down segment sandwiching the main q2 DDC scan segment. The exact amplitude, time, and q2 RF applied during the DDC segment will be detailed in each set of figures.

Differential ion mobility spectrometry (DMS) related experiments were also performed on the TripleTOF 5600 mass spectrometer. After injection of ions via nESI, the ions are then separated by the DMS device (mounted previous where the curtain plate was), sent through Q1, and stored in q2 high pressure cell. Ions can be subjected to q2 DDC prior to TOF analysis or just sent directly into the TOF for mass analysis.

5.2.3 Sample Preparation.

Samples of monoclonal antibodies were filtered through the G-25 column to remove as much salt and small molecules as possible from the solution. The G-25 columns were first equilibrated with three 5 mL washes of the final solvent, either water or 1% AcOH, before small amounts of sample was loaded onto the column. The sample amount varied between 50 μL to 300 μL depending on the initial concentration of mAbs in solution. Solvent is then added to the column so that the total sample amount loaded equals 1 mL. The sample is then eluted from the

column with 500 μL of solvent and collected. The cleaned up sample is used as is or can be further diluted in desired solvent.

5.2.4 Disulfide Cleavage Photochemistry Setup.

A mercury lamp with a primary emission wavelength of 254 nm purchased from BHK, Inc (Ontario, Canada) was used in a homemade photochemical reaction device. A syringe pump linked to a 100 μm diameter silicate capillary was exposed to UV light within an enclosed box. Samples eluted from the capillary was directly collected in a nanoelectrospray borosilicate capillary and used for mass spectrometry analysis. The degree of photo exposure for the sample within the enclosed box to the UV lamp was varied by modulating the syringe pump speed.

5.2.5 Reduction and Alkylation of Disulfide Bonds.

Ammonium bicarbonate and urea were added to 100 μL of IgG sample that has been cleaned up using the PD Mditrap G-25 column to a concentration of 100 mM and 6 M respectively. 10 μL of 0.05 M dithiothreitol (DTT) in water was added to the IgG solution. The sample was then incubated at 56 $^{\circ}\text{C}$ for 40 minutes in a water bath before a brief centrifuge to collect any condensation. 0.3 mg of iodoacetamide (IAA) was added to the solution and reaction at room temperature for 30 minutes in the dark. 10 μL of 0.05 M DTT was then added to the solution and reacted for 15 more minutes in the dark at room temperature. The finished reaction product was cleaned up using an Agilent 1200 Series HPLC system with a C3 column and collected offline followed by mass spectrometry analysis.

5.2.6 Circular Dichroism

Circular dichroism (CD) measurements were performed on a Jasco J-1500 Circular Dichroism Spectrophotometer in the Research Instrumentation Center (RIC) in the Department

of Chemistry here at Purdue University. Samples were loaded into a 1 mL quartz cell purchased from Starna Cells, Inc. (Atascadero, CA, USA) and scanned over 200-260 nm wavelength. Sample heating is controlled by the instrument and a gradual heating ramp of 0.5 °C/min with a one minute equilibration time at the desired temperature was used for the CD measurements.

5.3 Results and Discussions

5.3.1 Requirement for Sample Cleanup

The mechanism of electrospray ionization (ESI) has been previously describe in chapter one and three main models that has been widely accepted are the Ion Evaporation Model (IEM), Charge Residue Model (CRM), and Chain Ejection Model (CEM). The ionization pathway for native electrospray of large proteins such as IgG will proceed through CRM and as a consequence salt ion (Na^+ , K^+ , etc.) will condense upon the protein ion as the droplet shrinks and dries up. The increase in adduction onto the protein will result in a broad peak in the mass spectrum and an overall decrease in max signal intensity as the signal is spread out over a broader m/z range. Adduction of sodium ions is very much present upon electrospray of ubiquitin in water and the presence of these adducts is expected to increase with the mass of the protein involved. Removal of low molecular ions and adducts that may condense onto protein during the CRM process can be achieve via the use of offline size exclusion filter column. The PD MidiTrap G-25 columns are size exclusion columns containing the Sephadex G-25 gel filtration matrix that filters out biomolecules 5000 Da or higher while retaining lower molecular weight entities within the matrix. Electrospray of low viscosity 123.2 mg/mL mAb sample that has been diluted by 300x is shown in Figure 5.2a. While individual charge state peaks can be distinguished for some of the higher charged ions, the overall quality of peaks is not ideal and adduction is rampant. One point to note is how the peak resolution seems to decrease as the

charge state decreases for the monomeric mAb in Figure 5.2a. This phenomenon is consistent with our understanding of how CRM mechanism operates and has been previously reported by Karas et al. [22] According to their mechanism, this trend of increasing adduction for decreasing charge states can be attributed to different charge states formed at various extent of droplet evaporation during the electrospray process. The observed degree of adduction is closely tied to the concentration of adducts present in the charged droplet at the time of ion formation. Higher charge state ions are formed in the early phases of the droplet evaporation/fission process and thus contain adduct concentration similar to the bulk solution. Lower charge state ions are formed later in the electrospray process where droplets underwent more extensive evaporation and a higher concentration of adducts are present in the droplet which in turn condense upon the analyte ion per CRM.

5.3.2 Electrospray and DDC of mAbs.

The resulting spectrum after application of the G-25 column to the IgG sample as previously described is shown in Figure 5.2b. Overall, peaks are much better resolved with the lower charged monomeric IgGs ions also distinguished compared to pretreatment and even dimer peaks are observed. The post column treatment process did not introduce any artifacts in the spectrum as the features of the monomers and dimers are still present compared to the direct sampling spectrum. Glycoforms for the IgG are still not resolved in the spectrum. Another run through the columns did not change overall spectrum quality compared to a single run.

For the 5600, q0 and q2 has been modified with dipolar direct current (DDC) collisional activation. Webb et al. have demonstrated the use of DDC to decluster loosely-bound adducts on large biomolecules in q0 using a similar time-of-flight instrument, SCIEX QSTAR, [23] and the same technique was applied to the IgG ions on the 5600. The key characteristics of DDC have

been described by Tolmachev et al. and a very brief summary of DDC is given here. [24] DDC is a broadband collisional activation technique achieved by applying a potential difference, $\pm V_{\text{DDC}}$, between two of the rods in a linear quadrupole ion trap or the two end caps in a 3D ion trap. The entire population of ions is offset from the center of the trap and experience collision heating from higher order RF field present off-center from within the trap. The ions are slowly heated, similar to single frequency CID or inferred multiphoton dissociation (IRMPD), and upon collision with the bath gas shed off loosely bound neutral adducts. More details of equations governing DDC can be found in chapter one. Unlike what Webb et al. did on the QStar where they trapped the ions in Q0 and applied DDC there, in this case it was applied in the high pressure q2 collision cell instead. The advantage for application of DDC in q0 compared to q2 is the slightly higher pressure which can be helpful for better collisional activation of the ions; however, the limitation of q0 DDC is the high mass limit which is related to the DDC voltage and q0RF that applied. The q0RF voltage is not directly controllable on the 5600 and is capacitively coupled to the Q1RF thus limiting how much RF q0 can be supplied. The DDC voltage applied directly impacts the heating applied to the ions with a higher voltage leading to an overall higher temperature; however, higher DDC voltages also imparts a high mass cutoff to the spectrum where high m/z ions are ejected from the trap after been displaced too far away from the center. This effect can be mitigated with higher RF voltage from the quadrupoles but experimentation with q0DDC on the 5600 have shown that the high mass cutoff is very drastic and directly impedes analysis of m/z regions of interest using a DDC voltage which will knock off sufficient amount of adducts. The post q2DDC spectrum, Figure 5.2c, drastically improves the spectral quality compared to pre-DDC spectrum, Figure 5.2b, with monomer and dimer peaks now easily identifiable. Trimer peaks are also much more prevalent now and can be recognized.

However, information regarding the IgG's glycoforms is still not present as they are not resolved in the spectrum.

In order to get an accurate molecular weight measurement of the IgG and its glycoforms, the sample is ran through the desalting columns that has been pre-equilibrated with 1% acetic acid instead of water. By spraying the IgG in a denaturing solvent, the protein ions will be denatured in solution and the ionization mechanism will not be CRM but CEM. Unlike CRM where the native proteins reside in the nucleus of the droplet as the droplet dries off, in CEM the highly charged and unfolded protein, induced by low pH of the solution, will extrude out of the droplet instead. This pathway reduces the amount of salt adducts that might occur and will provide a much cleaner spectrum. Electrospray of IgG in 1% acetic acid drastically increased the overall charge distribution of IgG is way higher compared to native and four charge state distributions are observed compared to just the one in native. A closer look at any of the peaks in the spectrum still showed signs of heavy adduction onto the ion. Application of DDC to the ions showed a drastic change in the spectrum where peaks sharpened up drastically and finer details of the glycoforms for the IgG are observed, Figure 5.3a. Reconstruction of the peaks in the m/z 3500 to 4500 region for the zero-charge mass spectrum, Figure 5.3b, showed the glycoforms present on the mAb. A series of 162 Da separations between the base and subsequent peaks are indicative of the various glycoforms of the IgG with the 162 Da being extra fucose entities on the glycan..

Samples of mAbs were treated with PNGaseF enzyme to remove glycan from the IgG to confirm the possible molecular weight and identity of the glycans attached. Reconstruction of the post-PNGase F treated IgG in 1% acetic solution mass spectrum showed a difference of approximately two G0F glycans for the base peaks, Figure 5;thus, confirming the glycosylation

on the IgG. The additional glycoforms with their molecular weight difference of 162 Da are likely G1F or G2F glycans on the IgG.

The effects of DDC in both native and denatured spectra of mAb revealed a drastically improved spectrum that not only has sharpened up but also condensed the ion signal resulting in an overall higher signal, as shown in Figure 5.2c and Figure 5.3a respectively. This condensation effect is demonstrated in Figure 5.4 where the pre- and post-DDC spectrum are compared for a region of the denatured IgG spectrum and a 6x signal increase was observed. A combination of both offline sample preparation as well as gas-phase mass spectrometry technique was able to improve the overall spectra quality of large proteins such as mAbs when ionized by ESI. Using a volatile buffer, such as ammonium acetate, in the solvent is another method to decrease adduction. [25-27] One thing to note is that there are still other methods to desalt large proteins during electrospray, for example, using nano-electrospray, which was done here, to generate smaller droplets to decrease non-volatile salt concentration that occurs during droplet desolvation. [22] Various other interface options such as counter flow dry nitrogen (sometimes heated) has been previously used for solvent removal and declustering purposes. [28] A strong potential gradient applied between the orifice and sampling apparatus (skimmer, lenses, capillary, etc) causes collisional activation in the interface area which can be useful for declustering. [29] Unlike DDC, any form of beam-type collisional activation method will be an uneven heating method as the potential energy imparted onto the ions or droplets are dependent upon the mass and charge. DDC is a form of collisional activation method where all ions are heated uniformly. Another type of voltage gradient that can be induced in the interface is a type of wedge-shaped potential difference where ions are slowed down in the high pressure interface region to give the droplets more time to desolvate and decluster. It should also be noted that based on personal

experience with the SCIEX instrument in the lab a strong potential gradient between the curtain plate and the orifice is also very helpful in delivery of more ions into the mass spectrometer for increased signal.

5.3.3 Parameters for DDC.

The three key experimental parameters for DDC to decluster biomolecular ions are the quadrupole RF, DDC voltage applied, and time of DDC applied. As use of DDC in q_2 for the 5600 was never applied it was necessary to gauge how each of these parameters influence the resulting spectrum. The high pressure collision cell, q_2 , in the 5600 is limited by its ability to have a high low mass cutout due to its RF frequency of 1.1 MHz. The max setting for the low mass cutout in the 5600 is limited to m/z 510 at $q = 0.908$. Ions in the m/z 5000 region would naturally be at a q value of approximately 0.1 when the low mass cutoff for q_2 is at m/z 500. It is preferred for ions of interest to be trapped as deep in the potential well as possible for ion traps to prevent any chances those ions will be lost. The deepest potential well in the trap is at $q = 0.706$ which would require a fairly high low mass cutoff. For most applications in storing high molecular weight ions on the 5600, it has been observed using a low mass cutoff of m/z 200 is applicable for trapping ions in the m/z 5000 plus range with no significant degradation in signal intensity observed; however, in the case for application of q_2 DDC a higher low mass cutoff is beneficial not only because it gives greater leeway in terms of how much energy can be deposited into the ions before it is ejected out of the trap but also allows for a wider range of voltages that can be applied to finely tune the DDC to account for the high mass cutoff. It was initially decided that a q_2 RF value of 500 was sufficiently high enough with enough of a safety margin to tune the DDC voltage as well as duration. A DDC voltage of 80 V for duration of 50 ms with a 5 ms ramp-up and ramp-down time at a q_2 RF of $m/500$ gave sufficiently enough of

declustering as well as a high enough of high mass cutoff such that aggregates for the mAbs are still observed. No significant difference was observed when increasing duration of DDC time up to 300 ms which is why DDC time was kept at 50 ms. Increasing the DDC voltage up to 100 V lowered the high mass cutoff from m/z 11000 to around m/z 8000 and all the aggregates were lost. The increased in DDC voltage did provide slightly sharper peaks of the monomers but still not enough to see any signs of the glycoforms. For the denatured mAb spectrum, the DDC voltage was increased to 90 V while which put the high mass cutoff around m/z 10000. Further increases in the DDC voltage could be performed as the main distribution of ions are in the m/z 3000 region but fragmentation was observed in the m/z 1000 region at 90V and further increase in DDC voltage increased those fragment ions with no significant decrease in adduction compared to 90 V. Recently, the 5600 has been issuing alerts regarding the q2 current being too high resulting in overheating with the spectrum collected also being affected by this. It can only be surmised that prolonged settings of the q2RF close to its maximum value have degraded the electronics over time and that it cannot be ran at that settings in the near future; thus, recent and future q2DDC will be performed at a q2RF value of 450. Tuning of the DDC voltage and the time did yield comparable spectra to before but overall the quality was not as still as good as before in terms of adduction removal.

5.3.4 Agitation and Analysis of mAbs.

Another difference between biologicals and small molecule drugs is how the active pharmaceutical ingredient (API) is stored as well as the delivery method. The most common form of drug delivery system is typically a tablet or pill which suits small molecules but is unsuited for biologicals as the strong acidic environment of the stomach and intestines digests proteins, and therefore become ineffective. Biologicals are therefore administered by injection or

infusion instead. Biologics are also stored differently compared to small molecule drugs, solid vs liquid, and their molecular stability as well as tendency for aggregation is also very different. A key concern during the biopharmaceutical development is aggregation [30-34] and mass spectrometry is a helpful tool that can be used to measure and characterize mAb aggregation. A lot of previous research conducted in this area has mostly relied upon spectroscopic techniques. Protein aggregation typically comes in two forms, reversible and irreversible aggregation. Reversible aggregation is when the aggregates can come apart and not cascade into particles upon initial formation of dimers or trimers. These aggregates are typically non-covalent interactions often formed by electrostatic interaction or simply van-der Waals forces. Irreversible aggregation is aggregates formed by either covalent modification, in the case of IgGs typically intermolecular disulfide formations, or aggregation of denatured proteins which cascades into particulates. Aggregations formed by these pathways do not revert back to their monomeric form. Protein aggregation can occur via many pathways depending environmental factors such as solution pH, ionic strength, mechanical stress, light exposure, and so forth. [75-78] Conformation alteration of previously discussed factors may expose aggregation-prone sequences of the proteins [38] and mass spectrometry can be used to probe molecular changes in higher-order protein structure via the use of hydrogen-deuterium exchange (HDX) mass spectrometry. [1, 39-41]

Aggregation of IgG is an important area to look at during the formulation, storage, transport, and delivery of the active pharmaceutical ingredient (API) into the human body. Dosages of IgG can vary from tens of milligrams up to hundreds of milligrams in terms of solution concentration depending on the form of delivery device: a low concentration high volume intravenous (IV) injection or a high concentration low volume single shot injection.

Pharmaceutical companies are aware of IgG aggregation and typically mix in surfactants, such as polysorbate 80, [33] or specialized buffers within the solvent to mitigate aggregation occurring; however, external factors after formulation such as temperature change, photon exposure, physical stress on the solution, or etc. can all occur and are factors in formation of aggregation. Research into these external factors is ongoing and as part of the Eli Lilly collaboration it was important to look into IgG aggregates.

A particular type of mechanical stress was of particular interest: bubbles formed by cavitation in syringe of an autoinjector containing a high concentration, low volume (a couple mL) amount of IgG intended for subcutaneous injection. Cavitation occurs when the plunger of an auto injectors come into contact with the liquid surface of injectable solution with sufficient velocity and force forming microbubbles in the solution that form, grow, and collapse. [42] It was important to look how bubbles formed by cavitation might influence the IgG within solution prior to injection.

Samples of IgG were collected after they have been ejected out from the auto injectors provided by Eli Lilly and obtained from the Pavlos Group. Two types of IgG solutions were provided: low viscosity 123.23 mg/mL and high viscosity 192.5 mg/mL. Triplicate runs of each mAb solution ejected from various types of autoinjectors were performed as well as a standard solution that has not been passed through the autoinjection process. Using the methods previously described, comparison of mass spectra between the standard solution and post-ejected samples were very similar with example spectra shown in Figure 5.6, 5.7, and 5.8. The butterfly comparison plots reveal little to no difference for the native, denatured, or deconvoluted spectra. No changes in aggregation pattern or changes to the molecular weight as well as glycoforms of the IgG were observed across all the samples, for both low viscosity and high viscosity. No signs

of any denatured dimer or trimer IgG peaks are present in the mass spectrum or reconstructed spectrum indicating the dimers and trimer peaks observed in the native mass spectrum are not covalent bound aggregates. The aggregation observed are most likely to be loosely bound that came together either by weak intermolecular forces or a cause of the initially high concentration of IgG in the original solution. Based on these results the effect of cavitation on the IgG is little to none.

5.3.5 Thermal Denaturation

Structural stability of proteins is inherently important as the protein's functionality is directly linked to its structure. Structural alteration can be as simple as deamidation to large changes such as overall tertiary and quaternary structure. Denaturation of proteins, or the unfolding of protein's native structure, can occur in various ways, the two most common methods to achieve this can be done through chemical or thermal. Chemical denaturation of proteins can easily be achieved by modulating the pH of the solution and is a common method to study how proteins denature. Electrospray of protein ion in an acetic solvent generates highly charged denatured protein ions. Thermal denaturation allows study of denatured proteins in their native solution conditions. For mass spectrometry, protein conformations are determined by their charge state distributions and can usually be used to determine if a protein is folded or unfolded. [43] Drift tube ion spectrometry is another method that can be used to look at gas-phase structural change through the measurement of the ion's collisional cross section in a low potential field gradient. [44, 45] Recently, a new spectrometry method called differential mobility spectrometry (DMS) or high-field asymmetric waveform ion mobility spectrometry (FAIMS) has also been used to separate an ion's mobility based on its mobility in high and low electric field. [46] DMS device has been used to separate peptides, [47] proteins, [48] lipids,

[49] isomers, [49] and conformationally different molecules [50] in the gas-phase but never been applied to large molecules such as IgG. DMS on the 5600 has since been applied to thermally denatured BSA and IgG samples. Circular dichroism (CD) is an analytical technique that measures secondary structures such as the presence of alpha helices or beta sheets and can be employed as a secondary method for validating protein denaturation. The charge state distribution of proteins is more closely related to tertiary and quaternary structure of proteins compared to the secondary structure information from CD measurements but can serve as an indicator of protein structural change that ESI might not be sensitive to.

Thermal denaturation of bovine serum albumin (BSA) was performed in a CD spectrometer with temperature control. Each BSA sample was heated up to the desired temperature within the spectrometer before a CD spectrum was taken. The solution of said sample was then sprayed into the mass spectrometer for mass analysis. Figure 5.9 details the resulting CD spectrum of BSA at various temperatures and the accompanying mass spectrum at some of those temperatures. BSA is populated by various alpha helix secondary structures and the resulting CD spectrum reflects that. No drastic change was observed for both the mass and CD spectra up till 60 °C. Minor changes in the CD spectra up until 60 °C indicates changes in the secondary structure of BSA but the mass spectra for those temperatures remains similar, showing the same charge state distribution of BSA monomers, dimers, and trimers. Only at 70 °C, where the CD spectrum has a significant shift did the mass spectrum at that temperature also showed that BSA was highly charged and denatured. The melting point of BSA in literature is 68 °C and CD as well as mass spectrometry data is consistent with that. This result validates that mass spectrometry is not particularly sensitive to secondary structural changes, while CD is, as the protein undergoes structural changes due to thermal denaturation but once significant changes

occur to both secondary and higher order protein structure CD and mass spectrometry are both sensitive to that.

The same experiment was performed with IgG and the results are shown in Figure 5.10. The CD spectrum does not indicate any specific secondary structure information such as alpha helix or beta coil, unlike BSA. Changes in temperature had almost little to effect on the CD spectrum until 70 °C. Mass spectra for those temperatures are also in agreement with the CD data. Mass spectra for the IgG at temperatures up to 60 °C are close to identical copies with the presence of monomers, dimers, and trimers observed. At 70 °C the mass spectrum does not show the presence of highly charged denatured IgG ions, unlike BSA, but aggregate ions are no longer present. The melting point of this particular IgG molecule is not provided but judging by the CD spectrum it would be between 60-70 °C. CD and mass spectrometry were both able to detect changes in protein structure upon thermal denaturation for both BSA and IgG. CD was not able to provide complimentary information when paired with mass spectrometry but does act as a form of secondary analytical technique for confirmation.

Analysis of BSA ions using the DMS interface is presented in Figure 5.11. Native and denatured BSA ions were subjected to gas-phase separation before analysis by mass spectrometry. Little to no separation of individual native ion charge states were observed in DMS separation space and the ions overall combine to form a fairly wide gaussian peak. The denatured BSA DMS spectrum is wider than native BSA and overall lap between individual charge states is still very significant. Increase in the denatured charge state of BSA showed a gradual shift in the DMS spectrum where signal increased in the lower CV range. When the entirety of the DMS and mass spectrum is considered, the DMS spectrum is dependent on the charge state of the protein ion and do not provide enough separation of separation to cleanly

separate any charge state of BSA. The principle for which DMS operates on, separation of ions based on their high and low field mobility, does not appear to be a great analytical technique for detailed separation of high m/z ions such as proteins.

5.3.6 Photochemical Cleavage of disulfide bonds.

Xia et al. has developed a photochemical system has since then been used for cleavage of disulfide bonds in peptides and proteins with the proposed reaction scheme described in Figure 5.12. [51] The same reaction setup was then applied to IgG, the largest protein ever tried by this method, Figure 5.13. The reaction condition as well as the flowrate was experimented with and optimized to the final condition of 50/50 water/isopropanol with 2% acetone and 0.5 % formic acid with an exposure time of ~4.4 s to the ultraviolet light providing the best quality spectrum. An increase in acetone percentage in the solution resulted in formation of side products where the acetone covalently bond to the cysteine. A long exposure time can also cause this side reaction to occur as well. It is a balancing act between the percentages of acetone added as well as exposure time. The sample was collected from the reaction in a borosilicate nESI tip and ionized. The resulting spectrum from this reaction, Figure 5.14b, depicts both the light and heavy chain of IgG. The light chain is much more abundant in signal compared to the heavy chain which could be due to ionization efficiency differences as both should be equal molar. Reconstruction of the post-PB reaction spectrum gave the molecular weight of a light chain and heavy chain. Based on the molecular weight difference between a fully intact IgG and the individual light and heavy chain, a 22 Da difference is present which constitutes 11 disulfide bonds. Comparing the sum of the light and heavy chain MW information obtained from a traditional reduction and alkylation of disulfide bonds by DTT and IAA to the intact IgG molecular weight revealed the presence of a total of 32 cysteines present on the IgG, a total of 16

disulfide bonds. 16 disulfide bond would fit the typically IgG1 subclass. [52]. Based on this result, the photochemical method broke 11 out of 16 total disulfide bonds. All the intermolecular disulfide bonds have been broken and some of the intramolecular are broken as well. Based on molecular weight information, all disulfide bonds in the light chains were broken with remaining unreacted disulfide bonds present on the heavy chain.

5.4 Conclusions

Methods and results for the analysis of IgG are discussed here. An offline method to desalt the solution combined with gas-phase broadband collisional heating, q2DDC, greatly reduced the amount of adducts observed on the IgG ions thereby increasing spectral peak quality. Native analysis of IgGs preserved loosely bound aggregates present in solution and denatured analysis gave the most accurate molecular weight information. Comparison of IgG spectra before and after the effects of cavitation in an autoinjector revealed little to no change in aggregates as well as molecular weight. This indicates that cavitation has not effect on the IgG or simply IgGs that have been affected cannot be observed in the mass spectrometer due to their low abundance. Denaturation of IgGs by thermal and chemical methods was investigated using mass spectrometry, circular dichroism spectroscopy, and differential mobility spectrometry. Denaturation is most apparent in the mass spectrum by the high protein charge states and CD as well as DMS provided complimentary information reaffirming the mass spectrometry results. Photochemical reaction successfully cleaved 11 out of 16 disulfide bonds in the IgG using only 4.4 seconds of photo exposure and confirms the viability of this reaction for large proteins. This is the first time IgGs have been analyzed in the McLuckey lab and a variety of analytical methods was applied. May this chapter serve as a template and guide for future work in the analysis of large biological molecules.

5.5 References

- [1] R. Majumdar, C.R. Middaugh, D.D. Weis, D.B. Volkin, Hydrogen-deuterium exchange mass spectrometry as an emerging analytical tool for stabilization and formulation development of therapeutic monoclonal antibodies, *J Pharm Sci*, 104 (2015) 327-345.
- [2] A. Mullard, 2018 FDA drug approvals, *Nature reviews. Drug discovery*, 18 (2019) 85-89.
- [3] G.d.l.T. B, F. Albericio, The Pharmaceutical Industry in 2018. An Analysis of FDA Drug Approvals from the Perspective of Molecules, *Molecules*, 24 (2019).
- [4] Z. Chen, J. Wang, L. Bao, L. Guo, W. Zhang, Y. Xue, H. Zhou, Y. Xiao, J. Wang, F. Wu, Y. Deng, C. Qin, Q. Jin, Human monoclonal antibodies targeting the haemagglutinin glycoprotein can neutralize H7N9 influenza virus, *Nat Commun*, 6 (2015) 6714.
- [5] T. Oliphant, M. Engle, G.E. Nybakken, C. Doane, S. Johnson, L. Huang, S. Gorlatov, E. Mehlhop, A. Marri, K.M. Chung, G.D. Ebel, L.D. Kramer, D.H. Fremont, M.S. Diamond, Development of a humanized monoclonal antibody with therapeutic potential against West Nile virus, *Nat Med*, 11 (2005) 522-530.
- [6] J. Bayry, S. Lacroix-Desmazes, M.D. Kazatchkine, S.V. Kaveri, Monoclonal antibody and intravenous immunoglobulin therapy for rheumatic diseases: rationale and mechanisms of action, *Nat Clin Pract Rheumatol*, 3 (2007) 262-272.
- [7] P.M. Hogarth, G.A. Pietersz, Fc receptor-targeted therapies for the treatment of inflammation, cancer and beyond, *Nature reviews. Drug discovery*, 11 (2012) 311-331.
- [8] L.M. Weiner, R. Surana, S. Wang, Monoclonal antibodies: versatile platforms for cancer immunotherapy, *Nat Rev Immunol*, 10 (2010) 317-327.
- [9] C. Mauri, L.T. Mars, M. Londei, Therapeutic activity of agonistic monoclonal antibodies against CD40 in a chronic autoimmune inflammatory process, *Nat Med*, 6 (2000) 673-679.
- [10] D. Berman, A. Korman, R. Peck, D. Feltquate, N. Lonberg, R. Canetta, The development of immunomodulatory monoclonal antibodies as a new therapeutic modality for cancer: the Bristol-Myers Squibb experience, *Pharmacol Ther*, 148 (2015) 132-153.
- [11] J.R. Yates, C.I. Ruse, A. Nakorchevsky, Proteomics by mass spectrometry: approaches, advances, and applications, *Annual review of biomedical engineering*, 11 (2009) 49-79.
- [12] Y. Song, R.L. Schowen, R.T. Borchardt, E.M. Topp, Effect of 'pH' on the rate of asparagine deamidation in polymeric formulations: 'pH'–rate profile, *Journal of Pharmaceutical Sciences*, 90 (2001) 141-156.
- [13] T.K. Toby, L. Fornelli, N.L. Kelleher, Progress in Top-Down Proteomics and the Analysis of Proteoforms, *Annu Rev Anal Chem (Palo Alto Calif)*, 9 (2016) 499-519.

- [14] F. Meng, B.J. Cargile, L.M. Miller, A.J. Forbes, J.R. Johnson, N.L. Kelleher, Informatics and multiplexing of intact protein identification in bacteria and the archaea, *Nat Biotechnol*, 19 (2001) 952-957.
- [15] G.E. Reid, J.L. Stephenson, Jr., S.A. McLuckey, Tandem mass spectrometry of ribonuclease A and B: N-linked glycosylation site analysis of whole protein ions, *Anal Chem*, 74 (2002) 577-583.
- [16] J.B. Shaw, W. Li, D.D. Holden, Y. Zhang, J. Griep-Raming, R.T. Fellers, B.P. Early, P.M. Thomas, N.L. Kelleher, J.S. Brodbelt, Complete protein characterization using top-down mass spectrometry and ultraviolet photodissociation, *Journal of the American Chemical Society*, 135 (2013) 12646-12651.
- [17] B.Q. Tran, C. Barton, J. Feng, A. Sandjong, S.H. Yoon, S. Awasthi, T. Liang, M.M. Khan, D.P.A. Kilgour, D.R. Goodlett, Y.A. Goo, Comprehensive glycosylation profiling of IgG and IgG-fusion proteins by top-down MS with multiple fragmentation techniques, *J Proteomics*, 134 (2016) 93-101.
- [18] C. Wu, J.C. Tran, L. Zamdborg, K.R. Durbin, M. Li, D.R. Ahlf, B.P. Early, P.M. Thomas, J.V. Sweedler, N.L. Kelleher, A protease for 'middle-down' proteomics, *Nature methods*, 9 (2012) 822-824.
- [19] N.L. Kelleher, H.Y. Lin, G.A. Valaskovic, D.J. Aaserud, E.K. Fridriksson, F.W. McLafferty, Top Down versus Bottom Up Protein Characterization by Tandem High-Resolution Mass Spectrometry, *Journal of the American Chemical Society*, 121 (1999) 806-812.
- [20] V.C. Cotham, J.S. Brodbelt, Characterization of Therapeutic Monoclonal Antibodies at the Subunit-Level using Middle-Down 193 nm Ultraviolet Photodissociation, *Anal Chem*, 88 (2016) 4004-4013.
- [21] S. Rojas-Betancourt, J.R. Stutzman, F.A. Londry, S.J. Blanksby, S.A. McLuckey, Gas-Phase Chemical Separation of Phosphatidylcholine and Phosphatidylethanolamine Cations via Charge Inversion Ion/Ion Chemistry, *Anal Chem*, 87 (2015) 11255-11262.
- [22] R. Juraschek, T. Dülcks, M. Karas, Nanoelectrospray—More than just a minimized-flow electrospray ionization source, *Journal of the American Society for Mass Spectrometry*, 10 (1999) 300-308.
- [23] I.K. Webb, Y. Gao, F.A. Londry, S.A. McLuckey, Trapping mode dipolar DC collisional activation in the RF-only ion guide of a linear ion trap/time-of-flight instrument for gaseous bio-ion declustering, *J Mass Spectrom*, 48 (2013) 1059-1065.
- [24] A.V. Tolmachev, A.N. Vilkov, B. Bogdanov, L. Pasa-Tolic, C.D. Masselon, R.D. Smith, Collisional activation of ions in RF ion traps and ion guides: the effective ion temperature treatment, *Journal of the American Society for Mass Spectrometry*, 15 (2004) 1616-1628.
- [25] H. Hernandez, C.V. Robinson, Determining the stoichiometry and interactions of macromolecular assemblies from mass spectrometry, *Nat Protoc*, 2 (2007) 715-726.

- [26] A.T. Iavarone, O.A. Udekwu, E.R. Williams, Buffer loading for counteracting metal salt-induced signal suppression in electrospray ionization, *Anal Chem*, 76 (2004) 3944-3950.
- [27] H.J. Sterling, J.D. Batchelor, D.E. Wemmer, E.R. Williams, Effects of buffer loading for electrospray ionization mass spectrometry of a noncovalent protein complex that requires high concentrations of essential salts, *Journal of the American Society for Mass Spectrometry*, 21 (2010) 1045-1049.
- [28] T.R. Covey, R.F. Bonner, B.I. Shushan, J. Henion, The determination of protein, oligonucleotide and peptide molecular weights by ion-spray mass spectrometry, *Rapid communications in mass spectrometry : RCM*, 2 (1988) 249-256.
- [29] B.B. Schneider, D.D. Chen, Collision-induced dissociation of ions within the orifice-skimmer region of an electrospray mass spectrometer, *Anal Chem*, 72 (2000) 791-799.
- [30] J.F. Carpenter, T.W. Randolph, W. Jiskoot, D.J. Crommelin, C.R. Middaugh, G. Winter, Y.X. Fan, S. Kirshner, D. Verthelyi, S. Kozlowski, K.A. Clouse, P.G. Swann, A. Rosenberg, B. Cherney, Overlooking subvisible particles in therapeutic protein products: gaps that may compromise product quality, *J Pharm Sci*, 98 (2009) 1201-1205.
- [31] E.Y. Chi, S. Krishnan, B.S. Kendrick, B.S. Chang, J.F. Carpenter, T.W. Randolph, Roles of conformational stability and colloidal stability in the aggregation of recombinant human granulocyte colony-stimulating factor, *Protein Sci*, 12 (2003) 903-913.
- [32] H.C. Mahler, W. Friess, U. Grauschopf, S. Kiese, Protein aggregation: pathways, induction factors and analysis, *J Pharm Sci*, 98 (2009) 2909-2934.
- [33] H.C. Mahler, R. Muller, W. Friess, A. Delille, S. Matheus, Induction and analysis of aggregates in a liquid IgG1-antibody formulation, *Eur J Pharm Biopharm*, 59 (2005) 407-417.
- [34] S.J. Shire, Formulation and manufacturability of biologics, *Curr Opin Biotechnol*, 20 (2009) 708-714.
- [35] B.A. Kerwin, R.L. Remmele, Jr., Protect from light: photodegradation and protein biologics, *J Pharm Sci*, 96 (2007) 1468-1479.
- [36] B.D. Mason, C. Schoneich, B.A. Kerwin, Effect of pH and light on aggregation and conformation of an IgG1 mAb, *Mol Pharm*, 9 (2012) 774-790.
- [37] A. Hawe, M. Wiggenhorn, M. van de Weert, J.H. Garbe, H.C. Mahler, W. Jiskoot, Forced degradation of therapeutic proteins, *J Pharm Sci*, 101 (2012) 895-913.
- [38] C.J. Roberts, Therapeutic protein aggregation: mechanisms, design, and control, *Trends Biotechnol*, 32 (2014) 372-380.
- [39] H. Wei, J. Mo, L. Tao, R.J. Russell, A.A. Tymiak, G. Chen, R.E. Iacob, J.R. Engen, Hydrogen/deuterium exchange mass spectrometry for probing higher order structure of protein therapeutics: methodology and applications, *Drug Discov Today*, 19 (2014) 95-102.

- [40] C.E. Bobst, R.R. Abzalimov, D. Houde, M. Kloczewiak, R. Mhatre, S.A. Berkowitz, I.A. Kaltashov, Detection and characterization of altered conformations of protein pharmaceuticals using complementary mass spectrometry-based approaches, *Anal Chem*, 80 (2008) 7473-7481.
- [41] D. Houde, Y. Peng, S.A. Berkowitz, J.R. Engen, Post-translational modifications differentially affect IgG1 conformation and receptor binding, *Mol Cell Proteomics*, 9 (2010) 1716-1728.
- [42] J.C. Veilleux, J.E. Shepherd, Pressure and stress transients in autoinjector devices, *Drug Deliv Transl Res*, 8 (2018) 1238-1253.
- [43] Z. Hall, C.V. Robinson, Do charge state signatures guarantee protein conformations?, *Journal of the American Society for Mass Spectrometry*, 23 (2012) 1161-1168.
- [44] R. Cumeras, E. Figueras, C.E. Davis, J.I. Baumbach, I. Gracia, Review on ion mobility spectrometry. Part 1: current instrumentation, *The Analyst*, 140 (2015) 1376-1390.
- [45] R. Cumeras, E. Figueras, C.E. Davis, J.I. Baumbach, I. Gracia, Review on ion mobility spectrometry. Part 2: hyphenated methods and effects of experimental parameters, *The Analyst*, 140 (2015) 1391-1410.
- [46] B.M. Kolakowski, Z. Mester, Review of applications of high-field asymmetric waveform ion mobility spectrometry (FAIMS) and differential mobility spectrometry (DMS), *The Analyst*, 132 (2007) 842-864.
- [47] D.S. Levin, R.A. Miller, E.G. Nazarov, P. Vouros, Rapid separation and quantitative analysis of peptides using a new nanoelectrospray- differential mobility spectrometer-mass spectrometer system, *Anal Chem*, 78 (2006) 5443-5452.
- [48] H.J. Cooper, To What Extent is FAIMS Beneficial in the Analysis of Proteins?, *Journal of the American Society for Mass Spectrometry*, 27 (2016) 566-577.
- [49] A.A. Shvartsburg, G. Isaac, N. Leveque, R.D. Smith, T.O. Metz, Separation and classification of lipids using differential ion mobility spectrometry, *Journal of the American Society for Mass Spectrometry*, 22 (2011) 1146-1155.
- [50] S. Zhu, J.L. Campbell, I. Chernushevich, J.C. Le Blanc, D.J. Wilson, Differential Mobility Spectrometry-Hydrogen Deuterium Exchange (DMS-HDX) as a Probe of Protein Conformation in Solution, *Journal of the American Society for Mass Spectrometry*, 27 (2016) 991-999.
- [51] S. Adhikari, X. Yang, Y. Xia, Acetone/Isopropanol Photoinitiating System Enables Tunable Disulfide Reduction and Disulfide Mapping via Tandem Mass Spectrometry, *Anal Chem*, 90 (2018) 13036-13043.
- [52] H. Liu, K. May, Disulfide bond structures of IgG molecules: structural variations, chemical modifications and possible impacts to stability and biological function, *MAbs*, 4 (2012) 17-23.

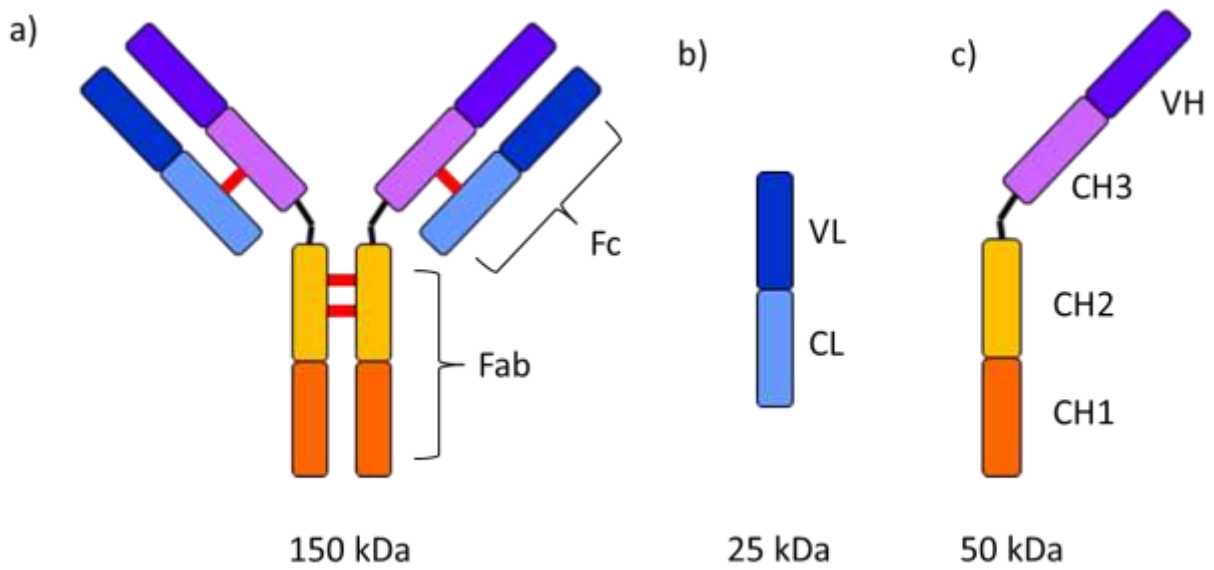


Figure 5.1 a) A generic diagram of IgG1 with its two regions, disulfide bonds (red), and its approximate molecular weight labeled. The b) light chain and c) heavy chain of IgG with their various domains labeled as well each chain's molecular weight.

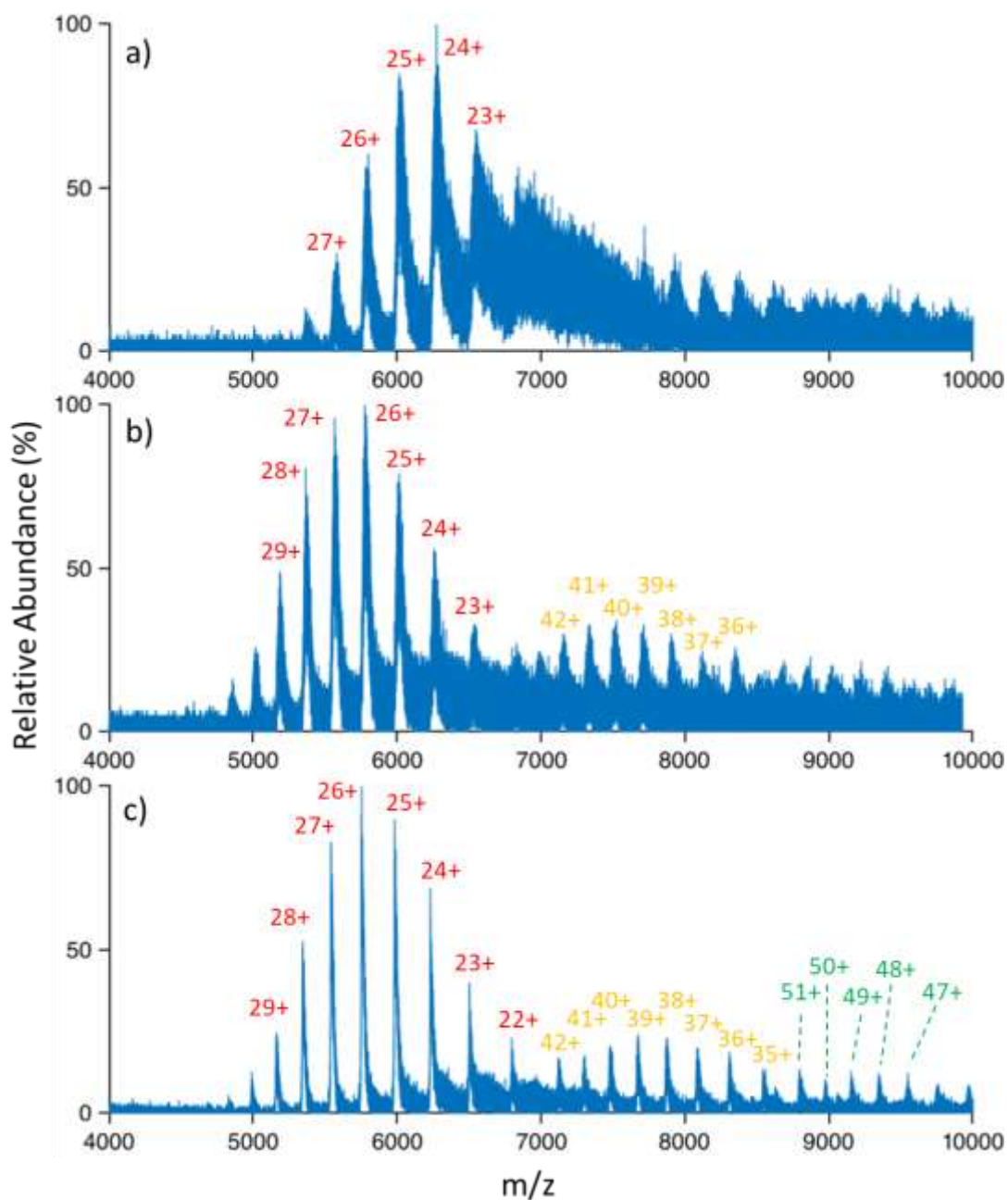


Figure 5.2 nESI spectrum for a) 300x dilution of 123.23 mg/mL mAb sample in water, b) 50 μ L of sample ran through PD MidiTrap G-25 followed by a 20x dilution in water, and c) q2DDC (50 ms, \pm 40V, q2RF 500) applied to the ions before injection into time-of-flight for mass analysis. The IgG ion's charge states are label in red for monomer, orange for dimers, and green for trimers.

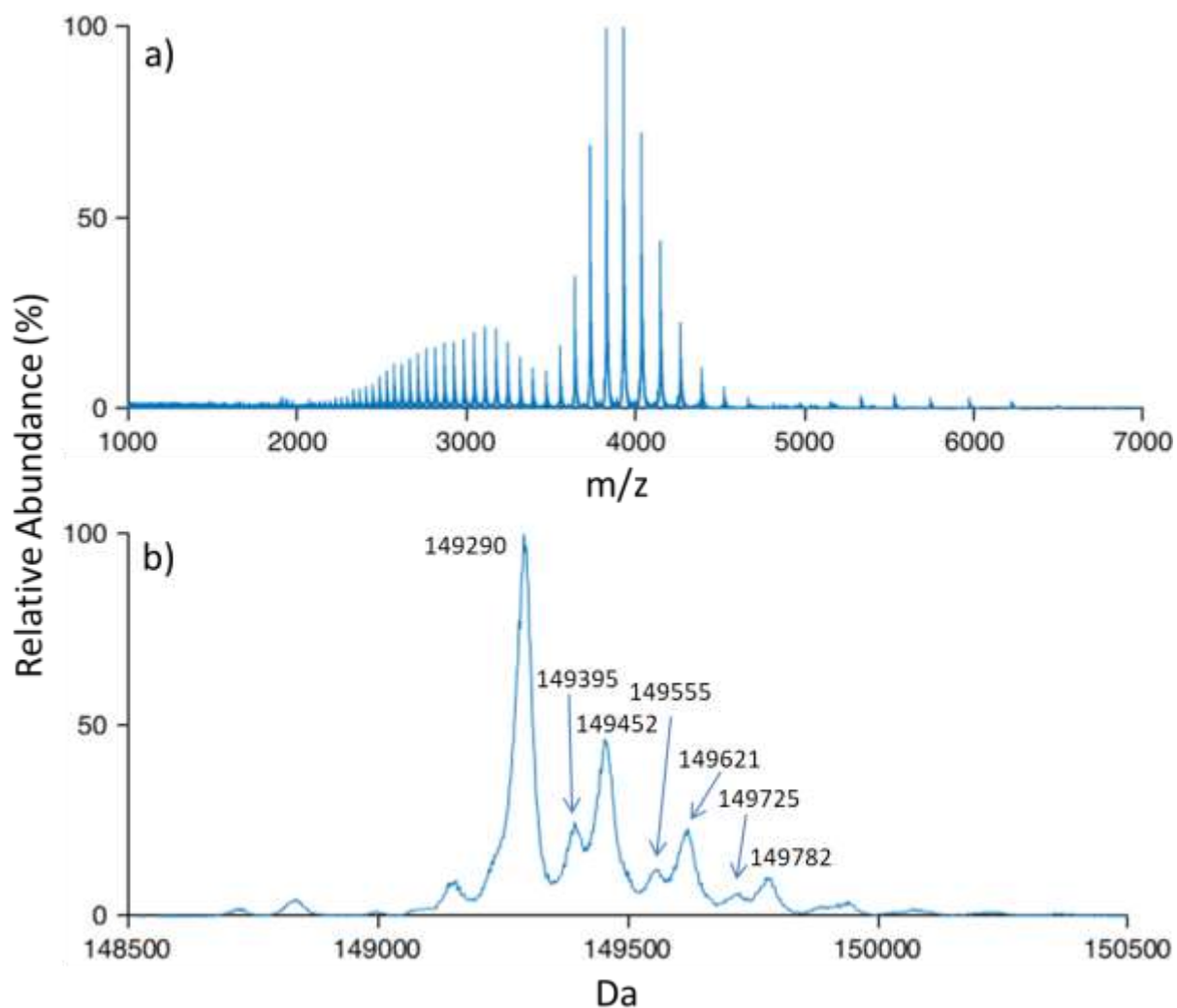


Figure 5.3 a) Mass spectrum of IgG in 1% acetic acid after filtered through PD Miditrap G-25 with q2 DDC applied. b) Reconstruction of denatured IgG mass spectrum from m/z region 3500 to 4500 using PeakView software.

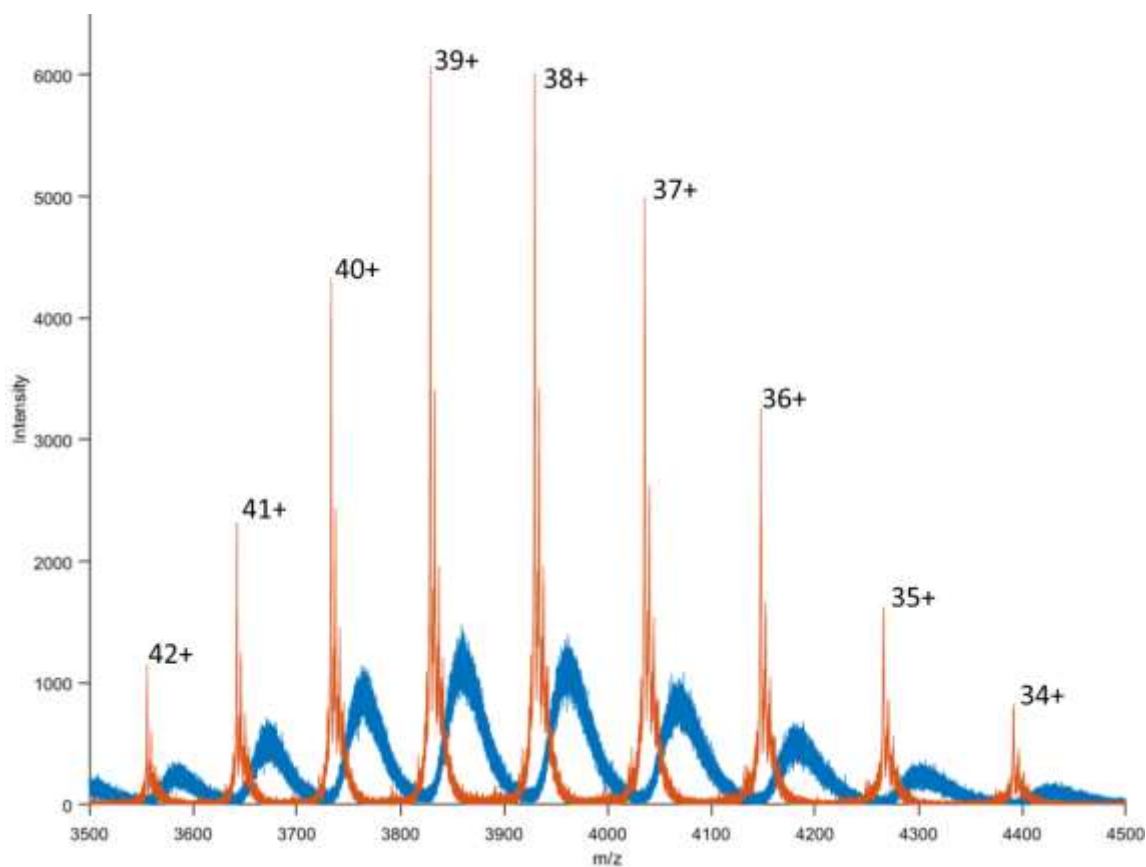


Figure 5.4 Zoomed in region (m/z 3500-4500) of the denatured IgG spectrum where no DDC has been applied (blue) and q2 DDC has been applied (orange). The y-axis shows the absolute intensity of the two spectra where the only difference is whether DDC voltage was applied or not. The scan segment lengths are the same and the same nESI tip was used for both spectra.

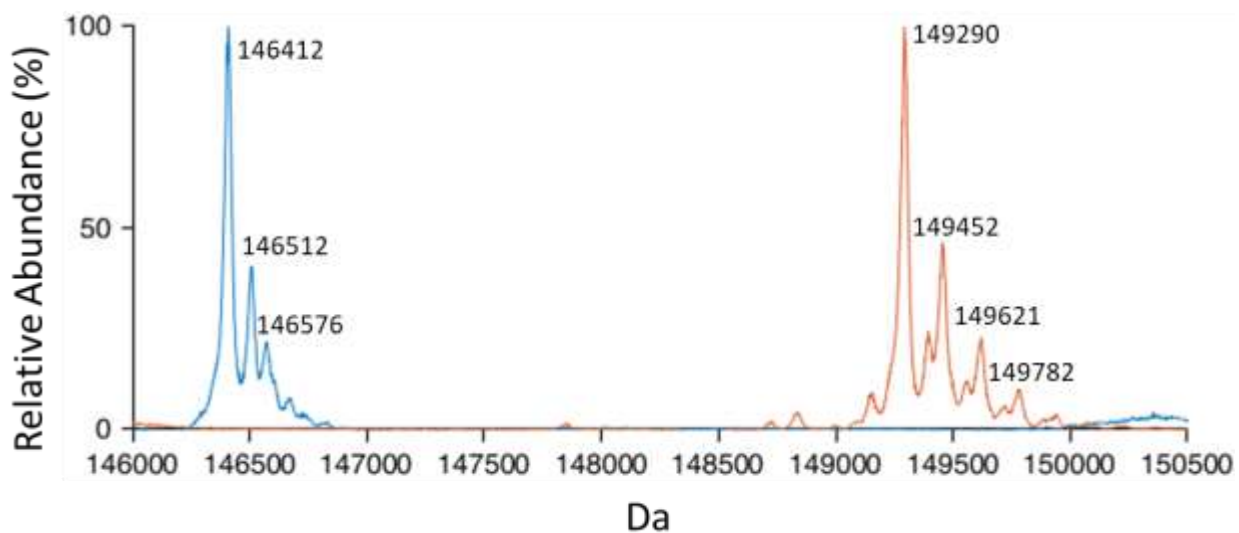


Figure 5.5 Reconstructed mass spectrum of IgG (orange) and deglycosylated IgG using PNGase F (blue). The molecular weight difference between the two base peaks is 2878 Da corresponding to approximately two G0F glycan groups.

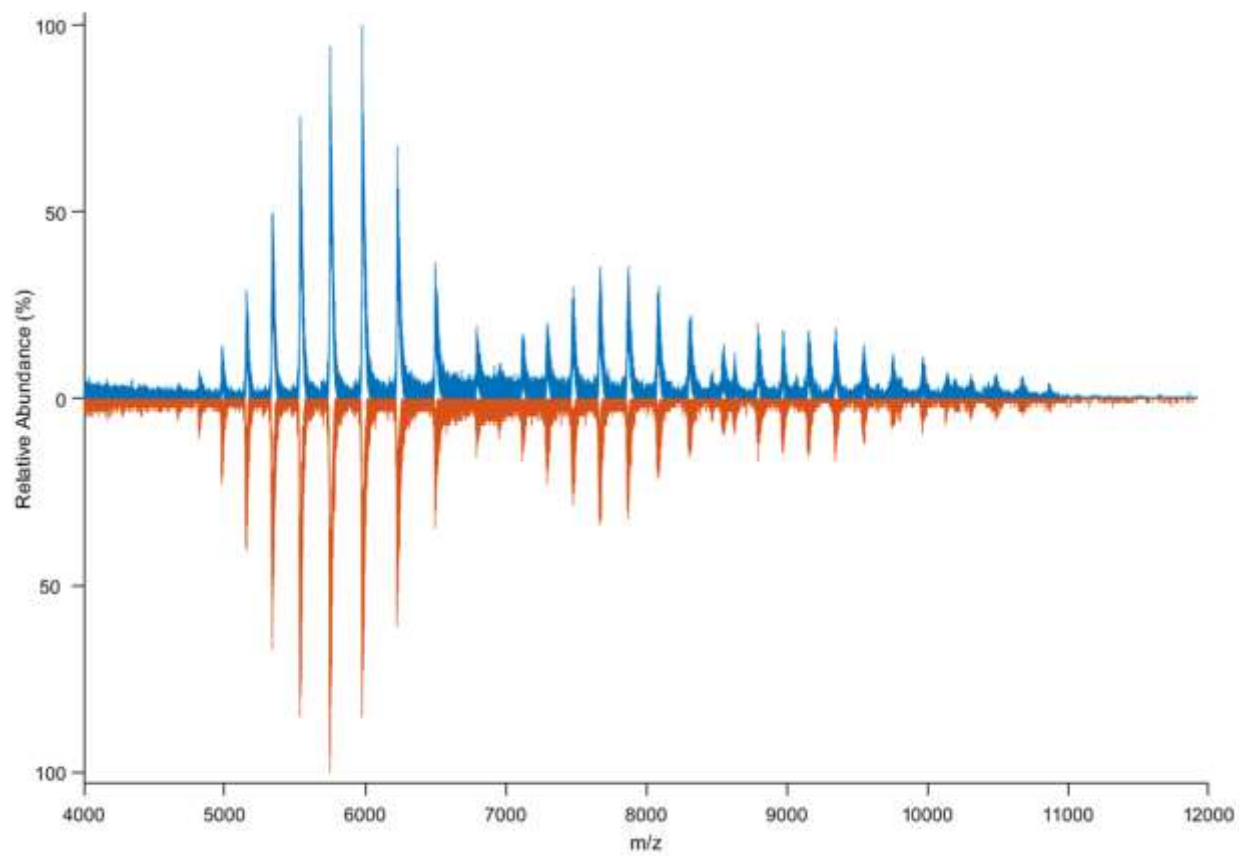


Figure 5.6 Butterfly spectrum of IgG in native solution condition before (blue) and after (orange) ejection of sample from the auto injector.

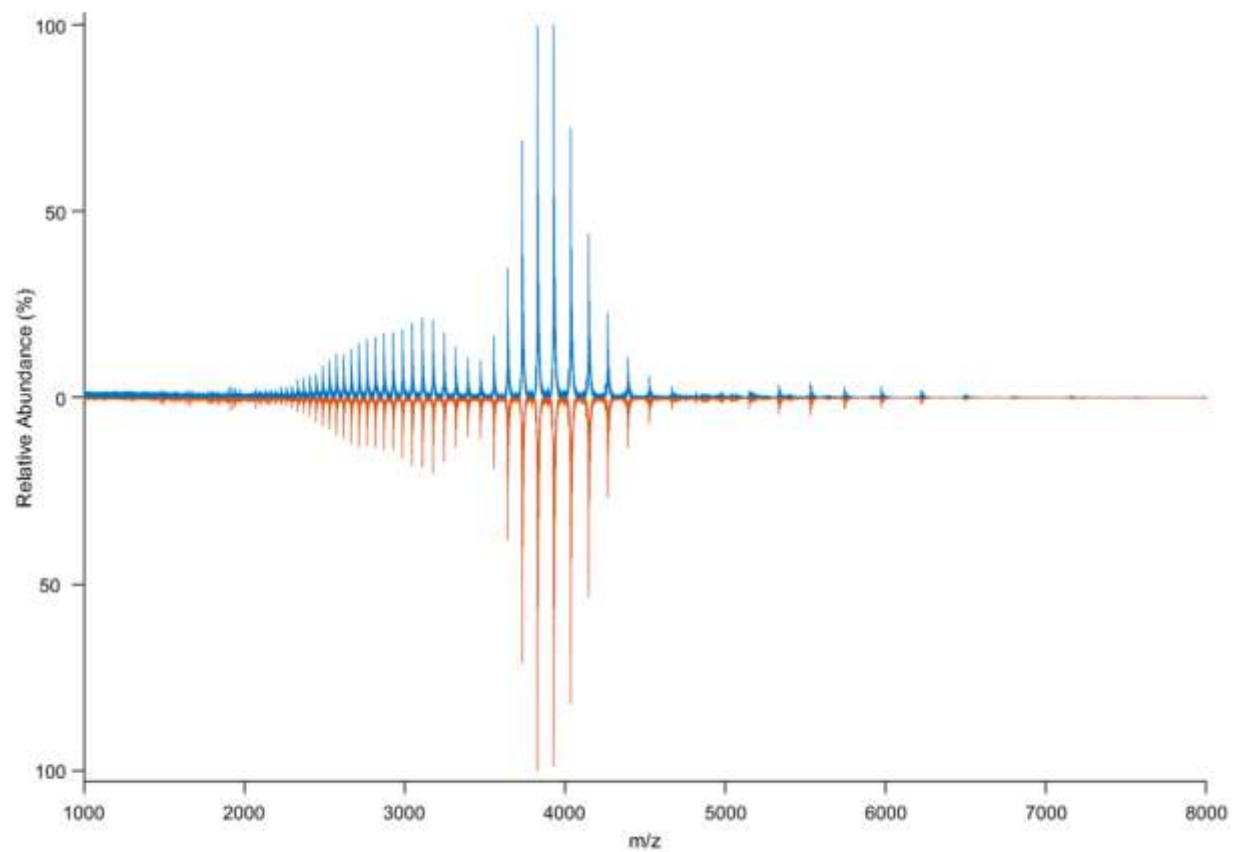


Figure 5.7 Butterfly spectrum of IgG in denatured solution condition before (blue) and after (orange) ejection of sample from the auto injector.

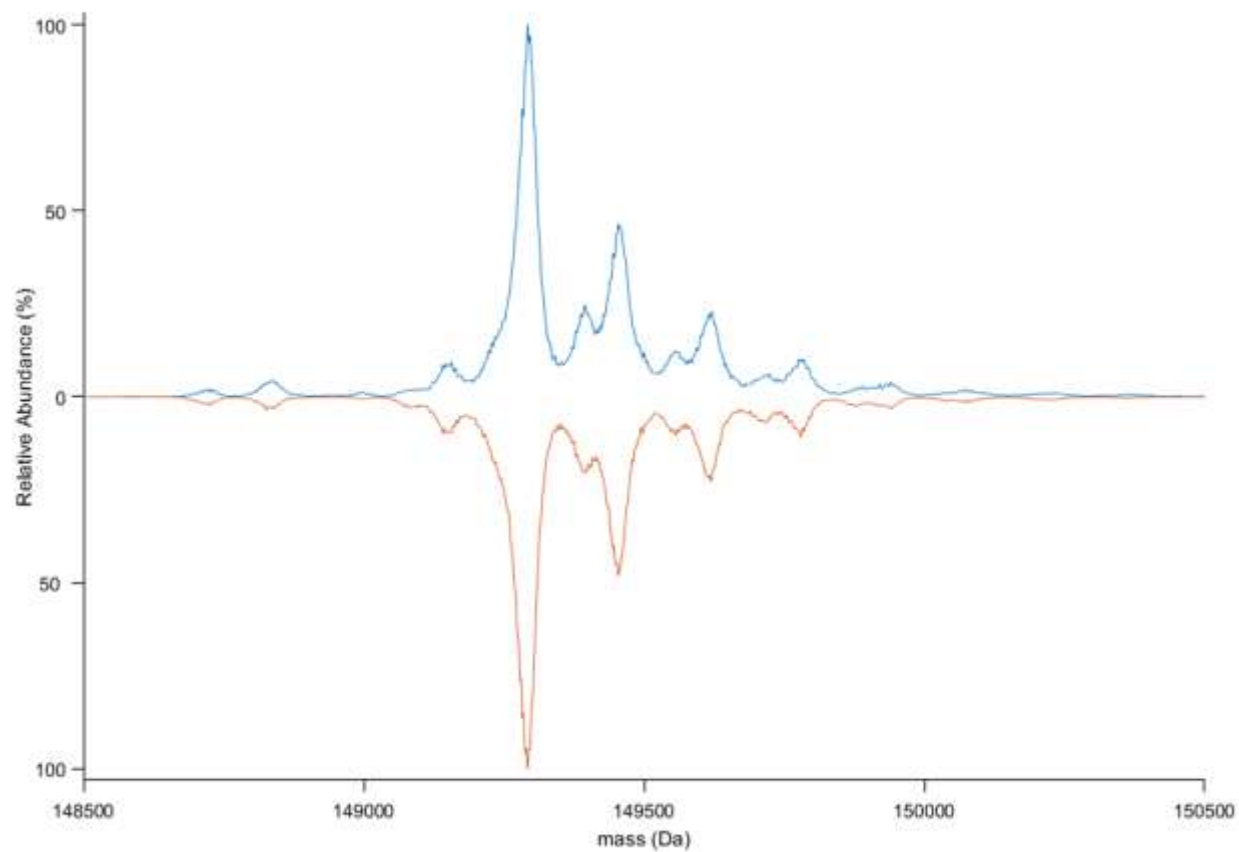


Figure 5.8 Butterfly spectrum of the MW of IgG reconstructed from the denatured condition mass spectrum before (blue) and after (orange) ejection of sample from the auto injector.

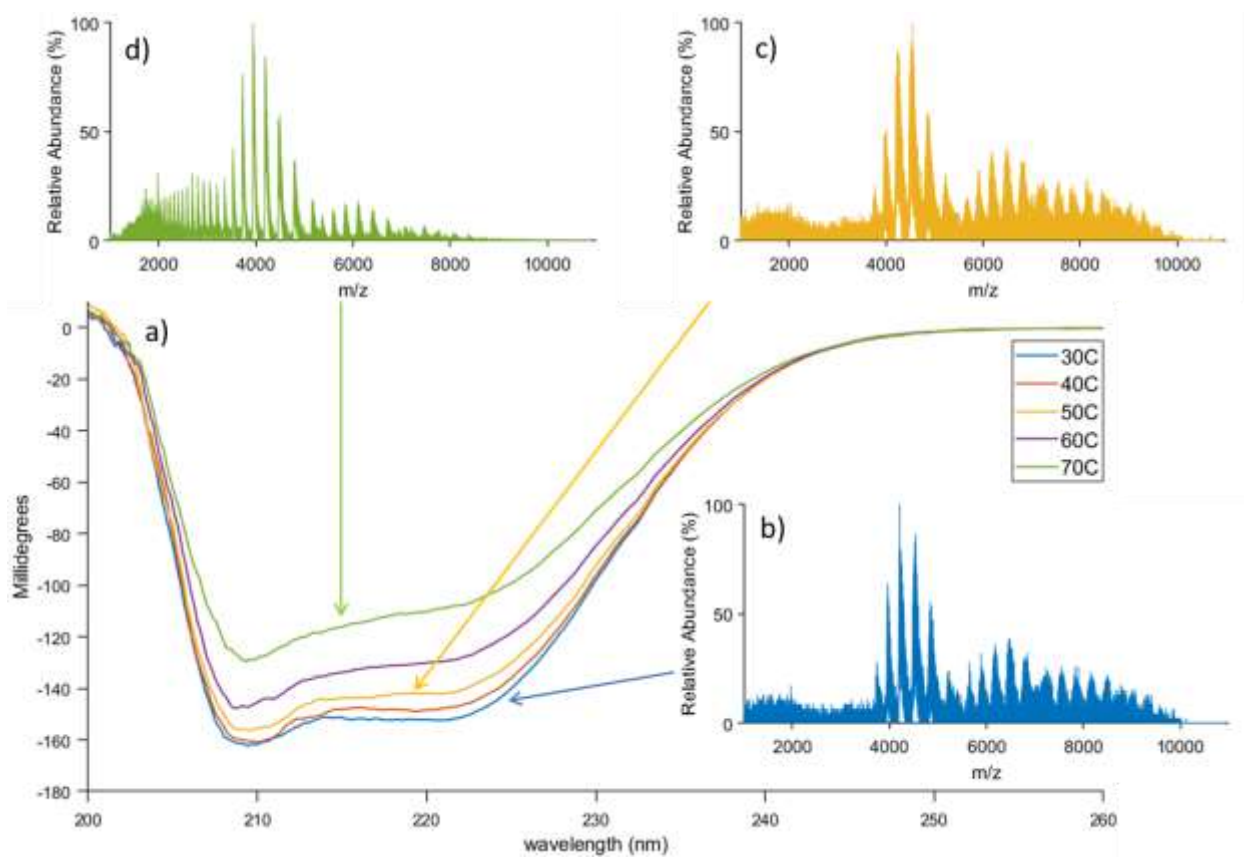


Figure 5.9 Circular dichroism (CD) of BSA from 30 °C to 70 °C in 10 °C steps with the mass spectrum of BSA at b) 30 °C, c) 50 °C, and d) 70 °C shown.

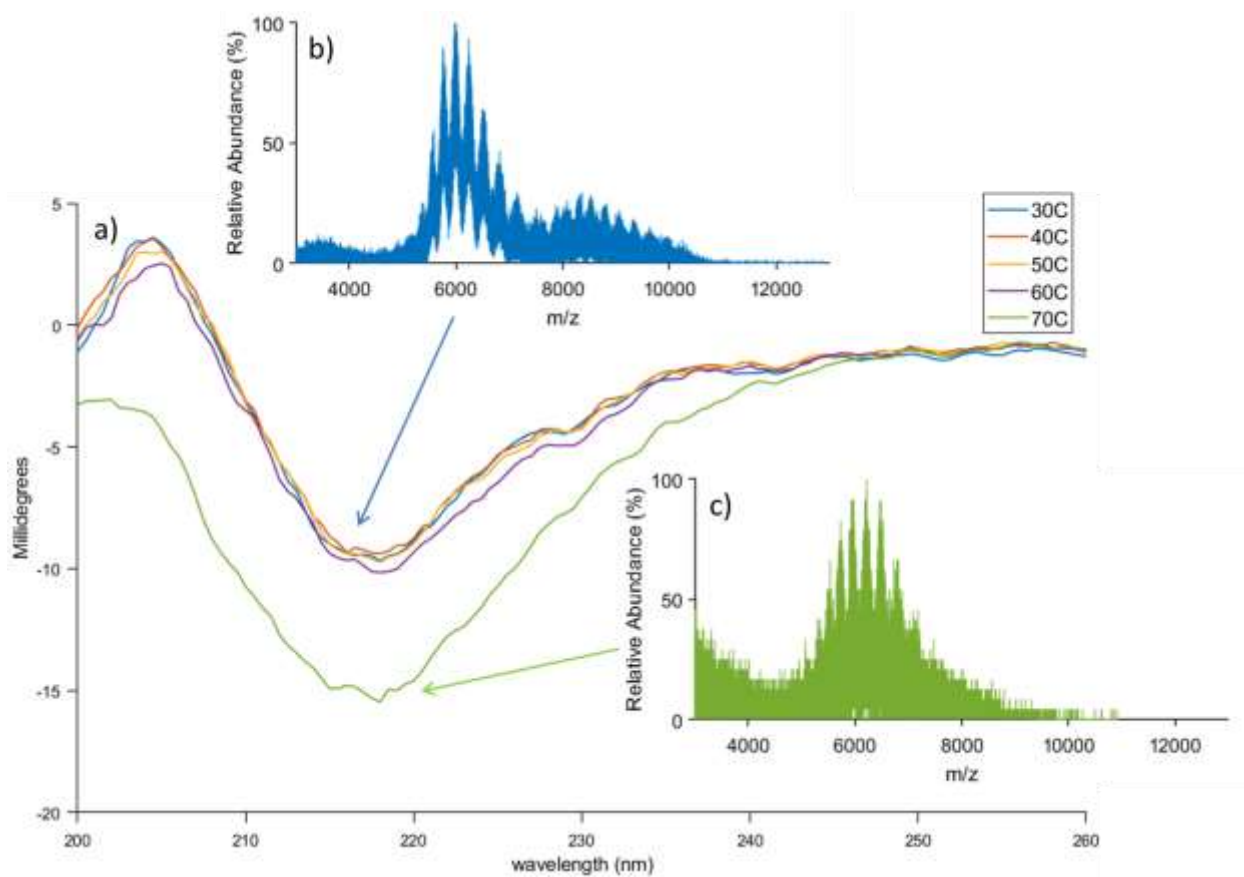


Figure 5.10 a) Circular dichroism (CD) of IgG from 30 °C to 70 °C in 10 °C steps with the mass spectrum of IgG at b) 30 °C and c) 70 °C shown.

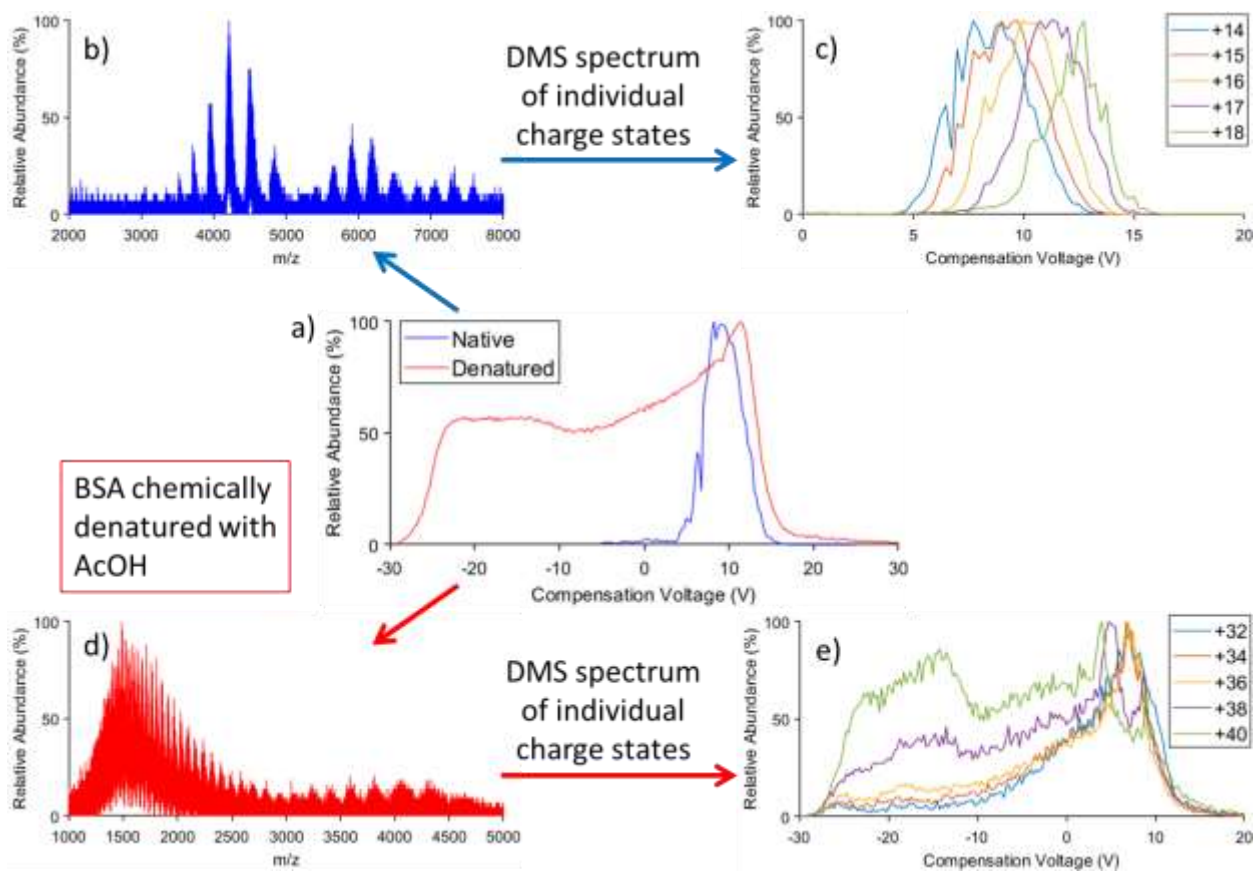
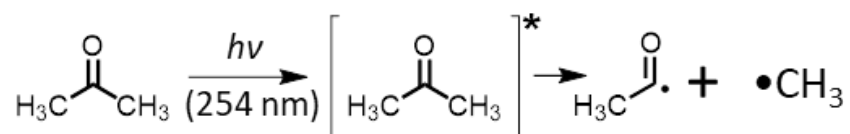
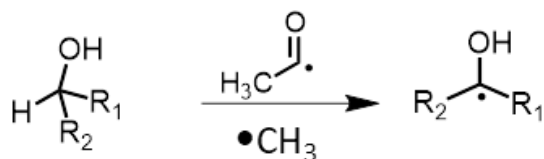


Figure 5.11 a) DMS spectrum of BSA native (blue) and denature (red). The overall mass spectrum of the DMS spectrum for b) native BSA and d) denatured BSA as well as the DMS spectrum of individual charge states for c) native and e) denatured are shown.

a) Radical Initiation



b) Formation of Alkyl Hydroxyl Radical



MeOH: $\text{R}_1 = \text{R}_2 = \text{H}$ EtOH: $\text{R}_1 = \text{H}, \text{R}_2 = \text{CH}_3$

IPA: $\text{R}_1 = \text{R}_2 = \text{CH}_3$

c) Cleavage of S-S

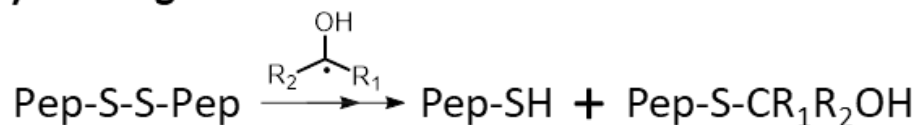


Figure 5.12 Proposed reaction schematic of the photochemical disulfide bond cleavage reaction starting with a) radical initiation on the acetone followed by b) formation of alkyl hydroxyl radical which initiates the c) cleavage of disulfide bonds.

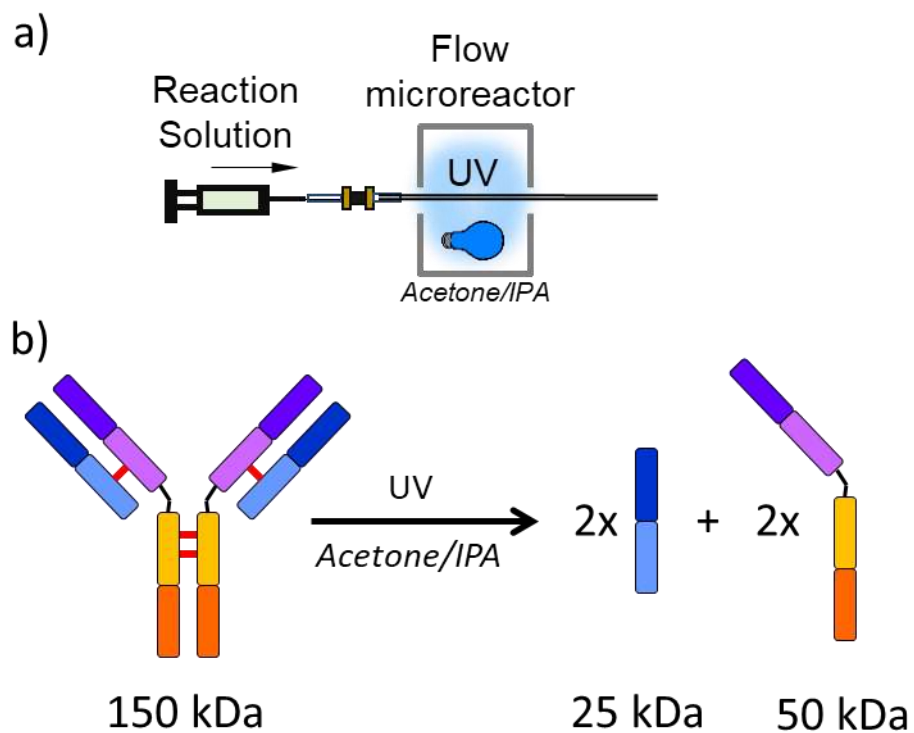


Figure 5.13 a) General schematic of the reaction cell used for the offline UV photoreaction where the sample is collected at the end of the tubing straight into the nESI tip. b) A generic structure for IgG1 showing four intermolecular disulfide bonds (labeled in red) that are broken after the UV photoreaction resulting in the light (25 kDa) and heavy (50 kDa) chain.

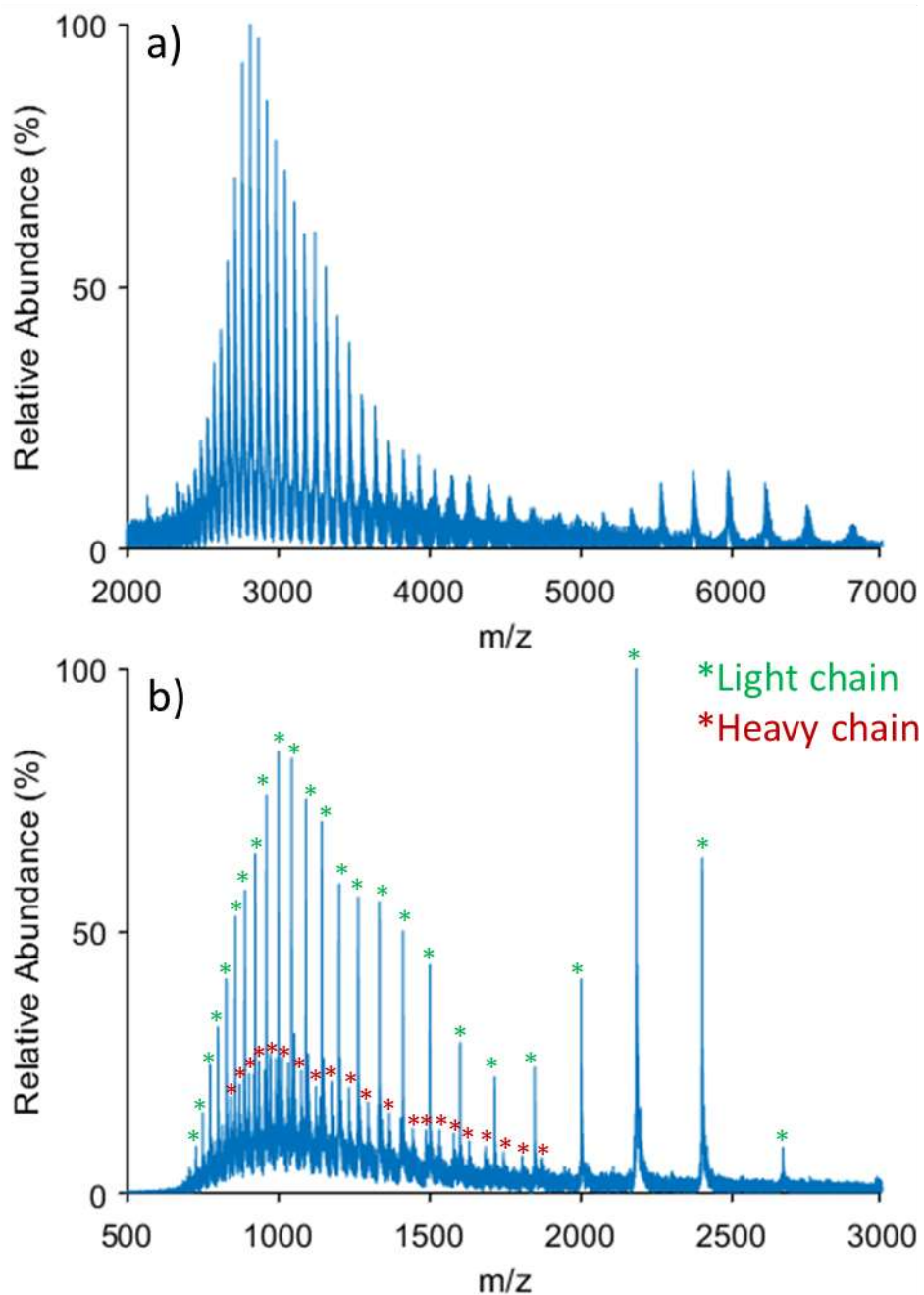


Figure 5.14 Mass spectra of IgG in 50/50 water/isopropanol with 2% acetone and 0.5 % formic acid a) before and b) after UV photochemistry. The peaks corresponding to the light chain and heavy chain are respectively labeled in green and red.

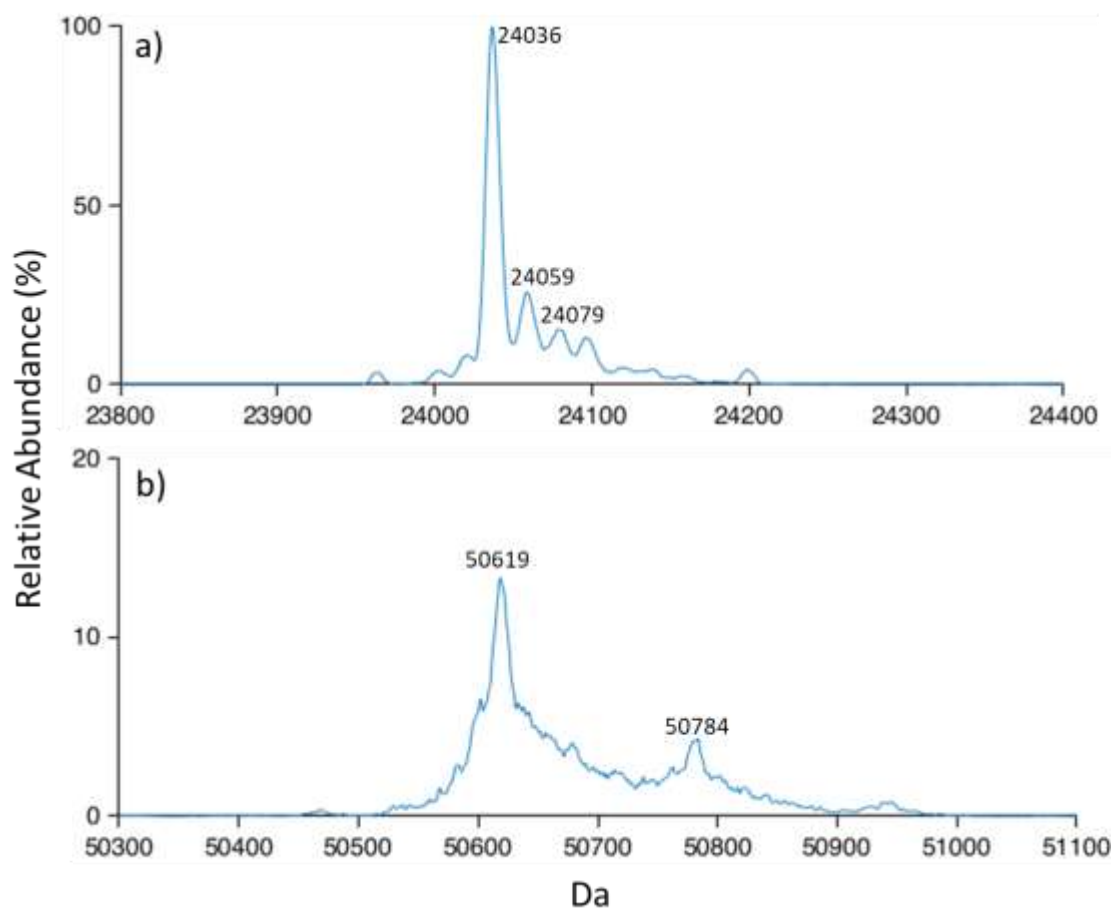


Figure 5.15 Reconstruction of post UV photochemistry reaction IgG mass spectrum revealing molecular weight of a) light chain and b) heavy chain.

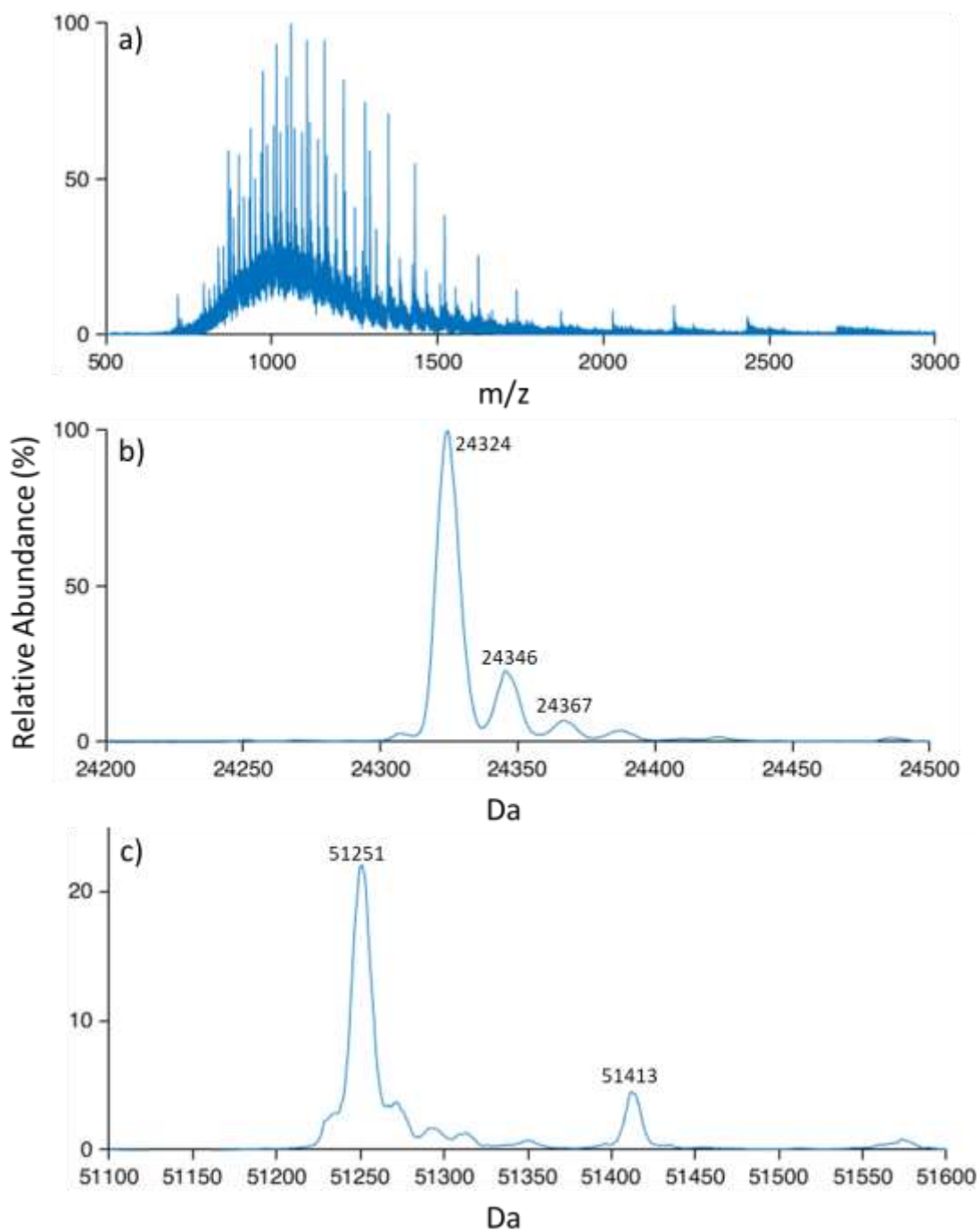


Figure 5.16 a) Mass spectrum of IgG post reduction and alkylation using *dithiothreitol* (DTT) and iodoacetamide (IAA). Reconstruction of above mass spectrum and the resulting molecular weight of b) light chain and c) heavy chain.

PUBLICATION

Shih, M.; McLuckey, S. A. Ion/ion charge inversion/attachment in conjunction with dipolar DC collisional activation as a selective screen for sulfo- and phosphopeptides. *Int. J. Mass Spectrom* 444, 116181 (2019)



Contents lists available at ScienceDirect

International Journal of Mass Spectrometry

journal homepage: www.elsevier.com/locate/ijms

Ion/ion charge inversion/attachment in conjunction with dipolar DC collisional activation as a selective screen for sulfo- and phosphopeptides

Mack Shih, Scott A. McLuckey*

Department of Chemistry, Purdue University, West Lafayette, IN, 47907, USA



ARTICLE INFO

Article history:
 Received 27 May 2019
 Received in revised form
 9 July 2019
 Accepted 10 July 2019
 Available online 11 July 2019

Keywords:
 Phosphopeptide
 Sulfopeptide
 Ion/ion reaction
 Charge inversion
 Dipolar DC collisional activation

ABSTRACT

We describe a gas-phase approach for the rapid screening of polypeptide anions for phosphorylation or sulfonation based on binding strengths to guanidinium-containing reagent ions. The approach relies on the generation of a complex via reaction of mixtures of deprotonated polypeptide anions with dicationic guanidinium-containing reagent ions and subsequent dipolar DC collisional activation of the complexes. The relative strengths of the electrostatic interactions of guanidinium with deprotonated acidic sites follows the order carboxylate < phosph(on)ate < sulf(on)ate. The differences between the binding strengths at these sites allows for the use of an appropriately selected dipolar DC amplitude leading to significantly different dissociation rates for complexes derived from unmodified peptides versus phosphorylated and sulfated peptides. The difference in binding strengths between guanidinium and phosph(on)ate versus guanidinium and sulf(on)ate is sufficiently great to allow for the dissociation of a large fraction of phosphopeptide complexes with the dissociation of a much smaller fraction of sulfopeptide complexes. DFT calculations and experimental data with model peptides and with a mixture of tryptic peptides spiked with phosphopeptides are presented to illustrate and support this approach. Dissociation rate data are presented that demonstrate the differences in binding strengths for different anion charge-bearing sites and reveal the DDC conditions most likely to provide the greatest discrimination between unmodified peptides, phosphopeptides, and sulfopeptides.

© 2019 Elsevier B.V. All rights reserved.

1. Introduction

Protein post-translational modifications (PTMs) increase the functional diversity as well as the overall complexity of the proteome. Phosphorylation is one of the most abundant PTMs present in proteomes with as much as a third of eukaryotic proteins estimated to be phosphorylated [1]. Phosphorylation plays a central role in signaling and regulatory process and, as a result, phosphoproteomics is widely practiced [2,3]. A common phosphoproteomics strategy involves a bottom-up work flow that relies on enrichment and/or separation using liquid chromatography and structural characterization via tandem mass spectrometry (MS/MS) techniques [4]. Enrichment prior to analysis is typically used, as phosphorylation is a low stoichiometry modification and must be

separated from the high backgrounds of non-phosphorylated peptides. Enrichment strategies such as immobilized metal affinity chromatography (IMAC) and metal oxide affinity chromatography (MOAC) are common metal-based affinity chromatography methods. Evaluation of other affinity materials, such as amine-based species, is also being undertaken but traditional metal-based affinity chromatography remain dominant [5].

Phosphopeptide analyses typically involve positive ionization in conjunction with MS/MS using one or more activation methods. Collision induced dissociation (CID) remains the most popular activation method for peptide sequencing, based partly on its widespread availability, but is ill-suited for phosphopeptide analysis due to the lability of the phosphate bond, which often leads to loss of the PTM [6]. This is particularly problematic with ion trap CID and somewhat less so with beam-type CID and higher energy collisional activation (HCD), the latter of which tend to lead to greater contributions from amide bond cleavages [7]. Electron-based activation methods, such as electron transfer dissociation (ETD) and electron capture dissociation (ECD) preserve PTMs on

* Corresponding author. 560 Oval Drive, Department of Chemistry, Purdue University, West Lafayette, IN, 47907-2084, USA.
 E-mail address: mcluckey@purdue.edu (S.A. McLuckey).

<https://doi.org/10.1016/j.ijms.2019.116181>

1387-3806/© 2019 Elsevier B.V. All rights reserved.

peptides while cleaving the N-C α bond to form c- and z-type ions allowing determination of the PTM location [8,9]. Negative mode electrospray ionization (ESI) holds potential for phosphopeptide analysis as the presence of the acidic phosphate group facilitates efficient ionization in the negative mode [10]. However, similar issues with slow heating methods, such as ion trap CID, prevail in the negative mode where the PTMs are first lost upon dissociation. Alternative activation strategies for negative mode structure determination of phosphopeptides, such as negative electron transfer dissociation (nETD) and electron detachment dissociation (EDD), have since been described and applied [11,12].

Sulfonation is another PTM that appears in the proteome, although at a lesser abundance compared to phosphorylation and is less extensively studied. Sulfonation primarily appears at tyrosine whereas phosphorylation primarily occurs at tyrosine, serine, and threonine. Tyrosine sulfonation is present in secretory and transmembrane proteins and has been shown to play a role in modulating extracellular protein-protein interactions for a variety of physiological and pathogenic responses [13,14]. Sulfopeptidomics research is hampered by the lack of an effective enrichment method and difficulties in distinguishing sulfopeptides from phosphopeptides in the mass spectrometer. Metal based IMAC methods have been applied for enrichment of sulfopeptides but lack the specificity that has been shown for phosphopeptides [15]. Application of novel antibodies for sulfopeptide enrichment has shown remarkable specificity for sulfotyrosine peptides and discrimination from phosphopeptides as well as sulfated glycans [16]. However, antibody enrichment has not been broadly adapted due to costs and concerns about their structural stability. Weak anion exchange chromatography has also been used for enrichment of sulfopeptides but modifications at the primary amines are required for better specificity [17,18].

The mass changes associated with sulfonation and phosphorylation are isobaric with the mass difference being only 9.5 mDa. Unless equipped with high resolution/high mass measurement accuracy mass spectrometers, such as an Orbitrap or FT-ICR, it can be challenging to distinguish between a given peptide that is either phosphorylated or sulfonated on the basis of mass. Both forms of modified peptide fragment similarly using low energy CID where major isobaric neutral losses occur (i.e., nominal losses of 80 Da (SO₃ or HPO₃) or -98 Da (H₂SO₄ or H₃PO₄)). While research has been done in comparing the spectra of ions derived from sulfopeptides and phosphopeptides under a variety of activation conditions, unless there is a comprehensive spectral library of sulfopeptides vs. phosphopeptides it remains challenging to distinguish a sulfopeptide from a phosphopeptide on the basis of fragmentation [19].

We have investigated gas-phase charge inversion reactions via ion/ion chemistry as means for addressing measurement challenges in mass spectrometry. For example, we demonstrated charge-inversion reactions applied to ions derived from precipitated blood plasma to result in a 200-fold improvement in signal-to-noise ratio due to a significant reduction in chemical noise [20]. Charge-inversion has also been used to separate isomeric phosphatidylethanolamine and phosphatidylcholine lipids [21] as well as to facilitate location of double bonds in unsaturated fatty acids [22]. Here we present another gas-phase ion/ion charge-inversion technique that allows for the distinction of phospho- and sulfopeptides from unmodified peptides as well as from each other. Research has demonstrated a relatively strong noncovalent interaction between guanidinium and phosphate and sulfate groups in both solution and in the gas phase [23–26]. Histidine interactions with acidic sites have also been studied and found to be somewhat weaker than those of guanidinium [27]. We seek to exploit the differences in the strengths of electrostatic interactions

between guanidinium and deprotonated acidic sites (i.e., carboxylate vs. phosph(on)ate vs. sulf(on)ate) in the context of ion/ion reactions. Ion/ion reactions are induced between singly-charged peptide anion mixtures and a guanidinium containing peptide dication. The resulting cationic peptide complex is then subjected to a broadband collisional activation using dipolar DC (DDC) [28]. The binding strength between the two peptides in the long-lived complex is dependent upon specific functional group interactions such that the complex stabilities are composition-dependent. This allows DDC to serve as an 'energy filter' to assist in the distinction of the functional groups involved in binding. We demonstrate this approach with model phosphopeptides and a sulfopeptide in both a simple mixture and a more complex mixture of tryptic ubiquitin peptides spiked with a phosphopeptide.

2. Experimental section

Materials. Peptides YGGFL, GAIDDL, NVVQIY, pSGGFL, pTGGFL, pYGGFL, and sYGGFL were custom synthesized by Biomatik (Wilmington, DE, USA). The custom peptides AAARAAARA and RKRARKA were synthesized by NeoBioLab (Cambridge, MA, USA). Water, Optima™ LC/MS Grade, was purchased from Fisher Scientific (Pittsburgh, PA, USA). Ubiquitin from bovine erythrocytes and trypsin from bovine pancreas were purchased from Sigma-Aldrich (St. Louis, MO, USA). All solutions for nano-electrospray (nESI), using capillaries pulled to tip diameter 3–4 μ m, were prepared in an aqueous solution at an initial concentration of ~1 mg/ml and diluted to desired concentration before use. The final concentration of each peptide in the peptide mixtures in aqueous solution is between 3 μ M and 30 μ M.

Trypsin digestion. Approximately 1 mg of ubiquitin was dissolved in 500 μ L of 50 mM NH₄HCO₃. A trypsin solution of 1 mg/mL was added to the protein solution at a 1:40 mass ratio. The solution was incubated at 37 °C for 12 hours before evaporated to dryness using a vacuum centrifuge. The resulting product was reconstituted in 500 μ L water.

N-terminal acetylation. Approximately 0.5 mg of peptide was dissolved in 250 μ L water before 15 μ L of 5 mM pH 6–7 borate buffer and 20 μ L of acetic anhydride were added. The solution was left at room temperature and allowed to react for 2 hours before quenching the reaction with 2 μ L glacial acetic acid. The resulting solution was evaporated to dryness using a vacuum centrifuge before being reconstituted in 500 μ L water.

Mass spectrometry. All experiments were performed on a TripleTOF 5600 mass spectrometer (SCIEX, Concord, ON, Canada) modified for ion/ion reactions and dipolar DC (DDC), in analogy with a previously described Q-TOF instrument [29,30]. Both reagent and analyte ions were formed via nano-electrospray emitters placed before the inlet aperture of the atmosphere vacuum interface. Cations and anions were formed alternately by pulsing the respective electrospray emitters [31]. For ion/ion reactions, the doubly protonated reagent was isolated by Q1 and accumulated in the q2 reaction cell before the negatively charged analyte ions were generated and introduced into q2. The oppositely charged ions were allowed to react within q2 for 20 ms. After mutual storage, a ramped ion trap resonance ejection scan was performed to eject remaining reagent and proton transfer products thereby leaving only the complex ions within q2. In the experiments associated with Figs. 2–4, a subsequent dipolar DC (DDC) excitation at a fixed amplitude was applied for 200 ms when the q2 RF voltage is set to be 250 m/z at a q value of 0.908 (i.e., low-mass cutoff = m/z 250) for broadband activation of the isolated complexes.

Dipolar DC Dissociation Kinetics. The rates of complex ion dissociation follow pseudo first order kinetics under DDC conditions, as indicated in Equation (1): [28,32–34].

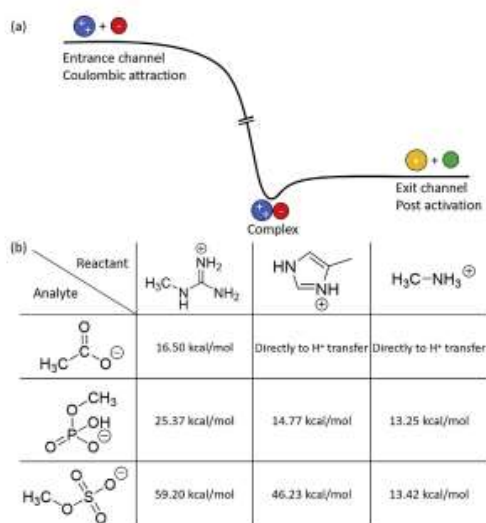


Fig. 1. (a) A generic energy diagram for a proton transfer ion/ion reaction involving a doubly-protonated reagent (blue) and a singly-deprotonated analyte (red). The reactants undergo a long-range attraction due to the Coulombic potential and, if they undergo an intimate collision, form a relatively long-lived complex. The complex can break up spontaneously to yield charged (yellow) and neutral (green) proton transfer products or the complex can be stabilized via collisions and/or emission. (b) The interaction strength between three basic groups and three deprotonated acids calculated via DFT. The model is a simplified version where only the interaction between positively charged basic groups and the negatively charged acidic groups are probed. The binding strength is the zero-point corrected energy difference between the complex and the sum of the products after proton transfer. (For interpretation of the references to colour in this figure legend, the reader is referred to the Web version of this article.)

$$[M]_t = e^{-k_{\text{dis}}t} \quad (1)$$

where $[M]_t$ is the molar fraction of the complex at time t , and k_{dis} is the pseudo-first order dissociation rate of the ion. The molar fraction of the complex is calculated as the ratio of complex ion's abundance over the abundance of all ions present. Complex ion dissociation kinetics were determined at a fixed RF amplitude (low-mass cutoff = m/z 250) as a function of dipolar DC amplitude. For a given DC and RF amplitude, the dissociation rate for a complex ion is determined from fitting the data to Equation (2):

$$\ln\left(\frac{[M]_t}{[M]_t + [\text{Fragment}]_t}\right) = -k_{\text{dis}}t \quad (2)$$

In all cases, the dominant fragment ion generated from DDC collisional activation of the complexes in this work was the protonated reagent. Error bars for k_{dis} correspond to the standard deviation from the linear fitting to Equation (2).

Density functional theory calculations. All optimizations and zero-point corrected energies (ZPE) were performed using the Gaussian 09 package [35] at the B3LYP/6-311++G(2d,p) level of theory. As the molecules are small, all structures were directly optimized in Gaussian 09. The anions and cations as well as their respective neutral forms were individually optimized for structure. The complex structure is a combination of the optimized anions and cations further subjected to optimizations.

3. Results and discussion

The general approach for screening of mixtures of anionic peptides with carboxylate, phosph(on)ate, or sulf(on)ate charge bearing sites is summarized schematically in Scheme 1.

The approach is based on reacting primarily singly-charged peptide anions with a doubly-charged cationic reagent that contains at least one arginine residue or, in this work, two protonated arginine residues. Of all the basic residues of the common amino acids, arginine has the highest proton affinity [36,37] and engages in the strongest electrostatic interactions with anionic sites. Reagent dications with arginine residues are therefore more likely to react with anions to yield a complex ion, rather than undergo proton transfer. It is also advantageous for the reagent cation to be relatively large, which increases the cross-section for intimate collision. The first step of the process is therefore intended to generate singly positively charged complexes comprised of the analyte anions attached to the doubly protonated reagent. The most weakly-bound complexes can be preferentially fragmented by the judicious choice of dipolar DC amplitude while the more strongly-bound complexes survive. Provided there is a sufficiently large difference between the binding strengths associated with the different anionic charge sites, the dipolar DC conditions can be used to distinguish between the types of anionic peptides. We show below that, according to DFT calculation, complex stability based on the electrostatic interaction between a guanidinium moiety (e.g., a protonated arginine residue) and a deprotonated site increase in the order of carboxylate < phosph(on)ate < sulf(on)ate. We then demonstrate that dipolar DC conditions can be established that are able to distinguish phospho- and sulfopeptides from unmodified peptides and from one another.

Density functional theory calculations of guanidinium interactions. The key characteristic of interest here is the gas-phase binding strength between the negatively charged peptide analytes and the positively charged dicationic reagent. Acid-base chemistry generally dominates in electrospray ionization such that excess protons are localized on the most basic sites of a peptide, such as the N-terminus or lysine, arginine, and histidine side-chains, in positive ion mode and removed at acidic sites, such as the C-terminus or aspartic, and glutamic acid side-chains, in negative ion mode. That logic can be further extended in the presence of PTMs such as phosphorylation and sulfonation. Phosphate and sulfate groups have a lower pKa values than carboxylate groups, which makes them more likely to be the charge site when ionized in the negative mode. Hence, a carboxylate group is likely to be the moiety involved in the interaction with a cationic reagent for unmodified peptides whereas for the phosphopeptides and sulfopeptides the charge site will be at the phosphate or sulfate groups, respectively. Density functional calculations were used to quantify the binding strength between the different types of negatively charged (i.e. carboxylate, sulfate, phosphate) and positively charged (i.e. primary amine, imidazole, guanidinium) chemical groups in the context of ion/ion reactions. A generic Brauman-type energy diagram (i.e., reactants shown from the left, products shown on the right, intermediate shown in the middle) for doubly protonated reagent and a singly deprotonated analyte proceeding via a long-lived complex is shown in Fig. 1(a). A more detailed analysis of energy surfaces for ion/ion reactions has been previously discussed [34]. In this case, reactions that proceed through a relatively long-lived intermediate (i.e., a complex) are of particular interest. (Proton transfer at a crossing point without formation of a complex is possible at large impact parameters and is minimized when the physical cross-sections of the reactants are large. [34]) Complex formation is always thermodynamically favorable in this type of reaction by roughly 100 kcal/mol per pair of opposite charges. The

4

M. Shih, S.A. McLuckey / International Journal of Mass Spectrometry 444 (2019) 116181

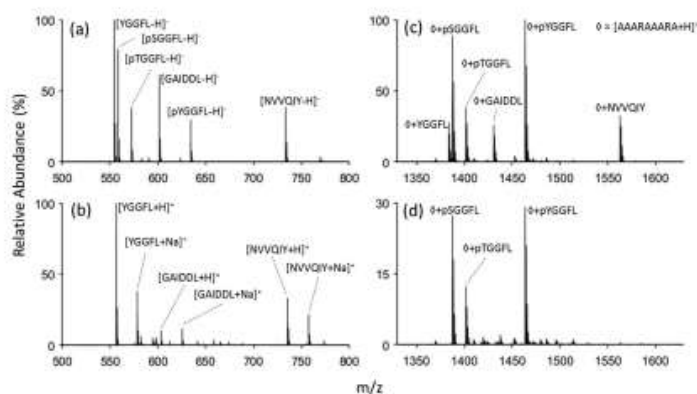


Fig. 2. NanoESI of six peptide mixture containing three phosphopeptides in (a) negative mode and (b) positive mode. Charge-inversion ion/ion reaction of the anionic peptide mixture with $[AAAAAARA+2H]^{2+}$ (c) with no DDC applied, and (d) DDC voltage of 22 volts applied.

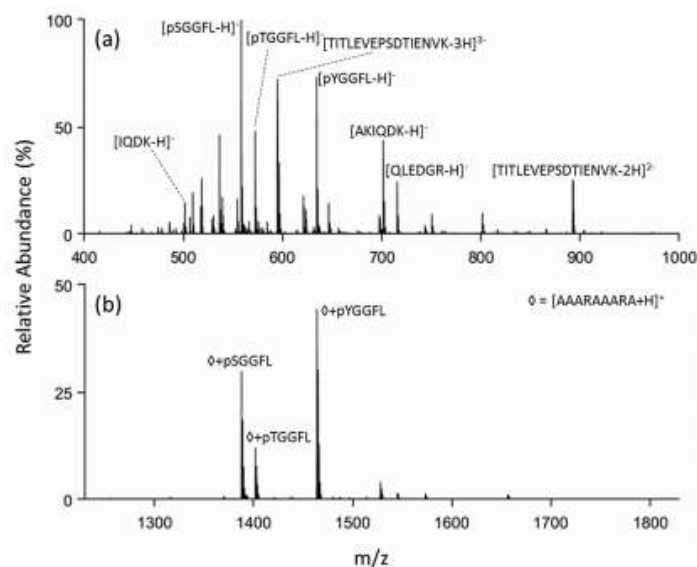


Fig. 3. (a) Negative mode nanoESI of trypsin digested ubiquitin with phosphopeptides pSGGFL, pTGGFL, and pYGGFL spiked in and (b) post ion/ion reaction with DDC at 22 V applied.

lowest energy exit channel from the complex involves proton transfer leading to a singly protonated product and a neutral product. The barrier to proton transfer from the complex is largely determined by the strength of the electrostatic interaction between the relevant protonated and deprotonated sites. The calculated energy barriers for proton transfer from a basic group cation to each of the three anionic groups of interest are listed in the table of Fig. 1(b). The energies calculated via DFT shown in the table are the difference between the zero-point corrected energies (ZPE) of the complex and the sum of the two neutrals after proton transfer has

occurred. (Reverse critical energies for proton transfer reactions are typically small and are expected to largely cancel so that the calculated values here are expected to be suitable for comparisons.) The calculations clearly show that interaction strength between guanidinium and the various negative charge sites follow the order sulf(on)ate > phosph(on)ate > carboxylate. For a given anionic site, the binding strengths for the cationic sites follows the order guanidinium > imidazole > primary amine. The energy-minimized structures of the complexes formed between the various cations and anions are provided in Figs. S1–S7. (Protonated imidazole/

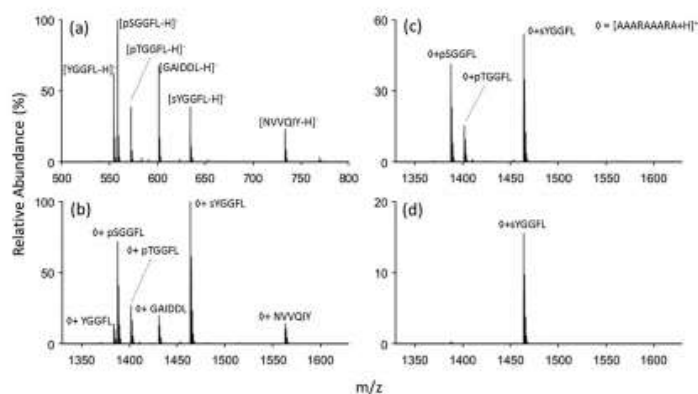
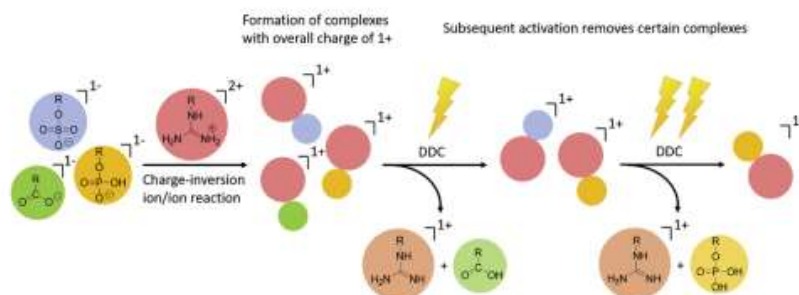


Fig. 4. (a) Negative mode nanoESI of a sulfopeptide, sYGGFL, two phosphopeptides, pTGGFL and pSGGFL, and three non-PTM peptides, YGGFL, GAIDDL, and NVVQIY. (b) Post-ion/ion reaction spectrum of the anionic peptide mixture with [AAAAAARA+2H]²⁺ followed by (c) DDC using 22 V and (d) 25 V.



Scheme 1. Schematic depiction of the use of a guanidinium-containing dicationic reagent and dipolar DC collisional activation for the discrimination between carboxylate, phosph(on)ate, and sulf(on)ate containing peptide anions.

carboxylate and protonated methylamine/carboxylate complexes were not found to be lower in energy than the proton transfer products and are therefore not shown in Supplemental Information.)

Complex formation and DDC for phosphopeptides vs. unmodified peptides. Model phosphopeptides, pSGGFL, pTGGFL, and pYGGFL, as well as a variety of other small model peptides of similar size, YGGFL, GAIDDL, and NVVQIY, were used to evaluate the relative stabilities of complexes formed with a doubly protonated reagent with two arginine residues. Mass spectra of this peptide mixture in both positive mode and negative mode nESI are shown in Fig. 2(a) and (b), respectively. In the positive mode spectrum, signals from the phosphopeptides are essentially absent as only the protonated and sodiated versions of unmodified peptides are present. In contrast, the three phosphopeptides give rise to strong signals in the negative ion mode. Ion/ion reaction between the negatively charged peptides and doubly-protonated AAAAARA formed a long-lived stable complex with 1+ charge that was detected in the positive mode, as shown in Fig. 2(c). (Residual reagent cations as well as singly-protonated AAAAARA generated via proton transfer were ejected by a resonance ejection ramp prior to mass analysis in generating Fig. 2(c). The complete spectrum prior to the voltage sweep is shown in Fig. S8.) It is clear from a

comparison of the relative abundances of the peptide anions (Fig. 2(a)) with the relative abundances of the complexes observed in Fig. 2(c) that the relative propensities for stable complex formation are peptide anion dependent. Stable complex formation competes with proton transfer at a crossing on the energy surface (without complex formation) and proton transfer via break-up of an initially formed complex [33]. The likelihood for the initial formation of a long-lived complex increases with the physical sizes of the reactants (i.e., a larger analyte anion and a larger reagent increase the relative likelihood for a 'sticky' collision between the reactants). The relative likelihood for the survival of the initially formed complex, which leads to the observation of a stable complex, is related, in part, to the binding strength in the complex. The factors of peptide anion size and the strengths of the interactions in the complex largely determine the changes in relative abundances in Fig. 2(a) and (c). Based on the calculations discussed above, the binding strengths of the phosphopeptide complexes are expected to be significantly greater than those involving unmodified peptides. The selective dissociation of the more weakly-bound complexes can be effected via dipolar DDC collisional activation. DDC is a broad-band collisional activation technique that provides a roughly uniform degree of excitation across a wide range of masses [27,31,32]. As shown in Fig. 2(d), a DDC amplitude of 22 V applied

for 200 ms leads to the dissociation of essentially all of the complexes comprised of the unmodified peptides while prominent signals from the phosphopeptide-containing complexes remain. The resulting spectrum provides an illustration for how phosphopeptide anions can be distinguished from unmodified peptide anion via ion/ion complex formation and DDC collisional activation.

Application of this approach to a more complex sample containing phosphopeptides was also performed. Peptides derived from tryptic digestion of ubiquitin along with phosphopeptides spiked into solution were subjected to analysis. In the positive mode (see Fig. S9), very little indication of the presence of the phosphopeptides is apparent while prominent signals are present in the negative mode spectrum (Fig. 3(a)). Applying the charge inversion DDC process to the mixture highlights the phosphopeptide anions (Fig. 3(b)). It is worthy of note that doubly- and triply-deprotonated TITLVEPSDTIENVK ions, one of the ubiquitin tryptic peptides, are prominent in Fig. 3(a). The doubly-deprotonated ion would be neutralized as a result of complex formation and the triply-deprotonated species would form a negatively charged complex. Therefore, evidence for this peptide would not be expected via a single ion/ion reaction. However, there are several pathways for generating cations with this peptide via two ion/ion reactions, such as a single proton transfer to the di-anion followed by reagent cation attachment. However, there is no evidence that any TITLVEPSDTIENVK-containing cations survived the DDC experiment associated with Fig. 3(b).

Complex formation and DDC for phosphopeptides vs. sulfopeptides. Substituting sYGGFL for pYGGFL in the model peptide

mixture of Fig. 2 and repeating the ion/ion reaction experiment showed that the reagent cation formed a stable complex with the sulfopeptide in analogy with the phosphopeptides (see Fig. 4(a)). Application of 22 V DDC, as above, resulted in the survival of only the phosphopeptide and sulfopeptide complexes. Application of 25 V DDC for the same time (200 ms) resulted in the disappearance of almost all of the phosphopeptide complexes while retaining a significant fraction of the sulfopeptide containing complexes. This result is consistent with the expectation that the stronger binding for sulf(on)ate relative to phosph(on)ate to guanidinium, as predicted by the DFT calculations, leads to more stable electrostatic complexes. The differences in binding strengths for the three anionic sites discussed here suggests that the amplitude of DDC applied to complexes generated in reaction with guanidinium-containing reagents can be used to distinguish between unmodified peptides and modified peptides at intermediate values and between phosphopeptides and sulfopeptides at higher DDC values.

DDC dissociation kinetics. Differences in complex dissociation rates form the basis for the use of DDC to discriminate between different classes of anions (i.e., carboxylate, phosph(on)ate, sulf(on)ate). In order to evaluate reagents and conditions for optimal discrimination between anion classes, it is instructive to determine complex ion dissociation rates over a range of conditions. Fig. 5(a) shows a series of kinetic plots at various DDC amplitudes for the complex formed from deprotonated pYGGFL and doubly-protonated AAARAAAARA. Examples of the spectra collected at 23 V DDC across various activation times are shown in Fig. S10. Fig. 5(b) summarizes the dissociation rates of the complexes

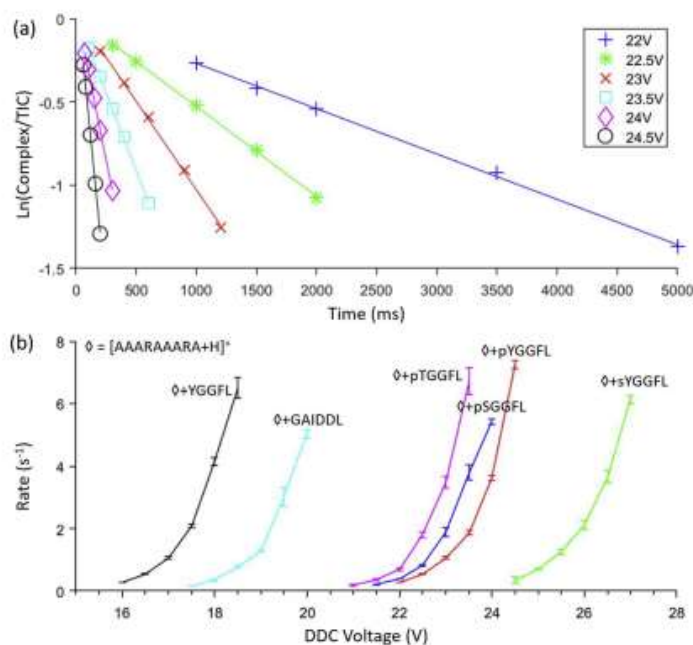


Fig. 5. (a) The kinetic data for determining the dissociation rate of the peptide complex between $[pYGGFL-H]^+$ and $[AAARAAAARA+2H]^{2+}$. The natural log of the peak area of the complex over the peak area of the total ion current (TIC) is plotted against the activation time of DDC. (b) The complex dissociation rate of each peptide complex, k_{diss} , is plotted against the DDC voltage. The error bar is two standard deviations of the slope's fitting error in the kinetic data.

formed from ion/ion reaction between doubly protonated AAARAARA and deprotonated YGGFL, GAIDDL, pTGGFL, pSGGFL, pYGGFL, and sYGGFL. It is clear that the complexes of the unmodified peptides YGGFL and GAIDDL fragment at the lowest DDC amplitudes, which is consistent with the DFT calculations that show relatively weak interaction between guanidinium and carboxylate. With three acidic sites in GAIDDL, the opportunity for additional interactions in the complex likely underlies the requirement for higher DDC voltages to achieve dissociation rates similar to the complex with YGGFL. The complexes derived from three phosphopeptides show similar dissociation kinetics while the sulfopeptide complex requires significantly higher DDC voltages. Fig. 5(b) shows why a DDC amplitude of 22 V is effective in destroying the complexes comprised of the unmodified peptides while the complexes of the modified peptides largely survive. Likewise, a DDC amplitude of 25 V is effective in destroying the complexes of the unmodified and phosphorylated peptides while the sulfopeptide complex remains intact.

The rate data of Fig. 6 illustrate how the measurement of DDC kinetics can be used to evaluate the discriminatory value of a reagent cation. Fig. 6(a), for example, summarizes the dissociation rate data obtained using doubly protonated RKRARKA as the reagent for deprotonated pYGGFL, pTGGFL, pSGGFL, and sYGGFL. For comparison, the rate data for the doubly-protonated AAARAARA reagent are also provided. The more basic reagent (i.e., RKRARKA) leads to more stable complexes for all of the peptides, as reflected by the shift of the rate data to the right on the DDC amplitude scale. In the case of the phosphopeptides, the stability order changed

from the pYGGFL/AAARAARA complex being the most stable of the three AAARAARA complexes to being the least stable of the peptide/RKRARKA complexes. This observation highlights the importance of the additional interactions that are introduced by the incorporation of another arginine residue and two lysine residues. The sulfopeptide/RKRARKA complex was found to be significantly more stable than those of all of the phosphopeptides. However, the separation between the phosphopeptides and the sulfopeptide on the DDC scales was narrower with the RKRARKA reagent than with the AAARAARA reagent. Overall, therefore, doubly-protonated AAARAARA appears to be a more discriminatory reagent cation for phospho-versus sulfopeptides.

The comparison of Fig. 6(a) suggests that interactions beyond those of a single guanidinium cation with a deprotonated acidic site can have a measureable effect on complex stability and can impact the discriminatory value of a doubly-protonated reagent for distinguishing between unmodified peptides and phospho- and sulfopeptides. Fig. 6(b) compares DDC rate data for doubly-protonated AAARAARA and N-terminally acetylated AAARAARA to determine a possible role for the N-terminus in stabilizing the complexes with deprotonated pYGGFL, pSGGFL, and sYGGFL. Interestingly, neither of the tyrosine-containing peptide complexes showed a significant change in dissociation kinetics when the reagent peptide was N-terminally acetylated while the pSGGFL complex was observed to be less stable. This result suggests that the serine residue of pSGGFL interacts with the N-terminus in complexes with AAARAARA more strongly than the tyrosine residues of pYGGFL and sYGGFL. It is beyond the scope of this work to examine all of the

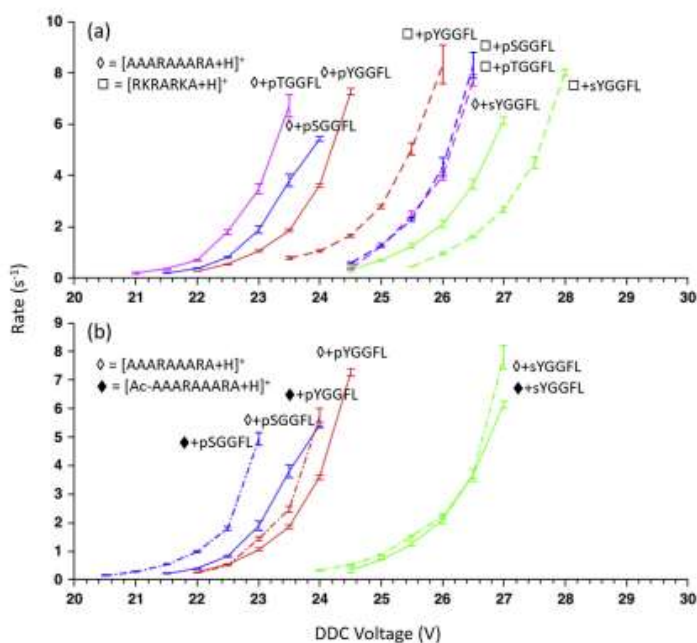


Fig. 6. (a) Kinetic data comparison between peptide complexes of AAARAARA (○) and RKRARKA (□) for three phosphopeptides and a sulfopeptide. Kinetic data for AAARAARA complexes are solid lines and dashed lines for RKRARKA complexes. (b) Kinetic data comparison of select peptides between AAARAARA (○) and Ac-AAARAARA (◆). The error bar is two standard deviations of the slope's fitting error in the kinetic data.

possible interactions that might take place in a complex formed between reagent and analyte polypeptides. In any case, in order to maximize the contribution from the targeted guanidinium/deprotonated acid interaction to the overall binding strength of the complex, it is desirable to minimize the possibility for other strong non-covalent interactions. Along these lines, competition between fragmentation of covalent bonds and cleavage of the phosphate-guanidinium bond in some peptide complexes has been noted under low energy collision conditions, [26,38] as has intermolecular phosphate transfer between complex components [39,40]. No evidence for such processes for either the phospho- or sulfopeptides was observed in the DDC step in this work but these possibilities should be recognized when examining other reagent/peptide combinations.

4. Conclusions

This work provides proof-of-concept for an ion/ion reaction approach to distinguishing between unmodified, phosphorylated, and sulfated peptides. The basis for discrimination is the relative strengths of interaction between guanidinium and carboxylate, phosph(on)ate, and sulf(on)ate in the gas phase. The relative strengths of the electrostatic interactions between guanidinium and conjugate bases of the relevant acidic sites, determined by DFT calculations and supported experimentally, increase in the order carboxylate < phosph(on)ate < sulf(on)ate. The interaction is generated by reacting a doubly protonated reagent peptide with at least two arginine residues with singly deprotonated peptides in the gas phase to form a long-lived complex. The relative stabilities of the complexes are probed via dipolar DC (DDC) collisional activation, a broad-band collisional excitation technique. With an appropriately selected DDC amplitude and time, it was shown to be possible to fragment a large majority of complexes comprised of unmodified peptide anions while retaining large fractions of complexes comprised of phosphopeptides and sulfopeptides. Likewise, at a higher DDC amplitude, it was possible to fragment a large majority of phosphopeptide complexes while preserving a large fraction of the sulfopeptide complexes. The discriminatory value of the reagent and DDC conditions is readily apparent from dissociation kinetics experiments that provide dissociation rates as a function of DDC amplitude for a fixed RF amplitude. Such data point to DDC conditions that provide the greatest degree of discrimination between anion types and are useful in evaluating reagent cations used to generate complexes. The results shown here highlight the roles that non-covalent interactions other than the guanidinium-anion interaction can affect complex ion stabilities. To maximize the role of the guanidinium interaction and to avoid other interactions that may vary with the analyte ion sequence/composition, it is desirable to minimize the presence of polar groups other than the arginine residues.

Acknowledgments

This work was supported by the National Institutes of Health (NIH) under Grant GM R37-45372.

Appendix A. Supplementary data

Supplementary data to this article can be found online at <https://doi.org/10.1016/j.ijms.2019.116181>.

References

- [1] P. Cohen, The regulation of protein function by multisite phosphorylation – a 25 year update, *Trends Biochem. Sci.* 25 (2000) 596–601.
- [2] J.A. Ubersax, J.E. Ferrell Jr., Mechanisms of specificity in protein phosphorylation, *Nat. Rev. Mol. Cell Biol.* 8 (2007) 530–541.
- [3] P. Cohen, The origins of protein phosphorylation, *Nat. Cell Biol.* 4 (2002) E127–E130.
- [4] N.M. Riley, J.J. Coon, Phosphoproteomics in the age of rapid and deep proteome profiling, *Anal. Chem.* 88 (2016) 74–84.
- [5] Z.G. Wang, N. Lv, W.Z. Bi, J.L. Zhang, J.Z. Ni, Development of the affinity materials for phosphorylated proteins/peptides enrichment in phosphoproteomics analysis, *ACS Appl. Mater. Interfaces* 7 (2015) 8377–8392.
- [6] J.S. Brodbelt, Ion activation methods for peptides and proteins, *Anal. Chem.* 88 (2016) 30–51.
- [7] M.P. Jedrychowski, E.L. Huttlin, W. Haas, M.E. Sowa, R. Rad, S.P. Gygi, Evaluation of HCD- and CID-type fragmentation within their respective detection platforms for murine phosphoproteomics, *Mol. Cell. Proteom.* 10 (2011), 009910. M111.
- [8] A. Chi, C. Huttenhower, L.V. Geer, J.J. Coon, J.E. Syka, D.L. Bai, J. Shabanowitz, D.J. Burke, O.G. Troyanskaya, D. F. Hunt Hunt, Analysis of phosphorylation sites on proteins from *Saccharomyces cerevisiae* by electron transfer dissociation (ETD) mass spectrometry, *Proc. Nat. Acad. Sci. USA* 104 (2007) 2193–2198.
- [9] A. Stensballe, O.N. Jensen, J.V. Olsen, K.F. Haselmann, R.A. Zubarev, Electron capture dissociation of singly and multiply phosphorylated peptides, *Rapid Commun. Mass Spectrom.* 14 (2000) 1793–1800.
- [10] J.W. Flora, D.C. Muddiman, Selective, sensitive, and rapid phosphopeptide identification in enzymatic digests using ESI-FTICR-MS with infrared multiphoton dissociation, *Anal. Chem.* 73 (2001) 3305–3311.
- [11] B.A. Budnik, K.F. Haselmann, R.A. Zubarev, Electron detachment dissociation of peptide di-anions: an electron-hole recombination phenomenon, *Chem. Phys. Lett.* 342 (2001) 299–302.
- [12] J.J. Coon, J. Shabanowitz, D.F. Hunt, J.E. Syka, Electron transfer dissociation of peptide anions, *J. Am. Soc. Mass Spectrom.* 16 (2005) 880–882.
- [13] K.L. Moore, Protein tyrosine sulfation: a critical posttranslational modification in plants and animals, *Proc. Nat. Acad. Sci. USA* 106 (2009) 14741–14742.
- [14] Y.S. Yang, C.C. Wang, B.H. Chen, Y.H. Hou, K.S. Hung, Y.C. Mao, Tyrosine sulfation as a protein post-translational modification, *Molecules* 20 (2015) 2138–2164.
- [15] G. Dimesa Baldeviana, E.P. Meneses, L. Hernandez Orihuela, O. Villa Hernandez, R. Castro Franco, V. Pasdo Robles, C.V. Ferreira Batista, Analysis of sulfated peptides from the skin secretion of the *Pachymedusa dactylos* frog using IMAC-Ga enrichment and high-resolution mass spectrometry, *Rapid Commun. Mass Spectrom.* 25 (2011) 1017–1027.
- [16] A.J. Hofflines, E. Darnoc, K.C. Bridges, J.A. Leary, K.L. Moore, Detection and purification of tyrosine-sulfated proteins using a novel anti-sulfotyrosine monoclonal antibody, *J. Biol. Chem.* 281 (2006) 37877–37887.
- [17] Y. Amano, H. Shinohara, Y. Sakagami, Y. Matsubayashi, Ion-selective enrichment of tyrosine-sulfated peptides from complex protein digests, *Anal. Biochem.* 346 (2005) 124–131.
- [18] M.R. Robinson, J.S. Brodbelt, Integrating weak anion exchange and ultraviolet photodissociation mass spectrometry with strategic modulation of peptide basicity for the enrichment of sulfopeptides, *Anal. Chem.* 88 (2016) 11037–11045.
- [19] G. Chen, Y. Zhang, J.C. Trinidad, C. Dann, III distinguishing sulfotyrosine containing peptides from their phosphotyrosine counterparts using mass spectrometry, *J. Am. Soc. Mass Spectrom.* 29 (2018) 455–462.
- [20] K.M. Hassell, Y. LeBlanc, S.A. McLuckey, Conversion of multiple analyte cation types to a single analyte anion type via ion/ion charge inversion, *The Analyst* 134 (2009) 2262–2266.
- [21] S. Rojas-Betancourt, J.R. Stutzman, S.J. Blanksby, S.A. McLuckey, Gas-phase chemical separation of phosphatidylcholine and phosphatidylethanolamine cations via charge inversion ion/ion chemistry, *Anal. Chem.* 87 (2015) 11255–11262.
- [22] C.E. Randolph, D.J. Foreman, S.K. Betancourt, S.J. Blanksby, S.A. McLuckey, Gas-phase ion/ion reactions involving tris-phenanthroline alkaline earth metal complexes as charge inversion reagents for the identification of fatty acids, *Anal. Chem.* 90 (2018) 12861–12869.
- [23] K.A. Schug, W. Lindner, Noncovalent binding between guanidinium and anionic groups: focus on biological- and synthetic-based arginine/guanidinium interactions with phosph(on)ate and sulf(on)ate residues, *Chem. Rev.* 105 (2005) 67–114.
- [24] S.N. Jackson, H.Y. Wang, A. Yegorov, A.S. Woods, Phosphate stabilization of intermolecular interactions, *J. Proteome Res.* 5 (2006) 122–126.
- [25] A.L. Patrick, N.C. Poller, H2SO4 and SO3 transfer reactions in a sulfopeptide-basic peptide complex, *Anal. Chem.* 87 (2015) 9551–9554.
- [26] A.S. Woods, S.C. Moyer, S.N. Jackson, Amazing stability of phosphate-quaternary amine interactions, *J. Proteome Res.* 7 (2008) 3423–3427.
- [27] L. Muller, S.N. Jackson, A.S. Woods, Histidine, the less interactive cousin of arginine, *Eur. J. Mass Spectrom.* 25 (2019) 212–218.
- [28] A.V. Tolmachev, A.N. Vilkov, B. Bogdanov, L. Pasa-Tolic, C.D. Masselon, R.D. Smith, Collisional activation of ions in RF ion traps and ion guides: the effective ion temperature treatment, *J. Am. Soc. Mass Spectrom.* 15 (2004) 1616–1628.
- [29] Y. Xia, P.A. Chrisman, D.E. Erickson, J. Liu, X. Liang, F.A. Londry, M.J. Yang, S.A. McLuckey, Implementation of ion/ion reactions in a quadrupole/time-of-flight tandem mass spectrometer, *Anal. Chem.* 78 (2006) 4146–4154.
- [30] I.K. Webb, F.A. Londry, S.A. McLuckey, Implementation of dipolar DC CID in

- storage and transmission modes on a quadrupole/time-of-flight tandem mass spectrometer, *rapid commun. Mass Spectrom.* 25 (2011) 2500–2510.
- [31] Y. Xia, X. Liang, S.A. McLuckey, Pulsed dual electrospray ionization for ion/ion reactions, *J. Am. Soc. Mass Spectrom.* 16 (2005) 1750–1756.
- [32] B.M. Prentice, R.E. Santini, S.A. McLuckey, Adaptation of a 3-D quadrupole ion trap for dipolar DC collisional activation, *J. Am. Soc. Mass Spectrom.* 22 (2011) 1486–1492.
- [33] B.S. Prentice, S.A. McLuckey, Dipolar DC collisional activation in a “stretched” 3-D ion trap: the effect of higher order fields on RF-heating, *J. Am. Soc. Mass Spectrom.* 23 (2012) 736–744.
- [34] J. Liu, C.M. Fisher, J.D. Gilbert, R.M. Prentice, S.A. McLuckey, Selective covalent chemistry via gas-phase ion/ion reactions: an exploration of the energy surfaces associated with N-hydroxysuccinimide ester reagents and primary amines and guanidine groups, *J. Am. Soc. Mass Spectrom.* 27 (2016) 1089–1098.
- [35] M.J. Frisch, G.W. Trucks, M.J. Frisch, G.W. Trucks, H.B. Schlegel, G.E. Scuseria, M.A. Robb, J.R. Cheeseman, G. Scalmani, V. Barone, B. Mennucci, G.A. Petersson, H. Nakatsuji, M. Caricato, X. Li, H.P. Hratchian, A.F. Izmaylov, J. Bloino, G. Zheng, J.L. Sonnenberg, M. Hada, M. Ehara, K. Toyota, R. Fukuda, J. Hasegawa, M. Ishida, T. Nakajima, Y. Honda, O. Kitao, H. Nakai, T. Vreven, J.A. Montgomery Jr., J.E. Peralta, F. Ogliaro, M. Bearpark, J.J. Heyd, E. Brothers, K.N. Kudin, V.N. Staroverov, R. Kobayashi, J. Normand, K. Raghavachari, A. Rendell, J.C. Burant, S.S. Iyengar, J. Tomasi, M. Cossi, N. Rega, J.M. Millam, M. Klene, J.E. Knox, J.B. Cross, V. Bakken, C. Adamo, J. Jaramillo, R. Gomperts, R.E. Stratmann, O. Vazquez, A.J. Austin, R. Cammi, C. Pomelli, J.W. Ochterski, R.L. Martin, K. Morokuma, V.G. Zakrzewski, G.A. Voth, P. Salvador, J.J. Dannenberg, S. Dapprich, A.D. Daniels, Ö. Farkas, J.B. Foresman, J.V. Ortiz, J. Cioslowski, D.J. Fox, *Gaussian 09, Revision A.02*, Gaussian, Inc., Wallingford, CT, 2009.
- [36] A.G. Harrison, The gas-phase basicities and proton affinities of amino acids and peptides, *Mass Spectrom. Rev.* 16 (1997) 201–217.
- [37] C. Bleiholder, S. Subai, B. Fairs, Revising the proton affinity scale of the naturally occurring α -amino acids, *J. Am. Soc. Mass Spectrom.* 17 (2006) 1275–1281.
- [38] J. Laskin, Z. Yang, A.S. Woods, Competition between covalent and noncovalent bond cleavages in dissociation of phosphopeptide-amine complexes, *Phys. Chem. Chem. Phys.* 13 (2011) 6936–6946.
- [39] A.M. Palumbo, G.E. Reid, Evaluation of gas-phase rearrangement and competing fragmentation reactions on protein phosphorylation site assignment using collision induced dissociation MS/MS and MS3, *Anal. Chem.* 80 (2008) 9735–9747.
- [40] M.-B. Gonzalez-Sanchez, F. Lamucara, G.E. Hardman, C.E. Eyers, Gas-phase intermolecular phosphate transfer within a phosphohistidine phosphopeptide dimer, *Int. J. Mass Spectrom.* 367 (2014) 28–34.